Exercise under Artificial Gravity – Experimental and Computational Approaches

by

Ana Díaz Artiles

Ingeniero Aeronáutico Superior, Universidad Politécnica de Madrid, Spain (2006)

SUBMITTED TO THE DEPARTMENT OF AERONAUTICS AND ASTRONAUTICS
IN PARTIAL FULFILLMENT OF THE REQUIREMENTS FOR THE DEGREE OF

DOCTOR OF PHILOSOPHY IN AERONAUTICS AND ASTRONAUTICS
AT THE
MASSACHUSETTS INSTITUTE OF TECHNOLOGY

JUNE 2015

Signature redacted

Signature of Author.....
Ana Díaz Artiles
Department of Aeronautics and Astronautics
June 2015

Signature redacted

Certified by.....
Prof. Laurence R. Young
Professor of Aeronautics and Astronautics and Health Science and Technology
Thesis Supervisor

Signature redacted

Certified by.....
Prof. Thomas Heldt
Hermann L.F. von Helmholtz Career Development Professor
Professor of Electrical and Biomedical Engineering
Committee Member

Signature redacted

Certified by.....
Prof. Dava J. Newman
Professor of Aeronautics and Astronautics and Engineering Systems
MacVicar Faculty Fellow, Director Technology Policy Program, Director MIT-Portugal Program
Committee Member

Signature redacted

Accepted by.....
Prof. Paulo C. Lozano
Associate Professor of Aeronautics and Astronautics
Chair, Graduate Program Committee

Exercise under Artificial Gravity – Experimental and Computational Approaches

By

Ana Díaz Artiles

Submitted to the Department of Aeronautics and Astronautics
on May 15th, 2015 in Partial Fulfillment of the Requirements for the Degree of
Doctor of Philosophy in Aeronautics and Astronautics

Abstract

Humans experience strong physiological deconditioning during space missions, primarily due to the weightlessness conditions. Some of these adverse consequences include bone loss, muscle atrophy, sensory-motor deconditioning, and cardiovascular adaptation, which may lead to orthostatic intolerance when astronauts are back on Earth. In order to mitigate the negative effects of weightlessness, several countermeasures are currently in place, particularly very intensive exercise protocols. However, despite these countermeasures, astronaut physiological deconditioning persists, highlighting the need for new approaches to maintain the astronauts' physiological state within acceptable limits.

Artificial gravity has long been suggested as a comprehensive countermeasure that is capable of challenging all the physiological systems at the same time, therefore maintaining overall health during extended weightlessness. Ground studies have shown that intermittent artificial gravity using a short-radius centrifuge combined with ergometer exercise is effective in preventing cardiovascular and musculoskeletal deconditioning. However, these studies have been done in very different conditions, and confounding factors between the studies (including centrifuge configuration, exposure time, gravity level, gravity gradient, and use/intensity of exercise) make it very difficult to draw clear conclusions about the stimuli needed to maintain physiological conditioning in space.

The first objective of this research effort is to analyze the effects of different artificial gravity levels and ergometer exercise workload on musculoskeletal and cardiovascular functions, motion sickness and comfort. Human experiments are conducted using a new configuration of the MIT Compact Radius Centrifuge, which has been constrained to a radius of 1.4 meters, the upper radial limit to fit within an ISS module without extensive structural alterations.

The second objective is to develop a computational model of the cardiovascular system to gain a better understanding of the effects of exercise under a high gravity gradient on the cardiovascular system. The gravity gradient generated when using a short-radius centrifuge has not previously been investigated in detail. The model is validated with the experimental measurements from the MIT CRC. Then, the model is used to explore the cardiovascular responses to new centrifuge configurations and from 0g adapted subjects.

Thesis supervisor: Laurence R. Young
Professor of Aeronautics and Astronautics and Professor of Health Science and Technology

Acknowledgments

This has been an incredible journey. It seems it was yesterday when I decided to come back to grad school to follow my passion, and here I am, four years later trying to summarize in a couple of pages how grateful I am for this incredible experience and, most of all, for all the amazing people that I encountered and supported me along the way.

First and foremost, I would like to thank my PhD Thesis advisor Prof. Larry Young. You took me as your student when I was in need of support, and you provided me with great opportunities, both personal and professional. Your energy and passion about everything you do is amazingly contagious. You are a remarkable teacher and mentor, and it is truly an honor to be your last PhD student.

I would also like to thank all the others mentors and committee members that have been incredible helpful during my four years at MIT. Prof. Jeff Hoffman: as my very first advisor, thank you for giving me the opportunity to join MIT and start this adventure. You guided my first steps into the spacesuit research, sharing your incredibly useful first-hand experience with me (and with the rest of the lab when we went to the movies to watch "Gravity"!). Prof. Dava Newman: thank you for your support since day one. Although I have officially never been your student, you have always treated me like one. During these years, you have provided me with opportunities off all kinds, including research, teaching, personal development, and also research trips (I wish I could have gone to Honduras at least once). Thank you for investing in me and my education, and for being such an inspiration to me. Prof. Thomas Heldt: thank you for teaching me everything I know about cardiovascular modeling. You introduced me to this field and you helped me as if I were part of your own lab. My thesis readers Prof. Jay Buckey, and Peter Norsk: thank you for your time invested in reading my dissertation and you valuable and insightful feedback and comments from an M.D. perspective.

Many other professors and members of the MIT community also deserve special mention. Prof. Leia Stirling, Dr. Chuck Oman, Dr. Andy Liu, Dr. Alan Natapoff, and Prof. Julie Shah, thank you for your guidance and support. During my time at MIT I had the chance to interact and work in one way or another with you all, and all of you have contributed to my personal and professional development. Liz Zotos and Beth Marois, you both deserve a really big thank you for your help, patience, and kindness dealing with all my questions and administrative tasks.

Dear MVLers: you really are the best lab in the world. The path towards a PhD is not always easy, but there will be always a labmate to help you get through the though moments. I want to start with my lovely officemate Raquel Galvan. You were there when I first arrived to our office, and you have been by my side this entire time. We have laughed together, and we have cried together. You have been an incredible support to me, and I am really grateful for having you around. Alexandra Hilbert, you arrived to the "girls office" a little bit later, but it seems we know each other for ages. Thank you for always being so positive and believing in me (you were right! I did it!). Chris Trigg, you did an amazing job putting the centrifuge together so I could do the experimental work with it. Your contribution to this research project was extremely important I will always be grateful to you. To the previous MVL generation, Allie Anderson (best trip to Iowa ever!), Aaron Johnson (you know you made me laugh every Friday morning), Torin Clark (you have been my MEEI biggest support and I am so grateful for having you around this past year), Justin Kaderka (thanks to you and your family to welcome us during every single trip to Houston as

if we were family), Brad Holschuh (and your incredible help during my preparation for quals), and Rita (so greateful for having an European buddy!). Thank you all for making this lab one of the best working environments I have ever seen. To the rest of the MVLers, every single one of you have made my time here very special, and I wish you all a happy graduation (first things first) and all the best in the future.

Dear Spanish mafia: you have become family and I am really blessed to have you around all these years. Even if most of you are already somewhere else, you have been an extremely important part of my years in Boston. To all of you: Carlos, Maite, Jorge, Alessandro, Majota, Maria, Ada, Fernando, Marc, Romina, and Iñigo, thank you and see you soon for new adventures!

At last, but not least, I would like to thank my family for their unconditional and eternal support. My parents have always encouraged me to follow my dreams and they have given me everything I needed along the way. When I told them I was going back to school, they encouraged me and supported me in every way possible. My sister has always been by my side and I wish I had you here. And most of all, I would like to thank my husband Dani for being my most unconditional supporter through all these years. Thank you for your patience and your love. I couldn't have done it without you.

This research was done thanks to the financial support of the Fulbright Commission, the MIT-Skolkovo development project (seed grant 6925991), and National Space Biomedical Research Institute (NSBRI) through NASA NCC 9-58.

Table of Contents

List of Acronyms

ADH	Antidiuretic Hormone
AG	Artificial Gravity
AGREE	Artificial Gravity with Ergometric Exercise
ANP	Atrial Natriuretic Peptide
ARED	Advance Resistive Exercise Device
BMD	Bone Mineral Density
CEVIS	Cycle Ergometer with Vibration Isolation System
CO	Cardiac Output
COLBERT	Combined Operational Load Bearing External Resistance Treadmill
COUHES	Committee on the Use of Humans as Experimental Subjects
CRC	Compact-Radius Centrifuge
CV	Cardiovascular
CSF	Cerebrospinal Fluid
DBP	Diastolic Blood Pressure
DLR	German Aerospace Center
EMG	Electromyography
GIF	Gravito-Inertial Force
GLCS	Gravity Loading Countermeasure Skinsuit
HDBR	Head Down Bed Rest
IBMP	Institute for Biomedical Problems
IPFM	Integral Pulse Frequency Modulation
iRED	Interim Resistive Exercise Device
ISS	International Space Station
IU	International Unit
LBNP	Lower Body Negative Pressure
LEM	Lode Ergometry Manager
LEO	Low Earth Orbit
MAP	Mean Arterial Pressure
MBP	Mean Blood Pressure
MIT	Massachusetts Institute of Technology
NASA	National Aeronautics Space Administration
NTS	Nucleus Tractus Solitarious
PMM	Permanent Multipurpose Module
PSA	Pulsatile Systolic Area
RPM	Revolutions per Minute
SBP	Systolic Blood Pressure
SRC	Short-Radius Centrifuge
SV	Stroke Volume
TVIS	Treadmill with Vibration Isolation System
US	United States
VIIP	Visual Impairment and elevated Intracranial Pressure

List of Figures

List of Tables

1 Introduction

Human deconditioning in weightlessness conditions has been considered from the very beginning of the human spaceflight era in the early 1960s. Since then, medical scientists have been involved in maintaining human health and performance in space under a new discipline called "Space Medicine" [1]. Over more than 50 years, an extensive research effort has been realized to identify, study, and resolve the medical problems that astronauts face in the 0g environment. Some of the physiological issues due to the weightlessness environment include bone loss, muscle atrophy, changes in body weight, fluid shift, cardiovascular deconditioning, and neurovestibular effects [1], [2].

Investigations on space physiology through the years led to a set of countermeasures to mitigate the effects of microgravity on the human body. For example, astronauts on the ISS currently follow an intense exercise protocol using anaerobic (or resistive) and aerobic devices, such as the Advanced Resistive Exercise Device (ARED) or the Cycle Ergometer with Vibration Isolation System (CEVIS), respectively. In addition, astronauts use nutrition supplements such as calcium and vitamin D, and wear special devices such as the lower body negative pressure (LBNP) vacuum chamber or the elastic "penguin" suit to stress the physiological systems in a similar way to standing [2]. However, the current countermeasures have proven to be only partially effective, and each one of them intends to mitigate one aspect of physiological deconditioning suffered in space [3].

Artificial Gravity (AG) has been discussed as an integrated countermeasure capable of mitigating most of the physiological deconditioning due to long duration exposure to weightlessness conditions. The inertial forces generated by centrifugation have the potential to affect multiple physiological systems at the same time, including musculoskeletal, cardiovascular, and the sensory-motor system [3]. Two different concepts, short radius and long radius AG, are considered in order to generate inertial forces using centrifugation in space. The first one consists of the use of a small radius centrifuge located inside a space vehicle or a specific module of a space station. This option involves high rates of rotation during intermittent sessions of artificial gravity. The second option considers the permanent rotation of the entire space station, involving lower rates of rotation but much higher system complexity [3].

Artificial gravity is not a new concept in human spaceflight. It was proposed by the Russian Konstatin Tsiolkovsky in his manuscript *"Free Space"* written in 1883 [3]. Since then, many designs have been envisioned, including the famous rotating wheel-like space station concept in the film "*2001: A Space Odyssey*" directed by Stanley Kubrick in 1968, based on Arthur C. Clarke's story "*The Sentinel*" from 1948. However, even after all these years many fundamental questions remain unanswered. It is believed

that exercise during centrifugation is one of the best combinations to maintain physiological functions in microgravity conditions [4], but the aerospace community has not agreed on a standardized protocol that will be effective. Many parameters still need to be defined, such as spacecraft design, artificial gravity exposure duration, rotation rates or exercise type, intensity and duration.

The objective of this research effort is to deepen the understanding of the physiological effects of artificial gravity generated by a short-radius centrifuge. The purpose is to take a first step towards a full trade space analysis of the most important artificial gravity parameters, examining through experimentation, modeling, and simulation the effects of different artificial gravity and exercise workload levels on multiple physiological systems (cardiovascular, musculoskeletal, and motion sickness and comfort) using the MIT Compact Radius Centrifuge.

2 Background

2.1 Physiological Deconditioning in Space

In the past 50 years humankind has made remarkable progress in space exploration. The Russian Yuri Gagarin was the first man launched into space on 12th August 1961, completing one orbit in 108 minutes. Even before then, the aerospace community was already raising the question about the possible reactions of humans to weightlessness. Through the years, the manned space programs conducted by the United States and Russia (or Soviet Union until 1991) have been key elements in the advance of physiological and biomedical understanding of human deconditioning in space [1]. Currently, more than 500 people have been to space and several institutions around the world are working on understanding and mitigating the negative effects of the weightlessness environment. Thus, the discipline of "Space Medicine" has become well established, providing a scientific base for physiological performance of astronauts in space.

Astronauts experience physiological changes when they go to space due to the weightlessness environment. The primary changes and their time course through several months are presented in Figure 1. Some of the physiological functions present shifts at the very early phases of spaceflight, such as the neurovestibular system, which makes adjustments during the first few days in orbit. On the other hand, cardiovascular shifts and adjustments are more likely to peak after three weeks in orbit, although this has only been demonstrated to a limited extent, since very little is known for long duration missions [5], [6].

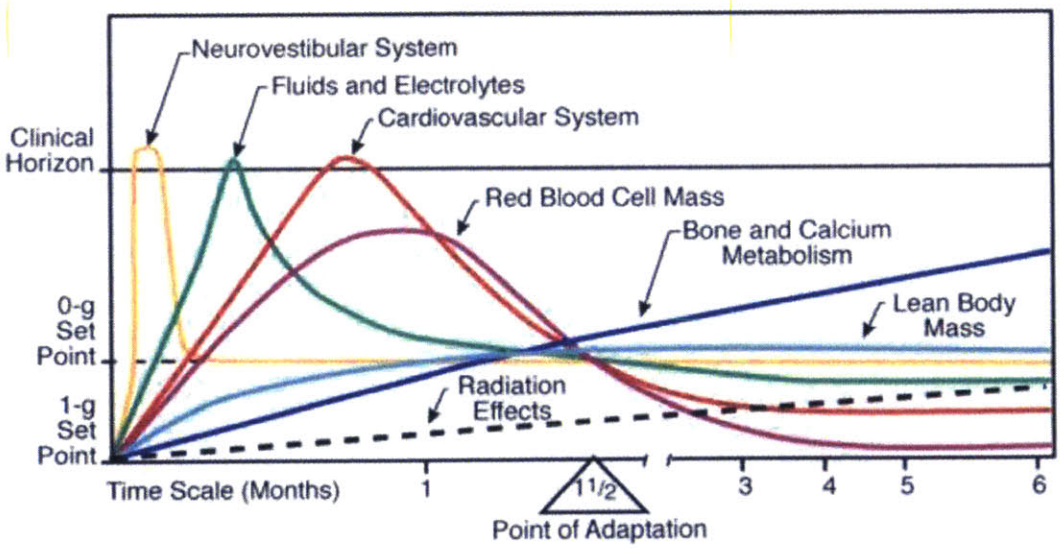

Figure 1 – Time course of physiological shifts associated with acclimation to weightlessness (adapted from [1]).

After some time in space (≈1.5 months), some of the physiological systems reach a new point of equilibrium after adaptation to the weightlessness environment. This is the case for the cardiovascular system, and the red blood cell mass among others. However, the skeletal system does not seem to reach a new point of equilibrium as astronauts continue to lose bone and calcium even after 6 months in orbit [1], [2].

When astronauts come back to the Earth, the physiological systems undergo new shifts and changes to readapt to the 1-g environment. These changes depend on individual differences, the type and intensity of the countermeasures applied during the spaceflight, and the duration of the space mission. Despite these differences, all astronauts present similar trends as represented in Figure 2. As an example, most astronauts experience orthostatic intolerance or difficulties with postural equilibrium associated with the re-adaptation of the cardiovascular and neurovestibular systems. In general, these physiological systems return to their preflight baselines one to three months post flight [1], [2].

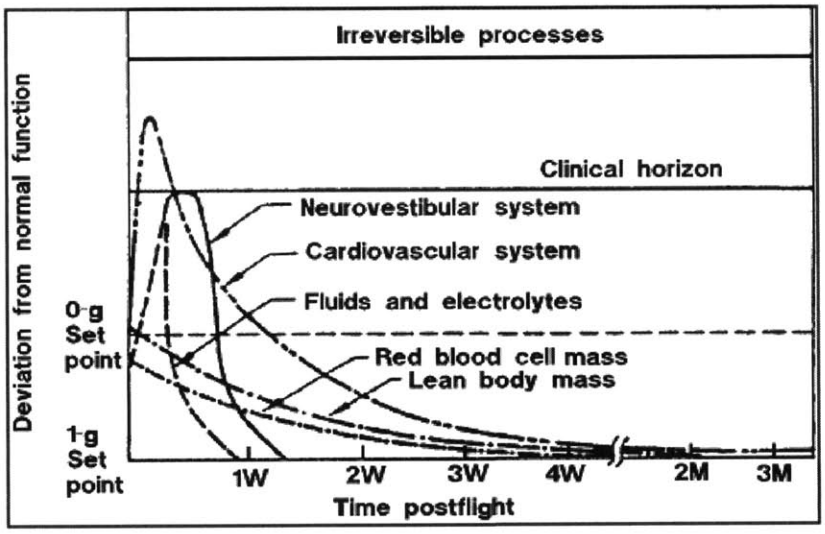

Figure 2 –Time course of physiological shift during adaptation to 1-g (adapted from [1]).

2.1.1 Skeletal Deconditioning

Bone loss is one of the most serious biomedical problems during spaceflight [1]. It occurs primarily because of the absence of skeletal loading in microgravity [2], [7], [8]. Other factors also affect skeletal properties, such as dietary factors (including calcium, vitamin D, and vitamin K), low light levels, high concentrations of CO_2, and genetic factors [2], [8].

Bone is a living tissue and it is under constant remodeling throughout its lifetime. Frost's mechanostat theory suggests that the response of bone to mechanical loads is controlled by a "mechanostat" that adjusts and adapts bone tissue according to the needed mechanical function [9]. Depending on the load applied, bone could be resorbed (i.e. loss of bone mass and therefore strength), remodeled (bone replacement), or modeled (i.e. bone gain). During the remodeling process old bone is replaced by new bone, helping to avoid the accumulation of microdamage [3]. This remodeling process is affected by the quantity and frequency of loading applied to the skeleton [2], [3], [8], [10], [11]. Two types of mechanical loading can be distinguished: static loading and dynamic loading. A clear example of static loading is the gravity force. People on Earth are continuously subjected to the gravity force, and this gravitational acceleration has an important role in skeleton remodeling. On the other hand, dynamic loading may include short periods of high-impact peak loads (such as ground reaction forces while running or jumping) or frequent low-level loading (such as low frequency vibration). Peak loads are particularly important in bone remodeling [12]. Lastly, muscle contraction also plays an important role in skeleton loading [8], [11]. In weightlessness conditions, mechanical loading of the skeleton is largely reduced because of the absence of gravitational stress and ground reactions forces. In addition, the muscle forces generated to move in space are significantly reduced, especially in the lower limbs [1], [8]. All in all, in space the skeleton adapts to the 0-g condition, increasing bone resorption and decreasing bone formation. This leads to a net decrease in Bone Mineral Density (BMD), and overall weaker bone [2], [10].

The loss of BMD is not equally distributed throughout the body. The lower extremities, which normally receive the greatest gravity loading, are the most affected with losses as big as -1.7 % per month in the great trochanter [2]. Astronauts show a gradient of loss that increases beginning at the lower spine and moving lower in the body [10]. The upper extremities are usually unaffected, and the skull may gain bone mass [2]. These results can be explained by the way astronauts move and work in space. They do not use their lower extremities to displace themselves from one place to another, as they do on Earth. Instead, astronauts use their fingers, arms, or upper extremities to do so. Changes in BMD after spaceflight observed through the MIR program are shown in Table 1. Bone loss persists even with an intense exercise program in place, although very recent data from the International Space Station (ISS) suggest that improving nutrition and resistance exercise can attenuate the expected BMD deficits observed after long duration missions [13].

Recovery time after spaceflight may exceed the time spent in microgravity conditions [2], [10]. Additionally, even if the preflight values of BMD are recovered, the internal structure of the bone may be altered. Finally, it is important to mention that there are large inter-individual differences in bone loss and bone recovery rates [2].

Table 1 – Bone loss rates from long-duration Mir missions [2].

Bone	% Change/month
Skull	+0.60
Humerus	+0.10
Lumbar Spine	-1.07
Pelvis	-1.35
Femoral Neck	-1.16
Greater Tronchanter	-1.58
Tibia	-1.25
Calcaneus	-1.50

2.1.2 Muscle Deconditioning

Astronauts experience muscle deconditioning during spaceflight [2], [14], [15]. In this unloading environment, muscles experience an imbalance between two processes - muscle protein synthesis and muscle protein degradation - leading to losses of muscle mass and strength. Eventually, muscle protein synthesis and muscle protein degradation will stabilize at a reduced equilibrium point involving lower muscle mass. Causes of muscle deconditioning include the lack of activity, under-nutrition and stress, oxidative stress (refers to the balance between oxidants/antioxidants), and hormonal influences [2].

Not all the muscles undergo the same level of changes during a space mission. The "antigravity muscles", or the muscles involved in maintaining posture and stability under gravity conditions, are most affected by the weightlessness environment. They contain a high percentage of type I (slow twitch) fibers, given their continuous role in posture and balance under Earth gravity. These type I fibers seem to be most sensitive to lack of activity and weightlessness conditions. In addition, some type I fibers will transform into type II fibers (fast twitch) during spaceflight due to the changes in their activation patterns while in space. Table 2 shows the changes in muscle volume after long-duration spaceflight in some of the antigravity muscles:

Table 2 – Changes in muscle volume for different muscle groups [2].

Muscle Group	% Loss after long-duration flight
Back	-10.9
Iliopsoas	-20.0
Quadriceps	-12.1
Hamstrings	-15.7
Soleus	-19.6

2.1.3 Cardiovascular Deconditioning

The cardiovascular system experiences important changes during spaceflight in order to adapt to a weightlessness environment. In general, this adaptation process is successful. Some cardiac rhythm disturbances have been documented in the past for crew members, although it is very difficult to associate them with weightlessness instead of other factors such as stress, exercise or electrolyte imbalance [2]. However, the readaptation process when crew members return to a gravity environment is more problematic. Their cardiovascular system is not adapted to normal gravity conditions, and orthostatic intolerance occurs [2], [16].

One of the main cardiovascular effects that astronauts experience during spaceflight is the central fluid shift phenomenon. Blood pressure and volume distribution are directly affected by gravity. In standing position on Earth, the blood is pulled to the lower extremities. Similarly, venous pressure decreases due to the presence of the gravity force. Nevertheless, the human body has mechanisms to deal with gravity effects. For example, leg muscles are used as secondary pumps to facilitate venous return to the heart [16]. In space, part of the blood that is usually located in the lower part of the body is shifted upwards to the upper body, the upper trunk, and the head. Consequently, there is a significant increase in central blood volume (volume in the heart cavities, lungs and central arterial tree). The cardiopulmonary receptors, situated in the atria and pulmonary arteries, sense this pressure change and start acting upon the "excess" body fluid (plasma and red cell mass), increasing the output of urine, and making the astronauts less thirsty, among other resulting processes [2], [16]. As a consequence, the overall quantity of fluids and electrolytes decreases, leading to a reduction in total circulation blood volume of up to 11% [2], and stabilization in a new "cardiovascular state" associated with weightlessness conditions.

The increase in transmural central venous pressure in weightlessness induce an increase in stroke volume and cardiac output by as much a 22% in short-duration spaceflight [6], and by 35 and 41% respectively between 3 and 6 months on the ISS [5]. Heart rate remains unchanged or decreased. Systemic vascular resistance decreases by 14% in short-duration spaceflight and therefore blood pressure is reduced to approximately the supine level on the ground [6]. These changes seem to be accentuated during long-duration flights, with a reduction in the systemic vascular resistance of approximately 39%, and a reduction in blood pressure of 8-10 mmHg [5].

The cardiovascular system also experiences other changes in space. During the first stages of weightlessness, the heart enlarges in order to handle the fluid shift and the increase in central blood volume. In later stages, when the fluid adjustments occur and the total circulating blood decreases, the heart does not need to work as hard. Moreover, the heart does not need to work against gravity either.

These changes, and the reduction of the overall level of activity, lead to a decrease in heart size (both chamber size and wall thickness) causing cardiac atrophy [2], [16]. Other effects in microgravity include an increase in venous compliance resulting in blood pooling to the lower extremities and a reduction in the baroreflex sensitivity [3]. In addition, the initial increase in fluid volume in the head can cause facial edema, headaches, nasal congestion, and venous engorgement [17].

When astronauts return to Earth, their cardiovascular system may not be adapted to deal with the gravity force. This may be due to a combination of different factors, such as reduced blood volume, cardiac atrophy, reduced vasoconstriction, increased venous compliance, reduced stroke volume and cardiac output, or decrease in the baroreceptor reflex. Aerobic capacity is also reduced up to 22% after short duration spaceflight (9-14 days) [18]. As a consequence, crew members suffer what is known as postflight orthostatic intolerance. Once, back on Earth, gravity pulls the blood to the lower extremities again. The arterial pressure decreases and the heart rate increases as a result of the baroreflex response, but the body may not be able to generate the necessary pressure to force the blood back up to the head. In some cases, this postflight orthostatic stress is strong enough to make it impossible for astronauts to stand up for several minutes without losing consciousness. After short-duration spaceflight, up to 63% of crew members presented signs of orthostatic intolerance [2].

2.1.4 Sensory-motor Deconditioning

In order to successfully control balance and posture, the human brain integrates information that comes from the different vestibular sensors including semicircular canals, otoliths organs, as well as vision, and proprioception. The integration of the vestibular inputs is also altered in space, and astronauts must adapt to these changes during their space missions. As a result, perception, body orientation and equilibrium are affected, which may lead to detriments in astronaut performance and well-being. These alterations are particularly significant during the first days of a space mission [2], [3], [16].

During spaceflight, the otoliths organs no longer sense the continuous gravitational force and therefore the vestibular system must learn how to interpret the otolith information in this new environment. These changes in otolith stimulation can cause conflicting vestibular cues in space, and may lead to disorientation and space motion sickness. Symptoms may include nausea, headache, dizziness, vomiting, drowsiness, and cold sweat. Space motion sickness is very common during spaceflight. Approximately two-thirds of the Space Shuttle astronauts experiences some degree of motion sickness during the first few days of spaceflight [19]. In addition, astronauts' sense of proprioception is highly reduced in space, unless they wear bungee cords that push them against the floor in order to stand up, walk or run (e.g.

using the treadmill). As a result, past evidence suggests that crew members put more weight on visual cues than on other vestibular sensors [20], [21].

Sensorimotor activities such as walking heel-to-toe or standing with eyes closed can be very challenging after spaceflight. Nevertheless, these symptoms generally disappear within a few days of landing, demonstrating again the high adaptability of the balance system [2].

2.2 Current countermeasures

Several countermeasures are currently in place to keep astronauts healthy and mitigate as much as possible the negative effect of weightlessness on the human body. In general, these countermeasures are system specific, focusing on one particular aspect of human deconditioning in space.

Exercise is the principal countermeasure used in space, and it is part of the daily activities of crew members. Astronauts exercise around 2.5 hours a day, 6 days a week, using different devices including treadmills, ergometers, a resistance exercise device, as well as bungees and expanders. Together, these devices provide a comprehensive exercise plan that includes aerobic, anaerobic and resistive training to alleviate skeletal, muscular and cardiovascular deconditioning [2]. The exercise devices on the ISS are the Treadmill with Vibration Isolation System (TVIS), the T2 Treadmill or Combined Operational Load Bearing External Resistance Treadmill (COLBERT), the Cycle Ergometer with Vibration Isolation System (CEVIS), the VELO Ergometer, and the Advanced Resistive Exercise Device (ARED) [22]. These exercises devices are shown in Figure 3.

The T2/COLBERT treadmill was added to the existing TVIS treadmill to cover the larger crew of 6 astronauts on the ISS. Both treadmills can be operated in either active mode or passive mode (powered by the astronauts), and they have bungee cords to pull the users against the treadmill and create some compressive loading [23]. The Russian VELO ergometer is used in the recumbent position and provides workload levels between 50-250 W at 40-120 rpm. The CEVIS ergometer is operated in the United States Laboratory Module (US LAB) and is able to provide workload levels between 25-350 W at 50-120 rpm. This ergometer provides a very accurate workload independent of the pedaling of the crew member [24]. The ARED device was sent to the ISS in November 2008 to replace the Interim Resistive Exercise Device (iRED). The ARED primary goal is to maintain astronaut muscle mass and strength during their space missions. It simulates free-weight exercises up to 1675 N of load, and allows crew members to follow a personalized exercise plan [25].

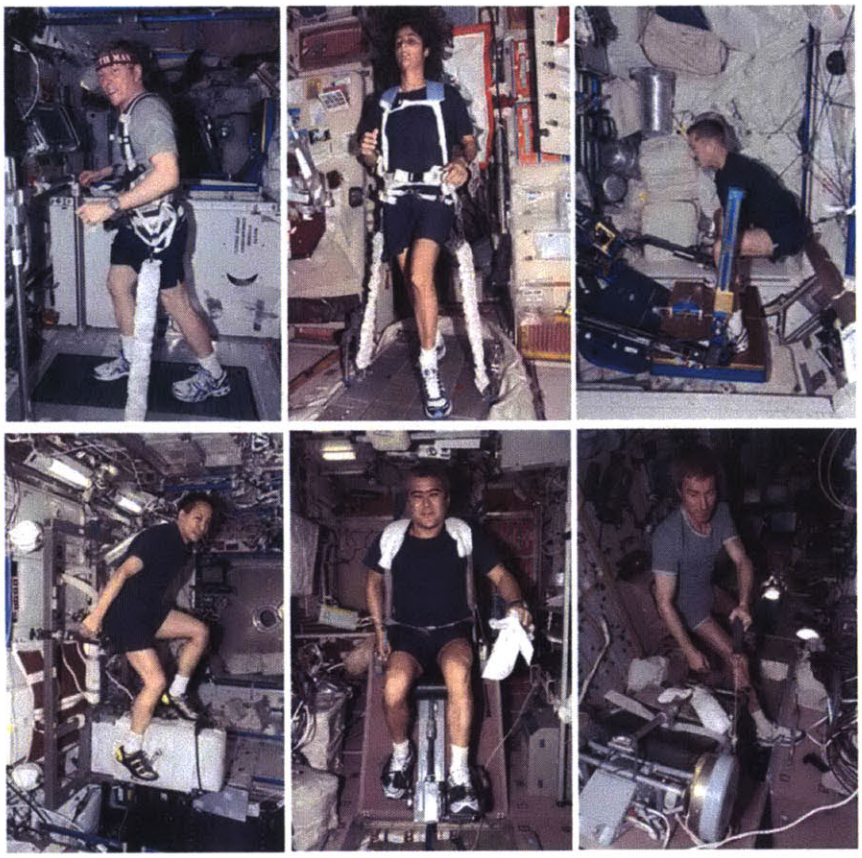

Figure 3 - Exercise devices in the ISS (top left to bottom right): T2/COLBERT, TVIS, ARED, CEVIS, VELO Ergometer, VELO Ergometer with cable (NASA) [22].

Additional countermeasures are also being used during spaceflight. Leg cuffs are used soon after reaching orbit to reduce the amount of fluid shift from the lower extremities to the upper extremities, ameliorating the symptoms resulting from fluid distribution such as facial edema, engorgement of the external neck veins, nasal congestion, and headache [17]. The Lower Body Negative Pressure (LBNP) system consists of a chamber that covers the lower extremities and induces a cardiovascular stress by applying negative pressure over the lower body. It increases blood pressure to the legs and restores the blood pressure gradient, creating a cardiovascular state similar to upright standing on Earth. The LBNP system is mostly used one month before landing to improve orthostatic stability upon landing and to reduce the risk of pre-syncope and loss of consciousness [26]. LBNP is used in association with fluid loading, which consists of the consumption of water and salt tablets to increase plasma volume [3]. Figure 4 shows the Russian "Chibis" LBNP device currently on board.

Figure 4: The "Chibis" LBNP device [26].

The Zvezda Penguin suit is a whole-body suit that includes elastic bungee cords to partially simulate gravitational loading on the human body. Two sets of elastic cords attached to a leather belt provide upper body loading (cords from the shoulder to the belt) and lower body loading (cords from the belt to the feet). The suit creates compression along the body longitudinal axis (z-axis), providing constant static loads and resistance to movement and thus, stressing and stimulating the musculoskeletal system [8], [27]. The "Penguin" suit can produce a static axial load up to 70% of bodyweight during treadmill training. The upper body can produce axial and static loading up to 40 kg [28]. This load can be increased by shortening the leg cords. The calf muscles are also loaded by adjusting the cords on the boots [8]. Despite all of the potential musculoskeletal benefits provided by the use of the "Penguin" suit, cosmonauts have found the suit highly uncomfortable and very hot. Thus, they have individually loosened, or even cut, the elastic cords to improve their comfort. In addition, the suit has been used in conjunction with other countermeasures, making a proper evaluation and quantification of its effectiveness very difficult [8].

The Gravity Loading Countermeasure Skinsuit (GLCS) developed by the Massachusetts Institute of Technology also provides the wearer a continuous static loading replicating that of gravity on Earth. In contrast to the "Penguin' suit, the GLCS gradually increases the vertical load from the shoulders to the feet (z axis), mimicking the loads imposed on the different parts of the body under gravitational conditions. A first prototype of the GLCS was developed for a pilot study conducted under microgravity conditions during a parabolic flight campaign, showing reasonable suit comfort and mobility [8]. New prototypes are in development, and the GLCS will be used in the ISS for the first time in September 2015 [29]. Figure 5 shows the Russian "Penguin" suit (left, center), and the GLCS (right):

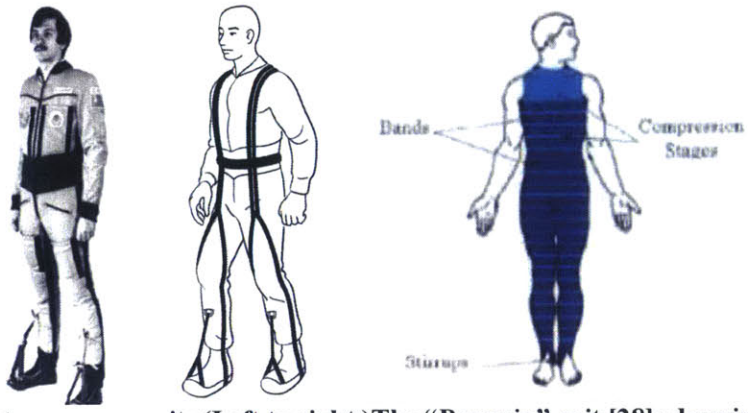

Figure 5 - Countermeasure suits (Left to right)The "Penguin" suit [28]; drawing by Philippe Tauzin, [Clement 2005], and the Gravity Loading Countermeasure Skinsuit or GLCS [8].

Nutrition is also a very important aspect of spaceflight. It has been shown that astronauts usually burn more calories than they take in and therefore are in negative caloric balance. This fact, combined with an intense exercise program, may lead to a significant mass loss (in particular muscle mass) and strength reduction [2]. Astronauts need an adequate energy intake and dietary supplements, such as calcium (1000-1200 mg/day) and vitamin D (600 IU) to mitigate bone loss. Table 3 summarized the main physiological effects during spaceflight and the countermeasures to mitigate them.

Table 3 – Summary of the main physiological effects and countermeasures.

Main Physiological Effects	Countermeasures
Skeletal deconditioning	Exercise (aerobic and resistive), Penguin suit, GLCS, LBNP, fluid loading, nutrition and dietary supplements (calcium, vitamin D)
Muscle deconditioning	
Cardiovascular deconditioning	
Sensory-motor deconditioning	

2.3 Artificial gravity as a multi-system countermeasure

Despite the large variety of countermeasures in place, their effectiveness has not been adequately demonstrated in terms of maintaining preflight levels of bone, muscle, aerobic fitness, and cardiovascular conditioning [2], [3], [28], [30], [31]. Each countermeasure targets one particular aspect of human deconditioning in space, making it very difficult and time consuming to maintain an overall good state across systems. For example, different exercise protocols are designed to counteract muscle loss (resistive exercise), cardiovascular deconditioning (aerobic exercise), or bone loss (high peak forces during treadmill exercise) and therefore, the crew members spend more than 2 hours/day exercising. On the other hand, these exercise protocols have not been shown to fully protect astronauts from weightlessness deconditioning during long duration spaceflight (6 months in Low Earth Orbit (LEO)) [30]. Hence, even with these countermeasures, astronauts will almost certainly suffer the negative effects of weightlessness during longer missions in the future such as a trip to Mars (up to 30-month round-trip mission). After the 6-month trip to Mars, the crew members will have suffered bone loss, muscle atrophy, cardiovascular deconditioning, and vestibular changes, and they will not have the support to deal with these changes as they do when they return to Earth. In addition, the reduced Mars gravity (0.38g) may not be sufficient to maintain a sufficient physiological conditioning without additional countermeasures [3].

Artificial gravity is introduced as a multi-system countermeasure. It consists of the recreation of a gravity environment that challenges all the physiological systems like on Earth. Artificial gravity will not mitigate all the risks associated with human spaceflight (for example, it will not be effective against psychological issues or radiation exposure), but it is proposed as a solution for the physiological deconditioning associated with long duration spaceflight, including bone loss, muscle atrophy, cardiovascular deconditioning, neurovestibular disturbances, space anemia, and immune system deficiency [2], [3], [32], [33]. In addition, besides reducing or eliminating physiological deconditioning, artificial gravity could potentially improve hygiene, habitability and medical operations [3], [34].

2.3.1 General principles of Artificial Gravity

Artificial gravity in a spacecraft can be generated using various techniques such as linear acceleration (accelerating or decelerating in a straight line), or centrifugal force (artificial gravity generated by rotation). In the second category, two main methods can be differentiated:

- **Continuous artificial gravity**

  Continuous artificial gravity can be generated by rotation of a large spacecraft. This concept was first proposed by Tsiolkovsky in 1883. In the 1950s, Von Braun envisioned a large spinning

space station in order to generate continuous artificial gravity (see Figure 6). A different option refers to the rotation of a rigid truss, which would have the astronaut's habitat in one side, and a counterweight or perhaps a nuclear power plant on the other side. It could also have another module at the center of rotation to perform 0g gravity experiments (see Figure 6). Providing continuous artificial gravity is highly desirable from the physiological point of view. However, many engineering challenges arise with this concept, and, considering the large mass needed on orbit, a very large budget would be necessary to carry out such an endeavor.

Figure 6 – Continuous artificial gravity: Wernher von Broun's rotating space station and rigid truss designed by NASA to provide 1g in the astronaut habitat (Credit: NASA).

- **Intermittent artificial gravity by rotation on an on-board small radius centrifuge**
  A small radius centrifuge is a more affordable approach to generate artificial gravity in space. The engineering challenges as well as budget constraints would certainly be reduced. In this scenario, astronauts would be subject to intermittent artificial gravity for short periods of time. It is unknown if the reduced gravity on Mars will be enough to maintain a healthy physiological state, and this concept would provide a way to create artificial gravity on the Mars surface as well as in space.

The next subsection reviews the physical principles of artificial gravity, in particular the principles associated with an on-board small radius centrifuge.

2.3.1.1 Artificial gravity generated by a small radius centrifuge

Inertial forces are generated by rotation during centrifugation. The centrifugal force is directed radially towards the rim of the centrifuge. It recreates the gravity force and hence, objects (or people) on the

centrifuge are stressed as if they were subjected to a true gravity environment (except for the gravity gradient, see below). In a rotating environment, the magnitude of the centrifugal force is:

$$F_{centrifugal} = m\omega^2 r \tag{1}$$

where m is the mass of the object (kilograms), ω is the angular velocity (radians per second), and r is the radius from the object to the center of rotation (meters). The force generated depends on the angular velocity and the radius. Thus, a small radius centrifuge needs to rotate faster to generate the same amount of force as a big rotating station, affecting how people feel in this rotating environment. This is mainly due to the presence of other inertial forces generated by movement during rotation: namely the Coriolis forces.

The Coriolis forces appear as a result of linear movement in a rotating environment and are perpendicular to the direction of the movement. The Coriolis forces are:

$$\boldsymbol{F}_{coriolis} = -2m\boldsymbol{\Omega} \times \boldsymbol{v} \tag{2}$$

where m is the mass of the object (kilograms), $\boldsymbol{\Omega}$ is the angular velocity vector which has magnitude ω and is directed along the axis of rotation (radians per second), and $\boldsymbol{v}$ is the velocity vector of the linear movement (m/s). Figure 7 shows the Coriolis forces in a spinning carousel:

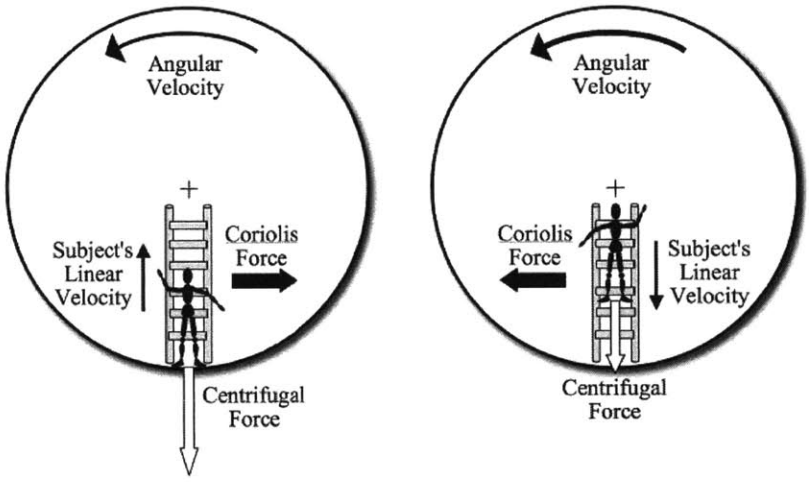

Figure 7 – Coriolis Forces in a rotating environment (Adapted from Stone 1973) [3].

Thus, the Coriolis forces are zero if $\boldsymbol{v}$ is zero or if $\boldsymbol{v}$ is parallel to the rotation axis. If $\boldsymbol{v}$ is in a plane normal to the rotation axis, the Coriolis forces are perpendicular to both the velocity and the rotation axis.

Coriolis forces are independent of the radius and therefore, their magnitude is the same at all distances from the center of rotation, assuming constant linear velocity. Figure 8 shows the Coriolis forces generated at four different rotation rates when the linear velocity is $v = 0.1\ m/s$. Note that the magnitude does not change with the radius.

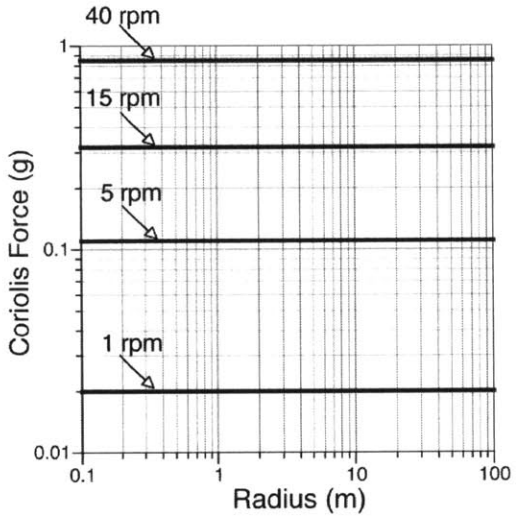

Figure 8 – Coriolis forces as a function of radius for four different rotation rates [3].

The gravity gradient is another extremely important parameter in a small radius centrifuge. The centripetal forces generated by rotation depend on the distance to the center of rotation and therefore, there is a force gradient along the centrifuge radius. As an example, when a subject is lying down on a centrifuge with her head located at or near the center of rotation and her feet at the rim of the centrifuge, she will experience different gravity levels along her body. For a subject of height h lying on a centrifuge of radius r with her feet at the rim, the general expression for the gravity gradient is:

$$\text{Gravity gradient} = 1 - \frac{a_{head}}{a_{foot}} = 1 - \frac{\omega^2(r-h)}{\omega^2 r} = 1 - \frac{(r-h)}{r} = \frac{h}{r} \tag{3}$$

where $(r-h)$ is the radius of rotation of the head. In the extreme case where the head is located at the center of rotation $(r-h) = 0$, the head will experience no force, and the subject will experience a gravity gradient of 100%. Figure 9 shows the relationship between gravity gradient and radius for a subject of height $h = 2\ m$ lying on a centrifuge with his/her feet at the rim, and her head pointing to the center of rotation.

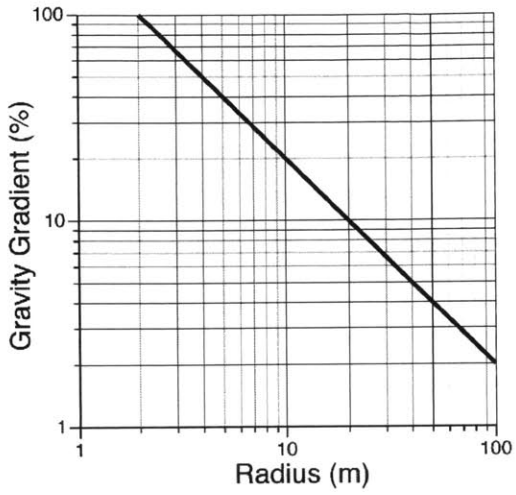

Figure 9 – Gravity gradient as a function of radius for an astronaut of height h=2m standing on the rim [3].

Many questions regarding the appropriate artificial gravity configuration and parameters still need to be answered. First, the level of artificial gravity required to maintain the physiological state of the astronauts is not known. Ground-based bed rest studies suggest that gravity levels up to 2 g at the feet could be useful, in particular if they are combined with exercise [3]. In addition, the tradeoff between angular velocity and radius to generate the desired gravity level needs to be further explored. Furthermore, most of the ground-based studies have been conducted using long-radius centrifuges. The physiological effects of the gravity gradient have not been thoroughly investigated [3].

2.3.2 Artificial Gravity Coupled With Exercise in a Short-Radius Centrifuge.

Performing exercise during centrifugation in a short-radius centrifuge has several advantages. Exercise during centrifugation may help increase tolerance to acceleration. The physiological stress of the centrifuge may be too high, inducing some degree of orthostatic intolerance. Active exercise during centrifugation activates the leg muscle pumps facilitating the venous flow towards the heart, keeping blood from pooling in the legs and therefore, protecting the astronauts against syncope or fainting [3], [35]. In addition, the use of artificial gravity could make exercise programs more efficient and reduce in-flight resources, such as in-flight mass (food and oxygen), power, crew time, and therefore, cost. Artificial gravity has the potential to provide a greater overall physiologic benefit for a given amount of exercise and resources. [33].

Centrifugation combined with exercise has been shown to be effective in preventing cardiovascular deconditioning [36]–[42]. Few ground-based studies have evaluated the combination of intermittent artificial gravity in a short-radius centrifuge with exercise as a comprehensive countermeasure for long duration spaceflight. One of the most implemented exercise devices used is a cycle ergometer. Greenleaf et al. showed that exercise in a short-radius centrifuge (1.9 m) adds a significant physiological stress that could attenuate orthostatic intolerance [36]. Iwase and his colleagues demonstrated that combining intermittent artificial gravity with ergometric exercise is effective in preventing cardiovascular deconditioning [37], [38]. Yang et al. confirmed the improvement of the cardiovascular function due to combined use of a short-arm centrifuge and aerobic exercise during a one-week training [39]. Katamaya et al. demonstrated that the use of a short-arm centrifuge combined with exercise training is effective in maintaining respiratory and cardiovascular responses to upright exercise during 20 days of -6° Head Down Bed Rest (HDBR) [41]. Iwasaki et al. showed that AG couple with moderated ergometer exercise successfully maintained plasma volume [42]. In addition, researchers have also implemented other types of exercise during short-radius centrifugation, such as squats [43], [44] and stair-steppers [4], demonstrating the feasibility of these types of exercise protocols in hypergravity rotating environments.

However, the effectiveness of centrifugation with or without exercise in mitigating the deconditioning of the musculoskeletal system is still inconclusive [45], [46]. Pure aerobic exercise seems to be ineffective because the mechanical loads exerted are not high enough to prevent bone and muscle deconditioning [3]. Too few studies have been conducted to date and no conclusions can be drawn concerning their effectiveness due to the short duration of Ag studies, and the large amount of confounding factors [35].

2.3.3 Confounding factors

Although several studies have investigated the effectiveness of artificial gravity exposure, these studies have been conducted in different conditions, making it very difficult to define clear conclusions about the parameters needed to maintain physiological conditioning in space. Confounding factors include centrifuge configuration, exposure time, gravity level, gravity gradient, and use/intensity of exercise. Kaderka et al. identified differences in research design among 14 AG studies used in a meta-analysis performed to compare the efficacy of AG with more traditional countermeasures. Differences included centrifuge configuration, subject selection criteria, experiment protocol (i.e. time of exposure, study duration, g level, gravity gradient, etc.) and choice of dependent measures [35]. Table 4 summarizes the short-radius centrifuges currently operational. This table gives an indication of the variety of centrifuge designs across multiple studies.

Table 4 – Existing short-radius centrifuges [3], [22].

Name	Location	Radius	Max g	Mode	Exercise
Space Cycle	UC Irvine, Irvine, USA	1-2 m	5.0 g	Gondola	Cycling /Squats
Short Arm Human Centrifuge	Nihon U, Nishi-Funabashi, Japan	1.8 m	3.0 g	Gondola	N/A
NASA Ames Human Powered Centrifuge	Moffet Field, USA	1.9 m	5.0 g	Bed	Cycling
Short-Radius Human Centrifuge	Nagoya U, Japan	1.4 m	2.0 g	Chair	Cycling
MIT Compact Radius Centrifuge	MIT, Cambridge, USA	2.0 m	1.8 g	Bed	Cycling
Short-Arm Centrifuge	Fourth Military Medical U, Xi'An, China	2.0 m	4.0 g	Chair	Cycling
Short-Radius Centrifuge	IBMP, Moscow, Russia	2.5 m	2.0 g	Bed	Cycling
DLR Short-Radius Centrifuge	DLR, Cologne, Germany	2.8 m	5.0 g	Bed/Chair	N/A
ESA Short-Arm Centrifuge	MEDES, Toulouse, France	2.9 m	3.5 g	Bed/Chair	N/A
EnviFuge	DLR, Cologne, Germany	3.8 m	6.0g	Bed	Cycling

These findings highlight the need for more exhaustive AG studies, with strategic isolation of some of the confounding factors. These experiments will help answering fundamental questions that are important and critical to the future implementation of artificial gravity in space. In addition, more standardized approaches to AG studies among the international research community are needed, fostering collaboration between the different facilities around the world.

2.4 Quantitative analysis of the cardiovascular system

Guyton was the "pioneer' of the quantitative physiology system analysis of circulation regulation. He developed a large circulatory model with hundreds of equations used to quantify the different subsystems of the circulation and their control [47]. His main contributions include (but are not limited to) the understanding of the interaction between venous return and cardiac function, the whole body autoregulation, renal body-fluid feedback mechanism in long-term blood pressure control, graphical analysis of physiological regulation, and quantitative computer modeling of physiological systems.[48]–[50]. Although Guyton's work was focused on long-term steady-state cardiovascular responses, the principles he developed are still applicable and are widely used in the field [51].

The cardiovascular system can be modeled using different approaches depending on the modeling objective and the assumptions on the spatial degrees of freedom. Three-dimensional (3D) models are used when detailed information about the blood flow in a particular region is needed. In these models, the fluid behavior is usually described by the Navier-Stokes equation for incompressible fluids. Despite the progress of current numerical methods, the computational cost of these models is very high, limiting their application to small localized regions. One-dimensional (1D) models assume axial symmetry and only have one degree of freedom, namely translation along the axial direction. These models are useful to analyze arterial wave propagation, and they are described by hyperbolic partial differential equations. Finally, zero-dimensional models (0D), or lumped-parameter models, represent the spatial variation in a highly aggregated manner, as they compartmentalize the cardiovascular system into discrete functional units. They describe the time evolution of the pressure and flow in each compartment using ordinary differential equations [52].

The objective of this modeling effort is to capture the beat-to-beat, short-term hemodynamic response to artificial gravity generated by a compact-radius centrifuge. Thus, a lumped-parameter model seems the logical choice, since it provides beat-to-beat average variables (including pressures, flows, and volumes) at a low computational cost.

2.4.1 Modeling orthostatic stress

With regard to the cardiovascular adaptation to gravitational stress, many computational models have been developed with a large variety of temporal and spatial resolutions, depending on the representation and the objective of the model [53]. Various mathematical models investigate the physiological responses to postural changes, such as active standing [54], head-up tilt [55]–[58], or lower body negative pressure [55], [59]. Some models were designed to explain observations seen during human spaceflight [58], [60], [61], including the recent Visual Impairment and elevated Intracranial Pressure (VIIP) syndrome [62].

For our purpose, the cardiovascular model to be developed needs to have enough compartments to capture the strong hydrostatic gradient generated by the compact-radius centrifuge. Heldt developed a lumped-parameter model using 21 compartments in order to simulate the short-term ($\approx$ 5 minutes), transient, beat-to beat hemodynamic response to gravitational stress, such as head-up tilt and lower body negative pressure [63]. The hemodynamic model includes the systemic circulation (arterial system, micro-circulation, and the venous system), the cardiac chambers, and the pulmonary circulation. The cardiovascular system is represented by seventeen vascular and four cardiac compartments grouped into four main sections: head and arms, thorax, abdomen, and legs. The full 21-compartment model is shown in Figure 10 and is currently incorporated in the expanded research version of CVSim, a computational

platform developed at the Harvard-MIT Division of Health Science and Technology [64]. Parameters such as compliance, volume, resistance, or vascular length (to determine the hydrostatic pressure) were estimated from the literature. The model also incorporates the arterial baroreflex and the cardiopulmonary reflex to maintain blood pressure homeostasis during orthostatic stress. Finally, the cardiovascular effects of exercise were modeled, including the effects of muscle blood flow (decreasing legs resistance), the effects of the muscle pumps (varying the external pressure at the venous leg compartment), and the increase of the intra-abdominal pressure.

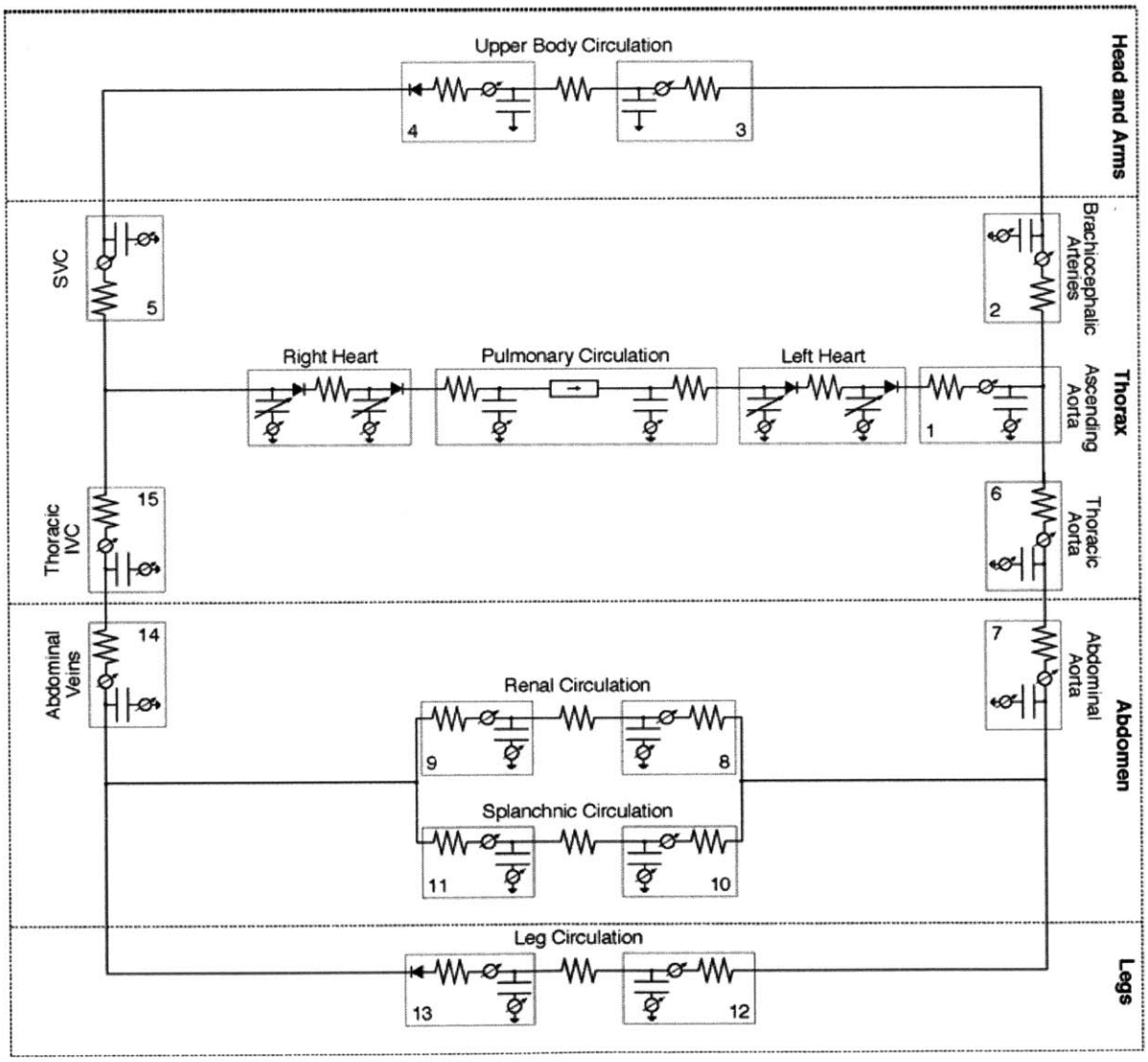

Figure 10 – Circuit representation of the cardiovascular model developed by Heldt [63].

Based on the 21-compartment model developed by Heldt, Zamanian built a lumped-parameter hemodynamic model for the cardiovascular response to centrifugation [65]. This new model introduced the simulation of the hydrostatic pressure resulting from centrifugation as well as a model for the collapsibility of blood vessels under high orthostatic stress (negative transmural pressure). Simulations at 11.6 rpm, 22.9 rpm, and 29.4 rpm were validated with experimental measurements conducted in the Man Vehicle Laboratory using the MIT short-radius centrifuge.

In the current modeling effort, Heldt's and Zamanian's approaches are combined to develop a new cardiovascular model capable of capturing the short-term, beat-to-beat hemodynamic responses to artificial gravity generated by a compact-radius centrifuge combined with ergometer exercise.

3 Thesis Aims

3.1 Research Gaps

The review of the AG literature highlights several major research gaps to be addressed in this thesis:

- Previous studies have shown that hypergravity generated by a short-radius centrifuge associated with an ergometer exercise device may be beneficial to maintain musculoskeletal and cardiovascular functions in microgravity conditions [3], [4], [36]–[41], [43], [44]. However, the optimal AG level to maintain normal physiological function is unknown. Different levels of artificial gravity and their effects on musculoskeletal and cardiovascular response need to be explored.

- The gravity gradient generated when using a short-radius centrifuge has not been investigated in detail. Previous research on cardiovascular effects during exercise under artificial gravity using a short-radius centrifuge has been limited to studies conducted under one particular gravity gradient [32], [35]–[42].

- Previous literature has shown that short-radius centrifugation combined with exercise may prevent physiological deconditioning in microgravity conditions [4], [36]–[41], [43], [44]. However, the optimal exercise protocol has not been defined yet. In particular, different exercise workload intensities and their effects on musculoskeletal and cardiovascular response need further investigation.

3.2 Thesis Aims

This thesis addresses these research gaps through a combination of analysis, modeling, simulation, and human subject experiments. The two aims of the thesis are:

1. To empirically investigate the effects of different artificial gravity and exercise workload levels on musculoskeletal and cardiovascular functions, as well as motion sickness and comfort. In particular, these are the specific objectives:

    1.1. To determine if AG ergometer exercise can produce higher foot forces than those measured under simulated 0-g conditions

    - *Hypothesis 1: Higher AG ergometer exercise levels in a compact-radius centrifuge increase foot forces*

1.2. To determine if AG ergometer exercise can produce higher cardiovascular responses than those measured under simulated 0-g conditions.

- *Hypothesis 2: Higher AG ergometer exercise levels in a compact-radius centrifuge increase overall cardiovascular activity*

1.3. To assess motion sickness and comfort.

- *Hypothesis 3: Higher AG ergometer exercise in a compact-radius centrifuge is well-tolerated and comfortable as ergometer exercise in simulated 0-g*

2. To develop a cardiovascular model to capture the effects of AG and ergometer exercise in a compact-radius centrifuge. In particular, these are the specific objectives:

2.1. To develop a computational model of the cardiovascular system that captures the short-term hemodynamic regulation during exercise in a high AG gradient environment such as a compact-radius centrifuge.

2.2. To evaluate the cardiovascular model with experimental measurements from 1-g adapted subjects using the MIT compact radius centrifuge.

2.3. To explore the cardiovascular model to identify the influence of the gravity level, the exercise workload, and the gravity gradient.

2.4. To simulate the cardiovascular effects of AG on 0-g adapted subjects.

Aims 1 and 2 will be addressed in Sections 4 and 5, respectively.

4 Experimental Approach – Physiological Responses under Artificial Gravity and Exercise

This experiment explores the effects of different levels of artificial gravity and exercise intensities on the cardiovascular system, musculoskeletal system, and motion sickness and comfort. The experiment was conducted at the Man Vehicle Laboratory (Massachusetts Institute of Technology) using a new configuration of the MIT Compact-Radius Centrifuge (CRC). The facility has undergone major upgrades, which were motivated by the 2011 Artificial Gravity with Ergometric Exercise (AGREE) project [66], in order to be compatible with a future use in the International Space Station (see Section 4.1.1). Twelve subjects participated in three experimental sessions scheduled in the morning of different days within the same week. During each session subjects performed the same exercise protocol (see Section 4.1.3) under one of the three different gravity levels tested: "No rotation" (or 0 G in the centripetal direction), 1 G, and 1.4 G's in the centripetal direction, measured at the feet. Foot forces, cardiovascular variables, and subjective data were gathered during the experimental sessions (see Section 4.1.5). Experimental results are summarized in Section 4.2.

4.1 Experimental Methods

4.1.1 The MIT Compact Radius Centrifuge

The MIT centrifuge facility has undergone major upgrades motivated by the 2011 Artificial Gravity with Ergometric Exercise (AGREE) project [66]. The AGREE project, no longer in development, proposed the assembly of a short-radius centrifuge in the Permanent Multipurpose Module (PMM) on-board the ISS in order to study the effectiveness of intermittent AG exposure in microgravity. Given the limited space inside the module, the AGREE centrifuge radius was limited to 1.4 meters, requiring the subject to be in seated position, with the interaural axis parallel to the axis of rotation, and the head slightly off-center. The AGREE centrifuge also included a cycle ergometer, as exercise during centrifugation decreases the chances of presyncope by increasing blood flow to the head via muscle contractions and an elevated heart rate. Exercise further enhances the overall conditioning resulting from AG exposure [38]. Figure 11 shows the proposed design in the PMM module.

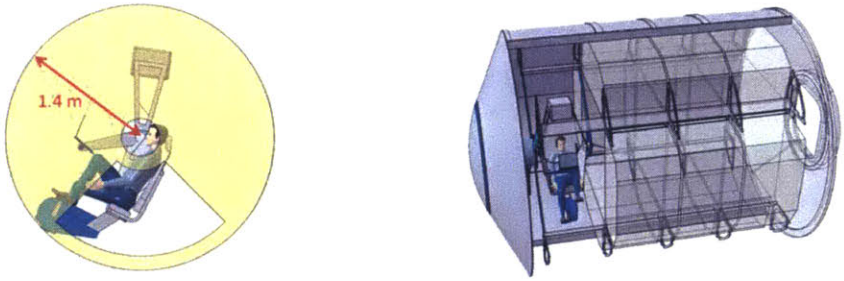

Figure 11 – AGREE centrifuge in the PMM [66].

Despite the cancelation of the project, AGREE provided important considerations and concerns for future inflight centrifuges. In particular, AGREE highlighted the fact that future centrifuges will most likely be constrained by space limitations, and therefore, subjects will be positioned in different configurations than they are in current centrifuges on Earth. AGREE highlighted the necessity to study these more compact configurations, particularly combined with exercise, in order to understand their effects on the physiological responses.

A compact-radius centrifuge (CRC) platform was designed and built on the centrifuge at the Massachusetts Institute of Technology (MIT), that complies with the AGREE criteria. A CRC is defined as a centrifuge with a radius of less than 1.95 meters [67], the height of the 99th percentile male astronaut as defined by NASA anthropometry standards [68]. Based on this definition, CRC's represent a class of centrifuges that cannot accommodate all subjects in a supine, radial position as is typically done in existing short-radius centrifuges (SRC's). Thus, the MIT centrifuge was constrained to a radius of 1.4 meters, the upper radial limit for a centrifuge to fit within an ISS module. In addition, an ergometer exercise device (Lode BV, Groningen, Netherlands) was also incorporated into the centrifuge and subjects can cycle at the same time as they are being centrifuged. This same exercise device is also being used on centrifuges at the Institute for Biomedical Problems (IBMP), the German Aerospace Center (DLR), and NASA Ames, opening the door to future research collaborations. The ergometer provides workloads up to 700 W and allows for exercise protocols to be preprogrammed in down to 1 W increments. The base on which the cycle ergometer is mounted has two possible adjustments, radial and tangential, to meet anthropomorphic differences. The ergometer can be exchanged with another exercise device, such as a stepper, or removed completely for exercise control runs. The Lode Angio ergometer includes the Lode Ergometry Manager (LEM) software package to control the ergometer from the on-board computer, allowing the experimenter to create custom exercise protocols, enter subject data, and save/export results for further analysis. Finally, the subject was positioned sidewise, facing "into the wind", to both reduce motion sickness and minimize potentially harmful knee lateral deflection due to Coriolis forces [22].

During the experimental sessions, subjects were positioned sidewise, with the head located near the center of rotation and the feet strapped on the ergometer device. The upper leg was suspended by adjustable leg cuffs to facilitate the exercise activity in a sideways position. They were secured with a three-point seat-belt, and a wireless camera mounted on the centrifuge monitored their facial expression for any signs of discomfort or presyncope. Figure 12 depicts the subject positioning on the final MIT CRC platform design.

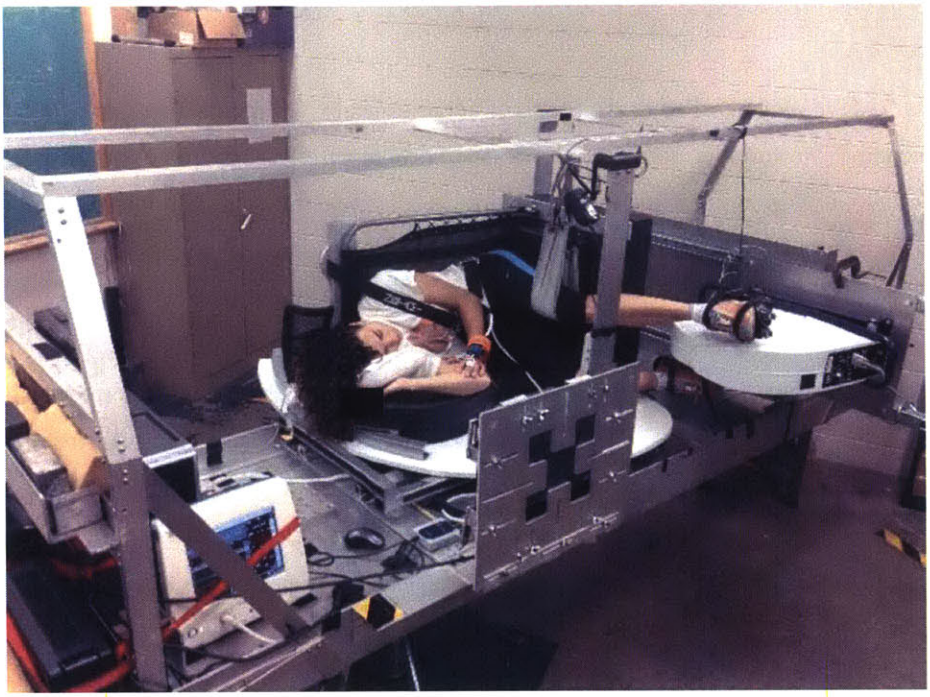

Figure 12 – Subject positioning on the MIT CRC platform.

4.1.2 Artificial Gravity Profile

At the beginning of each experimental session and once the subjects were positioned on the centrifuge, a wait time of 3 minutes was provided to allow the subjects to relax before the experiments, and to capture their initial physiological state before any stimuli .The centrifuge was then slowly spun up to the desired AG level over a time course of approximately 100 seconds. The centripetal G-levels studied were 0 (no rotation), 1, and 1.4 G's at the subject's feet level. The maximum artificial gravity value was limited by both the maximum angular velocity of the centrifuge as well as the radius constraint of 1.4 m. The required angular velocities to obtain the desired AG levels are given in Table 5. Rotation rate values varied slightly between subjects, since they depended on the centrifuge adjustments based on each subject's anthropometry, particularly on the location of the feet with respect to the center of rotation.

Table 5 – Centrifuge rotation rates for testing G-levels.

Gravity Level at the feet	Centrifuge rotation rate
0G Centripetal	0 RPM
1G Centripetal	28.6 RPM
1.4G Centripetal	33.9 RPM

Once the final G-level was reached, a wait time of approximately 100 seconds was provided to allow the subjects to become comfortable in the new gravity environment. Then, subjects completed a 15-minute exercise protocol while spinning using the ergometer device on-board. Once completed, another wait time of 2 minutes was provided to allow the subjects to recuperate from the exercise. Then, the centrifuge was spun-down over approximately 60 seconds. The shorter duration of the spin-down process is related to the capabilities of the MIT centrifuge motor. Subjects did not report motion sickness symptoms during this spin-down period. Completion of the entire protocol, including spin-up, exercise period, spin-down, and the various wait times lasted 25 minutes. Figure 13 shows an example of the centripetal acceleration profile during one experimental session at 1G. The accelerometer was located at ~ 1.2 m from the center of rotation, slightly further away than the subjects' feet (which were located at ~1.09 m from the center of rotation), and therefore the recorded acceleration is larger than the expected 9.8 m/s^2 at 1G. After each testing session, subjects were removed from the centrifuge and kept under observation for at least 10 minutes.

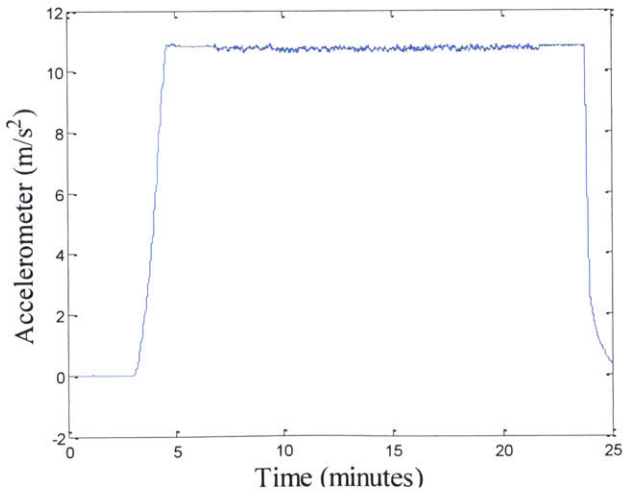

Figure 13 – Example Centripetal Acceleration Profile.

4.1.3 Exercise Protocol

The exercise protocol consisted of 15 minutes of ergometer exercise at three different workload levels:

- The first workload level was set to 25W. This is a low intensity exercise and was included to serve as a warm-up phase. Its duration was 3 minutes
- The second workload level was set to 50W. It corresponds to a moderate exercise intensity, and its duration was 5 minutes.
- The third and last workload level was set to 100W. This is considered as vigorous and high intensity exercise. Its duration was 5 minutes.

The workload levels were able to capture a good range of physiological states without reaching exhaustion. Workload changes between the workload levels were implemented gradually and smoothly. As already mentioned, extra time at the beginning and at the end was allotted to the spin-up and spin-down process to the desired level of artificial gravity. The entire protocol lasted 25 minutes, and is summarized in Figure 14. It was created using the Lode Ergometry Manager (LEM) software package and it was run automatically during the experiments. In addition, subjects were instructed to pedal at 60 RPM to get more homogeneous measurements across subjects and avoid additional confounding factors. In addition, the pedal cadence was also important for modeling purposes. This particular rhythm was maintained using a metronome.

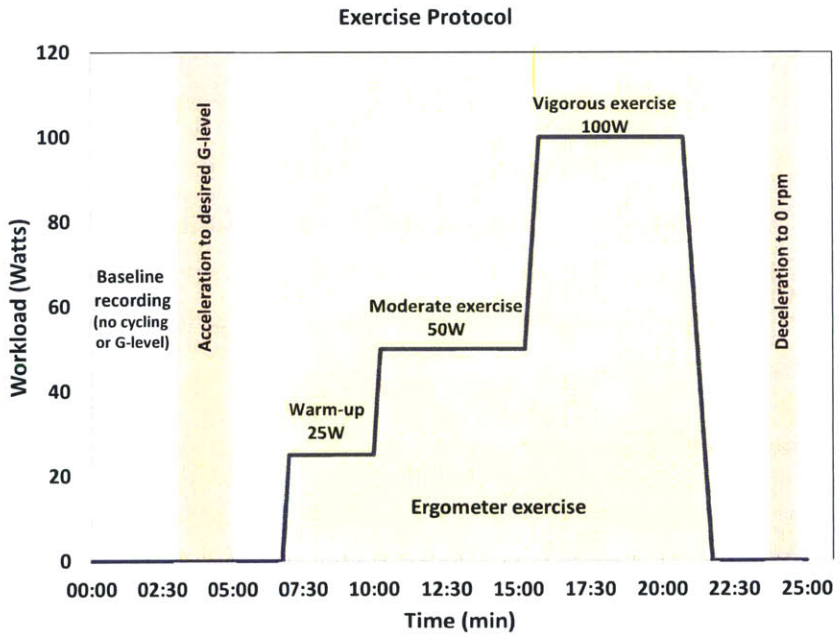

Figure 14 – Exercise Protocol.

4.1.4 Independent Variables

In each session, subjects followed the exercise protocol previously described at one specific gravity level. The gravity levels tested were "No centripetal" (0g or no rotation), 1 and 1.4 G's, measured at the feet. All subjects experienced all three conditions, and assignments were randomized across all subjects (see Table 6 below). Each AG level was tested in a different day of the same calendar week. In addition, all three centrifuge tests were scheduled in the morning, and the subjects were instructed not to drink caffeine or do exercise prior to the test.

Table 6 – Randomization of AG levels across subjects.

Subject ID	1st Session AG (g)	2nd Session AG (g)	3rd Session AG (g)
1	1.4	1	0
2	1	0	1.4
3	0	1	1.4
4	0	1.4	1
5	1.4	0	1
6	1	1.4	0
7	1	1.4	0
8	1	0	1.4
9	0	1.4	1
10	0	1	1.4
11	1.4	1	0
12	1.4	0	1

The exercise protocol involved three different workload intensities (25W, 50W, and 100W), and they were presented in the same order in every session (from warm-up to vigorous) in order to avoid potential injuries. Workload levels were chosen because they were able to capture a good range of physiological states without reaching exhaustion.

4.1.5 Dependent Variables

Foot force data were collected during the experiment using force plates mounted on the pedals (force range: -200N to +850N, where a positive value is a compression force; resolution: 0.3N; Vernier Software & Technology).

Cardiovascular variables were continuously recorded using the Nexfin monitor (BMEYE B.V. Amsterdam, the Netherlands). This non-invasive advance hemodynamic system monitored beat-to-beat cardiovascular parameters derived from the arterial pressure waveform. A finger cuff was used to continuously monitor changes in finger arterial volume using photo-plethysmography techniques [69], [70] (see Appendix A for details about the Nexfin system operation). Subjects were instructed to keep his/her hand at the heart level to avoid changes in blood pressure readings due to hydrostatic effects caused by the strong gravity gradient. Figure 12 shows the positioning held by subjects during the centrifuge experiments. The Nexfin monitor can be appreciated at the bottom left of the figure, as well as the subject's hand positioned at the heart level. Cardiovascular recordings included heart rate (HR), systolic (SBP), diastolic (DBP), and mean blood pressure (MBP), stroke volume (SV), cardiac output (CO), systemic vascular resistance (SVR), and pulse pressure (PP).

In addition, subjective data concerning motion sickness and comfort were also collected via an exit-survey. The questionnaire included 5–point Likert scales to get subjective data about comfort and difficulty of the exercise. Subjects also rated their overall motion sickness experience on a 0–10 scale (0 – no symptoms, 10 – vomiting). Finally, subjects also reported on their body soreness and their perception of the Coriolis forces.

4.1.6 Experimental Design

The experimental design was within-subjects and complete, such that every subject experienced all the combinations of AG level and exercise workload. A within-subjects design not only avoided potential existing differences between subjects, but also allowed for fewer total subjects. The complete design is critical to study interactions between independent variables. Table 7 summarizes the experimental design.

Table 7 – Summary of the experiment design.

Independent variables	Treatment Levels		
AG-Level (feet level)	0 G Centripetal	1 G Centripetal	1.4 G Centripetal
Exercise workload	25 W	50W	100 W
Dependent Variables			
Musculoskeletal: Foot Forces			
Cardiovascular monitoring: HR, CO, SBP, DBP, MBP, SV, SVR, PP			
Motion sickness and comfort: exit survey			

4.1.7 Subjects, Study Approval, and Statistical Significance

Participants were 12 healthy subjects (6 males and 6 females), between 23 and 29 years old (25.1 ± 2.1 years old; all values are presented as the average ± standard deviation). They had a good fitness level and had no known cardiovascular defects or conditions. Those selected exercised regularly and were able to perform aerobic exercise comfortably for an hour. Due to centrifuge structural limitations, maximum weight was restricted to 200 lb (90.7 Kg). Average weight and standard deviation were: 69.3 ± 11.6 Kg. Screening for recent injuries, recurrent pain or back problems, and severe motion sickness was also performed. Before participating, each subject provided written informed consent previously approved by the MIT Committee on the Use of Humans as Experimental Subjects. Statistical tests were performed using SYSTAT 13 Version 13.00.05 (SYSTAT Software Inc.2009). The level of significance was set to $\alpha = 0.05$.

4.2 Experiment Results

4.2.1 Musculoskeletal Results

Foot forces changed accordingly to the exercise workload level, as can be seen in Figure 15, Figure 16, and Figure 17. These figures depict the foot forces from one particular subject, recorded during the 25-min exercise protocol during each one of the three AG condition. In addition, the increase in foot forces due to the increase in artificial gravity during the spin-up process was highly noticeable (starting at Time = 3 minutes), both in the 1 G and 1.4 G condition. It was larger at higher spin-up rates. Likewise, the decrease in foot forces due to the spin-down process at the end of the protocol was also observed.

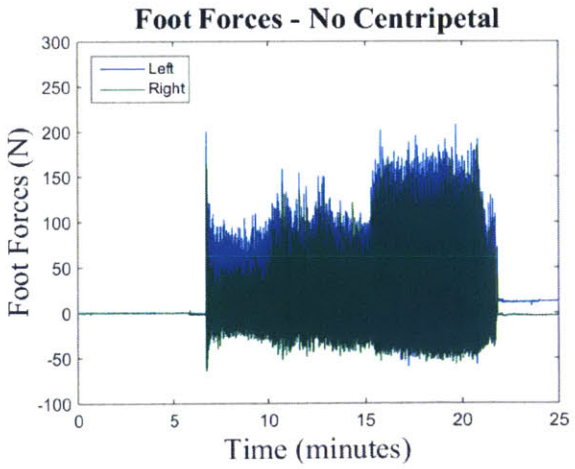

Figure 15 – Example of foot forces recorded from one subject during the 25-min ergometric exercise protocol in the "No centripetal" (no rotation) condition.

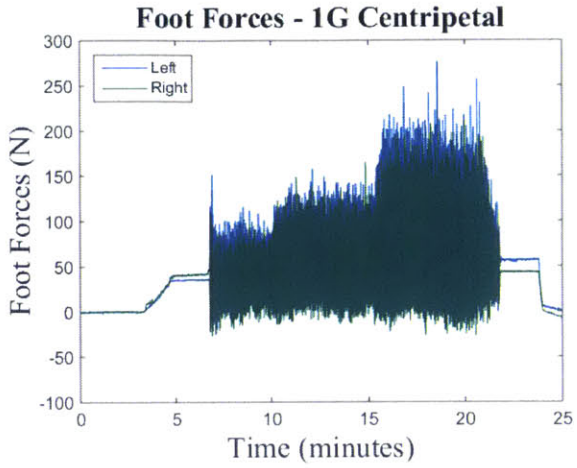

Figure 16 – Example of foot forces recorded from one subject during the 25-min ergometric exercise protocol in the 1 G condition.

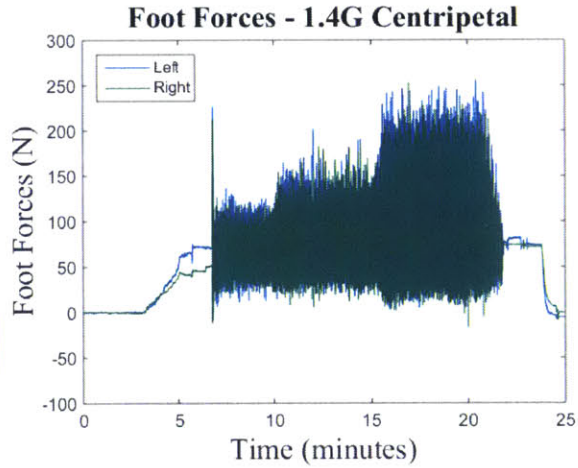

Figure 17 – Example of foot forces recorded from one subject during the 25-min ergometric exercise protocol in the 1.4 G condition.

Average peak forces values for the left and right foot were extracted from the experimental data. During each workload period, these values were calculated from all the peak forces generated during that period (excluding the transitions between periods). Figure 18 shows an example of the methodology to calculate the average peak forces exerted by the left foot during each exercise period at the 'No Centripetal" condition. Triangles identify all peaks generated during a particular period and the horizontal lines indicate the averaged value of those peaks.

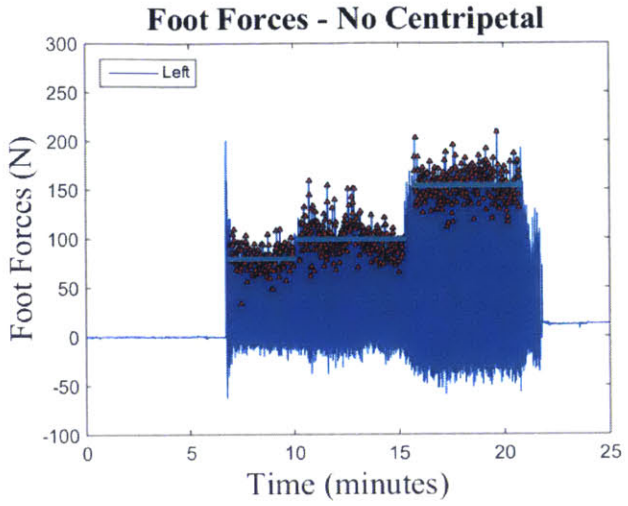

Figure 18 – Example of the methodology to calculate the average peak forces exerted by the left foot during each exercise period at the 0 G condition.

To continue with the example, in Figure 19, Figure 20 and Figure 21, peak force data during each one of the three workload conditions is presented as the average and standard deviation of those peaks, for each one of the three AG conditions ("No centripetal", "1G Centripetal", "1.4G Centripetal") respectively.

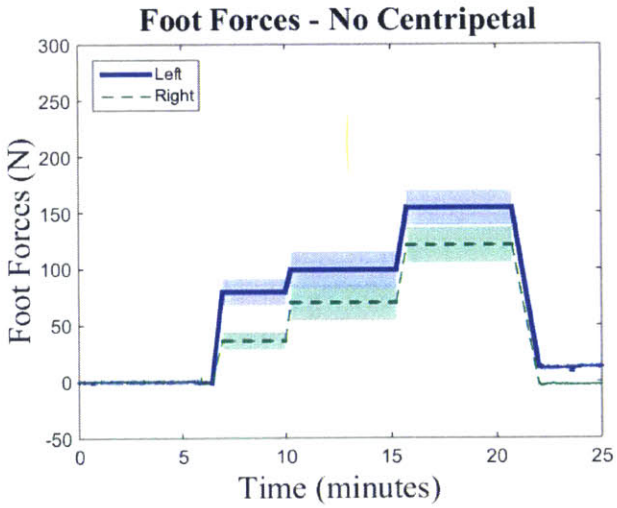

Figure 19 – Foot forces (average ± SD) from one subject during the 25-min ergometric exercise protocol in the "No Centripetal" condition.

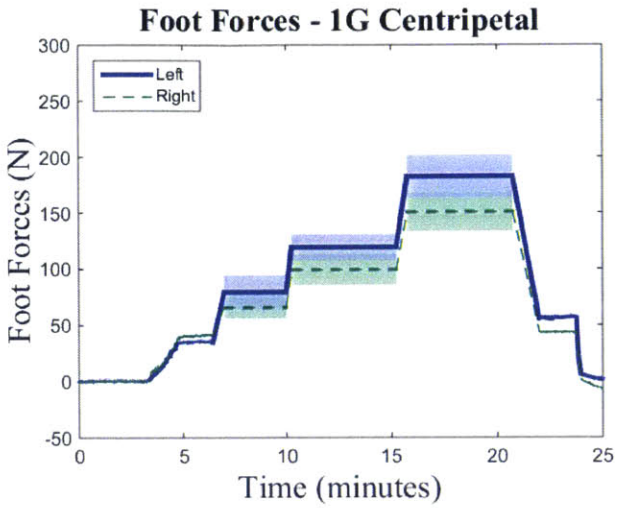

Figure 20 – Foot forces (average ± SD) from one subject during the 25-min ergometric exercise protocol in the "1G Centripetal" condition.

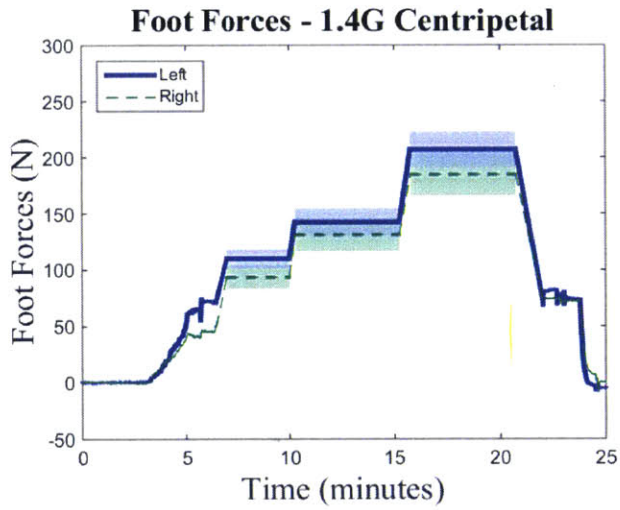

Figure 21 – Foot forces (average ± SD) from one subject during the 25-min ergometric exercise protocol in the "1.4G Centripetal" condition.

Finally, combining all subjects, average peak forces values for the left and right foot are summarized in Table 8 and Table 9 respectively (see Appendix A for foot forces data analysis). For two subjects, right foot force data were not available and therefore, these two subjects have been excluded from the right foot data analysis.

Table 8 – Left foot forces (N) average and standard deviation of the 12 subjects for each workload intensity and AG condition.

	Workload intensity		
AG level	25W	50W	100W
No Centripetal	65.6±12.4	90.9±15.6	154.8±22.1
1G Centripetal	89.9±14.5	127.0±17.4	189.6±13.1
1.4G Centripetal	108.0±10.4	150.5±14.8	211.4±14.9

Table 9 – Right foot forces (N) average and standard deviation of the 10 subjects for each workload intensity and AG condition.

	Workload intensity		
AG level	25W	50W	100W
No Centripetal	46.0±5.8	74.3±6.6	122.3±15.8
1G Centripetal	71.6±10.5	100.6±9.0	157.8±11.8
1.4G Centripetal	88.1±11.5	130.9±10.7	181.6±14.5

4.2.1.1 Left Foot Forces

A two-way repeated measures ANOVA showed that there was a significant effect of workload intensity on average left peak forces ($F(2,22)=1176.2$, $p < 0.0005$). Pairwise comparisons showed significant differences between the three workload conditions: "25W" and "50W" ($p<0.0005$); "25W" and "100W" ($p<0.0005$); and "50W" and "100W" ($p<0.0005$).

More interestingly, results also indicate that an increase in AG level significantly increased the left foot average peak forces ($F(2,22)=97.0$, $p < 0.0005$). Pairwise comparisons showed a significant increase in peak forces between "No Centripetal" and "1G Centripetal" ($p < 0.0005$), "No Centripetal" and "1.4G Centripetal" ($p < 0.0005$), "1G Centripetal" and "1.4G Centripetal" ($p < 0.0005$). Experimental data are shown in Figure 22.

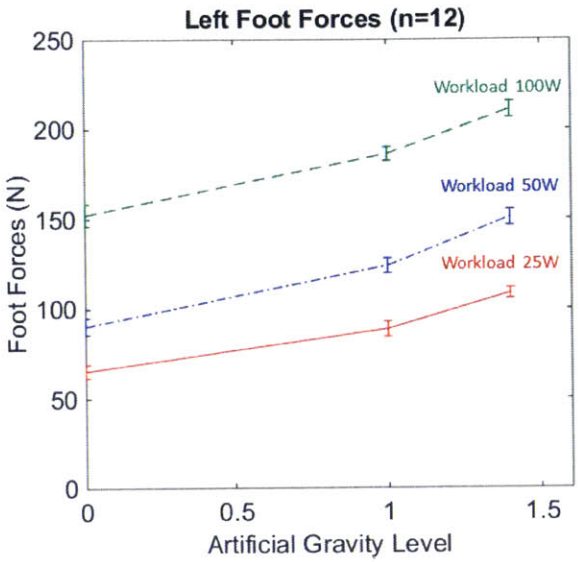

Figure 22 – Left foot forces across all conditions (error bars correspond to Standard Error).

Finally, a hierarchical regression model was fit with subject as the identifier, the average left foot forces as the dependent variable, and AG level and workload intensity as the independent variables.

$$(\mathrm{LFF})_{ij} = \rho_i + \beta_1(\mathrm{AG}) + \beta_2(\mathrm{Workload}) + \epsilon_{ij} \quad (4)$$

The left foot forces (LFF, in Newton) from the j^{th} measurements in the i^{th} subject are a function of the AG term (No Centripetal, 1G Centripetal, or 1.4G Centripetal), and the workload intensity in Watts (25W, 50W, and 100W). The model also includes subject-dependent intercepts (ρ_i, where i=1-12 subjects). AG level was statistically significant (β_1 =24.9, Z(94) =18.2 $p < 0.0005$) as well as workload intensity (β_2 =0.8, Z(94) =31.6, $p < 0.0005$). The interaction term was non-significant. The positive β coefficients support the hypothesis that higher AG and workload levels result in higher foot forces. The coefficients from the model fit are summarized in Table 10.

Table 10 – Results for the left foot forces hierarchical regression model.

Coefficients	Units	Estimate	SE	Z value	P-value
ρ_i	N	-13.1	2.7	-4.9	<0.0005
β_1	N/g	24.9	1.4	18.2	<0.0005
β_2	s/m	0.8	0.03	31.6	<0.0005

4.2.1.2 Right Foot Forces

The analysis of the average right foot peak forces yielded similar results. Statistical analysis revealed a significant effect of workload intensity ($F(2,18)=677.2$, $p < 0.001$) and artificial gravity level ($F(2,18)=87.8$, $p < 0.001$). In the same way as in the case of left foot forces, pairwise comparisons showed significant differences among the three workload conditions: "25W" and "50W" ($p<0.001$); "25W" and "100W" ($p<0.001$); and "50W" and "100W" ($p<0.001$). Similarly, pairwise comparisons showed a significant increase in right foot peak forces between "No Centripetal" and "1G Centripetal" ($p < 0.001$), "No Centripetal" and "1.4G Centripetal" ($p < 0.001$), "1G Centripetal" and "1.4G Centripetal" ($p = 0.001$). Experimental data are shown in Figure 23.

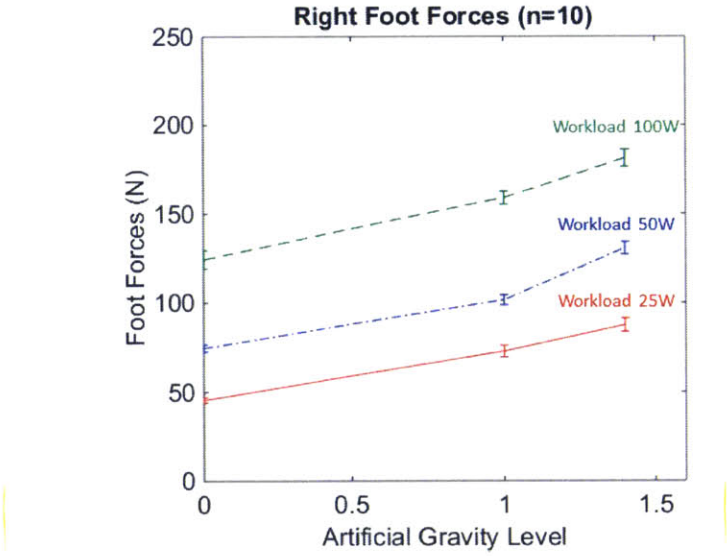

Figure 23 – Right foot forces across all conditions (error bars correspond to standard error).

As in the left foot forces analysis, a hierarchical regression model was fit with subject as the identifier, the average right foot forces as the dependent variable, and AG level and workload intensity as the independent variables. In the same manner, AG level was statistically significant ($\gamma_1 = 35.5$, $Z(84) = 17.3$, $p < 0.0005$) as well as the workload intensity ($\gamma_2 = 1.1$, $Z(84) = 28.7$, $p < 0.0005$. The interaction term was non-significant.

Table 11 summarizes the results of the model fit. .

$$(\mathrm{RFF})_{ij} = \rho_i + \gamma_1(\mathrm{AG}) + \gamma_2(\mathrm{Workload}) + \epsilon_{ij} \quad (5)$$

Table 11 – Results for the right foot forces hierarchical regression model.

Coefficients	Units	Estimate	SE	Z value	P-value
ρ_i	N	14.3	3.1	4.7	<0.0005
γ_1	N/g	35.5	2.0	17.3	<0.0005
γ_2	s/m	1.1	0.03	28.7	<0.0005

Another interesting observation is that right foot forces were generally smaller than left foot forces. On average, the difference between left and right foot forces was 21.5 ± 3.5 N. A paired t-test showed that this difference is statistically significant ($t(95) = 12.140$, p-value < 0.0005). This result could be explained by the sideway position of the subjects during the ergometer exercise. The right leg was partially supporting the body weight, and therefore its movement was more restricted. In addition, the larger surface area of contact likely resulted in higher friction. The left leg was supported by leg cuffs, having a better range of motion. This effect was unnoticeable to subjects and none of them reported any difference in pedaling between legs, either intentional or unintentional.

4.2.2 Cardiovascular Results

An example of blood pressure waveforms gathered from one subject during the three experimental session is shown in Figure 24. From these waveforms, the Nexfin monitor derived the rest of the beat-to-beat hemodynamic parameters analyzed in this work: heart rate (HR), systolic (SBP), diastolic (DBP), and mean blood pressure (MBP), stroke volume (SV), cardiac output (CO), systemic vascular resistance (SVR), and pulse pressure (PP). Raw signals were filtered using a low-pass Butterworth filter, both in forward and reverse directions (see Appendix B for details in data analysis).

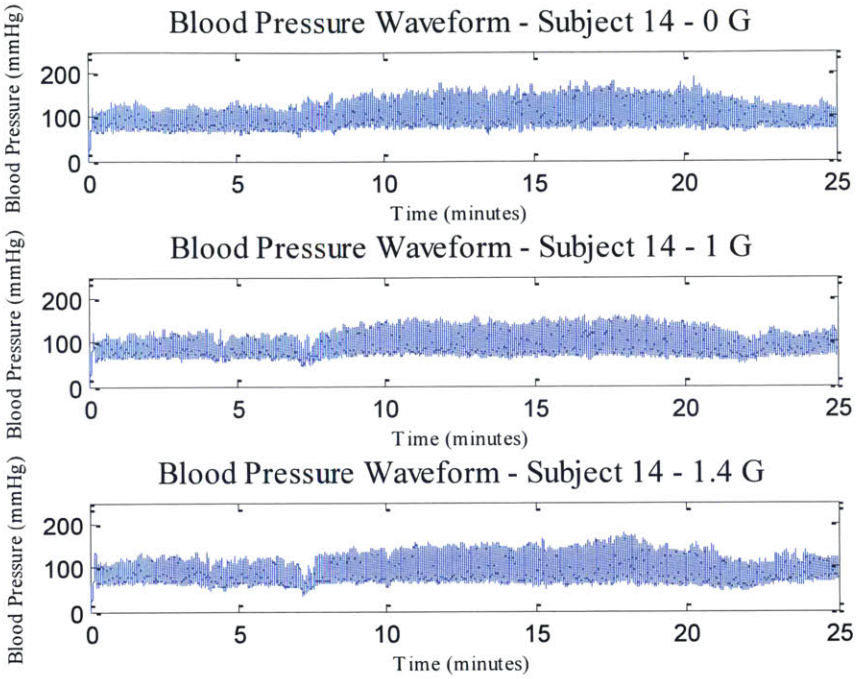

Figure 24 – Example of blood pressure waveform data measured with the Nexfin system from one subject.

Cardiovascular variables gathered during the centrifuge runs are shown from Figure 25 to Figure 32. Each figure contains three cardiovascular responses corresponding to the three AG level experienced: "No Centripetal" (red line), "1G Centripetal" (blue line), and "1.4G Centripetal" (green line). Gravity levels were measured at the feet. In addition, the spin-up phase (starting at Time = 3 min) and spin-down phase (starting at Time = 23:45 min), as well as the exercise phase (from Time = 6:45 min, to Time = 21:45 min) are also indicated in all figures.

4.2.2.1 Spin-up phase

During the spin-up phase, the artificial gravity force created by centrifugation started pulling the blood to the lower part of the body. Initially, this caused a slight decrease in blood pressure that can be appreciated in both **systolic and diastolic blood pressure** (Figure 26 and Figure 27 respectively). Therefore, it caused a decrease in **mean blood pressure** (see Figure 25), which is approximately MBP = DBP +1/3(SBP−DBP). This reduction was higher at the higher AG level ("1.4G Centripetal"), and was non-existent when the subject was not being centrifuged ("No Centripetal"). **Pulse pressure** (defined as PP = SBP – DBP) and **stroke volume** also showed a transient reduction that can be appreciated in Figure 28 and Figure 29 respectively.

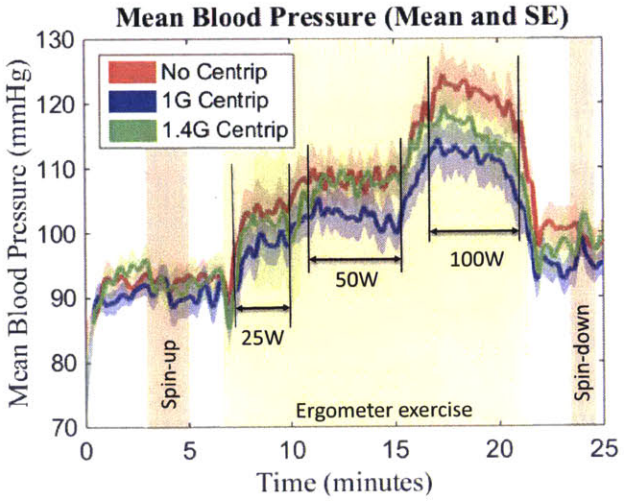

Figure 25 – Mean blood pressure from 12 subjects (Mean ± SE) during the 25-min protocol.

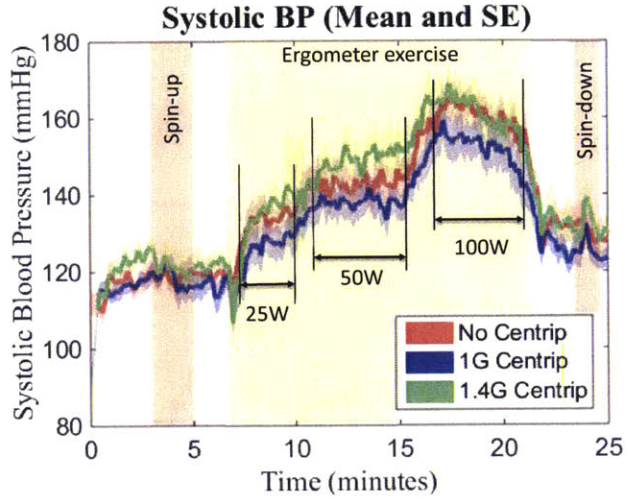

Figure 26 – Systolic blood pressure from 12 subjects (Mean ± SE) during the 25-min protocol.

When there is a significant blood pressure drop, the autonomic nervous system increases sympathetic stimulation triggered by the arterial baroreceptors, which are stretch receptors located in the carotid sinus and the aortic arch areas. The baroreceptors are the primary receptors for short-term control of the cardiovascular system. Consequences include an increase in heart rate and contractility of the heart to maintain the appropriate amount of blood flow to all the organs, in particular the brain (CO = SV×HR). In this experiment, a clear increase in heart rate can be observed during the spin-up phase at 1G and 1.4G, being more stable in the 1.4G condition (particularly between T = 5 min and T = 6:45 min), due to the cardiovascular response to a higher artificial gravity environment (see Figure 31).

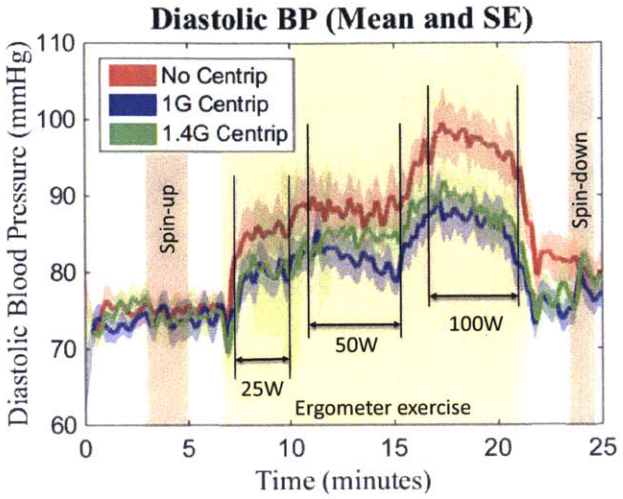

Figure 27 – Diastolic blood pressure from 12 subjects (Mean ± SE) during the 25-min protocol.

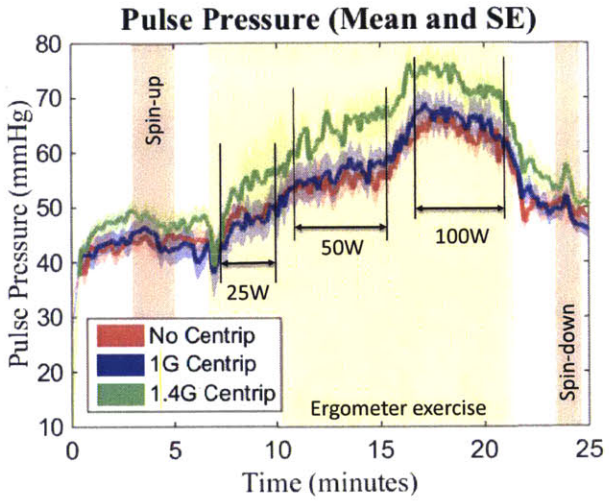

Figure 28 – Pulse pressure from 12 subjects (Mean ± SE) during the 25-min protocol.

As a consequence of the sympathetic stimulation, cardiac output did not decrease during the spin-up phase. On the contrary, it even showed a slight increase during this initial and very dynamic phase. (Figure 30). Other factors to take into account when interpreting cardiac output data include the enhancement of venous return caused by leg muscle activation due to the increase in foot forces during spin-up phase. As already mentioned in Section 4.2.1, foot forces increased during the spin-up phase and subjects responded by positioning themselves comfortably on the centrifuge chair and pressing against the pedals to counteract the effects of centrifugation. Again, cardiac output presented the largest responses at the highest G level, and as expected, no response was observed at the "No Centripetal" condition.

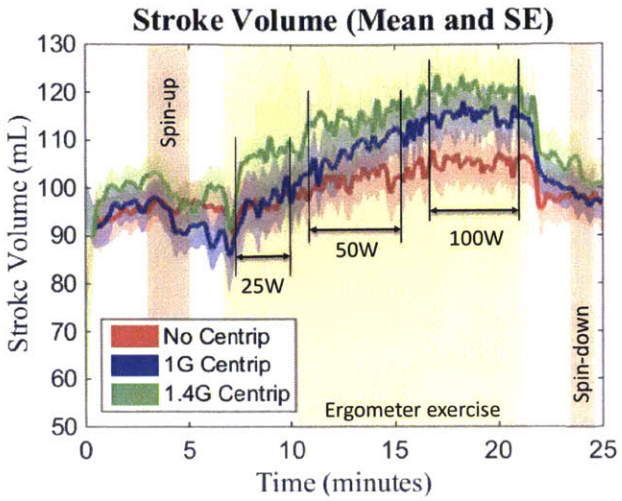

Figure 29 – Stroke Volume from 12 subjects (Mean ± SE) during the 25-min protocol.

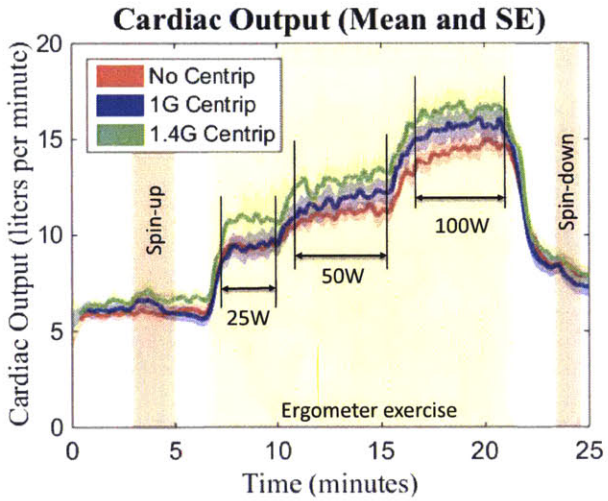

Figure 30 – Cardiac Output from 12 subjects (Mean ± SE) during the 25-min protocol.

Finally, at the beginning of the spin-up process, vascular resistance decreased slightly due to the blood pulling to the lower part of the body. After several seconds, the baroreceptor signal activated the sympathetic stimulation and the vascular resistance slowly increased. As expected, a larger drop was seen at 1.4G, and no changes were observed during the "No centripetal" condition (see Figure 32).

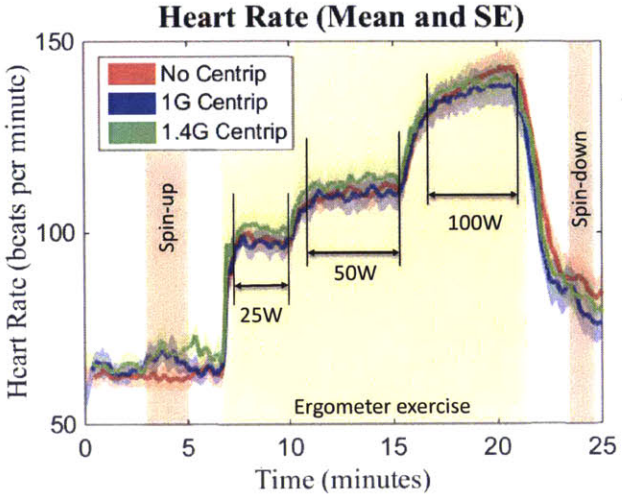

Figure 31 – Heart rate from 12 subjects (Mean ± SE) during the 25-min protocol.

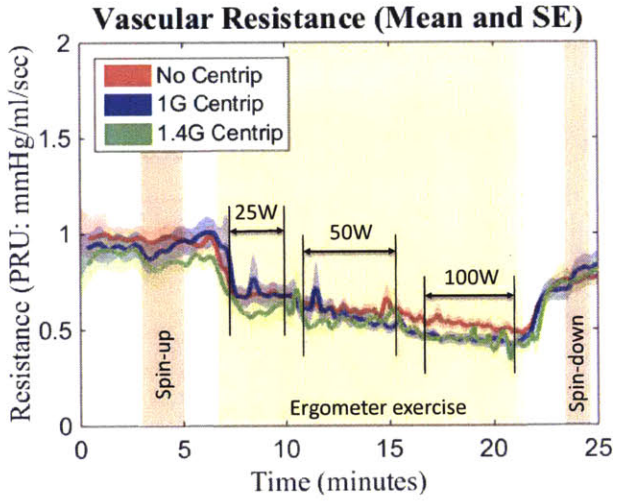

Figure 32 – Peripheral vascular resistance from 12 subjects (Mean ± SE) during the 25-min protocol.

4.2.2.2 Exercise Phase

Important physiologic changes occurred during exercise. The significant metabolic demand at the onset of exercise caused the blood pressure to suddenly decrease, causing the **stroke volume** to be reduced immediately, particularly at the most demanding 1.4G condition (see Figure 29). As expected, the **heart rate** increased rapidly at the beginning of the exercise phase (see Figure 31). In addition, the heart rate experienced significant increases right after every exercise workload transition (from 25W to 50 W at T = 10min, and from 50W to 100W at T=15:15 min). These transitions were also observed across all

cardiovascular variables, particularly **cardiac output** (Figure 30) and **all blood pressures** (Figure 25, Figure 26, Figure 27, and Figure 28).

Mean blood pressure also increased during exercise, particularly in the "0G Centripetal" condition, as can be appreciated in Figure 25. In this condition, the subject was not being centrifuged and therefore, there was not artificial gravity to pull blood towards his/her legs. Interestingly, blood pressure at "1.4G Centripetal" seemed generally higher than blood pressure at "1G.Centripetal". This behavior could be explained by the fact that at higher AG level ("1.4 Centripetal"), and despite the stronger blood pulling to the lower extremities, the venous return was facilitated during exercise due to the higher foot forces exerted on the ergometer. Therefore, this exercise effect, combined with the higher sympathetic activity, caused the **systolic blood pressure** to be maintained (or even to slightly increase) with respect to the "No Centripetal" case (Figure 26). On the other hand, **diastolic blood pressure** decreased in the presence of centrifugation driven by AG pulling blood to the lower body. As a result, **pulse pressure** increased with artificial gravity level during ergometer exercise, presenting larger values at higher G levels (see statistical analysis in Section 4.2.2.4). Pulse pressure recordings at "1G Centripetal" and "No Centripetal" did not differ as much compared to the "1.4G Centripetal" data, but a slight difference can still be appreciated between the two conditions (see Figure 28).

Stroke volume and **cardiac output** also increased according to exercise workload level, particularly cardiac output in which the three exercise phases can be clearly distinguished (Figure 30). Results indicate that these variables also increased with the artificial gravity level during the ergometer exercise (see statistical analysis in Section 4.2.2.4). Thus, in the "1.4G Centripetal" condition, stroke volume and cardiac output showed the largest changes across all exercise intensities. Moreover, results indicate that heart rate did not change between artificial gravity conditions and therefore, changes in cardiac output at different gravity levels were driven by changes in stroke volume.

Exercise increases muscle metabolism and, even though the level of sympathetic stimulation is high, vascular smooth muscle in the exercise muscles dilates to satisfy increasing metabolic demand. This process is called autoregulation. According to this mechanism, in this experiment the **vascular resistance** decreased during the exercise protocol, as seen in Figure 32. In particular, significant drops can be observed in the "1.4G Centripetal" condition at the beginning of the 25W and 50W exercise phases. After these initial drops, the resistance seemed to level-off, presumably due to an increase in sympathetic activity, reaching the steady decrease slope due to muscle dilation. Resistance seemed to be lower at higher AG levels to facilitate a higher blood flow during the more intense exercise caused by the higher centrifugal acceleration. During the exercise phase at 100W, the vascular resistances at "1G centripetal"

and "1.4G Centripetal" seemed to overlap and level off, probably indicating that maximal muscle dilation has been reached.

4.2.2.3 Post - Exercise and Spin-Down Phase

The exercise phase ended after one minute of ramp down from 100W to 0W (from T=20:45 min to T=21:45 min). During this one-minute period, subjects started recovering from the strenuous exercise and all cardiovascular variables slowly started to come back to their original values. In general, spin-down responses (starting at T = 23.45 min) were opposite to the spin-up responses, although a more exhaustive experiment and analysis should be performed to fully capture proper physiological responses during spin-down. The focus of the experiment presented in this work is not the post-exercise and spin-down phase, and both of these factors are certainly confounded in the results, since both phases are very close together due to time and protocol constraints on the centrifuge.

4.2.2.4 Statistical Analysis

In order to perform the statistical analysis, each one of the cardiovascular variables was averaged within the last two minutes of each workload phase. Therefore, three values were calculated for each CV variable, per subject, corresponding to workload at 25W, at 50W, and at 100W.

Results indicate that workload intensity had a significant effect in all variables. In addition, both workload intensity and AG level had significant effects in **cardiac output**, **stroke volume**, and **pulse pressure**. Hierarchical regression models were fitted to these variables, using subjects as identifiers to take into account the within-subjects design (ρ_i, where i=1-12 subjects), and AG level and workload intensity as the independent variables. Data were tested for homoscedasticity using the Levene's test, and for normality using the Kolmogorov-Smirnov test. In all cases, significance was taken at the $\alpha = 0.05$ level. The general formulation of the model follows the next equation:

$$(\text{CV Variable})_{ij} = \rho_i + \alpha_1(\text{AG}) + \alpha_2(\text{Workload}) + \epsilon_{ij} \quad (6)$$

In this equation, ρ_i is the intercept for subjects i = 1-12, AG level and workload intensity are the independent variables, and the CV variable is the dependent variable.

4.2.2.4.1 Cardiac output

The cardiac output (in l/min) from the j^{th} measurements in the i^{th} subject is a function of the AG term (0G Centripetal, 1G Centripetal, or 1.4G Centripetal), and the workload intensity in Watts (25W, 50W, and 100W). AG level was statistically significant ($\alpha_1 = 1.2$, Z(94) =13.1, $p < 0.0005$) as well as workload

intensity ($\alpha_2 = 0.07$, Z(94) =19.4, $p < 0.0005$). The interaction term was non-significant. The positive α coefficients support the hypothesis that higher AG and workload levels result in higher cardiac output. The coefficients from the model fit are summarized in Table 12, and experimental data are shown in Figure 33.

Table 12 – Results for the cardiac output hierarchical regression model.

Coefficients	Units	Estimate	SE	Z value	P-value
ρ_i	l/min	7.2	0.6	13.1	<0.0005
α_1	l/min/g	1.2	0.2	6.1	<0.0005
α_2	l/min/W	0.07	0.004	19.4	<0.0005

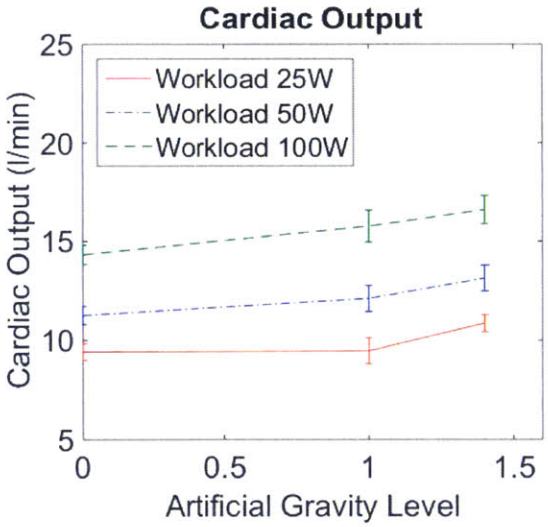

Figure 33 – Cardiac Output across all conditions (error bars correspond to standard error).

4.2.2.4.2 Stroke Volume

Similarly, stroke volume (in ml) from the j^{th} measurements in the i^{th} subject is a function of the AG term (0G Centripetal, 1G Centripetal, or 1.4G Centripetal), and the workload intensity in Watts (25W, 50W, and 100W). AG had a significant effect on stroke volume ($\alpha_1 = 9.1$, Z(94) =5.7, $p < 0.0005$), as well as workload intensity ($\alpha_2 = 0.14$, Z(94) =4.7, $p < 0.0005$). The interaction term was non-significant. The α coefficients are again positive, indicating that stroke volume increases with higher AG levels and

workload intensities. The coefficients from the model fit are summarized in Table 13, and experimental data are shown in Figure 34.

Table 13 – Results for the stroke volume hierarchical regression model.

Coefficients	Units	Estimate	SE	Z value	P-value
ρ_i	ml	92.2	5.0	18.6	<0.0005
α_1	ml/g	9.1	1.6	5.7	<0.0005
α_2	ml/W	0.14	0.03	4.7	<0.0005

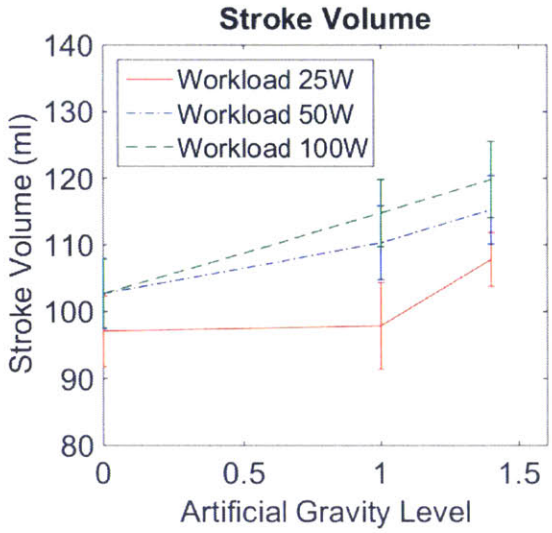

Figure 34 – Stroke Volume across all conditions (error bars correspond to standard error).

4.2.2.4.3 Pulse pressure

Finally, pulse pressure (in mmHg) from the j^{th} measurements in the i^{th} subject is a function of the AG term (0G Centripetal, 1G Centripetal, or 1.4G Centripetal), and the workload intensity in Watts (25W, 50W, and 100W). AG level was statistically significant ($\alpha_1 = 5.3$, Z(94) =3.7, $p < 0.0005$) as well as workload intensity ($\alpha_2 = 0.2$, Z(94) =7.3, $p < 0.0005$). The interaction term was non-significant. Once more, both α coefficients are positive, supporting the hypothesis that higher AG and workload levels result in higher pulse pressure. The coefficients from the model fit are summarized in Table 14, and experimental data are shown in Figure 35.

Table 14 – Results for the pulse pressure hierarchical regression model.

Coefficients	Units	Estimate	SE	Z value	P-value
ρ_i	mmHg	43.2	2.3	18.6	<0.0005
α_1	mmHg/g	5.3	1.4	3.7	<0.0005
α_2	mmHg/W	0.2	0.03	7.3	<0.0005

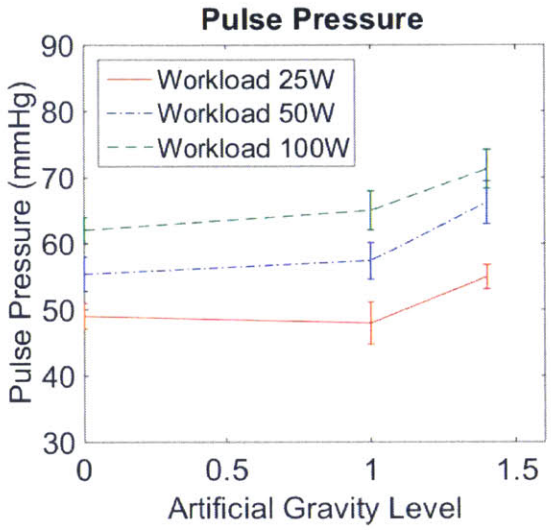

Figure 35 – Pulse Pressure across all conditions (error bars correspond to standard error).

4.2.3 Motion Sickness and Comfort Results

Subjects were generally comfortable and were able to complete the three-session experiment. Subjects reported no soreness other than normal exercise fatigue on the spinning centrifuge. None of the subjects reported an overall motion sickness rating higher than 1 in a 0-10 scale (see Table 15). Those subjects who had slight symptoms (motion sickness rating = 1) reported that they voluntarily moved their head, mostly to position themselves more comfortably on the chair. The spin-down process was also reported as a potential source of motion sickness. Finally, subjects did not notice the Coriolis forces on their knees acting in the lateral direction. These results were expected due to the sideways positioning of the subjects while cycling [43].

Table 15 – Motion Sickness Symptom Scale.

Rating	Motion Sickness Symptoms
0	No symptoms
1	Any symptom no matter how slight
2	Minimal warmth, fatigue
5	Stomach awareness
7	Moderate nausea
9	Incipient vomiting
10	Vomiting

Subjective data concerning the perceived "comfort" and "strenuousness" (or difficulty of exercise) during the experiment is summarized in Table 16. Data was collected using 5–point Likert scales, both for "comfort" (1 – very comfortable / natural, 5 – very uncomfortable / unnatural), and "strenuousness" (1 – easy, 5 – very strenuous). The Friedman test showed no significant effect of AG level on comfort ($\chi^2(2)=4.941$, $p = 0.085$). Similarly, the Friedman test showed no significant effects of AG level on difficulty of exercise ($\chi^2(2)=5.214$, $p = 0.074$).

Table 16 – Comfort and strenuousness subjective data average and standard deviation.

AG level	Comfort	Strenuousness
0 G	3.0±0.7	3.1±0.9
1 G	2.2±0.8	2.5±1.0
1.4 G	2.7±1.0	2.8±1.0

4.2.4 Summary of Results and Discussion

The new CRC at MIT is a unique AG platform capable of performing a wide range of human experiments. In particular, subjects have the capability to exercise while being rotated, which is a promising countermeasure against human deconditioning in space. Currently, the MIT CRC has a cycle ergometer in place, but it could be replaced by other exercise devices in the future.

This first human experiment validated both the mechanical aspects of the centrifuge and the capability of gathering physiological data during centrifugation and exercise. Twelve subjects were tested under three

AG levels ("No centripetal", "1G Centripetal", "1.4G Centripetal") during the same calendar week. At each AG level, subjects successfully completed a 25-minute exercise protocol that included 3 different ergometer intensities: 25W (warm-up phase), 50W (moderate exercise) and 100W (vigorous exercise). All subjects tolerated the centrifugation well, including the spin-up and spin-down process, and none of them presented signs of motion sickness. Foot forces during pedaling and non-invasive cardiovascular data were successfully recorded during all phases of the experiment. Three main hypothesis were tested and confirmed concerning the musculoskeletal system, the cardiovascular system, and motion and comfort.

- *Hypothesis 1: Higher AG ergometer exercise levels in a compact-radius centrifuge increase foot forces*

Recorded peak forces attained up to 42.5% body weight. Workload intensity and AG level both had a significant effect on peak foot forces. Therefore, these forces could be increased by using higher centrifuge rates, or increasing the ergometer resistance following the hierarchical regression models developed in this work. However, ergometer exercise does not produce foot forces as high as other types of exercise, such as stair-steppers. These are able to produce higher foot forces similar to treadmill running in space (up to 124% body weight [4].)

Previous studies using the CEVIS ergometer onboard the ISS showed that foot forces based on direct in-shoe insoles measurements [71] on astronauts ranged from 7.0% to 19.0% of body weight, depending on the workload, which varied from 75 to 210 W [72]. For the subjects in this study, peak forces ranged from 5.2% - 30.6% of body weight for the "No Centripetal" condition, 8.9% - 42.5% of body weight for AG level "1G Centripetal", and 10.7% - 42.0% of body weight for AG level "1.4G Centripetal". Average and standard deviation peak forces values (in % body weight), and their ranges in each condition are summarized in Table 17. Peak forces measured at AG level "No Centripetal" were within the same range as those measured in actual microgravity. Moreover, the increase in foot forces (% body weight) due to increase in AG level is also observed in the data (see Figure 36).

The ergometer was set to generate a particular workload profile during the exercise protocol (see Figure 14). Thus, the ergometer automatically adjusted its resistance based on the desired workload output, but also on the subject's pedaling speed: the faster the cycling RPM, the lower the ergometer resistance, in order to maintain a constant workload. Peak forces values obtained in this experiment correspond to a cycling rhythm of 60 RPM, which was maintained using a metronome. Different pedaling speeds would produce slightly different peak forces.

Table 17 – Foot Forces (% Body Weight) average and standard deviation for each workload intensity and AG condition.

AG level	Workload intensity					
	25W		50W		100W	
	Mean ± SD	Range	Mean ± SD	Range	Mean ± SD	Range
No Centripetal	8.7±2.7	5.2-13.8	12.7±2.7	8.6-17.5	21.3±4.9	14.2-30.6
1G Centripetal	12.3±2.3	8.9-18.4	17.4±3.3	11.7-25.4	26.5±5.2	18.3-42.5
1.4G Centripetal	14.9±2.3	10.7-19.0	21.5±3.4	14.8-29.1	30.1±5.3	20.1-42.0

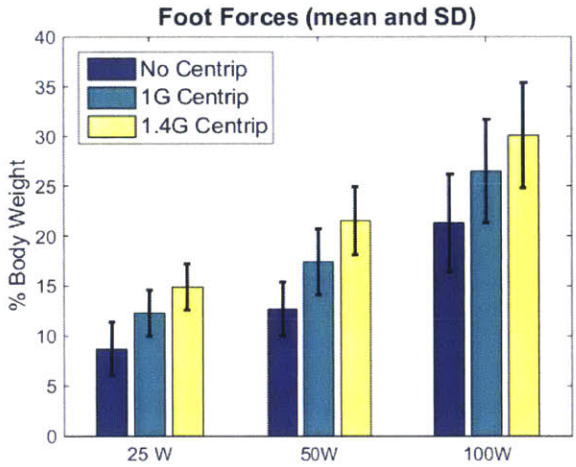

Figure 36 – Foot forces average and standard deviation for each workload intensity and AG condition.

- *Hypothesis 2: Higher AG ergometer exercise levels in a compact-radius centrifuge increase overall cardiovascular activity*

Exercise is a stressful condition to the cardiovascular system. During vigorous exercise, the cardiac output can increase to 6 or 7 times the normal values [73]. Muscle activation increases venous return and therefore mean systemic pressure. Autonomic stimulation increases heart rate and heart contractility. As a consequence, cardiac output also increases to meet the new metabolic demands imposed by the exercise activity. In addition, the higher muscle metabolism causes vasodilatation and the peripheral resistance decreases. These cardiovascular changes due to exercise are well captured in the cardiovascular data collected during this centrifuge experiment. The three exercise phases corresponding to the different exercise intensities (warm up at 25W, moderate exercise at 50W, and vigorous exercise at 100W) are

highly recognizable in most of the cardiovascular variables, in particular heart rate and cardiac output. Changes in these variables are the primary mechanism for the central nervous system to regulate the cardiovascular system.

The cardiovascular changes induced by the artificial gravity are also well captured in the data. The application of artificial gravity introduces a new stress condition that the cardiovascular system needs to overcome in order to assure the appropriate amount of blood flow to all parts of the body. This additional stress is reflected on the blood pressure drop that occurs when the subject is first exposed to artificial gravity. The higher the artificial gravity, the higher the cardiovascular stress, and therefore, the larger the initial blood pressure drop. The body respond to the pressure reduction by increasing the sympathetic stimulation, and therefore increasing heart rate, heart contractility, and peripheral resistance. This follows the same overall cardiovascular mechanisms and responses that someone on Earth experiences when changing from supine to upright position.

Data collected during this experiment suggest that pulse pressure, stroke volume, and as a consequence, the cardiac output, significantly increased with AG level to maintain a proper cardiovascular regulation. Higher AG levels combined with ergometer exercise increased venous return, presumably facilitated by a stronger muscle pump effect due to higher foot forces. This effect, combined with the stronger blood pulling to the lower part of the body due to higher levels of AG could explain these results.

It is important to acknowledge the strong gravity gradient when interpreting these results. The subject's head was located at the center of rotation and, as stated in previous sections, the gravity level was being measured at the feet. Cardiovascular sensors, in particular the baroreceptors, are located in the upper part of the body, and therefore, they were not exposed to gravitational changes as large as the feet or, more in general, the lower part of the body. Data show that significant cardiovascular changes (particularly in pulse pressure) occurred when artificial gravity at the feet is 1.4g, which corresponds to an artificial gravity level around 0.38g at the baroreceptors (assuming that they are located at 30 cm from the center of rotation). Similarly, when the feet were exposed to 1g, the baroreceptors were subjected to just 0.28g. This fact may explain why results concerning the "0G Centripetal" (no rotation) and "1G Centripetal" conditions do not differ too much, even though there was a considerable difference in the g level applied at the feet.

The Nexfin monitoring system is one of the best alternatives available to measure blood pressure and cardiac output non-invasively (see Appendix C for details about the Nexfin system operation). Measurements from invasive and non-invasive (Riva-Rocci/Korotkoff) methodologies showed good

correlations concluding that non-invasive blood pressure measurements are comparable to invasive monitoring [74]–[77]. Other studies compared the cardiac output measurements derived from Nexfin and transpulmonary thermodilution, showing adequate to excellent correlations [78]–[80]. However, some authors argue that the Nexfin system is not interchangeable with transpulmonary thermodilution techniques to monitor critical care patients [81]. Nevertheless, the Nexfin device provides fairly good results, and it is non-invasive, safe, convenient, and easy to use [79], definitely making it a suitable monitor for continuous measurements of CO, in particular in a non-clinical setting such as this centrifuge experiment.

- *Hypothesis 3: Higher AG ergometer exercise in a compact-radius centrifuge is well-tolerated and comfortable as ergometer exercise in simulated 0-g*

Subjective data show that subjects did not feel soreness or cycling difficulties other than normal discomfort due to the sideways positioning. None of the subjects noticed the Coriolis acceleration, or reported severe motion sickness. Subjects reported that exercising in the "No Centripetal" condition was more difficult and unnatural (see Table 16). This is probably due to the fact that, in this condition, there was no acceleration in the +Gz axis (or artificial gravity) to facilitate body positioning against the chair. In addition, the lack of wind in this "no rotation" condition made subjects to raise their body temperature, and therefore to be more sweaty and uncomfortable. The "No Centripetal" condition was chosen as the beginning of a linear AG spectrum (0g (no rotation), 1g, 1.4g in the centripetal direction), but these facts together could have had an impact in the CV data. In order to avoid this difficulties, futures experiments should consider AG levels between 0g (no rotation) and 1g centripetal (for example, 0.5g measured at the feet). Physiological data gathered at 0.5g would complement the existing dataset and would be used to refine the current regression models, and in general, to better understand the effects of AG on the human body.

This experiment has shown that AG combined with exercise in a compact-radius centrifuge indeed induces the expected acute physiological responses to the orthostatic stress generated by centrifugation. Furthermore, this initial parametric study provides a qualitative and quantitative analysis of human physiology and provides an initial step towards a full understanding of the effects of AG on the human body. Nevertheless, the effectiveness of AG as a countermeasure for space deconditioning is still "to be determined", since this will require the use and experimental testing of a centrifuge in space.

5 Computational Approach – Modeling Cardiovascular Responses under Artificial Gravity and Exercise

The second objective of this research effort is to develop a computational model that captures the cardiovascular behavior in the presence of a high gravity gradient environment during ergometer exercise. In particular, the model developed simulates the short-term hemodynamic response to orthostatic stress generated by a short-radius centrifuge (see a complete description of the model in Section 5.1). In the proposed modeling effort, the hydrostatic pressure resulting from the gravity gradient (see Section 0) and the effects of ergometer exercise during centrifugation (see Section 5.1.5) are combined to simulate the cardiovascular responses gathered experimentally using the MIT CRC (see Section 5.2). Additionally, the model is further explored to better understand the cardiovascular responses to new centrifuge configurations, or to different physiological states such as 0g-adapted subjects (see Section 5.3).

5.1 Model Description

The cardiovascular system can be represented as a fluid vessel network with regulatory control systems. This fluid network can also be represented by electric circuit analogues [63], [65], [82]. Thus, the cardiovascular system can be represented by a series of vascular segments modeled by electric circuit blocks or compartments. The model developed by Heldt [63] and used in this work consists of fifteen compartments representing the systemic circulation, four compartments representing the cardiac chambers, and two compartments representing the pulmonary circulation (see Section 5.1.1). In addition, the model includes the two major reflex mechanisms concerning the short-term hemodynamic response to orthostatic stress, namely the arterial baroreflex and the cardiopulmonary reflex (see Section 5.1.3).

Centrifugation using a short-radius centrifuge induces a significant orthostatic stress in the cardiovascular system. The artificial gravity induces both a primary rapid fluid shift from the upper body to the lower extremities, and a secondary slower fluid shift from the intravascular to the interstitial fluid compartment. These shifts induce a cardiovascular state of central hypovolemia that triggers the regulatory mechanisms to counteract the reduction in blood pressure and central blood volume. These effects of centrifugation were modeled by Zamanian [65] and are incorporated in the model described in this work (see Section 5.1.4).

Lastly, exercise has a significant impact in the cardiovascular system. Exercise increases cardiac output and blood flow to the exercising muscles, located in the legs in the case of ergometer exercise. This effect is accompanied by a decrease in peripheral resistance in the working muscles to facilitate the attainment of the muscle metabolic needs. Other exercise effects are related to muscular contraction, such as the

muscle-pump effect, which facilitates venous return, and an increase in intra-abdominal pressure. These effects, which were already considered by Heldt to some extent [63], are also incorporated in the model and they are further described in Section 5.1.5.

5.1.1 Systemic Circulation

A single vascular segment is modeled using the electric circuit analog show in Figure 37. The compartment is characterized by an inflow resistance R_n, an outflow resistance R_{n+1}, and the pressure-volume relationship $V_n(P_n - P_e)$, or the capacity of the segment to store volume V_n given a transmural pressure $\Delta P = P_n - P_e$.

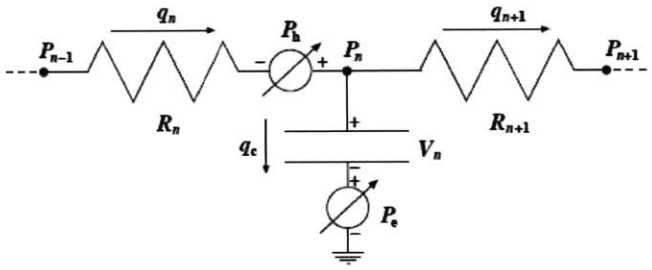

Figure 37 – Single compartment circuit representation [63].

In Figure 37, P_{n-1}, P_n, P_{n+1} are the compartment pressures; P_h is the hydrostatic pressure; P_e is the external pressure (such as the intra-thoracic pressure, intra-abdominal pressure, or the muscle-pump pressure); q_n, q_{n+1}, q_c are the flow rates; V_n is the compartment volume; and R_n, R_{n+1} are the flow resistances. The flows are calculated using the following constitutive relations:

$$q_n = q_{n+1} + q_c$$

$$q_n = \frac{P_{n-1} - P_n + P_h}{R_n}$$

$$q_{n+1} = \frac{P_n - P_{n+1}}{R_{n+1}}$$

$$q_c = \frac{d}{dt}V_n = \frac{dV_n}{d(P_n - P_e)} \cdot \frac{d}{dt}(P_n - P_e) = \frac{dV_n}{d\Delta P_n} \cdot \frac{d\Delta P_n}{dt}$$

Where $\frac{dV_n}{d\Delta P_n}$ is defined as incremental compliance C_n, that may be a function of transmural pressure.

Combining these equations yields an expression for the rate of change of transmural pressure in the nth compartment:

$$\frac{d\Delta P_n}{dt} = \frac{P_{n-1} - P_n + P_h}{C_n R_n} - \frac{P_n - P_{n+1}}{C_{n+1} R_{n+1}} \tag{7}$$

In Heldt's model, the systemic circulation is represented by fifteen compartments, connected in series and parallel, representing three different functional units: the arterial system (aorta and arteries), the micro-circulation (arterioles and capillaries), and the venous system (venules, veins, and venae cavae). Thus, the entire model is described by a set of coupled first-order differential equations. The model architecture is shown in Figure 38.

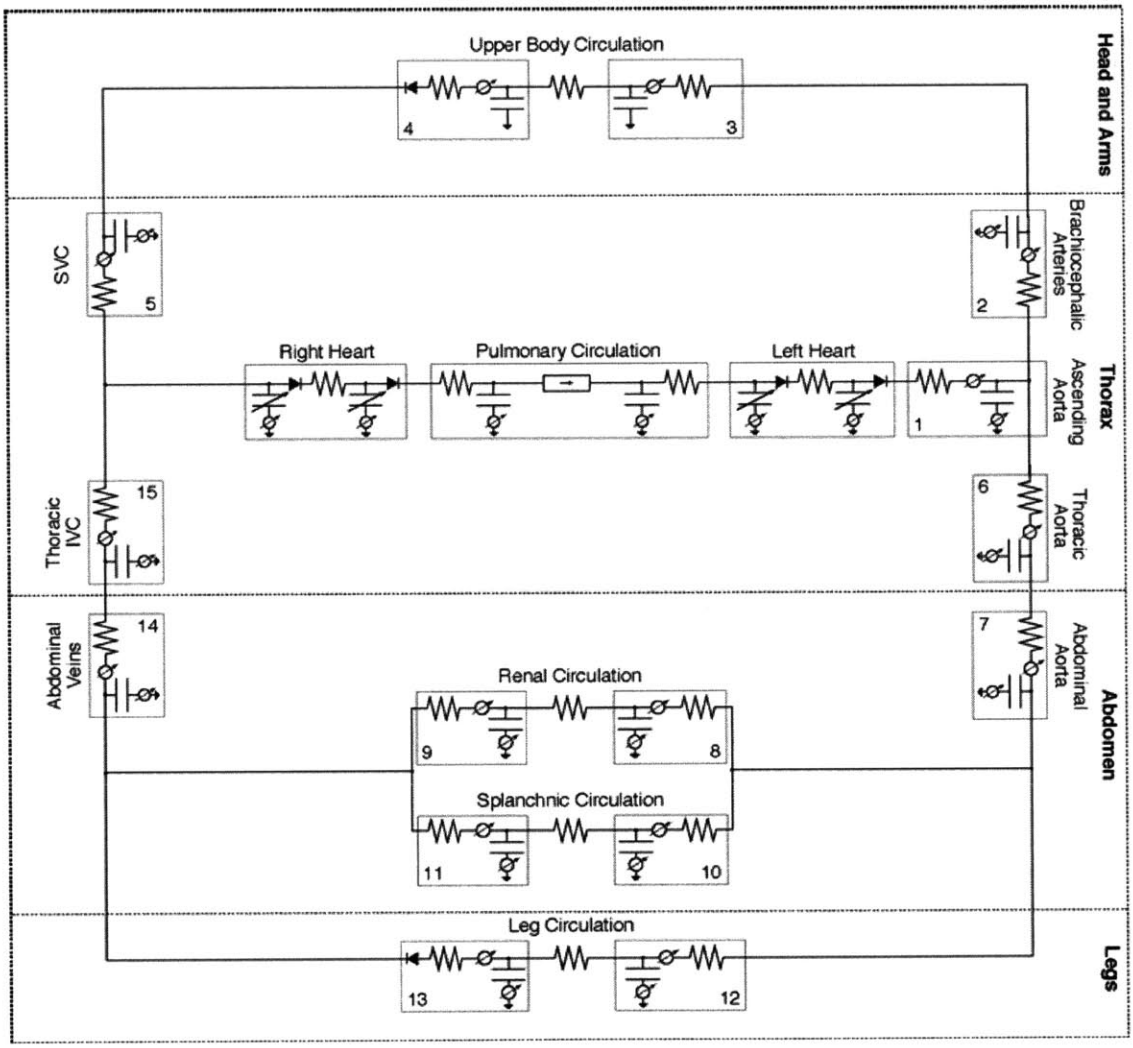

Figure 38 - Circuit representation of the cardiovascular model developed by Heldt [63].

As Heldt mentions, the circulation is divided in four vascular beds. The upper body comprises the circulation of the head, the neck and upper extremities, and this accounts for 10% of total skeletal muscle mass, one third of the blood supply to the skin, and one half of the blood supply to the skeleton. The renal compartment represents the kidneys and the adrenal glands. The splanchnic compartment includes the gastrointestinal track, one third of the skin, and one half of the adipose tissue. Lastly, the leg compartment comprises the lower extremities and the pelvic circulation. This accounts for 90% of the skeletal muscle, one half of the skeleton, one third of the skin, one half of the adipose tissue, and the pelvic organs [63].

5.1.1.1 Non-linear characteristics

Some parts of the systemic circulation show non-linear behaviors. For example, certain segments of the venous circulation only allow unidirectional flow due to the presence of unidirectional valves. Thus, unidirectional diodes are included in the compartments representing those areas, namely the venous upper body (compartment 4) and the venous leg circulation (compartment 13). The cardiac compartments also include unidirectional diodes representing the cardiac valves (see the cardiac model Section 5.1.2).

Under certain conditions of orthostatic stress, pressure-volume relationships in some venous circulation areas can reach regimes where they show a non-linear behavior. Generally, blood vessels operate in the linear range (low transmural pressures), but at high transmural pressures, the compliance decreases and the vessel can reach the elastic limit. Therefore, the following non-linear relation between total volume, V_t, and transmural pressure, ΔP, is implemented in the compartments likely to be exposed to these non-linear regimes, namely the splanchnic (compartment 11), leg (compartment 13), and abdominal (compartment 14) venous compartments:

$$V_t = V_0 + \frac{2V_{max}}{\pi} \cdot arctan\left(\frac{\pi C_0}{2V_{max}} \cdot \Delta P\right) \qquad for\ \Delta P > 0 \tag{8}$$

where V_{max} is the distending volume limit of the compartment, C_0 is the vascular compliance at zero transmural pressure, and V_0 is the venous unstressed volume or zero-pressure filling volume.

5.1.1.2 Parameter Assignments

The numerical values assigned to all the physical parameters were estimated by Heldt based on the literature. In the model description, Heldt includes a very detailed discussion about the rationale of all these choices [63]. For each compartment, these parameters include values for resistance R, compliance C, zero-pressure filling volume V_0, and anatomical vertical length l_v (superior-to-inferior extension of the vascular segment). The leg anatomical vertical lengths l_{v12} and l_{v13} were adjusted to take into account

the shorter configuration of the MIT centrifuge. In addition, the microvascular resistance values are also provided. Table 18, Table 19, Table 20, and Table 21 summarize the parameters of the systemic circulation.

Table 18 – Parameter values assigned to the systemic arterial compartments.

		Compartment Index							
Parameter	Units	1	2	3	6	7	8	10	12
C	$\frac{ml}{mmHg}$	0.28	0.13	0.42	0.21	0.10	0.21	0.42	0.42
V_0	ml	21	5	200	16	10	20	300	200
R	PRU	0.007	0.003	0.014	0.011	0.010	0.010	0.07	0.09
l_v	cm	10.0	4.5	20.0	16.0	14.5	0.0	10.0	85

Table 19 – Parameter values assigned to the systemic venous compartments.

		Compartment Index						
Parameter	Units	4	5	9	11	13	14	15
C	$\frac{ml}{mmHg}$	7	1.3	5	50	27	1.3	0.5
V_0	ml	645	16	30	1146	716	79	33
R	PRU	0.11	0.028	0.11	0.07	0.10	0.019	0.008
l_v	cm	20.0	14.5	0.0	10.0	85	14.5	6

Table 20 – Parameter values assigned to the systemic microvascular resistances.

		Microcirculation			
Parameter	Units	Upper body	Kidneys	Splanchnic	Legs
R	PRU	3.3	4.1	2.4	3.9

Table 21 – Parameters corresponding to the non-linear compartments.

		Compartment Index		
Parameter	Units	11	13	14
V_{max}	ml	1500	1000	650

5.1.2 Cardiac Model

The four cardiac chambers are represented using time-varying elastance models proposed by Heldt [63]. Both the right heart (right atrium and right ventricle) and the left heart (left atrium and left ventricle) are modeled using the same circuit representation, shown in Figure 39. The diodes represent the unidirectional nature of the blood flow in the cardiac chambers; R_{a-v} is the resistance due to the cardiac valves (tricuspid valve in the right heart, mitral valve in the left heart); P_a and P_v are the atrial and ventricular pressures; $C^a(t)$ and $C^v(t)$ are the atrial and ventricular capacitances; $E^a(t)$ and $E^v(t)$ are the atrial and ventricular elastances; and the time-varying pressure source P_{th} is the intrathoracic pressure.

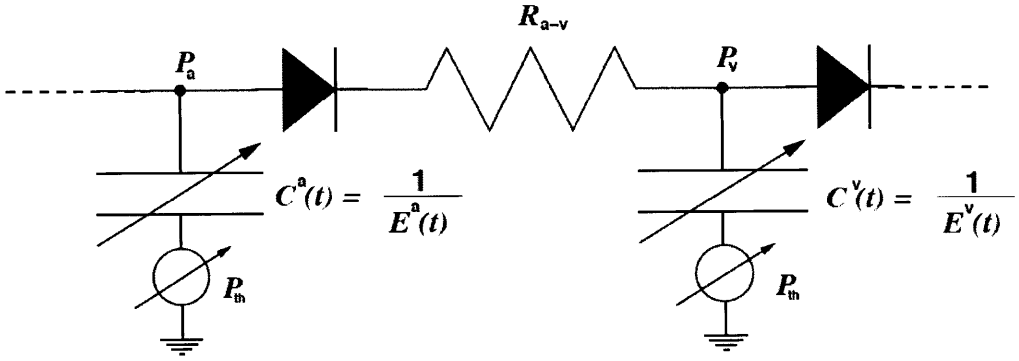

Figure 39 – Circuit representing the atrial and ventricular cardiac compartments. Figure taken from Heldt [63].

Previous research showed that the time-varying elastance waveform of the left ventricle can be reduced to a unique and universal curve when normalized and properly scaled [83]–[86]. Thus, as already assumed by Heldt [63], the normalized time-varying elastances for each one for the four cardiac chambers were taken to be identical, but each one scaled appropriately to account for the different end-systolic and end-diastolic compliances. Figure 40 depicts the normalized time-varying elastance of the human left ventricle.

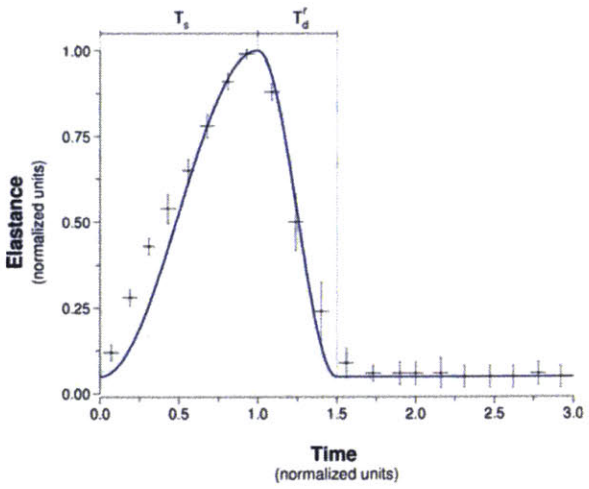

Figure 40 – Normalized time-varying elastance (figure taken from [63], as adapted from [87]).

In Figure 40, T_s is the systolic time interval and T_d^r is the time interval of diastolic relaxation. Then, the time-varying elastance in each one of the four chambers is modeled using the equation below, where the time interval of diastolic relaxation T_d^r is assumed to be one half of the systolic time interval T_s :

$$E(t) = \begin{cases} E_d + \frac{E_{es} - E_d}{2} \cdot \left\{1 - cos\left(\pi \frac{t}{T_s}\right)\right\} & 0 \le t \le T_s \\ E_d + \frac{E_{es} - E_d}{2} \cdot \left\{1 + cos\left(2\pi \frac{t}{T_s}\right)\right\} & T_s < t \le \frac{3}{2} T_s \\ E_d & \frac{3}{2} T_s < t \end{cases} \quad (9)$$

Lastly, E_d and E_{es} are the diastolic elastance and end-systolic elastances, respectively, and they take different values depending on the cardiac chamber. Table 22 summarizes the model parameters of the cardiac compartments.

Table 22 – Cardiac Parameters. Values taken from [63].

Parameters	Units	Right Heart		Left Heart	
		Atrium	Ventricle	Atrium	Ventricle
E_{es}	$\frac{mm\ Hg}{ml}$	0.74	1.3	0.61	2.5
E_d	$\frac{mm\ Hg}{ml}$	0.3	0.07	0.5	0.13
V_0	ml	14	46	24	55
R_{a-v}	PRU	0.005		0.010	

Lastly, the cardiac timing parameters also need to be defined. These parameters include the atrial and ventricular systole duration, T_S^a and T_S^v, as well as the "P-R interval", i.e. the delay between the onset of the atrial and ventricular contraction T_{a-v}. Their values are assumed to be proportional to the square root of the R-R interval length (inter-beat interval) T_{RR} [63], and they are summarized in Table 23.

Table 23 – Time parameters for the cardiac model. Values taken from [63], [65].

Parameter	Units	T_S^a	T_S^v	T_{a-v}
Time	s	$0.2\sqrt{T_{RR}}$	$0.3\sqrt{T_{RR}}$	$0.12\sqrt{T_{RR}}$

5.1.2.1 Cardiac Pacemaker

The generation of heartbeats is represented using an Integral Pulse Frequency Modulation (IPFM) model [63], [65], [88]. The model represents the dynamics of the transmembrane potential $M(t)$, whose value at time t depends on the cumulative automaticity, and the contribution of neural control (i.e. sympathetic or parasympathetic activity) since the last heartbeat or cardiac excitation time $t_k - 1$.

$$M(t) = \int_{t_k-1}^{t} m(t)dt = \int_{t_k-1}^{t} (m_0 + m_r(t))dt$$

where m_0 correspond to the automaticity, and $m_r(t)$ represents the neural input from the arterial baroreflex control system (see Section 5.1.3.1). A new heartbeat occurs when the transmembrane potential $M(t)$ reaches a predefined threshold potential Γ, and the time since the previous heartbeat is at least one fifth of the preceding cardiac cycle length. This last constraint represents the absolute refractory period of the heart cells. Therefore, the heartbeat occurs at $t_k$when:

$$\int_{t_k-1}^{t_k} m(t)dt = M(t_k) \geq \Gamma \quad \text{and} \quad t_k - t_{k-1} \geq 0.2(t_{k-1} - t_{k-2})$$

The automaticity m_0 is assumed to be constant, which leads to a constant heartrate in the absence of neural input form the sympathetic or parasympathetic control system. Then, the baroreceptor input can either increase (via sympathetic stimulation) or decrease (via parasympathetic stimulation) the slope of the transmembrane potential, increasing or decreasing the generation rate of heartbeats.

The function $m(t)$ is defined as the inverse of the instantaneous R-R interval $I(t)$:

$$m(t) = \frac{1}{I(t)} = \frac{1}{I_0 + \Delta I_{AB}(t)}$$

where I_0 is the nominal R-R interval, and $\Delta I_{AB}(t)$ represents the control input from the baroreceptor control system. The nominal heart rate is 67 beats/min and the threshold potential Γ is equal to 1.

5.1.3 Control Systems

The cardiovascular system must assure the delivery of oxygen and nutrients to all parts of the body, as well as the removal of waste. These mechanisms need to be maintained even in the presence of cardiovascular stress such as orthostatic stress due to centrifugation. The following cardiovascular control systems are the two major neurally-mediated reflex mechanisms responsible for the short-term hemodynamic response assuring a proper regulation of the cardiovascular system. The arterial baroreflex is described in Section 5.1.3.1 and the cardiopulmonary reflex is described in Section 5.1.3.2. Figure 41 shows a diagram of the cardiovascular controls systems represented in this model. This approach was previously used by Zamanian [65].

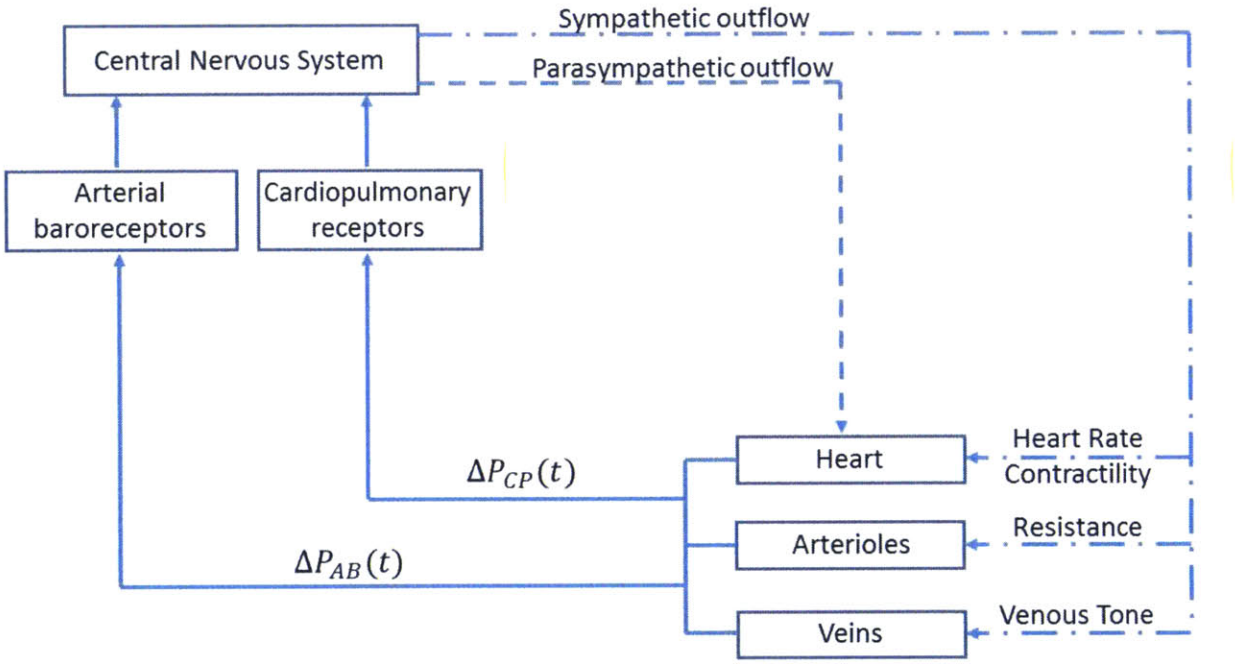

Figure 41 – Cardiovascular control system. $\Delta P_{AB}(t)$, $\Delta P_{CP}(t)$: arterial baroreceptors and cardiopulmonary receptors transmural pressures (figure adapted from [63], [65], [89]).

5.1.3.1 Arterial baroreflex

The arterial baroreceptors are stretch receptors located in the aortic arch and carotid sinus, and their main function is to regulate arterial blood pressure. These pressure sensors respond to stretching so that if arterial pressure increases, the arterial wall expands causing an increase in the firing rate of action potentials. Similarly, if pressure suddenly decreases the firing rate of action potentials decreases. These signals travel through the glossopharyngeal nerves (carotid sinus reflex) and the vagus nerves (aortic arch reflex) to the *nucleus tractus solitarious* (NTS) located in the medulla of the brainstem. The NTS integrates the autonomic responses and regulates the sympathetic or parasympathetic activity using efferent pathways to various organs.

The sympathetic efferent fibers exit from the central nervous system via the thoracic and lumbar spinal roots. The neurotransmitter for the sympathetic control system is norepinephrine. The effector mechanisms of the sympathetic stimulation include an increase in heart rate and cardiac contractility (via β-sympathetic receptors), and an increase in tone of vascular smooth muscle (via α-sympathetic receptors), which causes an increase in vascular peripheral resistance and a decrease in zero-venous filling volume. On the other hand, the parasympathetic efferent fibers exit from the central nervous system via the cranial nerves and the sacral spinal roots. The neurotransmitter for the parasympathetic control system is acetylcholine. The principal effector mechanism of the parasympathetic (or vagal) stimulation consists of a rapid decrease in heart rate. Figure 41 summarized the sympathetic and parasympathetic control loops previously described and included in this modeling effort.

5.1.3.1.1 Modeling the Arterial Baroreflex

The arterial baroreceptor mechanism can be represented using a negative feedback loop and an arterial pressure set-point P_A^{sp}as the reference pressure. Only one lumped baroreceptor in the carotid sinus is considered, and it is assumed to be located 25cm above the location of the heart (as represented by the aortic arch pressure P_1). Thus, taking into account the hydrostatic column due to centrifugation, the carotid sinus pressure P_{CS} (mmHg) is defined as:

$$P_{CS} = P_1 - \frac{1}{2} \cdot \rho \cdot \omega^2(t) \cdot ((25 + d)^2 - d^2) \tag{10}$$

where d is the distance between the head and the center of rotation measured in cm, ρ is the blood density in $\frac{mmHg}{1/s^2 cm^2}$, and $\omega(t)$ is the angular velocity of the centrifuge in rad/s. The feedback error signal $e_{AB}(t)$ is

then calculated by subtracting the arterial pressure set-point P_A^{sp} from the carotid sinus pressure P_{CS}, and scaling the resultant signal appropriately [63], [65] :

$$e_{AB}(t) = 18 \cdot arctan\left(\frac{P_{CS} - P_A^{sp}}{18}\right) \tag{11}$$

In nominal conditions (no exercise), the value of the arterial pressure set-point P_A^{sp} is close to be 95 mmHg.

The sympathetic and parasympathetic control systems are modeled as two linear time-invariant (LTI) filters, as proposed by Samar [89] and later used by Zamanian [65]. The sympathetic filter is represented using a triangular impulse response function, which is parameterized in terms of three timing variables: a delay, a peak, and an end. The transfer function used for the sympathetic filter is shown below:

$$s(s) = \frac{1}{42s^2}e^{-2s} + \frac{1}{75s^2}e^{-5s} + \frac{1}{300s^2}e^{-30s} \tag{12}$$

corresponding to a delay of 2s, a peak of 5 s, and an end of 30s (values taken from Samar [89]).

Samar [89] also proposed to represent the parasympathetic transfer function as a simple gain with zero delay. This approximation is valid due to the relatively rapid response of the parasympathetic system and its small time delay of less than one sec. Therefore, the parasympathetic filter is given by:

$$p(s) = 1 \tag{13}$$

The contribution of the autonomic control system to the effector variables is obtained by convolving the error signal with a linear combination of the sympathetic and parasympathetic control filters. The gains of the filters are specific to each effector variable. The arterial baroreflex contribution is then added to the cardiopulmonary reflex contribution (see 5.1.3.2) to constitute the total neurally-mediated global reflex contribution to each effector variable. Figure 42 shows a diagrammatic representation of the arterial baroreflex central nervous processing.

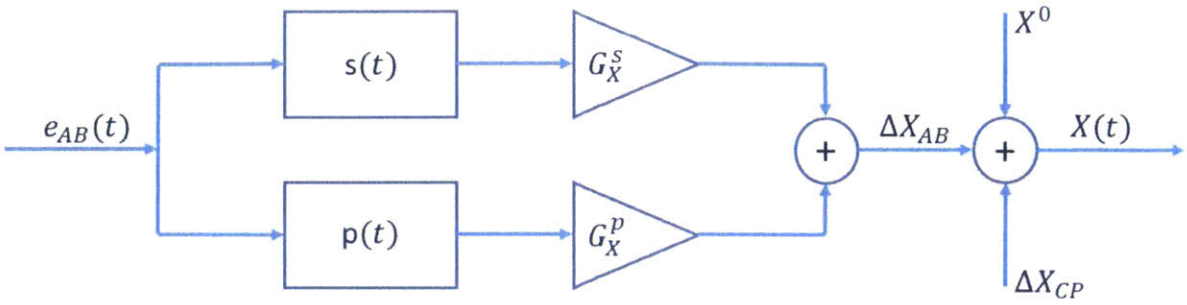

Figure 42 – Arterial baroreflex block diagram of the central nervous processing for an effector variable X (adapted from [65]).

The gain values are taken from Heldt's model [63] and later used by Zamanian [65]. They are summarized in Table 24.

Table 24 – Gain values for the arterial baroreflex model. Values taken from [63], [65].

Reflex Arc	Units	G^s	G^p
R-R Interval	$\frac{ms}{mm\ Hg}$	9	9
Left ventricular contractility	$\frac{ml}{mm\ Hg^2}$	0.007	0
Right ventricular contractility	$\frac{ml}{mm\ Hg^2}$	0.022	0
Upper body arterial resistance R_{ub}	$\frac{PRU}{mm\ Hg}$	-0.05	0
Renal circulation arterial resistance R_{rc}	$\frac{PRU}{mm\ Hg}$	-0.05	0
Splanchnic circulation arterial resistance R_{sc}	$\frac{PRU}{mm\ Hg}$	-0.05	0
Leg circulation arterial resistance R_{lc}	$\frac{PRU}{mm\ Hg}$	-0.05	0
Upper body venous unstressed volume V_{ub}	$\frac{ml}{mm\ Hg}$	5	0
Renal venous unstressed volume V_{rc}	$\frac{ml}{mm\ Hg}$	2	0
Splanchnic venous unstressed volume V_{sc}	$\frac{ml}{mm\ Hg}$	13	0
Leg venous unstressed volume V_{lc}	$\frac{ml}{mm\ Hg}$	7	0

5.1.3.2 Cardiopulmonary reflex

The cardiopulmonary receptors are located in the atria and the pulmonary arteries. They respond to increases in blood pressure in these low pressure areas caused by an increase in volume. Thus, when blood volume increases in these areas, the information travels through the vagal afferent nerves to the medulla, leading to a reduction in efferent sympathetic activity [63], [65], [90].

In addition, the cardiopulmonary reflex is related to the long-term neuro-humeral regulation. Stretch of the atria causes an increase of atrial natriuretic peptide (APN), a powerful vasodilator, and a decrease in the secretion of antidiuretic hormone (ADH), causing loss of fluid through urine.

5.1.3.2.1 Modeling the Cardiopulmonary Reflex

The cardiopulmonary reflex is also represented by a negative feedback loop, using a pressure set-point P_{CP}^{sp} as the reference pressure. The variable measured is the transmural right atrial pressure ΔP_{RA}. The feedback error signal $e_{CP}(t)$ is then calculated by subtracting the set-point pressure P_{CP}^{sp} from the transmural right atrial pressure ΔP_{RA}, and scaling the resultant signal appropriately [63], [65] :

$$e_{CP}(t) = 5 \cdot arctan\left(\frac{\Delta P_{RA} - P_{CP}^{sp}}{5}\right) \tag{14}$$

where the reference pressure P_{CP}^{sp} is set to 5 mmHg.

The contribution of the cardiopulmonary reflex to the effector variables is obtained using a similar process to the case of the arterial baroreflex. The cardiopulmonary error signal is fed to the sympathetic and parasympathetic filters previously described, and specific gains are applied to each effector variable. Finally, the cardiopulmonary contribution is added to the arterial baroreflex contribution to constitute the total neurally-mediated global reflex contribution to each effector variable. The effector variables taken into account in the model are the arterial resistance and the venous unstressed volume [63]. The gain values are taken from Heldt's model [63] and later used by Zamanian [65]. They are summarized in Table 25.

Table 25 - Gain values for the cardiopulmonary reflex model. Values taken from [63], [65].

Reflex Arc	Units	G^s	G^p
Upper body arterial resistance R_{ub}	$\frac{PRU}{mm\ Hg}$	-0.05	0
Renal circulation arterial resistance R_{rc}	$\frac{PRU}{mm\ Hg}$	-0.05	0
Splanchnic circulation arterial resistance R_{sc}	$\frac{PRU}{mm\ Hg}$	-0.05	0
Leg circulation arterial resistance R_{lc}	$\frac{PRU}{mm\ Hg}$	-0.05	0
Upper body venous unstressed volume V_{ub}	$\frac{ml}{mm\ Hg}$	13	0
Renal venous unstressed volume V_{rc}	$\frac{ml}{mm\ Hg}$	3	0
Splanchnic venous unstressed volume V_{sc}	$\frac{ml}{mm\ Hg}$	64	0
Leg venous unstressed volume V_{lc}	$\frac{ml}{mm\ Hg}$	30	0

5.1.4 Modeling Centrifugation

The effects of centrifugation are represented by changes in hydrostatic pressure, changes in intra-thoracic pressure, and changes in total blood volume.

5.1.4.1 Hydrostatic pressure

The effect of orthostatic stress is modeled by pressure sources, P_h, to account for the hydrostatic pressure resulting from centrifugation. These pressure sources are positioned in series within each compartment (see Figure 43) and their values depend on the subject positioning, particularly on the distance between each cardiovascular compartment and the center of rotation of the centrifuge. The hydrostatic pressure through a differential cross-section in the radial direction is given by:

$$dP_h = \rho * a(r) * dr$$

where $a(r)$ is the acceleration created by centrifugation, and it is defined as:

$$a(r) = \omega^2(t) * r$$

where $\omega(t)$ is the angular velocity of the centrifuge, and r is the distance from the axis of rotation.

Combining both expressions and integrating over the effective hydrostatic height of the compartment, a mathematical expression for the hydrostatic pressure is obtained:

$$P_h = \int_{R_i}^{R_o} \rho * \omega^2(t) * r = \rho * \omega^2(t) * \frac{r^2}{2}\Big|_{R_i}^{R_0} \tag{15}$$

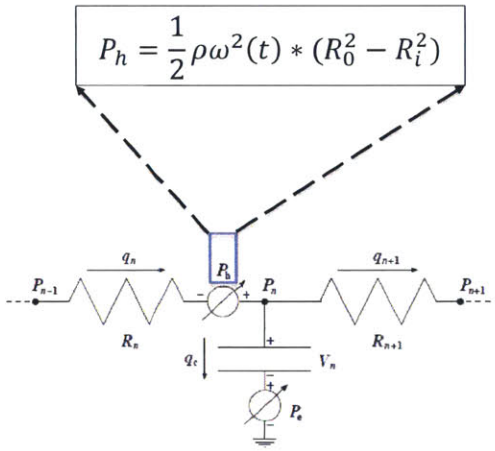

Figure 43 – Pressure sources accounting for the hydrostatic pressure resulting from centrifugation.

where the inlet radius R_i is the distance between the superior end of the compartment and the center of rotation, and the outlet radius R_o is the sum of the effective height of the compartment and the inlet radius. The effective height is assumed to be one half of the anatomical vertical length for each compartment, except the leg compartments where the effective length is defined as a third of the anatomical vertical length. As an example, Figure 44 shows a subject lying down on a centrifuge with the feet pointing at the rim of the centrifuge (radially outward direction). The leg compartment is located at a distance R_i from the center of rotation, and its effective height is $h_{lef} = R_o - R_i = \frac{1}{3} l_{v\,legs}$.

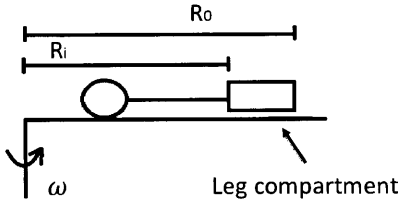

Figure 44 – Example of the hydrostatic pressure resulting from centrifugation in the leg compartment.

Assuming the subject has his/her head at the center of rotation, the inlet radii R_i for all compartments are shown in Table 26. In the particular case where the subject's head is located at a distance h from the center of rotation, the actual inlet radius R_i would be increased by the distance h. This configuration is further studied in Section 5.3.1.

Table 26 – Values for inlet radii R_i for all compartments.

Compartment Index	R_i (cm)	Compartment Index	R_i (cm)
1	24.5	9	55
2	20	10	55
3	0	11	55
4	0	12	55
5	20	13	55
6	24.5	14	40.5
7	40.5	15	34.5
8	55		

5.1.4.2 Intra-thoracic pressure

Intra-thoracic pressure also changes during orthostatic stress due to the weight of the liver being pulled down in the thoracic compartment [65], [91], [92]. Heldt modeled the intra-thoracic pressure during upright tilt according to:

$$P_{th}(t) = P_{th_0} - 3.5 \cdot \sin(\alpha_{\max}) \cdot \sin(\alpha(t))$$

where P_{th_0} is the nominal intra-thoracic pressure, and $\alpha(t)$ is the tilt angle, $\alpha_{\max}$ being the maximum tilt angle [63]. During upright tilt, the head-foot acceleration $a(t)$ can be written as a function of the tilt angle $\alpha(t)$:

$$\sin(\alpha(t)) = \frac{a(t)}{g}$$

$$\sin(\alpha_{\max}) = \frac{a_{max}}{g}$$

Using these relationships, the intra-thoracic pressure expression can be written as:

$$P_{th}(t) = P_{th_0} - 3.5 \cdot \frac{a_{max} \cdot a(t)}{g^2}$$

Finally, introducing the relationship between acceleration and angular velocity in a rotating environment ($a = \omega^2(t) * r$), the intra-thoracic pressure $P_{th}(t)$ during centrifugation is given by:

$$P_{th}(t) = P_{th_0} - 3.5 \cdot \frac{(r+h)^2 \cdot \omega_{max}^2}{g^2} \cdot \omega^2(t) \tag{16}$$

where $r = 55\ cm$ corresponding to the location of the liver in the thoracic compartment; h is the distance from the head to the center of rotation of the centrifuge; and $\omega(t)$ is the angular velocity.

5.1.4.3 Total Blood Volume

Orthostatic stress causes an increase in transcapillary fluid flow in the dependent vasculature and, as a consequence, a net decrease in intravascular volume. Changes in hydrostatic pressure alter the equilibrium between oncotic and hydrostatic gradients, directly affecting transcapillary fluid exchange.

Based on previous studies about transcapillary flow during orthostatic stress, Heldt characterized this phenomenon using additional RC compartments, as shown in Figure 45.

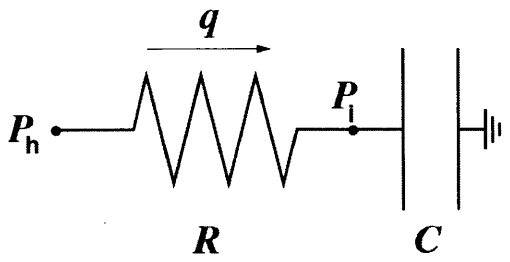

Figure 45 – RC model of interstitial compartment. Figure taken from Heldt [63] and Zamanian [65].

The transcapillary flow is solved analytically based on the orthostatic stress profile using the equations described in Appendix E. The solution of the equations depends on two parameters: the time constant $\tau = RC$, and the maximum interstitial volume change $V_{max} = P_h C$. For upright tilt and stand test simulations, Heldt proposed a time constant $\tau = 4.6\ min$, and the following expression for V_{max}:

$$V_{max} = 700ml \cdot \frac{\sin(\alpha_{\max})}{\sin(85)}$$

In order to get an expression for the V_{max} due to centrifugation, Zamanian used the previously mentioned relationship between tilt angle and acceleration in the head-foot direction $\sin(\alpha_{\max}) = \frac{a_{max}}{g}$:

$$V_{max} = 700ml \cdot \frac{a_{max}}{\mathrm{g} \cdot \sin(85)}$$

Again, introducing the relationship between acceleration and angular velocity in a rotating environment ($a = \omega^2(t) * r$), the maximum interstitial volume change V_{max} during centrifugation is given by:

$$V_{max} = 700ml \cdot \frac{(r+h) \cdot \omega_{max}^2}{\mathrm{g} \cdot \sin(85)} \tag{17}$$

where $r = 55\ cm$ corresponds again to the thoracic compartment; h is the distance from the head to the center of rotation of the centrifuge; and $\omega(t)$ is the angular velocity.

Once the equations are solved, the transcapillary flow is simply subtracted from the venous return at the selected compartments where this phenomenon is significant, namely splanchnic venous (compartment 11), leg venous (compartment 13), and abdominal venous (compartment 14). The fractions of interstitial volume and interstitial flow assigned to each compartment are defined as follows:

$$V^n(t) = \frac{P^n_{h,max}}{\sum_i P^i_{h,max}} \cdot V(t)$$

$$q^n(t) = \frac{P^n_{h,max}}{\sum_i P^i_{h,max}} \cdot q(t)$$

where $P^n_{h,max}$ is the maximum hydrostatic pressure in the nth compartment; and $\sum_i P^i_{h,max}$ is the sum of the maximum hydrostatic pressures of the three compartments (11, 13, and 14).

5.1.5 Modeling Exercise

One of the primary effects of exercise on the cardiovascular system is the large increase in the blood flow to the muscle groups that are exercising [63], [90]. During exercise, blood flow through skeletal muscle can increase from 3-4 ml/min per 100 grams of muscle (average during rest) to 50-80 ml/min per 100 grams of muscle [90]. Three major processes (although all three are interconnected) occur in the circulatory system to supply the increased blood flow required by the muscles:

- Mass sympathetic discharge throughout the body

  Sympathetic activity increases due to exercise. In addition, the parasympathetic signals to the heart are attenuated. As a consequence, the heart rate increases, and the arterioles of the peripheral circulation are strongly contracted (except the ones in the active muscles, which are strongly vasodilated), and veins and other capacitive areas are highly contracted. This facilitates venous return of blood to the heart, increasing the cardiac output.

- Increase in arterial pressure

  The increase can range from 20 to 80 mm Hg, depending on the exercise conditions. The increase in pressure is likely due to control command from the high control centers in the central nervous system in the brain.

  The total increase in arterial pressure depends on the type of exercise. Arterial pressure can increase to as high as 170 mmHg when exercising using just a few muscles, since the vasodilatation only occurs in those muscles while the sympathetic stimulation still generally increases. On the other hand, exercise like swimming or running generates muscle vasodilatation in almost every muscle in the entire body, and therefore, arterial pressure increases only by 20-40 mmHg [90]

- Increase in cardiac output

  This is necessary to supply large quantities of oxygen and nutrients to the muscles during exercise. The cardiac output can increase as much as six or seven times in a well-trained athlete [90].

Other effects of exercise include the pump effect of the leg muscles and the increase in intra-abdominal pressure due to the contraction of the abdominal muscles.

5.1.5.1 Exercise in the Cardiovascular Model

In the proposed cardiovascular model, the exercise effects will be modeled using four mechanisms: the increase in blood pressure, the increase in blood flow to the exercising muscles due to a decrease in resistance, the action of muscle pumps, and the increase in intra-abdominal pressure. These effects are summarized in Figure 46:

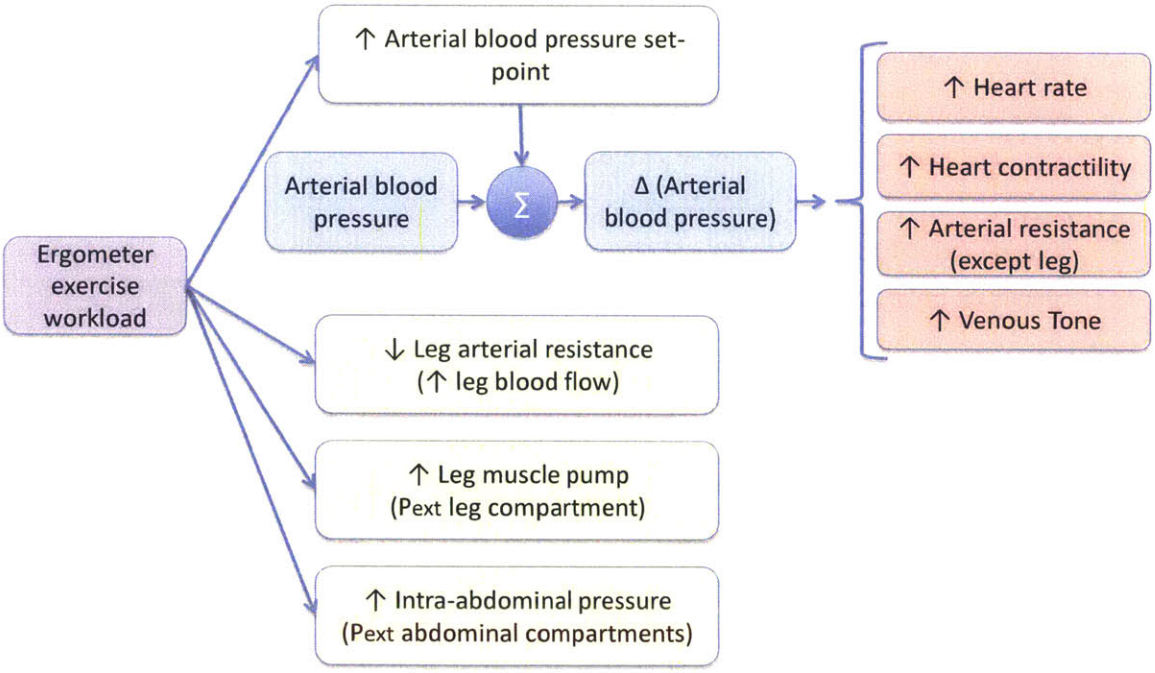

Figure 46 – Exercise Simulation Protocol.

5.1.5.1.1 Increase in Arterial Blood Pressure

In order to capture the effects of increased blood pressure during exercise, an exercise control system is incorporated using a set-point model [63]. The desired exercise workload sets a pre-defined set-point pressure of the arterial baroreflex P_A^{sp}. Thus, this is an adjustable parameter as a function of exercise intensity. Consequently, the model accounts for changes related to sympathetic activity, namely, increase in heart rate, increase in heart contractility, increase in arterial resistance (except in the active muscles), and increase in venous tone (decrease in venous zero pressure filling volume).

5.1.5.1.2 Decrease in Leg Arterial Resistance

The increase in leg blood flow during ergometer exercise is simulated by disconnecting the leg resistance from the baroreceptor and pulmonary control at the onset of exercise and decreasing it according to:

$$R_{lc}(t) = R_{lc}^{-} + \left(R_{lf} - R_{lc}^{-}\right)(1 - e^{-t/\tau}) \tag{18}$$

where R_{lc}^{-} is the leg vascular resistance immediately before the onset of an exercise phase, R_{lf} is the final leg vascular resistance for a given exercise intensity, and τ is a time constant. These parameters are chosen manually (trial and error procedure until best fit as judged by visual inspection) such that the total peripheral resistance matches the values seen experimentally at each workload intensity. As an example, Figure 47 shows the total peripheral resistance seen experimentally at the "1G Centripetal" condition (1G Exp), and the total peripheral resistance in the cardiovascular model (1G Sim). Three exponential curves can be observed during the exercise phase, corresponding to the three different workload intensities.

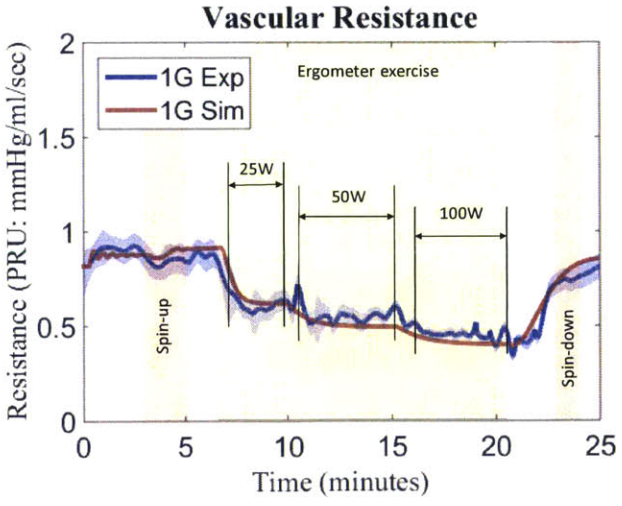

Figure 47 – Example of vascular resistance modeling.

5.1.5.1.3 Increase in Leg Muscle Pump

The action of the leg muscle pumps during cycling is simulated by varying the external pressure at the venous leg compartment assuming an ergometer exercise protocol cycling at 1 rev/sec, which is the cycling cadence used by the 12 subjects in the MIT CRC experimental protocol. The external pressure is represented according to:

$$P_{ext} = \begin{cases} P_{max}\frac{1}{2}(1-\cos(4\pi t)) & 0 \le t \le 1/4 \\ P_{max} & 1/4 \le t < 1/2 \\ P_{max}\frac{1}{2}(1+\cos(4\pi(t-1/2))) & 1/2 \le t < 3/4 \\ 0 & 3/4 \le t < 1 \end{cases} \quad (19)$$

where P_{max} is the maximal external pressure and it depends on the exercise workload. Figure 48 depicts an example of the muscle pump effect modeling, using $P_{max} = 20\ mmHg$.

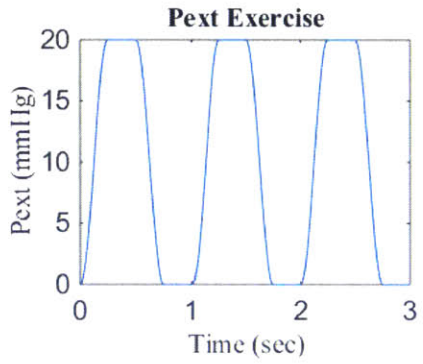

Figure 48 – Example of external pressure due to the muscle pump effect.

In addition to the periodic muscle pump effect during cycling, a constant external pressure is also added during the centrifugation periods with no exercise to take into account the action of the leg muscles when subjects are being pushed against the pedals.

5.1.5.1.4 Increase in Intra-Abdominal Pressure

The increase in intra-abdominal pressure is represented as an increase in external pressure on the abdominal compartments (compartments 7, 8, 9, 10, 11, and 14). The external pressure is represented according to:

$$P_{ext} = P_{ext}^{max}\,(1 - e^{-t/\hat{\tau}}) \quad (20)$$

where $\hat{\tau}$ is a time constant and P_{ext}^{max} is the maximal external pressure, which depends on the exercise workload. Figure 49 shows an example of the increase in the external pressure during the 25-min protocol exercise. The parameter P_{ext}^{max} takes different values depending on the intensity of exercise.

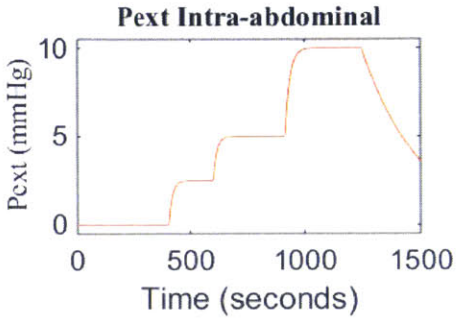

Figure 49 – Example of the external pressure increase in the abdominal compartments.

5.1.6 Matching the Experimental Data

It is important to mention that the purpose of these simulations is to intentionally limit the number of inputs and not to exert the full flexibility of the model to reduce the error between the experimental and simulated responses. A small number of parameters, namely total vascular resistance and mean blood pressure, have been constrained to evaluate if the resulting simulations capture the physiologic response over a range of exercise levels and AG regimes. The model has more than 100 parameters and it can certainly be manipulated to perfectly match the cardiovascular responses. However, the learning outcomes of this exercise are small, since most parameters will not contribute to the output and the resultant solution will not be unique.

5.1.7 Model Limitations

The cardiovascular model limitations are thoroughly detailed by Heldt [63], and only a summary is presented here. The objective of the cardiovascular model developed in this thesis is to simulate the short-term beat-to-beat hemodynamic responses to centrifugation and exercise. Therefore, a lumped parameter modeling approach is a reasonable choice, since it provides beat-to-beat averaged hemodynamic values, thus reducing the computational cost. However, this model is not suitable for other studies interested in detailed variations of pressure or other hemodynamic parameters within the cardiac cycle.

The compartmental nature of a lumped model entails some limitations, such as the inability to represent changes in hemodynamic variables as a function of the location through the body. For example, the

arterial pressure waveform slightly decreases when it travels far away from the heart. Similarly, the peak-systolic pressure increases and the diastolic pressure decreases, overall increasing pulse pressure up to 40%. However, the model simulates the pressures at the root of the aorta and therefore, does not take into account distal changes along the body.

Inertial effects are not included in the model. These effects become more important within a cardiac cycle or inter-beat (where there are large changes in flow rates) as opposed to from beat-to-beat. These effects have been estimated to contribute to less than 1% of the hemodynamic variables and therefore they are neglected.

Concerning the cardiac model, both the systolic and diastolic pressure-volume relationships are assumed to be linear. These relationships are fairly linear at normal filling pressures, but they do have a non-linear behavior at high filling pressures. Cardiovascular simulations in the non-linear region are beyond the scope of this work, and for the purpose of the simulations presented here, the pressure-volume relationships are assumed linear. Finally, the unstressed volume is assumed to be static throughout the cardiac cycle (intercept of the diastolic pressure-volume is the same as the intercept of the systolic pressure-volume). Generally, the systolic unstressed volume is 25-40% lower than the diastolic unstressed volume, which adds a small contribution to stroke volume. This effect was resolved by slightly decreasing the diastolic elastances so the stroke volume is slightly higher for a given end-diastolic pressure.

5.1.8 Model Implementation

The cardiovascular model is developed in Matlab Simulink, and it builds upon the previous model developed by Zamanian [65]. In order to avoid problematic numerical errors, the state variable is chosen to be the compartmental distending volume $V_d(t)$. Therefore, the state equation for the compartment n becomes:

$$\frac{d}{dt}V_{dn}(t) = q_{in_n} - q_{out_n} \tag{21}$$

where q_{in_n} and q_{out_n} correspond to the inward and outward compartmental flow respectively.

The model runs using the variable-step solver *ode23t* with a maximum step size of 0.01 s. The initial conditions are calculated using the methodology first implement by Davis [93], and further developed by Zamanian [65]. This methodology uses a non-linear system of 23 algebraic equations based on first principles to solve for luminal pressures in the compartments and from them, the initial compartmental volumes (see Appendix F for details on the initial conditions).

5.2 Model Evaluation

5.2.1 Reference Simulation 1G

The reference condition was chosen to be the "1G Centripetal". In this condition, subjects were exposed to 1G in the centripetal direction measured at the feet. Given the centrifuge configuration, this corresponded to an angular velocity of approximately 28.6 rpm. The centrifugation profile generated in the simulation matched the one used during the experimental approach: 3-minute rest, spin-up process to 28.6 rpm over 100 s, and spin-down deceleration at T = 23:45 over 1 min. The angular velocity profile is depicted in Figure 50.

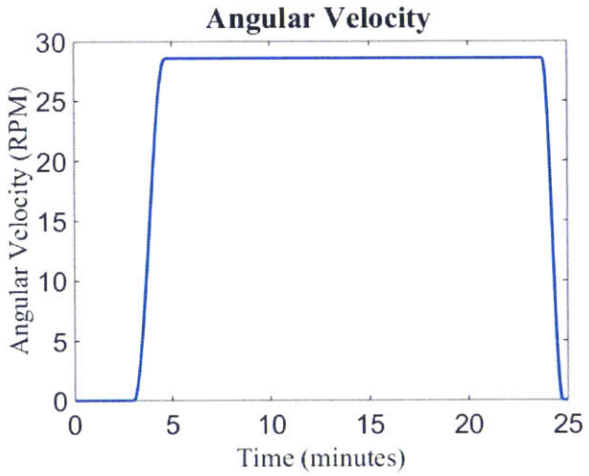

Figure 50 – Angular velocity profile during "1G Centripetal" simulation.

5.2.1.1 Simulation Inputs

The previously described mechanisms to simulate exercise were implemented, and the total vascular resistance and the mean blood pressure were chosen as input variables to the simulations. Therefore, the exercise parameters were manually adjusted to match, as well as possible (as judge by visual inspection), these two variables over time with their experimental values gathered during the centrifuge runs.

The decrease in total vascular resistance was primarily simulated by disconnecting the leg peripheral resistance from the control systems at the onset of exercise, and decreasing it using the exponential function described in Section 5.1.5.1.2 and reproduced here again:

$$R_{lc}(t) = R_{lc}^{-} + \left(R_{lf} - R_{lc}^{-}\right)(1 - e^{-t/\tau})$$

where R_{lc}^{-} is the leg vascular resistance immediately before the onset of an exercise phase, R_{lf} is the final leg vascular resistance for a given exercise intensity, and τ is a time constant. This process was repeated at every workload transition adjusting the final resistance and the time constant to match the experimental data.

In this model, the total peripheral resistance is composed of four systemic microvascular resistances: upper body R_{ub}, kidneys R_{rc}, splanchnic R_{sc}, and legs R_{lc}. The total peripheral resistance is then the parallel combination of the four microvascular resistances. To simulate the total vascular resistance more accurately, all four microvascular resistances were disconnected from the control systems at the onset of exercise, and their values were adjusted using the exponential function described above so that the total peripheral resistance matched the experimental data. The final resistances during each one of the exercises phases are presented in Table 27.

Table 27 – Microvascular resistance values during "1G Centripetal" simulations.

	Microcirculation (PRU)			
	Upper body	Kidneys	Splanchnic	Legs
Before exercise	3.3	4.1	2.4	3.9
Exercise: 25W	4.5	4.7	3.6	1.1
Exercise: 50W	4.6	4.8	3.7	0.75
Exercise: 100W	4.8	5.0	3.9	0.54

The leg resistance R_{lc} is the one that drove the total peripheral resistance to decrease in order to increase the blood flow to the working muscles located in the legs. The other three resistances slightly increased due to the increase in sympathetic outflow due to exercise and centrifugation.

Figure 51 shows the experimental (blue line: mean ± SE) and simulated (orange line) total vascular resistance at the reference condition "1G Centripetal". Before the exercise period, the simulated total vascular resistance responded appropriately to the orthostatic stress created by centrifugation. Thus, at the beginning of the spin-up phase the simulated resistance slightly decreased, followed by a noticeable increase due to the arterial baroreflex and cardiopulmonary reflex control systems. During the exercise period, the simulated total vascular resistance was composed of three exponentials curves corresponding each to one of the three workload intensities. The recovery after exercise was simulated using a quarter-sine functions.

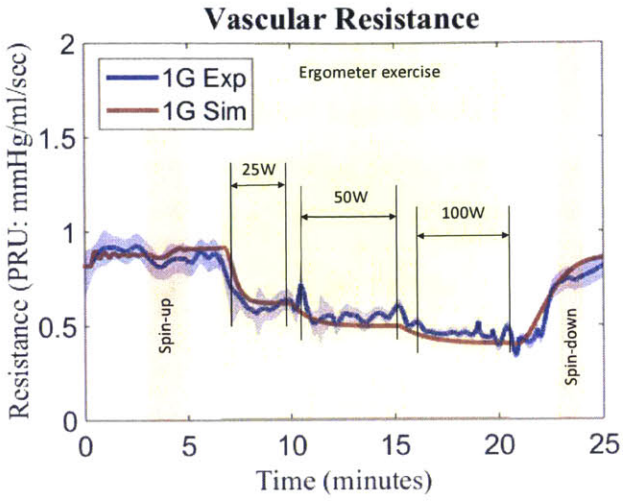

Figure 51 – Experimental (mean ± SE) and simulated total vascular resistance at condition "1G Centripetal".

The mean blood pressure was also selected as an input for the simulations. The arterial blood pressure set-point and the external pressure due to leg muscle pump were manually adjusted such that the mean blood pressure matched the experimental data to the best extent possible (visual criterion). Table 28 shows the values of these exercise parameters through the simulation.

Table 28 – Exercise parameters during the "1G Centripetal" simulation.

Simulation phase	Arterial set-point P_A^{sp} (mmHg)	Leg external pressure P_{max} due to muscle pump (mmHg)
Rest	95	0
After Spin-up	95	20 (constant)
Exercise: 25W	120	50 (periodic 1 sec)
Exercise: 50W	140	63 (periodic 1 sec)
Exercise: 100W	220	67 (periodic 1sec)
Before Spin-down	105	20 (constant)
Rest	105	0

The nominal arterial set-point P_A^{sp} was 95 mmHg. This value was maintained until the beginning of exercise. Then, the arterial set-point increased according to the exercise intensity. When the exercise was

completed, the arterial set-point was fixed to 105 mmHg, a slightly higher pressure than the nominal value of 95 mmHg, to capture the exercise recuperation process. Figure 52 shows the evolution of the arterial set-point P_A^{sp} during the exercise protocol simulation. The transitions between phases were defined by exponential functions in order to better capture the experimental responses. The time constants were chosen such that the simulation matched the experimental data as well as possible.

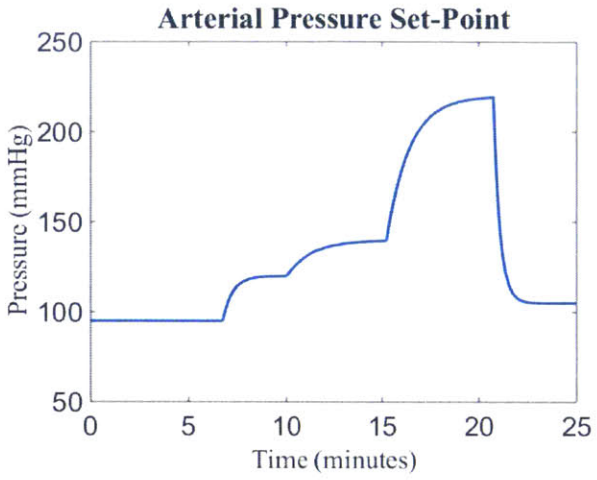

Figure 52 – Arterial pressure set-point P_A^{sp} during the "1G Centripetal" simulation.

The external pressure exerted by the leg muscles is represented in Figure 53. During the three exercise phases the external pressure is periodic (period = 1s, similar to the experimental protocol), according to the mathematical function described in Section 5.1.5.1.3 and reproduced here:

$$P_{ext} = \begin{cases} P_{max}\frac{1}{2}(1-\cos(4\pi t)) & 0 \le t \le 1/4 \\ P_{max} & 1/4 \le t < 1/2 \\ P_{max}\frac{1}{2}(1+\cos(4\pi(t-1/2))) & 1/2 \le t < 3/4 \\ 0 & 3/4 \le t < 1 \end{cases}$$

The maximal external pressure P_{max} (see Table 28) increased according to the exercise intensity. In Figure 53, the exercise period corresponds to the filled potion of the graph (pressure periodically attains P_{max} and 0 mmHg). In addition to this periodic external pressure during ergometer exercise, a constant pressure was added when subjects were not cycling but they were being centrifuged. Experimental data have shown that foot forces increased during centrifugation. This external pressure models the effects of leg muscle activation when subjects were being pushed against the pedals.

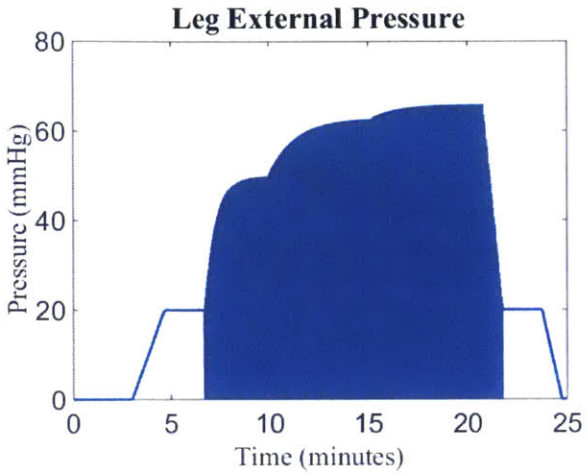

Figure 53 – Leg external pressure due to muscle pump during the "1G Centripetal" simulation.

Transitions between exercise phases were exponential to better capture the experimental behavior (the time constants were manually chosen such that the simulation matched the experimental data to be best extent possible using a visual criterion). Transitions between spin-up and spin-down phases were linear.

Figure 54 depicts the experimental (blue line: mean ± SE) and simulated (orange line) mean blood pressure at the reference condition "1G Centripetal". During the initial baseline period, the simulated mean blood pressure was still converging to a more stable pressure value. This was probably due to the low initial blood pressure calculated with the initial condition equations (see Appendix F). However, the pressure seemed to attain a stable value before starting the dynamic phases of the simulation. In general, the simulated mean blood pressure followed very closely the experimental data. The spin-up and spin-down processes were very well captured, and the transitions between exercise levels were also well reproduced. During the exercise phases the simulated pressure oscillated between a maximum and a minimum value caused by the muscle pump effect, but the average pressure simulated the experimental data reasonably well (within the SE). Pressure averages and differences (in %) between simulated and experimental data at each stage of the protocol are given at the end of the section in Table 30.

Finally, the increase in intra-abdominal pressure was the last mechanism to include in the exercise modeling methodology. The intra-abdominal pressure increased according to the exercise intensity. The intra-abdominal pressure values were estimated from the literature [63] and they are summarized in Table 29. Figure 55 depicts the intra-abdominal pressure simulated during the simulation. The transitions between exercise phases were also exponential functions, and the final decay represented the recuperation process after intense exercise.

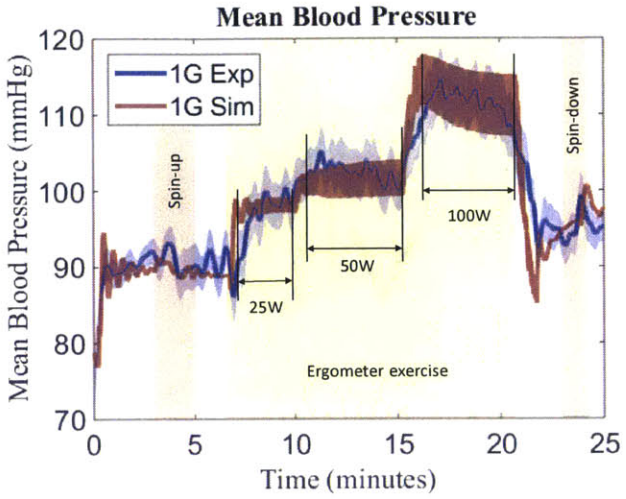

Figure 54 – Experimental (mean ± SE) and simulated mean blood pressure at condition "1G Centripetal".

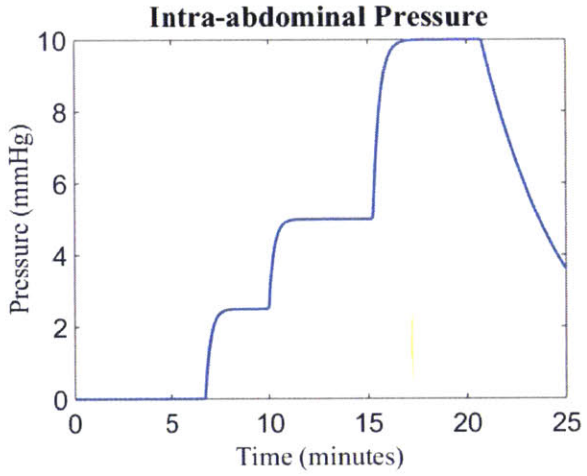

Figure 55 – Intra-abdominal pressure during the "1G Centripetal" simulation.

Table 29 – Intra-abdominal pressure during the "1G Centripetal" simulation.

Simulation phase	Intra-abdominal pressure (mmHg)
Before exercise	0
Exercise: 25W	2.5
Exercise: 50W	5
Exercise: 100W	10

5.2.1.2 Simulation Outputs

Two exercise parameters were used to adjust the simulated blood pressure (arterial pressure set-point, and leg muscles external pressure) and therefore, there are several combinations of these two parameters that would have yielded similar blood pressure results. Although the nature of the cardiovascular responses made these solutions very similar to one another (the exercise effect seemed to be predominant), there was a small ambiguity to be resolved while choosing the final exercise parameters. In order to select the final set of parameters amongst these close solutions, the heart rate data were also taken into account as a secondary input. Thus, although only to a very small extent, the final choice of the exercise parameters was somehow driven by the heart rate responses during the exercise phases. Figure 56 shows the experimental and simulated hear rate during the "1G Centripetal" condition.

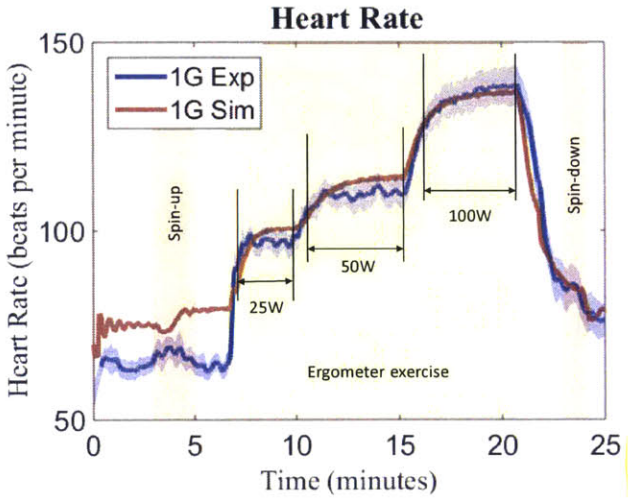

Figure 56 – Experimental (mean ± SE) and simulated heart rate at condition "1G Centripetal".

During the first three minutes of the simulation, the simulated average heart rate (75 bpm) was around 14% larger than the experimental data (66 bpm). Model results and comparisons during this baseline period are particularly interesting since they provide a good indication of the cardiovascular modeling performance without any other stressor such as centrifugation or exercise. The simulated heart rate responded properly to the orthostatic stress by increasing to 79 bpm during the spin-up phase. When the exercise started, the simulated heart rate followed within one SE the experimental data, partly because, as already mentioned, the exercise parameters were chosen to take into account to some extent the heart rate responses. Average data for HR and other CV variables are summarized in Table 30 at the end of the section.

Figure 57 and Figure 58 show the experimental (mean ± SE) and simulated cardiac output and stroke volume respectively. Both simulated variables captured very successfully the dynamics of the protocol, including the centrifugation phases as well as exercise phases. During the baseline period (first three minutes), the simulated cardiac output (5.6 l/min on average) was approximately within one SE of the experimental data (6.1 l/min on average). This corresponded to a difference of only -8%. However, the stroke volume during the same period was almost 21% smaller than the experimental stroke volume (75 ml vs. 95 ml). These results were in agreement with the higher simulated heart rate seen in Figure 56 (CO=SV*HR).

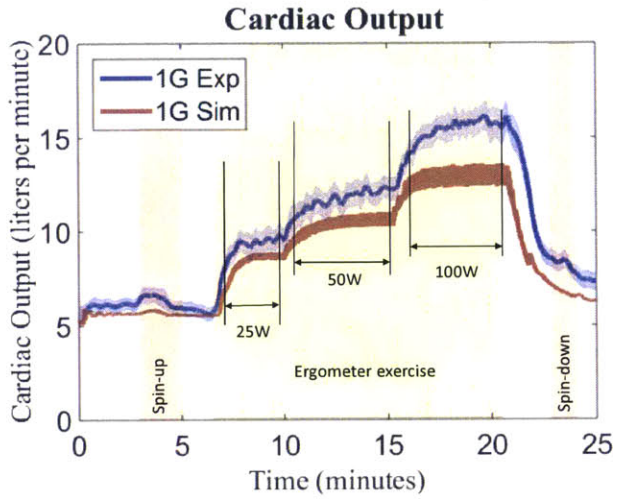

Figure 57 – Experimental (mean ± SE) and simulated cardiac output at condition "1G Centripetal".

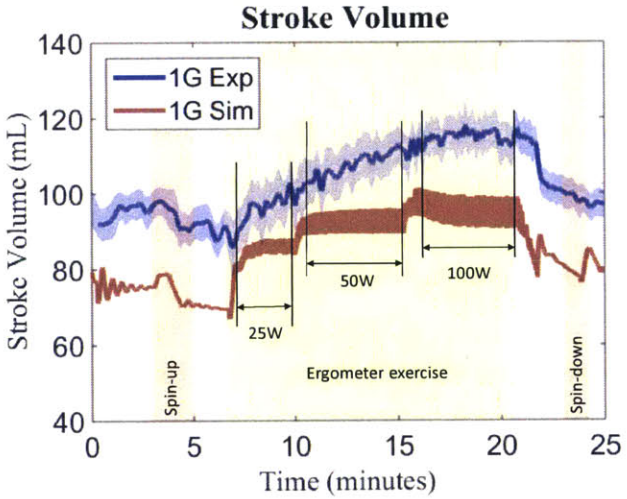

Figure 58 – Experimental (mean ± SE) and simulated stroke volume at condition "1G Centripetal".

The simulated cardiac output increased according to the exercise intensity, and the time constant at each transition consistently captured the dynamics of the cardiovascular progression. However, the difference with respect to the experimental data slightly increased with the exercise intensity. Then, the average cardiac outputs during the last two minutes at each exercise phase were smaller than the experimental values by 9% at 25W, 13% at 50W, and 18% at 100W.

Blood pressure data are shown in Figure 59, Figure 60 and Figure 61. Once more, the protocol dynamics were very well captured in the simulations, both the spin-up phase and the exercise transitions. Yet again, simulated data seemed to underestimate the experimental values. In the baseline period, systolic and diastolic blood pressures are 6% and 7% lower, respectively, than the data collected during the experiments. Since both pressures were reduced, the pulse pressure during this baseline period was fairly accurate (–5%), nearly within one SE until the beginning of the exercise period. During exercise, both systolic and diastolic pressure remained below the experimental data. The differences in percentages for each one of the three workload conditions (25W, 50W, and 100W) were –6%, –9%, and –10% for systolic blood pressure, and –8%, –7%, and –2% for diastolic blood pressure.

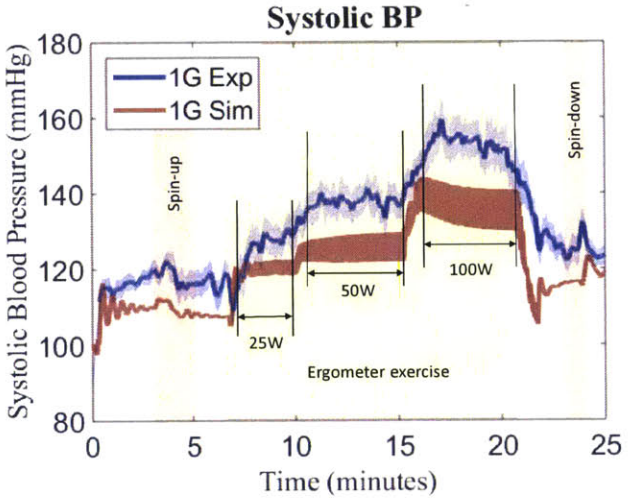

Figure 59 – Experimental (mean ± SE) and simulated systolic blood pressure at condition "1G Centripetal".

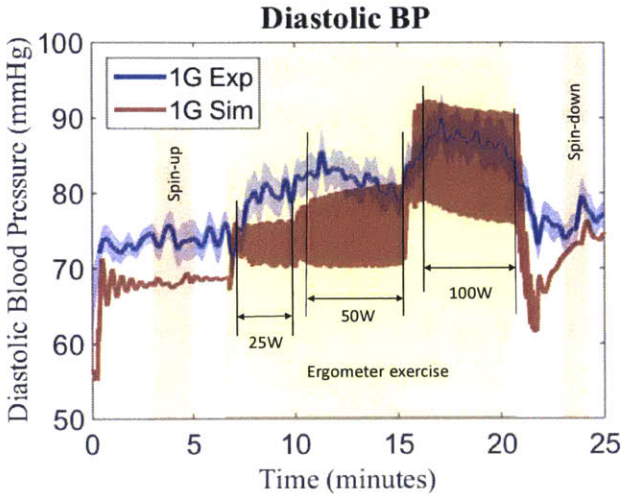

Figure 60 – Experimental (mean ± SE) and simulated diastolic blood pressure at condition "1G Centripetal".

The simulated pulse pressure showed an interesting behavior. Despite the lower systolic and diastolic pressures, the pulse pressure resulted to be within one SE of the experimental data during the baseline phase until the end of the 25W exercise period. In this first exercise phase, the difference with respect to the experimental data was just –2%. After the beginning of the 50W exercise phase, the simulated pulse pressure started deviating progressively from the experimental data, ending with an important difference in the 100W exercise phase of 13.5 mmHg (–21%). This difference was mostly due to the lower systolic pressure at 100W, since the diastolic pressure became fairly accurate, with a deviation of just –2%.

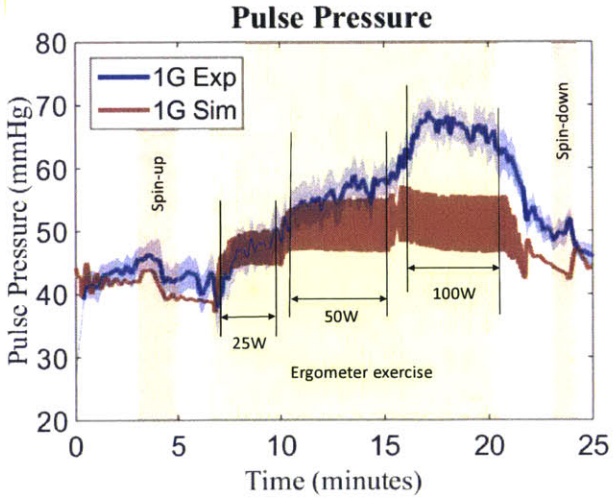

Figure 61 – Experimental (mean ± SE) and simulated pulse pressure at condition "1G Centripetal".

Table 30 summarized the averages of the CV variables during the different phases of the simulation: baseline (the first three minutes), exercise at 25W, exercise at 50W, and exercise at 100W. As in the experimental data, the averages during the exercise phases were calculated including only the last two minutes of each exercise period, in order to avoid the transitory episodes between phases. The last column of each phase (%) shows the deviation in percentage of the simulated results with respect to experimental data ($\frac{Sim-Exp}{Exp}$%).

Table 30 – Average of CV variables during the different periods of the simulation at "1G Centripetal".

CV	Baseline			Exercise 25W			Exercise 50W			Exercise 100W		
Variable	Sim	Exp	%	Sim	Exp	%	Sim	Exp	%	Sim	Exp	%
CO (l/min)	5.6	6.1	–8%	8.6	9.5	–9%	10.6	12.1	–13%	12.9	15.8	–18%
SV (ml)	75	95	–21%	86	98	–12%	93	110	–16%	94	115	–18%
HR (bpm)	75	66	14%	100	97	3%	114	110	3%	136	138	–1%
SBP (mmHg)	110	117	–6%	120	128	–6%	126	138	–9%	135	151	–10%
MBP (mmHg)	90	91	–1%	98	98	<–1%	102	102	<1%	111	111	<1%
DBP (mmHg)	67.8	73.1	–7%	73	80	–8%	75	81	–7%	84	86	–2%
PP (mmHg)	41.7	43.7	–5%	47	48	–2%	51	57	–12%	51	65	–21%

5.2.2 Simulation 1.4G

A similar analysis was completed concerning the "1.4G Centripetal" condition. In this case, subjects were exposed to 1.4G in the centripetal direction measured at the feet. This was equivalent to an angular velocity of approximately 33.9 rpm. The simulated centrifugation profile is shown in Figure 62 and it matched the experimental profile: 3-minute rest (baseline period), spin-up process to 33.9 rpm over 100 s, and spin-down deceleration at T = 23:45 over 1 min.

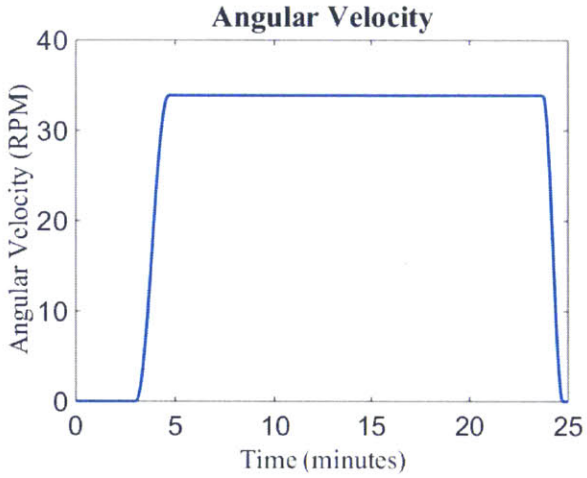

Figure 62 – Angular velocity profile during "1.4G Centripetal" simulation.

5.2.2.1 Simulation Inputs

As with the previous simulation, the total vascular resistance and the mean blood pressure were chosen as input variables, and the exercise parameters were manually chosen to match the simulations and the experimental data as well as possible, as judge by visual inspection.

The decrease in total peripheral resistance during the ergometer exercise was again simulated by disconnecting the four microvascular resistances (upper body R_{ub}, kidneys R_{rc}, splanchnic R_{sc}, and legs R_{lc}) from the baroreflex and cardiopulmonary control systems, and by adjusting their values using the exponential function described in the previous simulation. The resistance values during each one of the exercise phases are presented in Table 31. Since the experimental resistances in the "1G Centripetal" condition and "1.4G Centripetal" condition were very close to each other, these resistances values chosen here are almost identical to the ones used in the previous simulation. Figure 63 shows the experimental (blue line: mean ± SE) and simulated (orange line) total vascular resistance at the "1.4G Centripetal" condition.

Table 31 – Microvascular resistance values during "1.4G Centripetal" simulations.

	Microcirculation (PRU)			
	Upper body	Kidneys	Splanchnic	Legs
Before exercise	3.3	4.1	2.4	3.9
Exercise: 25W	4.5	4.7	3.6	1
Exercise: 50W	4.6	4.8	3.7	0.75
Exercise: 100W	4.8	5.0	3.9	0.54

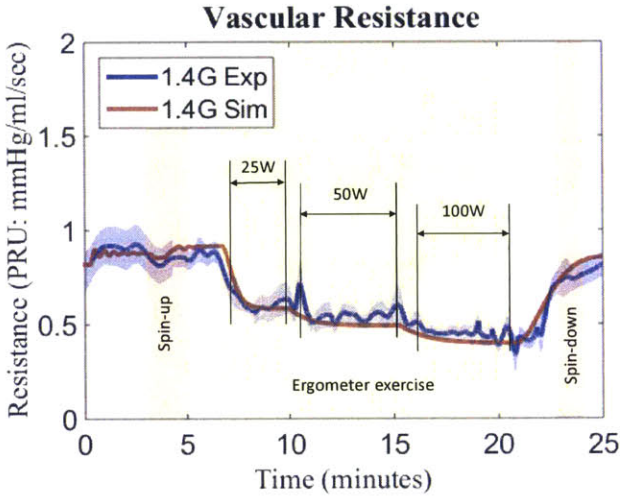

Figure 63 – Experimental (mean ± SE) and simulated total vascular resistance at condition "1.4G Centripetal".

During the spin-up phase, the simulated vascular resistance showed the expected dynamics due to the orthostatic stress and the consequent sympathetic reaction. The amplitude of the resistance response was slightly larger than in the previous simulation due to the higher AG level. This corresponded well with the experimental data. During the exercise period, the simulated total vascular resistance was composed of three exponential curves corresponding to each one of the three workload intensities. Finally, the recuperation after exercise was simulated using sinusoidal functions.

The second input variable was the mean blood pressure. Using the same procedure as in the previous simulation, the arterial blood pressure set-point and the external pressure due to leg muscle pump were manually adjusted such that the mean blood pressure matched the experimental data as well as possible (visual criterion). Table 32 shows the values of these exercise parameters throughout the simulation.

Table 32 – Exercise parameters during the "1.4G Centripetal" simulation.

Simulation phase	Arterial set-point P_A^{sp} (mmHg)	Leg external pressure P_{max} due to muscle pump (mmHg)
Rest	95	0
After Spin-up	95	30 (constant)
Exercise: 25W	127	83 (periodic 1 sec)
Exercise: 50W	150	96 (periodic 1 sec)
Exercise: 100W	240	100 (periodic 1sec)
Before Spin-down	105	30 (constant)
Rest	105	0

The nominal arterial set-point P_A^{sp} was again 95 mmHg, and this value was maintained until the beginning of the exercise. Then, the arterial set-point increased according to the exercise intensity. The magnitudes of these values were slightly larger than in the reference condition due to the effects of a higher gravity level. At the end of the exercise period, the arterial set-point was again fixed to 105 mmHg. The evolution of the arterial set-point P_A^{sp} throughout the simulation is shown in Figure 64. Transitions between levels were modeled as exponential functions, and the times constants were chosen to match the experimental data.

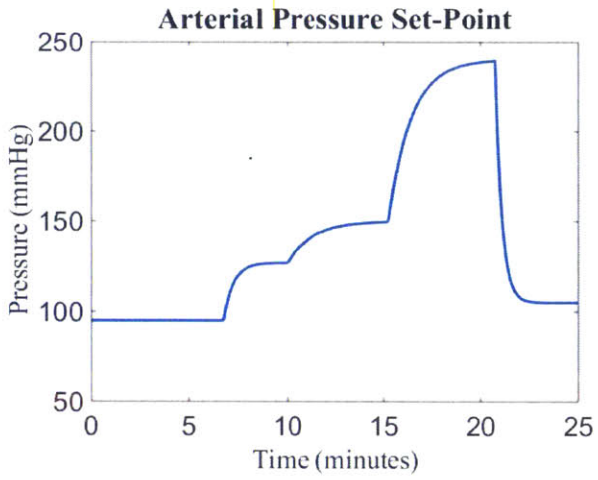

Figure 64 – Arterial pressure set-point P_A^{sp} during the "1.4G Centripetal" simulation.

The leg external pressure was simulated during the exercise phase using the same periodic function as before. The maximal external pressure P_{max} increased according to the exercise intensity. As with the arterial set-point pressure, the P_{max} values were slightly larger than the ones chosen in the reference simulation, due to the higher foot forces generated at higher AG level. Figure 65 shows the external pressure exerted by leg muscles during the simulation. The exercise period corresponded to the filled portion of the graph (pressure attaints periodically P_{max} and 0 mmHg). Furthermore, a constant pressure of 30 mmHg was also added when subjects were not cycling but they were being centrifuged, to take into account the leg muscle activation while subjects were pushed against the pedals.

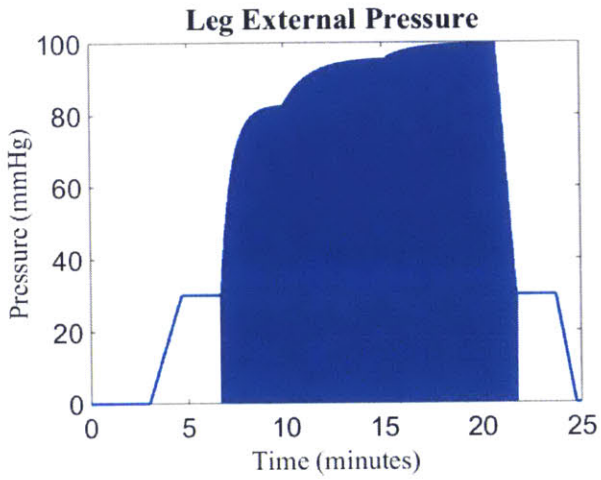

Figure 65 – Leg external pressure due to muscle pump during the "1.4G Centripetal" simulation.

Figure 66 shows the experimental (blue line: mean ± SE) and simulated (orange line) mean blood pressure at the"1.4G Centripetal" condition. The baseline period at "1.4G Centripetal" is exactly the same as at "1G Centripetal", and therefore the nominal arterial set-point P_A^{sp} was maintained to 95 mmHg, even though at "1.4G Centripetal" subjects showed an increasing blood pressure during this baseline period. Nevertheless, the difference is just around 3%. The simulated mean blood pressure replicated the experimental data remarkably well during the entire simulation. The average phase values for the mean blood pressure and other CV variables are listed in Table 34 located at the end of the section.

Finally, the intra-abdominal pressure was also included in the model, and it was characterized using the same parameters and exponential functions as in the reference simulation. The pressure values are summarized in Table 33, and Figure 55 shows the intra-abdominal pressure during the simulation.

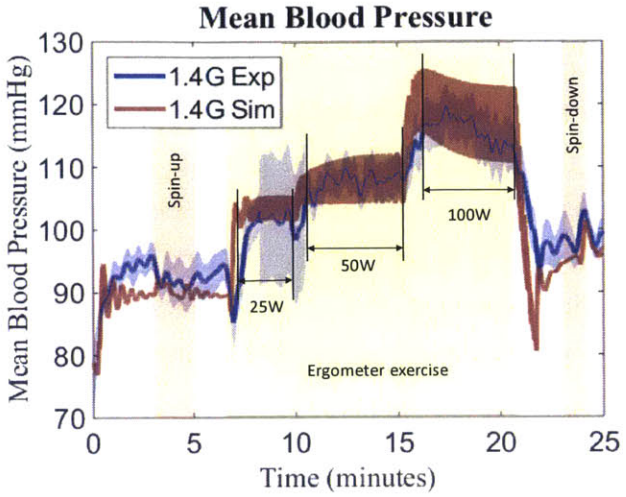

Figure 66 – Experimental (mean ± SE) and simulated mean blood pressure at condition "1.4G Centripetal".

Table 33 – Intra-abdominal pressure during the "1.4G Centripetal" simulation.

Simulation phase	Intra-abdominal pressure (mmHg)
Before exercise	0
Exercise: 25W	2.5
Exercise: 50W	5
Exercise: 100W	10

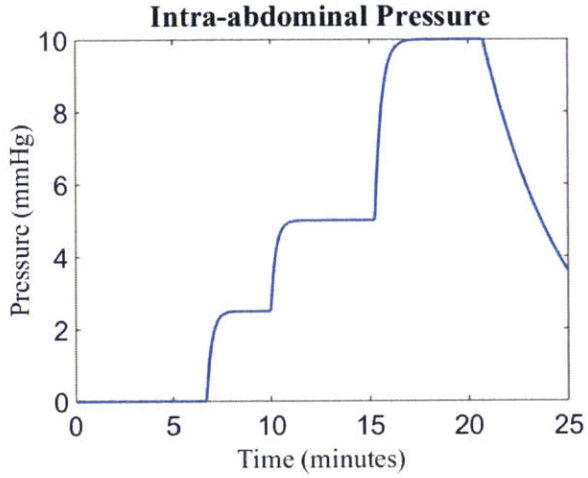

Figure 67 – Intra-abdominal pressure during the "1.4G Centripetal" simulation.

5.2.2.2 Simulation Outputs

As in the reference simulation, the final exercise parameters (arterial pressure set-point, and leg muscles external pressure) were also chosen taking into account to some extent the heart rate responses during the exercise phases. Figure 68 depicts the experimental (blue line: mean ± SE) and simulated (orange line) heart rate during the "1.4G Centripetal" condition.

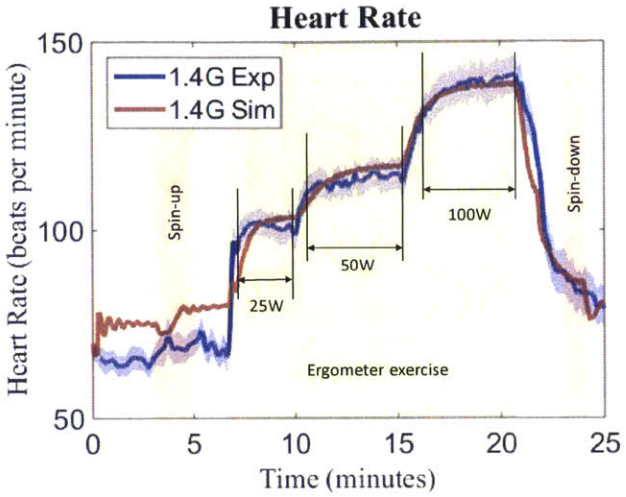

Figure 68 – Experimental (mean ± SE) and simulated heart rate at condition "1G Centripetal".

During the exercise period, and because of the previously mentioned parameter adjustments, the simulated heart rate response matched the experimental data extremely well (within 1 SE). Before the onset of the exercise, the simulation overestimated the subject's heart rate by around 15%. Nevertheless, the simulated heart rate responded appropriately to the higher 1.4G stress, increasing up to 80bpm after the spin-up phase. The simulation also followed very accurately the end of the exercise and the spin-down phase.

Figure 69 and Figure 70 show the experimental (mean ± SE) and simulated cardiac output and stroke volume respectively. Once more, both variables captured particularly well the dynamics of the protocol, both the centrifugation and the exercise. During the baseline period, results were expected to be very similar to "1G Centripetal" since the protocol was identical for both conditions. Thus, in the simulations at "1.4 Centripetal", the cardiac output was 5.6 l/min on average, while the experimental cardiac output was 6.3 l/min on average. This corresponded to an underestimation of 11%, which is very close to the 8% underestimation found in the "1G Centripetal" condition. During the same baseline period, the simulated stroke volume underestimated the experimental data by 23% (75ml vs. 78ml). This difference also

remains close to the 21% underestimation found in the "1G Condition". These results are in agreement with the higher simulated heart rate seen in Figure 68 (CO=SV*HR).

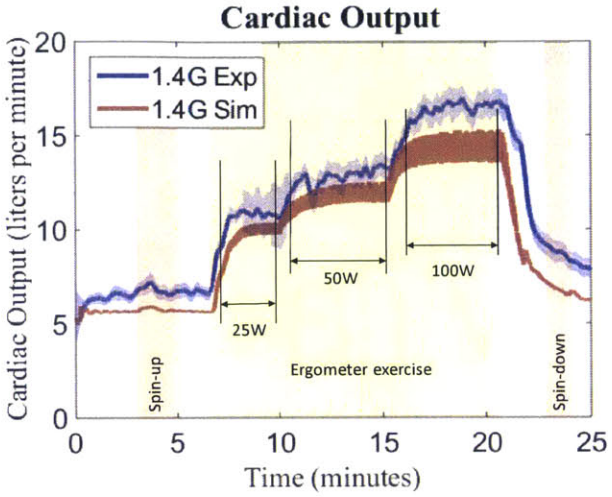

Figure 69 – Experimental (mean ± SE) and simulated cardiac output at condition "1.4G Centripetal".

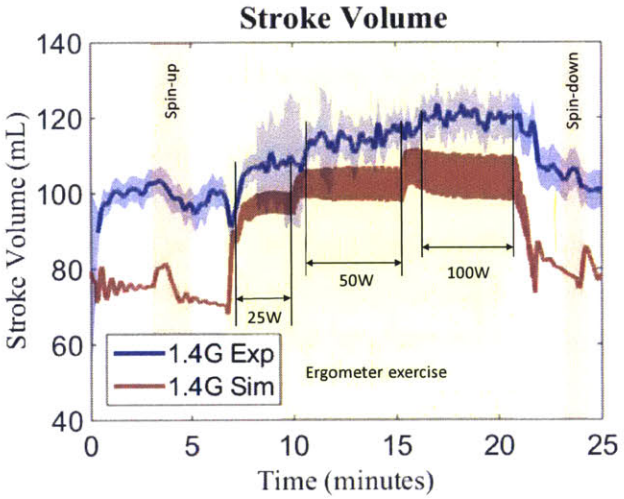

Figure 70 – Experimental (mean ± SE) and simulated stroke volume at condition "1.4G Centripetal".

Both the cardiac output and the stroke increased according to the exercise intensity, and they represented well the cardiovascular dynamics throughout the 25-min protocol. In particular, the cardiac output showed a very accurate time evolution during the exercise transitions. As already seen in the "1G Centripetal" simulation, both simulated variables underestimated the experimental responses during the

exercise period. The cardiac outputs, averaged over the last two minutes at each exercise phase, were smaller than the experimental cardiac outputs by 8% at 25W, 9% at 50W, and 14% at 100W. The underestimations in percentage for the stroke volume were 10% at 25W, 11% at 50W, and 14% at 100W. These differences were similar to the ones obtained for the reference condition.

Blood pressure data are shown in Figure 71, Figure 72, and Figure 73. The simulation data showed similar results to previous simulation: a good representation of the cardiovascular dynamics, and a general underestimation of the pressure throughout the protocol.

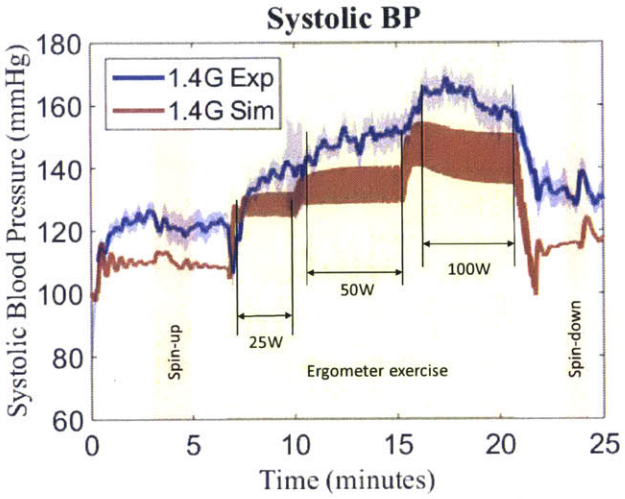

Figure 71 – Experimental (mean ± SE) and simulated systolic blood pressure at condition "1.4G Centripetal".

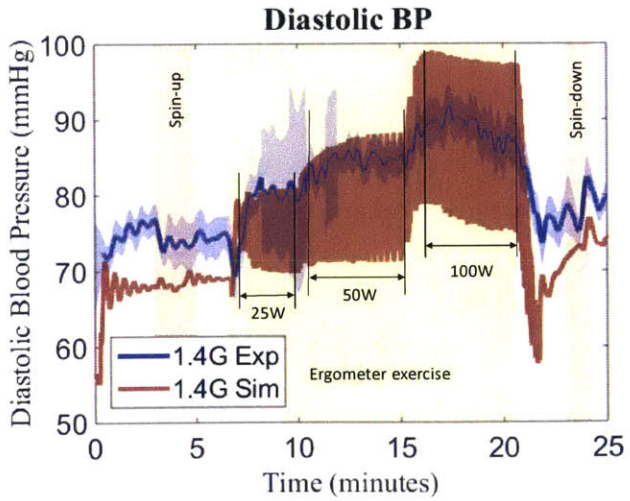

Figure 72 – Experimental (mean ± SE) and simulated diastolic blood pressure at condition "1.4G Centripetal".

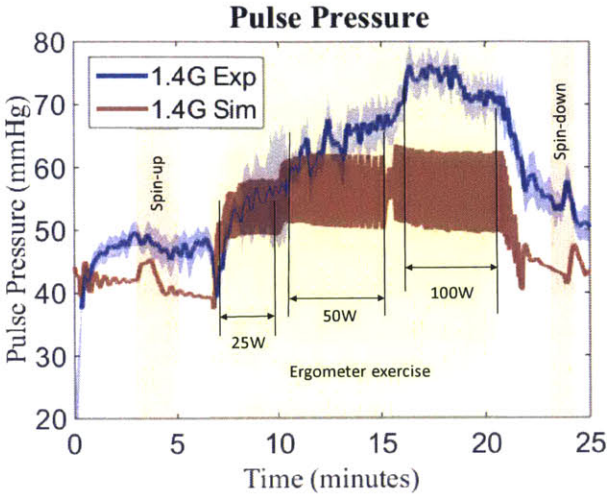

Figure 73 – Experimental (mean ± SE) and simulated pulse pressure at condition "1.4G Centripetal".

During the baseline period, the systolic and diastolic blood pressures were 10% and 9% lower than the data collected during the experiments. The pulse pressure was underestimated by 11% in this same period. Concerning exercise, the differences in percentages for each one of the three workload conditions (25W, 50W, and 100W) were –6%, –11%, and –10% for systolic blood pressure, and –7%, –7%, and <1% for diastolic blood pressure. The differences for pulse pressure were –3%, –16%, and –21%.

Table 34 summarizes the averages of the CV variables during the different phases of the "1.4G Centripetal" simulation. The averages during the exercise phases, for both the simulated and experimental data, have been calculated including only the last two minutes of each exercise period. As in Table 30 (equivalent data for "1G Condition"), the last column of each phase (%) shows the deviation in percentage of the simulated results with respect to the experimental data ($\frac{Sim-Exp}{Exp}$%). In general, both tables show very similar error percentages across all CV variables and phases, indicating that the model performs consistently and reliably at two different working points in the cardiovascular spectrum.

Table 34 – Average of CV variables during the different periods of the simulation at "1.4G Centripetal".

CV Variable	Baseline			Exercise 25W			Exercise 50W			Exercise 100W		
	Sim	Exp	%	Sim	Exp	%	Sim	Exp	%	Sim	Exp	%
CO (l/min)	5.6	6.3	–11%	10	10.9	–8%	11.9	13.1	–9%	14.3	16.6	–14%
SV (ml)	75	98	–23%	97	108	–10%	102	115	–11%	104	120	–14%
HR (bpm)	75	65	15%	103	101	2%	117	114	2%	138	140	–1%
SBP (mmHg)	110	122	–10%	129	137	–6%	135	151	–11%	143	159	–10%
MBP (mmHg)	90	93	–3%	104	103	<1%	108	108	<1%	117	114	3%
DBP (mmHg)	68	74	–8%	76	82	–7%	79	85	–7%	87	87	<1%
PP (mmHg)	42	47	–11%	53	55	–3%	56	66	–16%	56	71	–21%

5.3 Model Exploration

Once evaluated using the experimental data, the cardiovascular model could be further analyzed to identify the influence of different AG parameters. In this section, two case studies were explored. The objective of the first case study, detailed in Section 5.3.1, was to understand the effect of the distance from the head to the center of rotation (*h*). This is an important parameter because it affects two AG variables at the same time: the gravity level and the gravity gradient experienced by subjects (assuming constant angular velocity). Therefore, this parameter is particularly interesting to understand some of the important AG trade-offs.

In addition, cardiovascular responses of 0-g adapted subjects were also investigated in Section 5.3.2. Previous analyses have shown that total blood volume had a strong impact on the hemodynamic responses during orthostatic stress [63], making this case study particularly relevant and realistic for future in-flight AG related activities. Simulations of hypovolemic subjects were analyzed in order to investigate the effects of artificial gravity combined with exercise on physiologically deconditioned subjects.

5.3.1 Effect of distance to the center of rotation

The computational model was used to explore the cardiovascular responses to the 25-min exercise protocol while varying the subject's positioning on the centrifuge. In particular, the distance from the subject's head to the centrifuge center of rotation, h, was sequentially increased from $h=0$ cm to $h=60$ cm while keeping the rest of the centrifuge configuration constant. The "1G Centripetal" condition was chosen as the reference simulation, and the effects of centrifugation and exercise were simulated using the same methodology as already described.

Figure 74 depicts the vascular resistance simulated at various levels of h: 0, 20, 40, and 60 cm. As already explained in previous sections, the resistance was disconnected from the controls at the onset of exercise and it was manually adjusted to match the experimental data. Since the objective of this section is to study the isolated effect of the parameter h (distance from subject's head to the centrifuge center of rotation), the total peripheral resistance during the exercise phases was kept similar to the "1G Centripetal" reference condition. Thus, as seen in Figure 74, all four simulated cases were adjusted using the same resistance values.

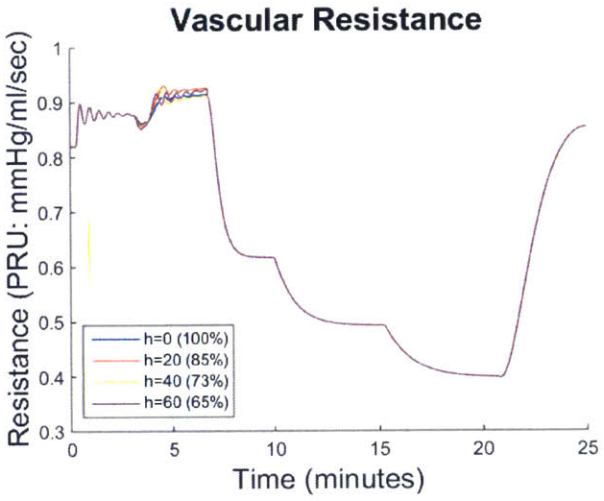

Figure 74 – Simulated total vascular resistance at different *h (cm)* values (h = distance from the head to the center of rotation. The value in parenthesis indicates the gravity gradient).

On the other hand, changes in h induced slight modifications in the exercise parameters, particularly in the arterial blood pressure set-point P_A^{sp}, and the leg muscle pump external pressure P_{max}. As seen in the model evaluation, the increase in artificial gravity from 1G to 1.4G (measured at subject's feet) led to higher foot forces and ultimately to an increase in the exercise parameters. In this case, increasing the

parameter h also led to an increase in artificial gravity (this time due to the increase in radius and not because of angular velocity, which was kept constant) and therefore the exercise parameters were changed accordingly. Exercise parameters at 1G and 1.4G were used as references and the exercise parameters concerning the simulated h levels were linearly adjusted based on those reference cases. For example, the artificial gravity level at the subject's feet when h=20 cm was approximately 1.2G in the centripetal direction. Therefore, the exercise parameters in this condition were midway between the values selected at 1G and 1.4G. In the same manner, for the rest of the conditions the exercise parameters were also properly interpolated. Table 35 summarizes the arterial pressure set-point P_A^{sp}, and the leg muscle pump external pressure P_{max}. corresponding to the simulated h values.

Table 35 – Exercise parameters at different h values.

Simulation phase	Arterial set-point P_A^{sp} (mmHg)				Leg external pressure P_{max} due to muscle pump (mmHg)			
	h = 0 (cm)	h = 20 (cm)	h = 40 (cm)	h = 60 (cm)	h = 0 (cm)	h = 20 (cm)	h = 40 (cm)	h = 60 (cm)
Rest	95	95	95	95	0	0	0	0
After Spin-up	95	95	95	95	20	24.7	29.3	33.9
Exercise: 25W	120	123.3	126.5	129.7	50*	65.6*	80.7*	95.7*
Exercise: 50W	140	144.7	149.3	153.9	63*	78.6*	93.7*	108.7*
Exercise: 100W	220	229.4	238.6	247.7	67*	82.6*	97.7*	112.7*
Before Spin-down	105	105	105	105	20	24.7	29.3	33.9
Rest	105	105	105	105	0	0	0	0

*Periodic 1 sec

Figure 75 and Figure 76 show the evolution of the selected exercise parameters for each one of the simulated h values during the exercise protocol. In Figure 75, the arterial pressure set-point P_A^{sp} during the exercise phases increased with h (the distance from subject's head to the centrifuge center of rotation in cm). The percentage seen in parenthesis corresponds to the gravity gradient experienced by subjects in these centrifuge configurations. Thus, given the CRC MIT configuration, a subject with his head at 60 cm from the centrifuge center of rotation would experience 0.55G at the head, and 1.55G at the feet, creating a gravity gradient along the body of 65%. Table 36 summarizes the G levels and gravity gradient percentages experienced at each one of the simulated h values. Similarly, Figure 76 shows the leg external pressure P_{max} due to the muscle pump effect during the four simulations (the periodic aspect of the function has not been included in the graph to facilitate the distinction of all 4 curves)

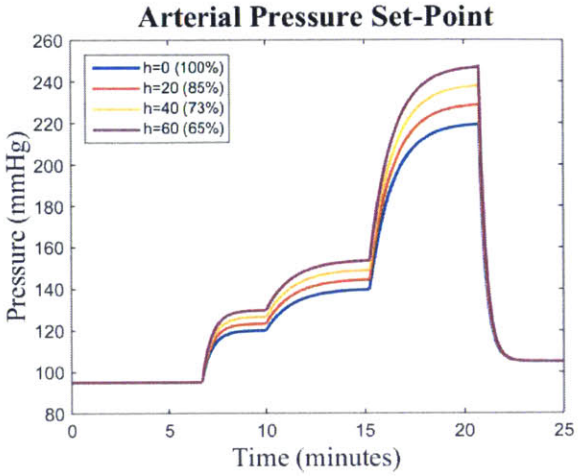

Figure 75 – Arterial pressure set-point P_A^{sp} at different *h (cm)* values.

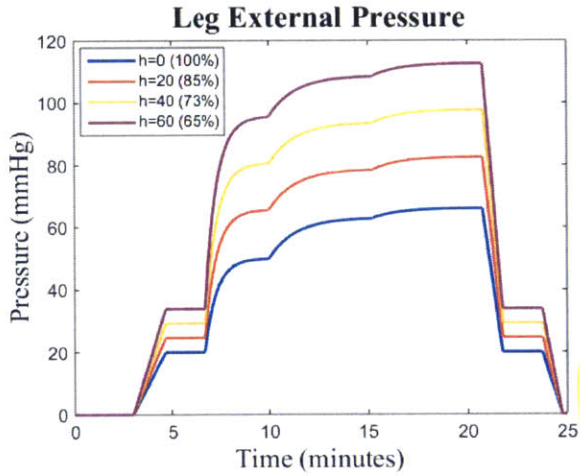

Figure 76 – Leg muscle pump external pressure P_{max} at different *h (cm)* values.

Table 36 – Acceleration levels and gravity gradient at different *h (cm)* values.

Head-Center Rotation	Acceleration Head (G's)	Acceleration Feet (G's)	Gravity Gradient
h = 0 cm	0	1	100%
h = 20 cm	0.18	1.19	84.6%
h = 40 cm	0.37	1.37	73.3%
h = 60 cm	0.55	1.55	64.7%

The following figures depict the simulated cardiovascular responses to increasing h values. In order to understand the results, it is important to acknowledge that in these particular conditions, the cardiovascular responses were driven by two separate and opposite phenomena. On one hand, larger h values induced higher artificial gravity levels and therefore, the more intense pulling of blood to the lower body made more difficult for the cardiovascular system to maintain a proper performance. On the other hand, larger h values created higher foot forces and a generally harder exercise workout, which ultimately increased venous flow towards the heart, facilitating the overall cardiovascular regulation. In the end, each cardiovascular solution was a compromise between these two opposite processes.

Figure 77 and Figure 78 show the mean blood pressure and the heart rate during the exercise protocol at the selected h values. In the baseline period (first three minutes), all simulations overlapped with each other since there was not any rotation yet. When the centrifugation started, blood was pulled to the lower extremities. The heart, stimulated by the sympathetic outflow due to the control systems, responded by increasing its rate in order to keep the blood pressure at appropriate levels. Mean blood pressure increased with h, even though the artificial gravity levels were higher at larger h values. These results are certainly due to the effects of exercise, particularly the increase in venous pressure caused by the influence of the more intense exercise parameters. The same tendency continued during the exercise phases where, despite the more elevated gravity levels generated at larger h values, the exercise conditions were able to maintain, and even increase the blood pressure.

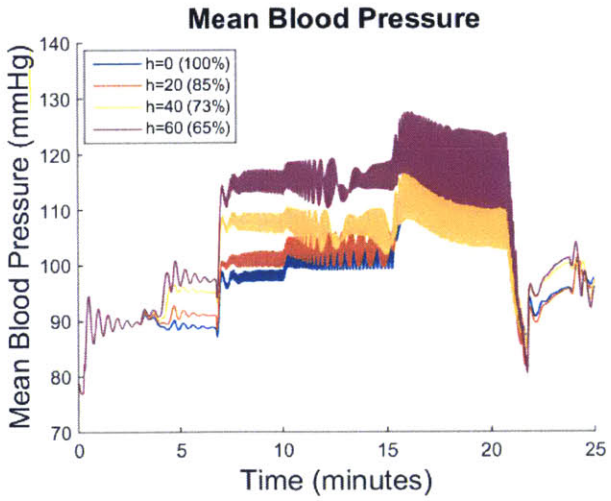

Figure 77 – Simulated mean blood pressure at different *h (cm)* values (*h* = distance from the head to the center of rotation. The value in parenthesis indicates the gravity gradient).

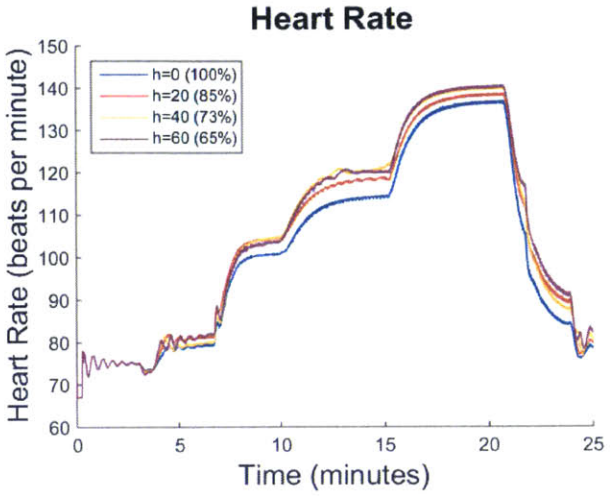

Figure 78 – Simulated heart rate at different *h (cm)* values (*h* = distance from the head to the center of rotation. The value in parenthesis indicates the gravity gradient).

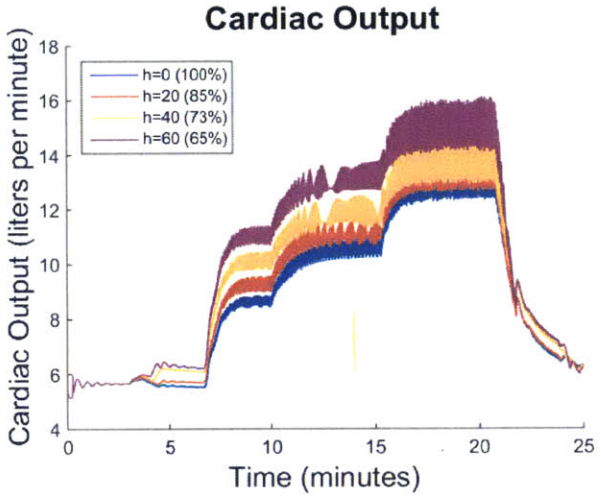

Figure 79 – Simulated cardiac output at different *h (cm)* values (*h* = distance from the head to the center of rotation. The value in parenthesis indicates the gravity gradient).

Averages of mean blood pressure and the rest of the cardiovascular variables at all conditions (including "Baseline", "After spin-up", "Exercise: 25W", "Exercise: 50W", and "Exercise: 100W") are summarized in Table 37 and Table 38. The averages in the exercise conditions were calculated taking into account the last two minutes of each phase. The column, $\%^{basel}$ shows the percentage change of the CV variables with respect to their baseline. This percentage gives an indication of how much the cardiovascular variables changed with respect to their baseline value due to centrifugation and exercise in each phase of the protocol.

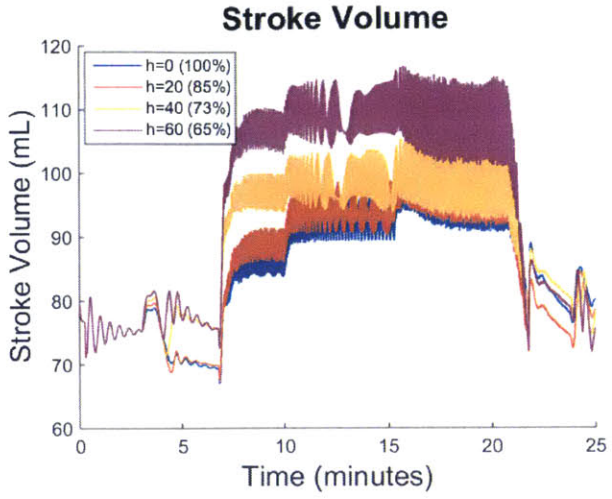

Figure 80 – Simulated stroke volume at different *h (cm)* values (*h* = distance from the head to the center of rotation. The value in parenthesis indicates the gravity gradient).

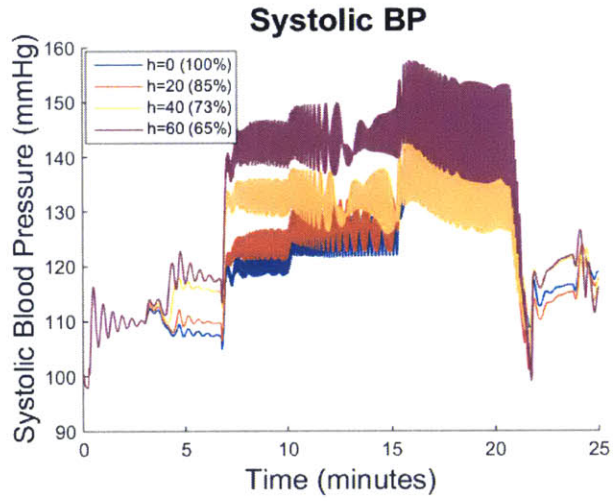

Figure 81 – Simulated systolic blood pressure at different *h (cm)* values (*h* = distance from the head to the center of rotation. The value in parenthesis indicates the gravity gradient).

The rest of the CV variables are shown from Figure 79 to Figure 83. In general, centrifugation at larger *h* levels increased the overall cardiovascular activity, as already seen in the mean blood pressure. Thus, at h=60 cm the cardiac output increased +13% (see Figure 79), the stroke volume increased +1% (see Figure 80), and the pulse pressure remained steady (instead of decreasing 7% when h=0 cm, see Figure 83). Similar results were seen in the systolic blood pressure (+7%, see Figure 81) and diastolic blood pressure (+10%, see Figure 82). Numerical values are summarized in the column "After Spin-up" in Table 37 and Table 38.

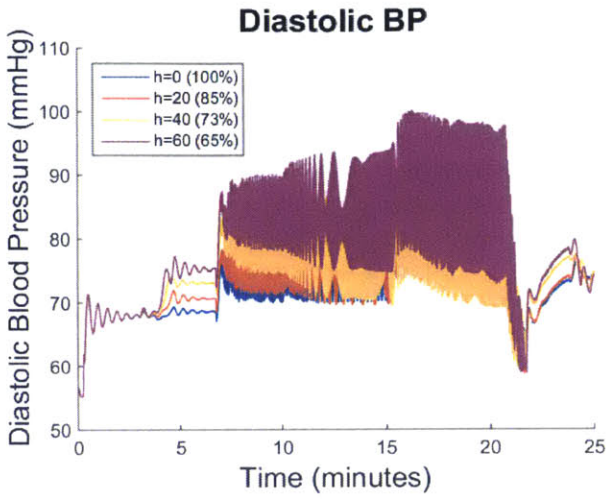

Figure 82 – Simulated diastolic blood pressure at different *h (cm)* values (*h* = distance from the head to the center of rotation. The value in parenthesis indicates the gravity gradient).

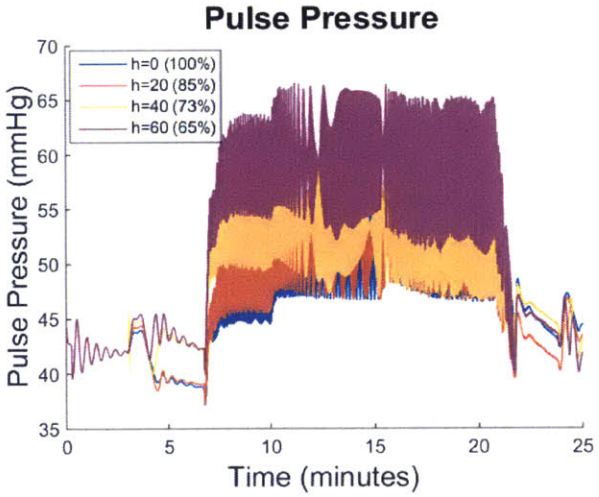

Figure 83 – Simulated pulse pressure at different *h (cm)* values (*h* = distance from the head to the center of rotation. The value in parenthesis indicates the gravity gradient).

As in the spin-up phase, the cardiovascular system seemed to perform adequately during the exercise phases. Again, despite the elevated artificial gravity levels generated at h=60 cm, the effects of exercise were able to maintain an appropriate overall cardiovascular regulation. In general, blood pressure, stroke volume, and cardiac output generally increased with *h* across all exercise conditions, indicating that the effect of exercise is more than enough to overcome the increasing pulling effect due to centrifugation.

These results emphasize the importance of exercise to maintain an appropriate and healthy cardiovascular regulation during orthostatic stress. In particular, ergometer exercise combined with artificial gravity facilitates venous return via periodic leg muscle contractions. In this simulation conditions, the ergometer exercise not only prevented the expected pressure loss due to increasing artificial gravity levels, but also produced a pressure increase that led to an intensification of the overall cardiovascular activity.

Averages values during the exercise phases are shown in Table 37 and Table 38, along with the % change with respect to their initial values at the baseline condition, which were similar for all *h* levels, since there was not any centrifugation yet.

Table 37 – Simulated CV variables systolic blood pressure (SBP), diastolic blood pressure (DBP), and pulse pressure (PP) varying the distance from head to center of rotation *h*.

Variable	Baseline	After Spin-up		Exercise: 25W		Exercise: 50W		Exercise: 100W	
SBP (mmHg)	Mean	Mean	$\%^{basel}$	Mean	$\%^{basel}$	Mean	$\%^{basel}$	Mean	$\%^{basel}$
h = 0 cm	110	107	–3%	120	9%	126	14%	135	23%
h = 20 cm	110	110	0%	124	13%	127	16%	135	23%
h = 40 cm	110	115	5%	133	21%	132	20%	134	22%
h = 60 cm	110	118	7%	143	30%	144	31%	144	31%
DBP (mmHg)	Mean	Mean	$\%^{basel}$	Mean	$\%^{basel}$	Mean	$\%^{basel}$	Mean	$\%^{basel}$
h = 0 cm	68	69	1%	73	8%	75	11%	84	23%
h = 20 cm	68	71	4%	76	11%	76	12%	82	21%
h = 40 cm	68	73	7%	80	17%	78	15%	81	18%
h = 60 cm	68	75	10%	84	24%	84	24%	86	27%
PP (mmHg)	Mean	Mean	$\%^{basel}$	Mean	$\%^{basel}$	Mean	$\%^{basel}$	Mean	$\%^{basel}$
h = 0 cm	42	39	–7%	47	12%	51	20%	51	23%
h = 20 cm	42	39	–7%	49	16%	51	22%	52	25%
h = 40 cm	42	42	0%	53	27%	54	28%	53	27%
h = 60 cm	42	42	0%	58	39%	60	42%	58	39%

Mean: average of CV variables in the indicated periods. In the exercise phases, the average has been calculated in the last two minutes to exclude transition effects. **$\%^{basel}$**: percentage with respect to the baseline value

Table 38 – Simulated CV variables mean blood pressure (MBP), heart rate (HR), cardiac output (CO), and stroke volume (SK) varying the distance from head to center of rotation *h*.

Variable	Baseline	After Spin-up		Exercise: 25W		Exercise: 50W		Exercise: 100W	
MBP (mmHg)	Mean	Mean	$\%^{basel}$	Mean	$\%^{basel}$	Mean	$\%^{basel}$	Mean	$\%^{basel}$
h = 0 cm	90	89	–1%	98	9%	102	13%	111	23%
h = 20 cm	90	91	1%	101	12%	103	15%	110	22%
h = 40 cm	90	95	6%	108	20%	107	18%	109	21%
h = 60 cm	90	97	8%	115	28%	116	29%	117	30%
HR (bpm)	Mean	Mean	$\%^{basel}$	Mean	$\%^{basel}$	Mean	$\%^{basel}$	Mean	$\%^{basel}$
h = 0 cm	75	79	5%	100	34%	114	52%	136	82%
h = 20 cm	75	81	8%	104	38%	118	58%	138	84%
h = 40 cm	75	80	7%	104	38%	120	61%	140	86%
h = 60 cm	75	82	9%	103	37%	120	60%	140	87%
CO (l/min)	Mean	Mean	$\%^{basel}$	Mean	$\%^{basel}$	Mean	$\%^{basel}$	Mean	$\%^{basel}$
h = 0 cm	5.6	5.5	–2%	8.6	54%	10.6	89%	12.9	130%
h = 20 cm	5.6	5.7	2%	9.2	64%	11.1	99%	13.3	138%
h = 40 cm	5.6	6.1	9%	10.1	80%	11.9	112%	13.7	145%
h = 60 cm	5.6	6.3	13%	11.0	96%	13.2	135%	15.0	169%
SV (ml)	Mean	Mean	$\%^{basel}$	Mean	$\%^{basel}$	Mean	$\%^{basel}$	Mean	$\%^{basel}$
h = 0 cm	75	69	–8%	86	14%	93	23%	94	26%
h = 20 cm	75	70	–7%	89	18%	94	25%	96	28%
h = 40 cm	75	76	1%	97	29%	99	32%	98	31%
h = 60 cm	75	76	1%	107	42%	110	46%	107	43%

Mean: average of CV variables in the indicated periods. In the exercise phases, the average has been calculated in the last two minutes to exclude transition effects. **$\%^{basel}$**: percentage with respect to the baseline value

5.3.2 Cardiovascular responses of 0-g adapted subjects

One of the main cardiovascular consequences of exposure to the microgravity environment is the reduction in total blood volume, plasma volume, and red blood cells. In space, the absence of hydrostatic pressure causes the blood that is usually located in the lower extremities to shift upwards to the upper extremities, creating an excess of fluid around the thorax. The stretch of the cardiopulmonary receptors leads to the inhibition of the sympathetic reflexes causing vasodilation, particularly in the renal arterioles and thus, increasing the urinary output. In addition, the stretch in the atrial stretch receptors produces a decrease in the secretion of antidiuretic hormone (ADH) and in the production of renin, also contributing to the decrease in blood volume. The cardiovascular deconditioning seen in space stabilizes over a period of four to six weeks [94]. After this period, blood volume losses reach a typical value of 11% [2]. This is thought to be an important factor in post-flight orthostatic intolerance experienced by astronauts when they come back to a gravity environment after a long exposure to microgravity.

In order to gain insight into the cardiovascular behavior of 0-g adapted astronauts, the computational model previously described was used to explore the cardiovascular responses to the 25-min exercise protocol while varying the total blood volume. The reference condition "1G Centripetal" was chosen as the underlying simulation and therefore, all the centrifugation and exercise parameters used in the reference condition were maintained. The total blood volume used in the reference simulation was $V_{tot\_ref} = 5150\ ml$. This number was based on the assumption that, in the human body, there are 75 ml of blood per kg of mass. Therefore, a total blood volume of 5150 ml corresponds to a subject of approximately 69 Kg (the 12 subjects' average weight and standard deviation were: 69.3 ± 11.6 Kg.). In this section, the reference volume is rounded to $V_{ref} = 5100\ ml$ and the volume simulated ranged from $V = 4500\ ml$ to $V = 5700\ ml$, corresponding to approximately +/- 12% of nominal blood volume.

The effects of centrifugation and exercise were simulated using the same methodology as in the "1G Centripetal" reference condition. Figure 84 shows the vascular resistance simulated at various levels of total blood volume. The resistance during the baseline period increased with the reduction of total blood volume, due to a more elevated sympathetic outflow. In addition, the resistance change induced by centrifugation was larger at lower blood volume. At the onset of exercise, the resistance was disconnected from the controls and, as detailed in previous sections, was manually adjusted to match the experimental data. Since the objective of this section is to study the isolated effect of the total blood volume, the rest of parameters in the simulation were not modified, including the total peripheral resistance during the exercise phases. Thus, as seen in Figure 84, all five simulated cases were adjusted using the same reference values.

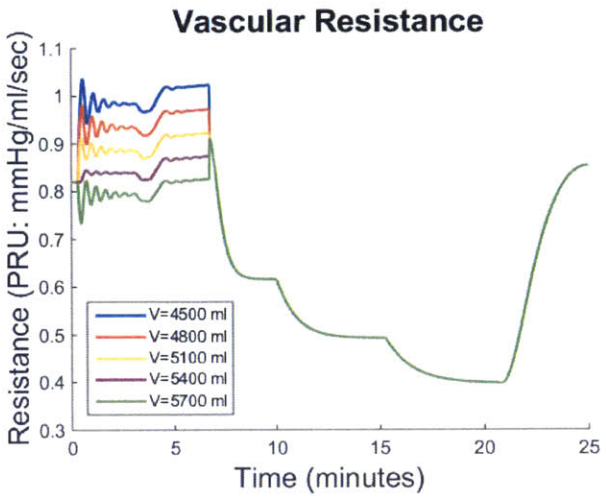

Figure 84 - Simulated total vascular resistance at different V (total blood volume).

Figure 85 and Figure 86 depict the mean blood pressure and the heart rate respectively at five different blood volume values. Simulations show that altering the total blood volume has two interesting outcomes: changes in the cardiovascular baseline operating point, and changes in the responses to centrifugation and exercise.

5.3.2.1 Changes in baseline cardiovascular operating points

Results showed that the level of total blood volume had an effect in the cardiovascular baseline operating point. Thus, in the baseline period (first three minutes), the MBP at the lowest total blood volume (V = 4500ml) was 81 mmHg, and the corresponding MBP at the reference total blood volume (Vref = 5100 ml) was 89 mmHg (see Figure 85). This is analogous to a decrease in 9%. The opposite behavior was seen when the total blood volume was increased. For example, the MBP at V=5700 ml was 95 mmHg, which is equivalent to a 7% increase with respect to the reference blood volume.

A similar change in the baseline operating point was observed in the rest of the cardiovascular variables. For example, as seen in Figure 85, the baseline heart rate increased 16% (82 to 88 bpm) from the reference condition (V = 5100 ml) to the lowest volume condition (V = 4500 ml). Averages of all cardiovascular variables at the baseline condition are summarized in the column "Baseline" in Table 39 and Table 40. The column $\%^{Vref}$ shows the percentage change of the baseline CV variables with respect to the Vref condition, where Vref = 5100 ml. Essentially this percentage gives an indication of how much the cardiovascular variables were shifted up or down when the total blood volume was manipulated.

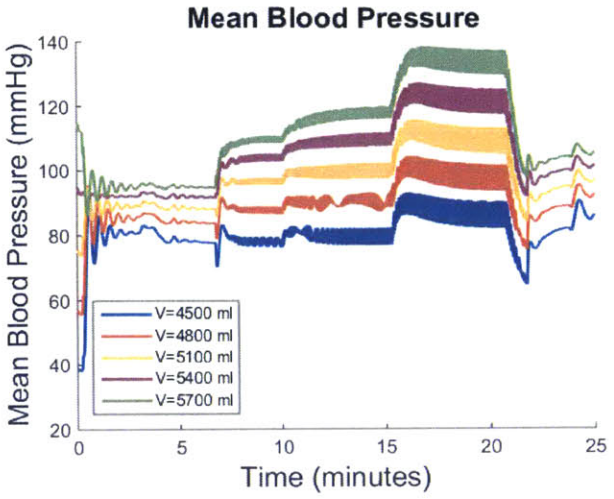

Figure 85 - Simulated mean blood pressure at different V (total blood volume).

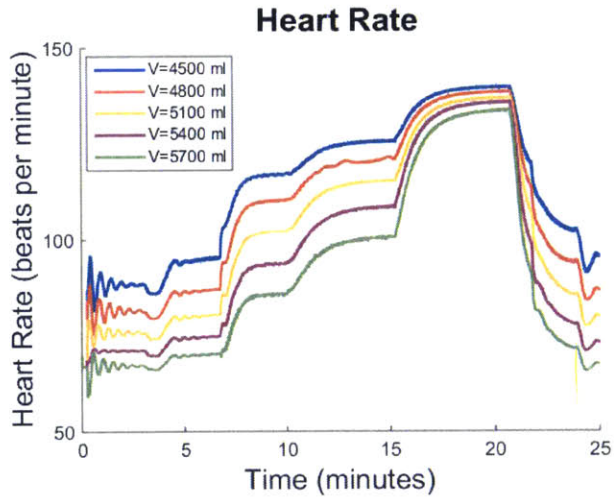

Figure 86 – Simulated heart rate at different V (total blood volume).

The rest of the CV variables are shown from Figure 87 to Figure 91. The manipulation of the blood volume resulted in shifts in the variables' baseline operating points, as already seen in the MBP or HR responses. At V= 4500 ml, where the blood volume was reduced by 12%, the blood pressure decreased, including systolic (–13%, see Figure 89), mean (–9%, see Figure 85), and to a lesser extent, diastolic blood pressure (–3%, see Figure 90). Consequently, the baseline pulse pressure also decreased (–27%, see Figure 91). In this cardiovascular conditions, the stroke volume operating point was highly reduced (–28%, see Figure 88), even though the control systems increased the heart rate (+16%, see Figure 86) in an attempt to compensate for the low pressure. In addition, cardiac output decreased by 16% (see Figure 87).

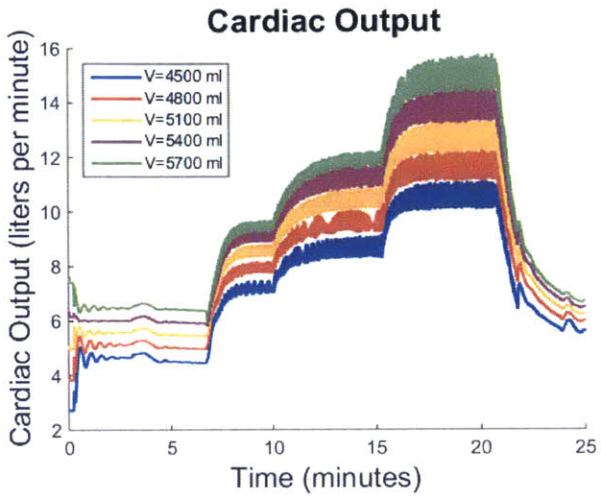

Figure 87 – Simulated cardiac output at different V (total blood volume).

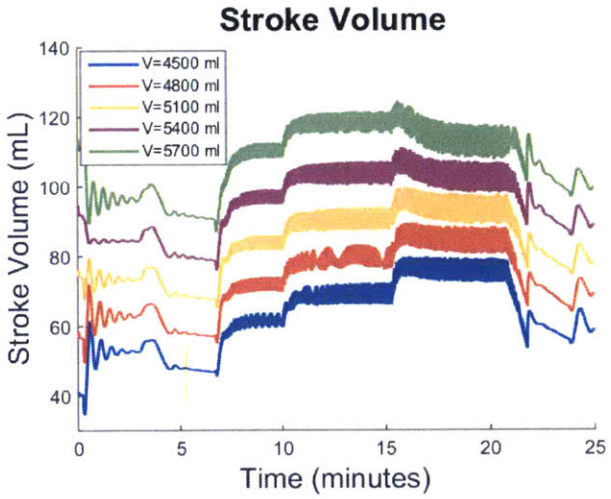

Figure 88 – Simulated stroke volume at different V (total blood volume).

In the case where the total blood volume was increased by 12 % to V=5700ml, the CV responses followed the opposite behavior. Hence, due to the larger blood volume, the blood pressure increased, including systolic (11%, see Figure 89), mean (7%, see Figure 85), and to a lesser extent, diastolic blood pressure (1%, see Figure 90). Consequently, the baseline pulse pressure also increased (30%, see Figure 91). In these cardiovascular conditions, the stroke volume operating point increased (+30%, see Figure 88). Due to the relatively high pressure, the control systems decreased the heart rate (–12%, see Figure 86). Finally, cardiac output increased by 16% (see Figure 87). Table 39 and Table 40 summarize the CV variables' baseline changes due to total blood volume alterations (first column "Baseline").

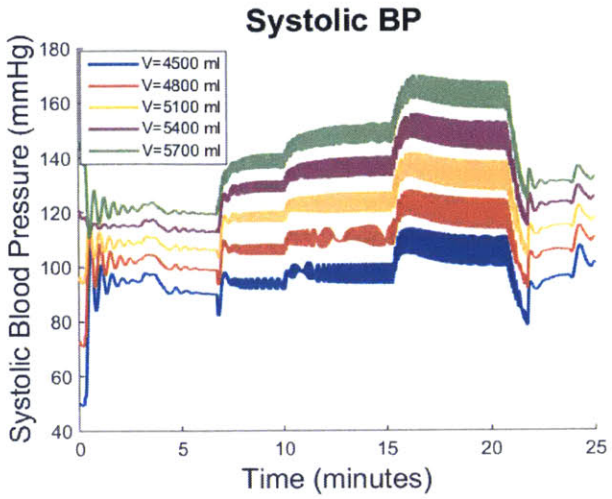

Figure 89 – Simulated systolic blood pressure at different V (total blood volume).

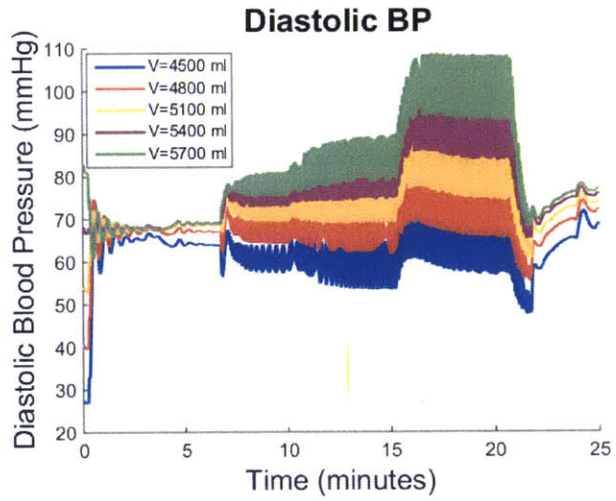

Figure 90 – Simulated diastolic blood pressure at different V (total blood volume).

5.3.2.2 Changes in cardiovascular responses to centrifugation and exercise

The second consequence of altering the total blood volume is the change in the cardiovascular system response capacity to stress such as centrifugation or exercise. The cardiovascular responses in the reference condition (Vref =5100 ml) during the centrifugation spin-up process included a slight increase in heart rate of 4 bpm (+5%, from 76 to 80 bpm, see Figure 86) in order to keep the mean blood pressure near constant (~89 mmHg, see Figure 85). As blood volume decreased, the changes experienced during spin-up by the heart rate and mean blood pressure became larger. Therefore, in the scenario with lower blood volume (V=4500 ml), the mean arterial pressure diminished by 4% (from 81 to 78 mmHg, see

Figure 85) even though the heart rate increased by 9% (from 88 to 99 bpm, see Figure 86) to compensate for the lower pressure. Hence, these simulations show that with a higher degree of hypovolemia, the blood pulling effect to the lower vasculature becomes more important, and therefore, it becomes more difficult for the cardiovascular system to maintain blood pressure at a proper level.

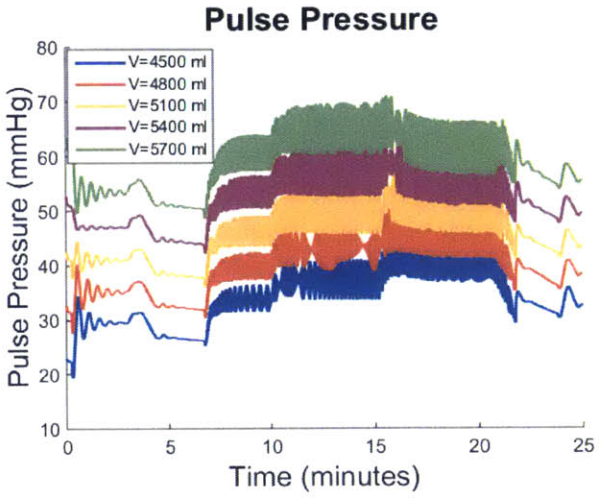

Figure 91 – Simulated pulse pressure at different V (total blood volume).

Averages of all cardiovascular variables at all conditions, including "Baseline", "After spin-up", "Exercise: 25W", "Exercise: 50W", and "Exercise: 100W", are summarized in Table 39 and Table 40. The averages in the exercise conditions were calculated taking into account only the last two minutes of each phase. As already mentioned, the column $\%^{Vref}$ shows the percentage change of the baseline CV variables with respect to the Vref condition, where Vref = 5100 ml. In addition, the column, $\%^{basel}$ shows the percentage change of the CV variables with respect to their own baseline (at the same V level). This percentage gives an indication of how much the cardiovascular variables changed with respect to their baseline value due to centrifugation and exercise.

In general, changes due to centrifugation were larger at the lower blood volume condition, as already seen in the blood pressure or heart rate responses described in previous paragraphs. Thus, at the lower blood volume level (V=4500ml) the cardiac output decreased –4%, the stroke volume decreased 11%, and the pulse pressure decreased 13 % due to centrifugation (see column "After Spin-up" in Table 39 and Table 40). These changes became less significant as blood is being added.

Table 39 – Simulated CV Variables mean blood pressure (MBP), heart rate (HR), cardiac output (CO), and strove volume (SV) varying the total blood volume *V*.

Variable	Baseline		After Spin-up		Exercise: 25W		Exercise: 50W		Exercise: 100W	
MBP (mmHg)	Mean	$\%^{Vref}$	Mean	$\%^{basel}$	Mean	$\%^{basel}$	Mean	$\%^{basel}$	Mean	$\%^{basel}$
V = 4500 ml	81	–9%	78	–4%	78	–3%	79	–2%	86	6%
V = 4800 ml	85	–4%	84	–1%	88	4%	91	7%	98	15%
V_{ref} = 5100 ml	89	0%	88	–1%	97	9%	100	13%	109	23%
V = 5400 ml	92	3%	92	0%	104	13%	110	20%	121	32%
V = 5700 ml	95	7%	95	0%	109	15%	118	24%	133	40%
HR (bpm)	Mean	$\%^{Vref}$	Mean	$\%^{basel}$	Mean	$\%^{basel}$	Mean	$\%^{basel}$	Mean	$\%^{basel}$
V = 4500 ml	88	16%	96	9%	117	33%	125	43%	140	59%
V = 4800 ml	82	8%	87	6%	110	34%	121	47%	138	69%
V_{ref} = 5100 ml	76	0%	80	5%	102	34%	115	51%	137	80%
V = 5400 ml	71	–7%	75	6%	93	31%	108	52%	135	91%
V = 5700 ml	67	–12%	70	4%	85	28%	100	50%	133	99%
CO (l/min)	Mean	$\%^{Vref}$	Mean	$\%^{basel}$	Mean	$\%^{basel}$	Mean	$\%^{basel}$	Mean	$\%^{basel}$
V = 4500 ml	4.7	–16%	4.5	–4%	7.1	52%	8.6	83%	10.5	124%
V = 4800 ml	5.2	–7%	5.0	–4%	7.9	52%	9.6	85%	11.6	123%
V_{ref} = 5100 ml	5.6	0%	5.8	4%	8.5	52%	10.4	86%	12.7	127%
V = 5400 ml	6.0	7%	5.9	–2%	9.0	50%	11.2	87%	13.8	131%
V = 5700 ml	6.5	16%	6.4	–2%	9.4	45%	11.9	83%	15.0	131%
SV (ml)	Mean	$\%^{Vref}$	Mean	$\%^{basel}$	Mean	$\%^{basel}$	Mean	$\%^{basel}$	Mean	$\%^{basel}$
V = 4500 ml	53	–28%	47	–11%	61	16%	69	30%	75	42%
V = 4800 ml	63	–15%	57	–10%	72	14%	80	26%	84	33%
V_{ref} = 5100 ml	74	0%	68	–8%	84	13%	90	22%	93	25%
V = 5400 ml	85	15%	79	–7%	97	14%	104	22%	102	20%
V = 5700 ml	96	30%	91	–5%	17%	17%	17%	17%	17%	17%

Mean: average of CV variables in the indicated periods. In the exercise phases, the average has been calculated in the last two minutes to exclude transition effects. **$\%^{Vref}$**: percentage with respect to the reference blood volume V_{ref} = 5100 ml. **$\%^{basel}$**: percentage with respect to the baseline value

Table 40 – Simulated CV variables systolic blood pressure (SBP), diastolic blood pressure (DBP), and pulse pressure (PP) varying the total blood volume *V*.

Variable	Baseline		After Spin-up		Exercise: 25W		Exercise: 50W		Exercise: 100W	
SBP (mmHg)	Mean	$\%^{Vref}$	Mean	$\%^{basel}$	Mean	$\%^{basel}$	Mean	$\%^{basel}$	Mean	$\%^{basel}$
V = 4500 ml	95	–13%	90	–5%	94	–1%	97	2%	105	11%
V = 4800 ml	102	–6%	99	–3%	107	5%	111	9%	119	17%
V_{ref} = 5100 ml	109	0%	106	–3%	119	9%	124	13%	133	22%
V = 5400 ml	115	6%	113	–2%	129	12%	137	19%	148	28%
V = 5700 ml	121	11%	120	–1%	139	15%	149	23%	162	34%
DBP (mmHg)	Mean	$\%^{Vref}$	Mean	$\%^{basel}$	Mean	$\%^{basel}$	Mean	$\%^{basel}$	Mean	$\%^{basel}$
V = 4500 ml	65	–3%	64	–2%	60	–7%	59	–9%	64	–1%
V = 4800 ml	67	0%	67	0%	67	0%	68	1%	73	10%
V_{ref} = 5100 ml	67	0%	68	1%	73	8%	74	11%	82	23%
V = 5400 ml	68	1%	68	0%	76	12%	80	18%	92	35%
V = 5700 ml	68	1%	69	1%	78	15%	84	24%	101	49%
PP (mmHg)	Mean	$\%^{Vref}$	Mean	$\%^{basel}$	Mean	$\%^{basel}$	Mean	$\%^{basel}$	Mean	$\%^{basel}$
V = 4500 ml	30	–27%	26	–13%	34	12%	37	25%	41	37%
V = 4800 ml	35	–15%	32	–9%	39	13%	44	24%	46	31%
V_{ref} = 5100 ml	41	0%	38	–7%	46	12%	49	21%	51	23%
V = 5400 ml	47	15%	44	–6%	53	13%	57	21%	56	19%
V = 5700 ml	53	29%	50	–6%	60	14%	65	22%	61	16%

Mean: average of CV variables in the indicated periods. In the exercise phases, the average has been calculated in the last two minutes to exclude transition effects. **$\%^{Vref}$**: percentage with respect to the reference blood volume V_{ref} = 5100 ml. **$\%^{basel}$**: percentage with respect to the baseline value

On the other hand, during the exercise phases at V=4500 ml, the cardiovascular system was unsuccessful in increasing the mean blood pressure to levels seen during the reference case (increase percentages at V=4500 ml are –3%, –2%, and 6% corresponding to exercise at 25W, 50W, and 100W). This occurred despite the increase in venous flow due to the muscle pump effect. As blood volume was expanded, the increase in blood pressure became more significant. Same trends were observed in the systolic and diastolic blood pressure (see Table 40).

The amount of blood volume highly affected all CV responses during the exercise phases. On one hand, the lower pressure attained at the lower volume condition determined the rest of the CV variables' trends. For example, the heart rate showed the largest values amongst all blood volume conditions, while the stroke volume and cardiac output presented the lowest values. On the other hand, at the largest blood volume condition (V=5700 ml), increases in blood pressure were substantial, leading to higher stroke volumes and cardiac outputs, as well as lower heart rates across exercises phases. Average values during the exercise phases are shown in Table 39 and Table 40, along with the % change with respect to their initial values at the baseline condition.

5.4 Summary of Results and Discussion

This cardiovascular model was developed to simulate the short-term hemodynamic responses to orthostatic stress and exercise. In particular, orthostatic stress was generated by centrifugation of a short-radius centrifuge, therefore generating a high gravity gradient along the body. This model recreated the difference in hydrostatic pressure between cardiovascular compartments caused by the gravity gradient. In addition, the effects of ergometer exercise were also incorporated in the model, including the increase in blood pressure, the muscle pump effect, the decrease in vascular resistance, and the slight increase in intra-abdominal pressure. Finally, the simulation recreated the exact 25-min exercise protocol already experienced by 12 subjects in a previous human experiment. The cardiovascular data taken during the experiments were used to calibrate and evaluate the computational model.

The simulation at "1G Centripetal" was chosen as the reference simulation. In this condition, subjects experienced 1G in the centripetal direction measured at the feet. This corresponded to an angular velocity of 28.6 rpm, which was replicated in the simulation protocol, including accurate acceleration and deceleration profiles. Concerning the cardiovascular variables, the total peripheral resistance and the mean blood pressure were used as inputs to the model. Three of the exercise parameters, namely the peripheral resistance, the arterial blood pressure set-point, and the leg external pressure, were chosen such that the input variables matched the data gathered experimentally. Thus, the microvascular resistances were disconnected from the controls at the onset of exercise and they were replicated to follow the resistance seen experimentally. On the other hand, the arterial blood pressure set-point and the leg external pressure due to muscle pump were selected to replicate the experimental mean blood pressure. In a second step, these two parameters were further adjusted taking into consideration the heart rate responses during the exercise period.

The simulated cardiovascular responses captured extremely well the cardiovascular dynamics during the entire protocol, including the spin-up and spin down phases, as well as the exercise period. The arterial baroreflex and the cardiopulmonary reflex responded properly to the cardiovascular stress created by centrifugation. In addition, the three exercise phases were very distinguishable from one another, and the time constants during transitions were particularly well replicated. In the baseline period (i.e. first three minutes of the protocol), the cardiovascular model overestimated the heart rate by 14%, and underestimated stroke volume and cardiac output by 21% and 8% respectively. Blood pressure, including systolic, diastolic, and pulse pressure were within less than 7% of underestimation.

During the exercise period, both the mean arterial pressure and the heart rate simulated the experimental data within an error of 3%. The underestimation seen in the cardiac output increased with the exercise intensity, starting at 9% at 25W, increasing to 13% at 50W, and reaching 18% at 100W. The stroke volume underestimation ranged from 12% at 25W (much smaller than the 21% seen in the baseline period) to 18% at 100W. The underestimation of the model seemed to be driven by the inability of the model to simulate higher systolic pressures, particularly during the intensive exercise phase at 100W, causing the pulse pressure underestimation to attain 21% at this particular exercise phase. That said, blood pressures (systolic, diastolic, and mean) were maintained within 10% error during all phases of the simulation.

Similar results were obtained in the "1.4G Centripetal" simulation. In this case, the angular velocity was increased to 33.9 rpm, and the exercise parameters were adjusted to take into account the higher centrifugation and muscle pump effect due to the higher foot forces. Once more, simulated results were successful at reproducing the cardiovascular dynamics caused by the simulated protocol. Cardiovascular responses to orthostatic stress were successfully captured during the spin-up and spin-down phases. In addition, the different exercise phases were also very well defined and the time constants reproduced well the transitions between phases.

A general underestimation of variables was also seen in this case study at "1.4 Centripetal". In the baseline period the stroke volume and cardiac output were underestimated by 23% and 11% respectively, and the heart rate was overestimated by 15%. Concerning the exercise periods, the same trends seen in the reference simulation were observed. Heart rate and mean blood pressure were simulated within an error of 3%, and the cardiac output and stroke volume underestimation increased with the exercise intensity, particularly at 100W. The cardiac output underestimation was 8% at 25W, 9% at 50W, and 14% at 100W. The stroke volume underestimation was 10% at 25W, 11% at 50W, and 14% at 100W. Again, the difference between the model results and the experimental data seemed to accrue at the higher exercise

intensity, where the systolic pressure is underestimated by 10%, but the diastolic pressure is within 1% error, causing the pulse pressure to be underestimated by 21%. Again, blood pressures (systolic, diastolic, and mean) were maintained within 10% error during all phases of the simulation.

Generally, the evaluation of the cardiovascular model showed a great performance simulating the cardiovascular dynamics during the 25-min exercise protocol. It also showed a slight underestimation of some of the cardiovascular variables, particularly stroke volume, and to a lesser extent, cardiac output (due to the overestimation of heart rate). These results could be better adjusted by modifying some of the numerous parameters that are built in the model. For example, as seen in the previous section, an increase in total blood volume would lead to a shift in the baseline operating point in the right direction: heart rate would decrease and stroke volume and cardiac output would increase. Other parameters could also be modified. However, the objective of this modeling effort was to simulate the cardiovascular responses using the minimum amount of inputs, and once those were decided, to evaluate the model prediction power using the experimental data.

Once evaluated, this model allows for further exploration to simulate and analyze the cardiovascular responses to other centrifuge configurations. The first parameter chosen was the distance from the subject's head to the center of rotation of the centrifuge, *h (cm)*. Changes in *h* led to changes in both artificial gravity level and gravity gradient, making this parameter especially attractive. The cardiovascular responses at higher h values were affected by the higher AG levels following two opposite processes: the increase of blood pulling to the lower extremities, and the increase in venous return caused by higher foot forces and generally harder workout. Results showed that, within the limits simulated here, despite the higher orthostatic stress generated at larger *h* values, the exercise conditions were able to overcome the blood pulling effect and maintain, or even increase, the overall cardiovascular activity. These results confirm the importance of exercise to maintain an appropriate cardiovascular regulation and a healthy cardiovascular system. This is particularly true under orthostatic stress conditions, where the exercise cardiovascular benefits (especially the increase in venous return), became essential.

Finally, the cardiovascular responses of subjects with varying total blood volumes were also simulated. Of particular interest were the 0-g adapted subjects, which were assumed to have a 12% decrease in total blood volume due to the microgravity environment. These subjects experienced not only changes in their baseline cardiovascular operating point, but also changes in the responses to centrifugation and exercise. Thus, during the baseline period, blood pressure decreased by 9% with respect to 1-g adapted subjects even though the heart rate increased +16% in an attempt to maintain the blood pressure to nominal levels. In addition, stroke volume and cardiac output also decreased by 28% and 16% respectively. On the other

hand, 0-g adapted subjects showed larger responses to the same cardiovascular stress caused by the centrifugation profile. Then, both the decrease in mean arterial pressure and the subsequent increase in heart rate seen in 0-g adapted subjects were larger than in 1-g adapted subjects. These simulation results are in agreement with the expected conclusion that the diminution of blood volume caused the blood pulling effect to become more important, making it more difficult for the cardiovascular system to maintain an appropriate overall cardiovascular regulation.

Overall, and despite the slight underestimation of some of the cardiovascular variables, the cardiovascular model developed in this research effort provides unique information about the cardiovascular responses to orthostatic stress and exercise. In particular, the cardiovascular dynamics due to the control systems in response to external stress were very well captured. The model was evaluated using experimental data gathered in the MIT compact-radius centrifuge, covering two different gravity levels and three different exercise intensities. Additionally, the model was further explored in new centrifuge configurations (varying the distance from the subject's head to the center of rotation), and in new subject's physiological conditions such as 0-g adapted subjects (simulated as a percentage of blood volume loss). Furthermore, this model, appropriately modified, can provide insightful information about other orthostatic stress profiles, types of exercise, or exercise intensities.

6 Conclusion

Artificial gravity is a promising countermeasure to mitigate human deconditioning in space, particularly during future long duration spaceflight missions beyond LEO. The use of a compact-radius centrifuge on-board is an affordable approach to generate gravity in space. However, many questions still remain unanswered regarding the appropriate configuration, parameters, and exercise protocols to keep astronauts in a healthy physiological state. This research effort aimed to investigate the human physiological responses to a variety of artificial gravity configurations in a compact-radius centrifuge, particularly when combined with ergometer exercise.

Two different approaches were employed: an experimental approach (Chapter 4) and a computational approach (Chapter 5). Both methodologies complemented each other, creating a coherent assessment of the use of artificial gravity and exercise on human physiology. The specific aims and hypothesis tested in this thesis are reproduced below:

1. Experimental approach: to empirically investigate the effects of different artificial gravity and exercise workload levels on musculoskeletal and cardiovascular functions, as well as motion sickness and comfort. In particular, these are the specific objectives:

    1.1. To determine if AG ergometer exercise can produce higher foot forces than those measured under simulated 0-g conditions

    - *Hypothesis 1: Higher AG ergometer exercise levels in a compact-radius centrifuge increase foot forces*

    1.2. To determine if AG ergometer exercise can produce higher cardiovascular responses than those measured under simulated 0-g conditions.

    - *Hypothesis 2: Higher AG ergometer exercise levels in a compact-radius centrifuge increase overall cardiovascular activity*

    1.3. To assess motion sickness and comfort.

    - *Hypothesis 3: Higher AG ergometer exercise in a compact-radius centrifuge is well-tolerated and comfortable as ergometer exercise in simulated 0-g*

2. Computational approach: to develop a cardiovascular model to capture the effects of AG and ergometer exercise in a compact-radius centrifuge. In particular, these are the specific objectives:

2.1. *To develop a computational model of the cardiovascular system that captures the short-term hemodynamic regulation during exercise in a high AG gradient environment such as a compact-radius centrifuge.*

2.2. *To evaluate the cardiovascular model with experimental measurements from 1-g adapted subjects using the MIT compact radius centrifuge.*

2.3. *To explore the cardiovascular model to identify the influence of the gravity level, the exercise workload, and the gravity gradient.*

2.4. *To simulate the cardiovascular effects of AG on 0-g adapted subjects.*

A summary of the results, main conclusion, contributions, and associated publications is presented in the following paragraphs, as well as suggestions for future research.

6.1 Summary and Contributions

The experimental approach consisted in the implementation of a comprehensive experimental study on human physiology during ergometer exercise using a new configuration of the MIT compact-radius centrifuge. The MIT centrifuge experienced several modifications in order to be compatible with a future use in the ISS. This experiment contributed to the identification and quantitative characterization of the short-term effects (~30 min) of different artificial gravity levels and exercise workload intensities on several aspects of human physiology, namely musculoskeletal system (in terms of foot forces), cardiovascular system (continuous beat-to beat cardiovascular monitoring using a Nexfin monitor), and motion sickness and comfort (subjective data collected during experimental sessions). This is the first experiment that covered multiple exercise and artificial gravity levels, including a reference point with no artificial gravity.

Twelve subjects completed the same ergometer exercise protocol under three different artificial gravity conditions. Results showed that there was a significant effect of artificial gravity level and workload intensity on peak foot forces generated during ergometer exercise (hypothesis 1 confirmed). In addition, results also showed that the amplitude of the cardiovascular responses adapted to the stress level generated not only by the exercise intensity, but also by the artificial gravity level to which the subjects were exposed (hypothesis 2 confirmed). In particular, pulse pressure, stroke volume, and cardiac output increased with the artificial gravity level, increasing the overall cardiovascular activity and therefore, suggesting that artificial gravity may be beneficial against cardiovascular deconditioning in space. Furthermore, all subjects tolerated the centrifugation well, including the spin-up and spin-down process,

and none of them presented signs of motion sickness. They were generally comfortable and did not notice Coriolis forces acting on their knees (hypothesis 3 confirmed).

The computational approach consisted in the development of a lumped-parameter model of the cardiovascular system that captured the transient hemodynamic responses to ergometer exercise under orthostatic stress generated by a short-radius centrifuge (Aim 2.1). This model was built upon previous work that was developed to study the short-term hemodynamic responses to either centrifugation or exercise, but not both mechanisms together at the same time, which was the object of this thesis. In addition to including the systemic circulation, the cardiac chambers, the pulmonary circulation, and the two major short-term neural control mechanisms (namely the arterial baroreflex and the cardiopulmonary reflex), the model presented in this thesis implemented the centrifugation profiles and the exercise mechanisms, thus replicating the experimental exercise protocol realized by the human subjects during the experimental study.

The model was evaluated with the empirical data gathered during the experimental part of this work (Aim 2.2). The simulated cardiovascular responses compared quite well with the experimental results. The model is capable of reproducing the cardiovascular changes due to both centrifugation and exercise (Aim 2.3), including the dynamic responses during transitions between the different phases of the protocol, which matched very well the experimental data. In addition, further exploration of the model was performed to study the impact of centrifugation parameters such as the distance between the subject's head and the center of rotation, which affects both the gravity level and the gravity gradient (Aim 2.3). Results revealed that, despite the increase in orthostatic stress at larger h, the overall cardiovascular regulation was properly maintained due to the beneficial effects of exercise, particularly the increase in venous return due to the muscle pump effect. Finally, the total blood volume was also altered to examine its impact on the cardiovascular regulation under orthostatic stress and exercise (Aim 2.4). Simulations of hypovolemic subjects were analyzed in order to investigate the hemodynamic responses of 0-g deconditioned subjects. The model simulations showed that decreasing the total blood volume affected the cardiovascular system's ability not only to maintain a constant baseline operating point, but also to respond to changes due to centrifugation and exercise. In these subjects, the blood-pulling effect during centrifugation became more important and it was more difficult for the cardiovascular system to sustain an appropriate overall cardiovascular regulation.

6.1.1 List of Associated Publications

1. A. Diaz and L.R. Young. "Human Modeling and Experimentation under Artificial Gravity using the MIT Compact Radius Centrifuge". Poster, presented at *2014 NASA Human Research Program (HRP) Investigators' Workshop*, February 2014.

2. A. Diaz, C. Trigg, and L.R. Young. "Combining Ergometer Exercise and Artificial Gravity". Technical manuscript, presented at *65th International Astronautical Congress*, September 2014.

3. A. Diaz and L.R. Young. "Artificial Gravity and Exercise on the MIT Compact Radius Centrifuge". Poster, presented at *2015 NASA Human Research Program (HRP) Investigators' Workshop*, January 13-15, 2015.

4. A. Diaz, T. Heldt and L.R. Young. "Cardiovascular Responses under Artificial Gravity Combined with Exercise". Technical manuscript, presented at *2015 IEEE Aerospace Conference*, March 2015.

5. A. Diaz, C. Trigg and L.R. Young. Combining ergometer exercise and artificial gravity in a compact-radius centrifuge. Technical manuscript, accepted in *Acta Astronautica*, vol. 113, pp. 80–88, 2015.

6.2 Suggestions for Further Research

This section contains some suggestions for future research based on this work.

6.2.1 Further Experimental Studies

This research effort constitutes just the beginning of the exploration of the multiple artificial gravity configurations that are possible in a compact-radius centrifuge. The MIT CRC offers the possibility of investigating intermediate artificial gravity levels from 0g centripetal (or no rotation) to 1.4g centripetal (measured at the feet, w=33.9rpm), which at the present time is considered as the maximal angular velocity at which this centrifuge can operate. Human responses to artificial gravity levels between 0g and 1g are relatively unknown and could be very important for a possible future use of artificial gravity. In addition, the exercise device in place allows for the implementation of other exercise protocols, using different durations and intensities. Furthermore, other exercise devices could be easily installed only with

small modifications on the centrifuge. The MIT CRC is a viable platform for continued and future AG ground research.

Bed rest studies combining artificial gravity and exercise would be the logical next step. The acute responses gathered during the MIT CRC experiments suggest that artificial gravity and exercise are a great combination that might be beneficial against human deconditioning in microgravity. Bed rests studies will provide an important step to answer this question. The ultimate confirmation will come with a human centrifuge in space.

6.2.2 Further modeling analysis

This lumped-parameter cardiovascular model has the capability of simulating orthostatic stress in a high gravity gradient environment such as a short-radius centrifuge. The model also has the capability to simulate the cardiovascular mechanisms during exercise. This opens a myriad of possible simulations combining these two stressors on the human body. New centrifugation profiles and exercise protocols can be easily simulated and, including the appropriate modifications, other types of exercise such as steppers or rowing.

In the context of VIIP, the current model could be combined with lumped-parameter models of the intracranial pressure mechanisms during fluids shift in altered gravity environments. The complete model could be used to investigate the potential effect of artificial gravity and/or exercise on the VIIP phenomenon.

Appendices

A. Foot Forces Data Analysis

The following Matlab codes show some of the most relevant foot forces data processing and analysis.

- The file "Get Logger Lite Data" reads the data files generated by the Logger Lite system. The forces are calibrated using the necessary offset. Only data concerning one subject is included, since the same process is applied for the rest of the subjects.
- The File "Process Logger Lite Data" calculates the average peak forces exerted by each foot during each exercise period, at each AG condition. Only data concerning one subject at one AG condition ("No Centripetal") is included. The same process is applied to other conditions and subjects.

```
% GET LOGGER LITE DATA

% This file gathers the Logger Lite data for the foot forces and accelerometer data
% Created by Aaron Ashley in August 2014

%% Get Data
% Define uniform sampling rate for use in statistical functions.
t_std_sequence = 0.001:0.001:25;
t_std = t_std_sequence(:);

% % % % % % % % % % % % % % % % % % % % % % % % % % % % % % % %
% To access a specific time, 5m = 5.000, 23m45s = 23.750, etc.%
% For indexing, 5.000 ~ 5/25 = 500/2500 = index of 500        %
% Another, 23.750 ~ 23.75/25 = 2375/2500 = index of 2375      %
% % % % % % % % % % % % % % % % % % % % % % % % % % % % % % % %

% Foot Force and Accelerometer Data

subjID = 11;
initials = 'XX';        (these are not the real initials for subject protection purposes)
s11LL0g = importdata([pwd '/../Subject' num2str(subjID) '-' initials '/0G-' initials '/LL-'
initials '-0G.csv']);
s11time0g = s11LL0g.data(:,1);
s11foot0gL = s11LL0g.data(:,5);
s11foot0gR = s11LL0g.data(:,6);
s11accX0g = s11LL0g.data(:,2);
s11accY0g = s11LL0g.data(:,3);
s11accZ0g = s11LL0g.data(:,4);
s11LL1g = importdata([pwd '/../Subject' num2str(subjID) '-' initials '/1G-' initials '/LL-'
initials '-1G.csv']);
s11time1g = s11LL1g.data(:,1);
s11foot1gL = s11LL1g.data(:,5);
s11foot1gR = s11LL1g.data(:,6);
s11accX1g = s11LL1g.data(:,2);
s11accY1g = s11LL1g.data(:,3);
s11accZ1g = s11LL1g.data(:,4);
s11LL14g = importdata([pwd '/../Subject' num2str(subjID) '-' initials '/1.4G-' initials '/LL-'
initials '-1.4G.csv']);
s11time14g = s11LL14g.data(:,1);
s11foot14gL = s11LL14g.data(:,5);
s11foot14gR = s11LL14g.data(:,6);
s11accX14g = s11LL14g.data(:,2);
```

```
s11accY14g = s11LL14g.data(:,3);
s11accZ14g = s11LL14g.data(:,4);

%% Interpolate
s11foot0gLI = interp1(s11time0g,s11foot0gL,t_std);
s11foot0gRI = interp1(s11time0g,s11foot0gR,t_std);
s11foot1gLI = interp1(s11time1g,s11foot1gL,t_std);
s11foot1gRI = interp1(s11time1g,s11foot1gR,t_std);
s11foot14gLI = interp1(s11time14g,s11foot14gL,t_std);
s11foot14gRI = interp1(s11time14g,s11foot14gR,t_std);
s11accX0gI = interp1(s11time0g,s11accX0g,t_std);
s11accY0gI = interp1(s11time0g,s11accY0g,t_std);
s11accZ0gI = interp1(s11time0g,s11accZ0g,t_std);
s11accX1gI = interp1(s11time1g,s11accX1g,t_std);
s11accY1gI = interp1(s11time1g,s11accY1g,t_std);
s11accZ1gI = interp1(s11time1g,s11accZ1g,t_std);
s11accX14gI = interp1(s11time14g,s11accX14g,t_std);
s11accY14gI = interp1(s11time14g,s11accY14g,t_std);
s11accZ14gI = interp1(s11time14g,s11accZ14g,t_std);

%% Zeroing the Force
% The offsets in this section are determined by the researcher.
% Enter a number to be subtracted from the interpolated foot force so that
% the the 0m-3m section lies closest to zero, thereby zeroing the force
% BEFORE the spin-up.
s11shift0gL = 16.5;
s11shift0gR = 44;
s11shift1gL = 7.8;
s11shift1gR = 43;
s11shift14gL = 13;
s11shift14gR = 46;

% Subtract the offset
s11foot0gLIz = s11foot0gLI - s11shift0gL;
s11foot0gRIz = s11foot0gRI - s11shift0gR;
s11foot1gLIz = s11foot1gLI - s11shift1gL;
s11foot1gRIz = s11foot1gRI - s11shift1gR;
s11foot14gLIz = s11foot14gLI - s11shift14gL;
s11foot14gRIz = s11foot14gRI - s11shift14gR;
```

```
% PROCESS LOGGER LITE DATA

% This script processes FOOT FORCE data from the
% Logger Lite device

% This file should be called immediately after 'getLLdata.m'
% atop the 'footforces.m' file.

% Created by Aaron Ashley in August 2014
% Modified by Ana Diaz in September 2014

%%%%%%%%%%%%% FORCE REFERENCE GUIDE %%%%%%%%%%%%%%%%%%%%%%
% Rest: 6m45s-7m,         6751-7000    % First rest
% 25W: 7m-10m,            7001-10000
% Rest: 10m-10m15s,       10001-10250  % 2nd rest
% 50W: 10m15s-15m15s,     10251-15250
% Rest: 15m15s-15m45s,    15251-15750 % Penultimate rest
% 100W: 15m45s-20m45s,    15751-20750
% Rest: 20m45s-21m45s,    20751-21750  % Last rest
%%%%%%%%%%%%%%%%%%%%%%%%%%%%%%%%%%%%%%%%%%%%%%%%%%%%%%%%%%

%% Subject 11
% CALCULATION OF THE PEAK FORCES MEAN (0g)

% 0g - LEFT %%%%%%%%%%
s11foot0gfirstL = s11foot0gLIz(6751:7000);      % First rest
s11foot0g25wL = s11foot0gLIz(7001:10000);     % 25W PHASE
s11foot0g2ndL = s11foot0gLIz(10001:10250);      % 2nd rest
```

```
s11foot0g50wL = s11foot0gLIz(10251:15250);     % 50W PHASE
s11foot0gpenultL = s11foot0gLIz(15251:15750);    % Penultimate rest
s11foot0g100wL = s11foot0gLIz(15751:20750);    % 100W PHASE
s11foot0glastL = s11foot0gLIz(20751:21750);      % Last rest

% Find the mean of peaks
[s11mean0g25wL,x] = findpeaks(s11foot0g25wL,'MinPeakHeight',30);
t_s11peaks0g25wL = (x + 7000)/1000; % unused
[s11mean0g50wL,x] = findpeaks(s11foot0g50wL,'MinPeakHeight',45);
t_s11peaks0g50wL = (x + 10250)/1000;
[s11mean0g100wL,x] = findpeaks(s11foot0g100wL,'MinPeakHeight',100);
t_s11peaks0g100wL = (x + 15750)/1000;

s11force0g25wL = mean(s11mean0g25wL);
s11force0g50wL = mean(s11mean0g50wL);
s11force0g100wL = mean(s11mean0g100wL);


% 0g - RIGHT %%%%%%%%%%
s11foot0gfirstR = s11foot0gRIz(6751:7000);       % First rest
s11foot0g25wR = s11foot0gRIz(7001:10000);      % 25W PHASE
s11foot0g2ndR = s11foot0gRIz(10001:10250);       % 2nd rest
s11foot0g50wR = s11foot0gRIz(10251:15250);     % 50W PHASE
s11foot0gpenultR = s11foot0gRIz(15251:15750);    % Penultimate rest
s11foot0g100wR = s11foot0gRIz(15751:20750);    % 100W PHASE
s11foot0glastR = s11foot0gRIz(20751:21750);      % Last rest

% Find the mean of peaks
 [s11mean0g25wR,x] = findpeaks(s11foot0g25wR,'MinPeakHeight',25);
t_s11peaks0g25wR = (x + 7000)/1000; % unused
[s11mean0g50wR,x] = findpeaks(s11foot0g50wR,'MinPeakHeight',45);
t_s11peaks0g50wR = (x + 10250)/1000;
[s11mean0g100wR,x] = findpeaks(s11foot0g100wR,'MinPeakHeight',90);
t_s11peaks0g100wR = (x + 15750)/1000;

s11force0g25wR = mean(s11mean0g25wR);
s11force0g50wR = mean(s11mean0g50wR);
s11force0g100wR = mean(s11mean0g100wR);
```

B. Cardiovascular Data Analysis

The following Matlab codes show some of the most relevant cardiovascular data processing and analysis.

- The file "Get Cardiovascular Data" reads the data files generated by the Nexfin system. It applies forward-reverse Butterworth filters to all the CV variables to get rid of motion artifacts and false readings. Only data concerning one subject is included, since the same process is applied for the rest of the subjects.
- The File "Process Cardiovascular Data" calculates the mean, standard deviation and standard error for all CV variables. In a second step, some of these values are manually adjusted removing the misreading data that were not removed by the Butterworth filter.
- The file "Plot all subjects" plots the 8 CV variables using the corrected mean and standard error.

```
% GET CARDIOVASCULAR DATA

% This script gathers, filters, and interpolates all the data from the
% CCNexfin cardiovascular device, but DOES NOT process the data or
% create any plots.
% Use other scripts to create plots to keep the MATLAB files organized.
% "getCVdata.m" and "processCVdata.m" should be called atop each plot file.
%
% Created by Aaron Ashley in July 2014
% Modified by Ana Diaz

%% Initialization
% This identifies the CCNexfin 'REC-90_100.csv' filename for later.
buildNexfin;

% Define uniform sampling rate for use in statistical functions.
t_std_sequence = 0.001:0.001:25; % 25,000 points
t_std = t_std_sequence(:);
t_stdw_sequence = 0.0001:0.0001:25; % 250,000 points --> waveform needs higher resolution
t_stdw = t_stdw_sequence(:);

% % % % % % % % % % % % % % % % % % % % % % % % % % % % % % % %
% To access a specific time, 5m = 5.00, 23m45s = 23.75, etc.%
% For indexing, 5.00 ~ 5/25 = 5000/2500 = index of 5000       %
% Another, 23.75 ~ 23.75/25 = 23750/2500 = index of 23750     %
% % % % % % % % % % % % % % % % % % % % % % % % % % % % % % % %

%% Filters
orderN = 6;

% Declare regular filters (The numerator is the frequency in Hz)
Wn_hr  = 8/100;
Wn_sys = 8/100;
Wn_dia = 5/100;
Wn_mbp = 5/100;
Wn_sv  = 6/100;
Wn_co  = 5/100;
Wn_r   = 4/100;
Wn_pp  = 8/100;

% Declare stronger filters
```

```
Wn_hr2  = 4/100;
Wn_sys2 = 4/100;
Wn_dia2 = 2/100;
Wn_mbp2 = 3/100;
Wn_sv2  = 4/100;
Wn_co2  = 3/100;
Wn_co3  = 0.5/100;
Wn_r2   = 4/100;
Wn_r3   = 2/100;
Wn_pp2  = 4/100;

% Create all filters
[b_hr,a_hr]     = butter(orderN,Wn_hr,'low');
[b_sys,a_sys]   = butter(orderN,Wn_sys,'low');
[b_dia,a_dia]   = butter(orderN,Wn_dia,'low');
[b_mbp,a_mbp]   = butter(orderN,Wn_mbp,'low');
[b_sv,a_sv]     = butter(orderN,Wn_sv,'low');
[b_co,a_co]     = butter(orderN,Wn_co,'low');
[b_r,a_r]       = butter(orderN,Wn_r,'low');
[b_pp,a_pp]     = butter(orderN,Wn_pp,'low');
[b_hr2,a_hr2]   = butter(orderN,Wn_hr2,'low');
[b_sys2,a_sys2] = butter(orderN,Wn_sys2,'low');
[b_dia2,a_dia2] = butter(orderN,Wn_dia2,'low');
[b_mbp2,a_mbp2] = butter(orderN,Wn_mbp2,'low');
[b_sv2,a_sv2]   = butter(orderN,Wn_sv2,'low');
[b_co2,a_co2]   = butter(orderN,Wn_co2,'low');
[b_co3,a_co3]   = butter(orderN,Wn_co3,'low');
[b_r2,a_r2]     = butter(orderN,Wn_r2,'low');
[b_r3,a_r3]     = butter(orderN,Wn_r3,'low');
[b_pp2,a_pp2]   = butter(orderN,Wn_pp2,'low');

%% Subject 5
subjID = 5;
initials = 'XX';
```
(these are not the real initials for subject protection purposes)

```
% 0G
s5all0g = importdata([pwd '/../Subject' num2str(subjID) '-' initials '/0G-' initials '/REC-'
num2str(s5num0g) '_100.csv']);
s5time0gSec = s5all0g.data(:,1);
    s5time0gMin = s5time0gSec/60;
s5hr0g = s5all0g.data(:,3);      % Heart Rate
s5sys0g = s5all0g.data(:,6);     % Systolic
s5dia0g = s5all0g.data(:,7);     % Diastolic
s5mbp0g = s5all0g.data(:,8);     % Mean Blood Pressure
s5sv0g = s5all0g.data(:,9);      % Stroke Volume
s5co0g = s5all0g.data(:,10);     % Cardiac Output
s5r0g = s5all0g.data(:,11);      % Resistance
s5pp0g = s5sys0g-s5dia0g;        % Pulse Pressure

s5hr0gFilt = filtfilt(b_hr,a_hr,s5hr0g);
s5sys0gFilt = filtfilt(b_sys,a_sys,s5sys0g);
s5dia0gFilt = filtfilt(b_dia,a_dia,s5dia0g);
s5mbp0gFilt = filtfilt(b_mbp,a_mbp,s5mbp0g);
s5sv0gFilt = filtfilt(b_sv,a_sv,s5sv0g);
s5co0gFilt = filtfilt(b_co,a_co,s5co0g);
s5r0gFilt = filtfilt(b_r,a_r,s5r0g);
s5pp0gFilt = filtfilt(b_pp,a_pp,s5pp0g);

s5hr0gI = interp1(s5time0gMin,s5hr0gFilt,t_std);
s5sys0gI = interp1(s5time0gMin,s5sys0gFilt,t_std);
s5dia0gI = interp1(s5time0gMin,s5dia0gFilt,t_std);
s5mbp0gI = interp1(s5time0gMin,s5mbp0gFilt,t_std);
s5sv0gI = interp1(s5time0gMin,s5sv0gFilt,t_std);
s5co0gI = interp1(s5time0gMin,s5co0gFilt,t_std);
s5r0gI = interp1(s5time0gMin,s5r0gFilt,t_std);
s5pp0gI = interp1(s5time0gMin,s5pp0gFilt,t_std);

wavename = [pwd '/../Subject' num2str(subjID) '-' initials '/0G-' initials '/REC-'
num2str(s5num0g) '_103.bin'];
waveID = fopen(wavename,'r');
```

```
wave = fread(waveID,'int16');
fclose(waveID);
waveUnit = wave*(0.25); % New integers are units of mmHg
tstar = 0:1:length(wave)-1;
tvec = tstar(:);
tsample = tvec/200; %seconds
t = tsample/60; %minutes
s5wave0gI = interp1(t,waveUnit,t_stdw);

% 1G
s5all1g = importdata([pwd '/../Subject' num2str(subjID) '-' initials '/1G-' initials '/REC-'
num2str(s5num1g) '_100.csv']);
s5time1gSec = s5all1g.data(:,1);
    s5time1gMin = s5time1gSec/60;
s5hr1g = s5all1g.data(:,3);      % Heart Rate
s5sys1g = s5all1g.data(:,6);     % Systolic
s5dia1g = s5all1g.data(:,7);     % Diastolic
s5mbp1g = s5all1g.data(:,8);     % Mean Blood Pressure
s5sv1g = s5all1g.data(:,9);      % Stroke Volume
s5co1g = s5all1g.data(:,10);     % Cardiac Output
s5r1g = s5all1g.data(:,11);      % Resistance
s5pp1g = s5sys1g-s5dia1g;        % Pulse Pressure

s5hr1gFilt = filtfilt(b_hr,a_hr,s5hr1g);
s5sys1gFilt = filtfilt(b_sys2,a_sys2,s5sys1g);
s5dia1gFilt = filtfilt(b_dia,a_dia,s5dia1g);
s5mbp1gFilt = filtfilt(b_mbp,a_mbp,s5mbp1g);
s5sv1gFilt = filtfilt(b_sv,a_sv,s5sv1g);
s5co1gFilt = filtfilt(b_co,a_co,s5co1g);
s5r1gFilt = filtfilt(b_r,a_r,s5r1g);
s5pp1gFilt = filtfilt(b_pp,a_pp,s5pp1g);

s5hr1gI = interp1(s5time1gMin,s5hr1gFilt,t_std);
s5sys1gI = interp1(s5time1gMin,s5sys1gFilt,t_std);
s5dia1gI = interp1(s5time1gMin,s5dia1gFilt,t_std);
s5mbp1gI = interp1(s5time1gMin,s5mbp1gFilt,t_std);
s5sv1gI = interp1(s5time1gMin,s5sv1gFilt,t_std);
s5co1gI = interp1(s5time1gMin,s5co1gFilt,t_std);
s5r1gI = interp1(s5time1gMin,s5r1gFilt,t_std);
s5pp1gI = interp1(s5time1gMin,s5pp1gFilt,t_std);

wavename = [pwd '/../Subject' num2str(subjID) '-' initials '/1G-' initials '/REC-'
num2str(s5num1g) '_103.bin'];
waveID = fopen(wavename,'r');
wave = fread(waveID,'int16');
fclose(waveID);
waveUnit = wave*(0.25); % New integers are units of mmHg
tstar = 0:1:length(wave)-1;
tvec = tstar(:);
tsample = tvec/200; %seconds
t = tsample/60; %minutes
s5wave1gI = interp1(t,waveUnit,t_stdw);

% 1.4G
s5all14g = importdata([pwd '/../Subject' num2str(subjID) '-' initials '/1.4G-' initials '/REC-'
num2str(s5num14g) '_100.csv']);
s5time14gSec = s5all14g.data(:,1);
    s5time14gMin = s5time14gSec/60;
s5hr14g = s5all14g.data(:,3);      % Heart Rate
s5sys14g = s5all14g.data(:,6);     % Systolic
s5dia14g = s5all14g.data(:,7);     % Diastolic
s5mbp14g = s5all14g.data(:,8);     % Mean Blood Pressure
s5sv14g = s5all14g.data(:,9);      % Stroke Volume
s5co14g = s5all14g.data(:,10);     % Cardiac Output
s5r14g = s5all14g.data(:,11);      % Resistance
s5pp14g = s5sys14g-s5dia14g;       % Pulse Pressure

s5hr14gFilt = filtfilt(b_hr,a_hr,s5hr14g);
s5sys14gFilt = filtfilt(b_sys,a_sys,s5sys14g);
s5dia14gFilt = filtfilt(b_dia,a_dia,s5dia14g);
```

```
s5mbp14gFilt = filtfilt(b_mbp,a_mbp,s5mbp14g);
s5sv14gFilt = filtfilt(b_sv,a_sv,s5sv14g);
s5co14gFilt = filtfilt(b_co,a_co,s5co14g);
s5r14gFilt = filtfilt(b_r,a_r,s5r14g);
s5pp14gFilt = filtfilt(b_pp,a_pp,s5pp14g);

s5hr14gI = interp1(s5time14gMin,s5hr14gFilt,t_std);
s5sys14gI = interp1(s5time14gMin,s5sys14gFilt,t_std);
s5dia14gI = interp1(s5time14gMin,s5dia14gFilt,t_std);
s5mbp14gI = interp1(s5time14gMin,s5mbp14gFilt,t_std);
s5sv14gI = interp1(s5time14gMin,s5sv14gFilt,t_std);
s5co14gI = interp1(s5time14gMin,s5co14gFilt,t_std);
s5r14gI = interp1(s5time14gMin,s5r14gFilt,t_std);
s5pp14gI = interp1(s5time14gMin,s5pp14gFilt,t_std);

wavename = [pwd '/../Subject' num2str(subjID) '-' initials '/1.4G-' initials '/REC-'
num2str(s5num14g) '_103.bin'];
waveID = fopen(wavename,'r');
wave = fread(waveID,'int16');
fclose(waveID);
waveUnit = wave*(0.25); % New integers are units of mmHg
tstar = 0:1:length(wave)-1;
tvec = tstar(:);
tsample = tvec/200; %seconds
t = tsample/60; %minutes
s5wave14gI = interp1(t,waveUnit,t_stdw);
```

```
% PROCESS CARDIOVASCULAR DATA

% This script does some basic processing for all the CCNexfin
% cardiovascular data, but DOES NOT create any plots.
% Use other scripts to create plots to keep the MATLAB files organized.
% "getCVdata.m" and "processCVdata.m" should be called atop each plot file.
%
% Created by Aaron Ashley in August 2014
% Modified by Ana Diaz in September 2014

%% Mean,SD, and SE
% This section builds matrices from each subject's interpolated data,
% then takes the mean standard deviation, and SE at each time step (t_std).
%%%%%%%%%%%%%%%%%%%%%%%%%%%%%%%%%%%%%%%%%%%%

% 0G (Centrifuge no rotation)
allhr0g = [s5hr0gI,s6hr0gI,s7hr0gI,s8hr0gI,s9hr0gI,s10hr0gI,s11hr0gI,s13hr0gI,s14hr0gI,s15hr0gI,
s16hr0gI,s17hr0gI];
allsys0g = [s5sys0gI,s6sys0gI,s7sys0gI,s8sys0gI,s9sys0gI,s10sys0gI,s11sys0gI,s13sys0gI,s14sys0gI,
s15sys0gI,s16sys0gI,s17sys0gI];
alldia0g = [s5dia0gI,s6dia0gI,s7dia0gI,s8dia0gI,s9dia0gI,s10dia0gI,s11dia0gI,s13dia0gI,s14dia0gI,
s15dia0gI,s16dia0gI,s17dia0gI];
allmbp0g = [s5mbp0gI,s6mbp0gI,s7mbp0gI,s8mbp0gI,s9mbp0gI,s10mbp0gI,s11mbp0gI,s13mbp0gI,s14mbp0gI,
s15mbp0gI,s16mbp0gI,s17mbp0gI];
allsv0g = [s5sv0gI,s6sv0gI,s7sv0gI,s8sv0gI,s9sv0gI,s10sv0gI,s11sv0gI,s13sv0gI,s14sv0gI,s15sv0gI,
s16sv0gI,s17sv0gI];
allco0g = [s5co0gI,s6co0gI,s7co0gI,s8co0gI,s9co0gI,s10co0gI,s11co0gI,s13co0gI,s14co0gI,s15co0gI,
s16co0gI,s17co0gI];
allr0g = [s5r0gI,s6r0gI,s7r0gI,s8r0gI,s9r0gI,s10r0gI,s11r0gI,s13r0gI,s14r0gI,s15r0gI,s16r0gI,
s17r0gI];
allpp0g = [s5pp0gI,s6pp0gI,s7pp0gI,s8pp0gI,s9pp0gI,s10pp0gI,s11pp0gI,s13pp0gI,s14pp0gI,s15pp0gI,
s16pp0gI,s17pp0gI];

% 1G
allhr1g = [s5hr1gI,s6hr1gI,s7hr1gI,s8hr1gI,s9hr1gI,s10hr1gI,s11hr1gI,s13hr1gI,s14hr1gI,s15hr1gI,
s16hr1gI,s17hr1gI];
allsys1g = [s5sys1gI,s6sys1gI,s7sys1gI,s8sys1gI,s9sys1gI,s10sys1gI,s11sys1gI,s13sys1gI,s14sys1gI,
s15sys1gI,s16sys1gI,s17sys1gI];
alldia1g = [s5dia1gI,s6dia1gI,s7dia1gI,s8dia1gI,s9dia1gI,s10dia1gI,s11dia1gI,s13dia1gI,s14dia1gI,
s15dia1gI,s16dia1gI,s17dia1gI];
```

```
allmbp1g = [s5mbp1gI,s6mbp1gI,s7mbp1gI,s8mbp1gI,s9mbp1gI,s10mbp1gI,s11mbp1gI,s13mbp1gI,s14mbp1gI,
s15mbp1gI,s16mbp1gI,s17mbp1gI];
allsv1g = [s5sv1gI,s6sv1gI,s7sv1gI,s8sv1gI,s9sv1gI,s10sv1gI,s11sv1gI,s13sv1gI,s14sv1gI,s15sv1gI,
s16sv1gI,s17sv1gI];
allco1g = [s5co1gI,s6co1gI,s7co1gI,s8co1gI,s9co1gI,s10co1gI,s11co1gI,s13co1gI,s14co1gI,s15co1gI,
s16co1gI,s17co1gI];
allr1g = [s5r1gI,s6r1gI,s7r1gI,s8r1gI,s9r1gI,s10r1gI,s11r1gI,s13r1gI,s14r1gI,s15r1gI,s16r1gI,
s17r1gI];
allpp1g = [s5pp1gI,s6pp1gI,s7pp1gI,s8pp1gI,s9pp1gI,s10pp1gI,s11pp1gI,s13pp1gI,s14pp1gI,s15pp1gI,
s16pp1gI,s17pp1gI];

% 1.4G
allhr14g = [s5hr14gI,s6hr14gI,s7hr14gI,s8hr14gI,s9hr14gI,s10hr14gI,s11hr14gI,s13hr14gI,s14hr14gI,
s15hr14gI,s16hr14gI,s17hr14gI];
allsys14g = [s5sys14gI,s6sys14gI,s7sys14gI,s8sys14gI,s9sys14gI,s10sys14gI,s11sys14gI,s13sys14gI,
s14sys14gI,s15sys14gI,s16sys14gI,s17sys14gI];
alldia14g = [s5dia14gI,s6dia14gI,s7dia14gI,s8dia14gI,s9dia14gI,s10dia14gI,s11dia14gI,s13dia14gI,
s14dia14gI,s15dia14gI,s16dia14gI,s17dia14gI];
allmbp14g = [s5mbp14gI,s6mbp14gI,s7mbp14gI,s8mbp14gI,s9mbp14gI,s10mbp14gI,s11mbp14gI,s13mbp14gI,
s14mbp14gI,s15mbp14gI,s16mbp14gI,s17mbp14gI];
allsv14g = [s5sv14gI,s6sv14gI,s7sv14gI,s8sv14gI,s9sv14gI,s10sv14gI,s11sv14gI,s13sv14gI,s14sv14gI,
s15sv14gI,s16sv14gI,s17sv14gI];
allco14g = [s5co14gI,s6co14gI,s7co14gI,s8co14gI,s9co14gI,s10co14gI,s11co14gI,s13co14gI,s14co14gI,
s15co14gI,s16co14gI,s17co14gI];
allr14g = [s5r14gI,s6r14gI,s7r14gI,s8r14gI,s9r14gI,s10r14gI,s11r14gI,s13r14gI,s14r14gI,s15r14gI,
s16r14gI,s17r14gI];
allpp14g = [s5pp14gI,s6pp14gI,s7pp14gI,s8pp14gI,s9pp14gI,s10pp14gI,s11pp14gI,s13pp14gI,s14pp14gI,
s15pp14gI,s16pp14gI,s17pp14gI];

%% %%%%%%%%%%%%%%%%%%%%%%%%%%%%%%%%%
%Calculation of the mean
meanhr0g = mean(allhr0g,2);
meansys0g = mean(allsys0g,2);
meandia0g = mean(alldia0g,2);
meanmbp0g = mean(allmbp0g,2);
meansv0g = mean(allsv0g,2);
meanco0g = mean(allco0g,2);
meanr0g = mean(allr0g,2);
meanpp0g = mean(allpp0g,2);
    meanhr1g = mean(allhr1g,2);
    meansys1g = mean(allsys1g,2);
    meandia1g = mean(alldia1g,2);
    meanmbp1g = mean(allmbp1g,2);
    meansv1g = mean(allsv1g,2);
    meanco1g = mean(allco1g,2);
    meanr1g = mean(allr1g,2);
    meanpp1g = mean(allpp1g,2);
        meanhr14g = mean(allhr14g,2);
        meansys14g = mean(allsys14g,2);
        meandia14g = mean(alldia14g,2);
        meanmbp14g = mean(allmbp14g,2);
        meansv14g = mean(allsv14g,2);
        meanco14g = mean(allco14g,2);
        meanr14g = mean(allr14g,2);
        meanpp14g = mean(allpp14g,2);
%% %%%%%%%%%%%%%%%%%%%%%%%%%%%%%%%%%
%%Calculation of the SD
SDhr0g = std(allhr0g,0,2);
        plusSDhr0g = meanhr0g + SDhr0g;
        minusSDhr0g = meanhr0g - SDhr0g;
    SDsys0g = std(allsys0g,0,2);
        plusSDsys0g = meansys0g + SDsys0g;
        minusSDsys0g = meansys0g - SDsys0g;
    SDdia0g = std(alldia0g,0,2);
        plusSDdia0g = meandia0g + SDdia0g;
        minusSDdia0g = meandia0g - SDdia0g;
    SDmbp0g = std(allmbp0g,0,2);
        plusSDmbp0g = meanmbp0g + SDmbp0g;
        minusSDmbp0g = meanmbp0g - SDmbp0g;
    SDsv0g = std(allsv0g,0,2);
        plusSDsv0g = meansv0g + SDsv0g;
```

```
        minusSDsv0g = meansv0g - SDsv0g;
    SDco0g = std(allco0g,0,2);
        plusSDco0g = meanco0g + SDco0g;
        minusSDco0g = meanco0g - SDco0g;
    SDr0g = std(allr0g,0,2);
        plusSDr0g = meanr0g + SDr0g;
        minusSDr0g = meanr0g - SDr0g;
    SDpp0g = std(allpp0g,0,2);
        plusSDpp0g = meanpp0g + SDpp0g;
        minusSDpp0g = meanpp0g - SDpp0g;
SDhr1g = std(allhr1g,0,2);
        plusSDhr1g = meanhr1g + SDhr1g;
        minusSDhr1g = meanhr1g - SDhr1g;
    SDsys1g = std(allsys1g,0,2);
        plusSDsys1g = meansys1g + SDsys1g;
        minusSDsys1g = meansys1g - SDsys1g;
    SDdia1g = std(alldia1g,0,2);
        plusSDdia1g = meandia1g + SDdia1g;
        minusSDdia1g = meandia1g - SDdia1g;
    SDmbp1g = std(allmbp1g,0,2);
        plusSDmbp1g = meanmbp1g + SDmbp1g;
        minusSDmbp1g = meanmbp1g - SDmbp1g;
    SDsv1g = std(allsv1g,0,2);
        plusSDsv1g = meansv1g + SDsv1g;
        minusSDsv1g = meansv1g - SDsv1g;
    SDco1g = std(allco1g,0,2);
        plusSDco1g = meanco1g + SDco1g;
        minusSDco1g = meanco1g - SDco1g;
    SDr1g = std(allr1g,0,2);
        plusSDr1g = meanr1g + SDr1g;
        minusSDr1g = meanr1g - SDr1g;
    SDpp1g = std(allpp1g,0,2);
        plusSDpp1g = meanpp1g + SDpp1g;
        minusSDpp1g = meanpp1g - SDpp1g;
SDhr14g = std(allhr14g,0,2);
        plusSDhr14g = meanhr14g + SDhr14g;
        minusSDhr14g = meanhr14g - SDhr14g;
    SDsys14g = std(allsys14g,0,2);
        plusSDsys14g = meansys14g + SDsys14g;
        minusSDsys14g = meansys14g - SDsys14g;
    SDdia14g = std(alldia14g,0,2);
        plusSDdia14g = meandia14g + SDdia14g;
        minusSDdia14g = meandia14g - SDdia14g;
    SDmbp14g = std(allmbp14g,0,2);
        plusSDmbp14g = meanmbp14g + SDmbp14g;
        minusSDmbp14g = meanmbp14g - SDmbp14g;
    SDsv14g = std(allsv14g,0,2);
        plusSDsv14g = meansv14g + SDsv14g;
        minusSDsv14g = meansv14g - SDsv14g;
    SDco14g = std(allco14g,0,2);
        plusSDco14g = meanco14g + SDco14g;
        minusSDco14g = meanco14g - SDco14g;
    SDr14g = std(allr14g,0,2);
        plusSDr14g = meanr14g + SDr14g;
        minusSDr14g = meanr14g - SDr14g;
    SDpp14g = std(allpp14g,0,2);
        plusSDpp14g = meanpp14g + SDpp14g;
        minusSDpp14g = meanpp14g - SDpp14g;


%% %%%%%%%%%%%%%%%%%%%%%%%%%%%%%%%%%%%%
%%Calculation of the Standard Error
n = 12;  %Number of subjects

SEhr0g = SDhr0g/sqrt(n);
        plusSEhr0g = meanhr0g + SEhr0g;
        minusSEhr0g = meanhr0g - SEhr0g;
    SEsys0g = SDsys0g/sqrt(n);
        plusSEsys0g = meansys0g + SEsys0g;
        minusSEsys0g = meansys0g - SEsys0g;
    SEdia0g = SDdia0g/sqrt(n);
```

```
        plusSEdia0g = meandia0g + SEdia0g;
        minusSEdia0g = meandia0g - SEdia0g;
    SEmbp0g = SDmbp0g/sqrt(n);
        plusSEmbp0g = meanmbp0g + SEmbp0g;
        minusSEmbp0g = meanmbp0g - SEmbp0g;
    SEsv0g = SDsv0g/sqrt(n);
        plusSEsv0g = meansv0g + SEsv0g;
        minusSEsv0g = meansv0g - SEsv0g;
    SEco0g = SDco0g/sqrt(n);
        plusSEco0g = meanco0g + SEco0g;
        minusSEco0g = meanco0g - SEco0g;
    SEr0g = SDr0g/sqrt(n);
        plusSEr0g = meanr0g + SEr0g;
        minusSEr0g = meanr0g - SEr0g;
    SEpp0g = SDpp0g/sqrt(n);
        plusSEpp0g = meanpp0g + SEpp0g;
        minusSEpp0g = meanpp0g - SEpp0g;
SEhr1g = SDhr1g/sqrt(n);
        plusSEhr1g = meanhr1g + SEhr1g;
        minusSEhr1g = meanhr1g - SEhr1g;
    SEsys1g = SDsys1g/sqrt(n);
        plusSEsys1g = meansys1g + SEsys1g;
        minusSEsys1g = meansys1g - SEsys1g;
    SEdia1g = SDdia1g/sqrt(n);
        plusSEdia1g = meandia1g + SEdia1g;
        minusSEdia1g = meandia1g - SEdia1g;
    SEmbp1g = SDmbp1g/sqrt(n);
        plusSEmbp1g = meanmbp1g + SEmbp1g;
        minusSEmbp1g = meanmbp1g - SEmbp1g;
    SEsv1g = SDsv1g/sqrt(n);
        plusSEsv1g = meansv1g + SEsv1g;
        minusSEsv1g = meansv1g - SEsv1g;
    SEco1g = SDco1g/sqrt(n);
        plusSEco1g = meanco1g + SEco1g;
        minusSEco1g = meanco1g - SEco1g;
    SEr1g = SDr1g/sqrt(n);
        plusSEr1g = meanr1g + SEr1g;
        minusSEr1g = meanr1g - SEr1g;
    SEpp1g = SDpp1g/sqrt(n);
        plusSEpp1g = meanpp1g + SEpp1g;
        minusSEpp1g = meanpp1g - SEpp1g;

SEhr14g = SDhr14g/sqrt(n);
        plusSEhr14g = meanhr14g + SEhr14g;
        minusSEhr14g = meanhr14g - SEhr14g;
    SEsys14g = SDsys14g/sqrt(n);
        plusSEsys14g = meansys14g + SEsys14g;
        minusSEsys14g = meansys14g - SEsys14g;
    SEdia14g = SDdia14g/sqrt(n);
        plusSEdia14g = meandia14g + SEdia14g;
        minusSEdia14g = meandia14g - SEdia14g;
    SEmbp14g = SDmbp14g/sqrt(n);
        plusSEmbp14g = meanmbp14g + SEmbp14g;
        minusSEmbp14g = meanmbp14g - SEmbp14g;
    SEsv14g = SDsv14g/sqrt(n);
        plusSEsv14g = meansv14g + SEsv14g;
        minusSEsv14g = meansv14g - SEsv14g;
    SEco14g = SDco14g/sqrt(n);
        plusSEco14g = meanco14g + SEco14g;
        minusSEco14g = meanco14g - SEco14g;
    SEr14g = SDr14g/sqrt(n);
        plusSEr14g = meanr14g + SEr14g;
        minusSEr14g = meanr14g - SEr14g;
    SEpp14g = SDpp14g/sqrt(n);
        plusSEpp14g = meanpp14g + SEpp14g;
        minusSEpp14g = meanpp14g - SEpp14g;

%% Calculation of Mean, SD and SE taking out some readings for filtering purposes

%% Cardiac Output 1.4g
```

```
mask = ones (size(allco14g));
mask(9600:10400,1)=0;  %Subject 5
mask(8250:10500,3)=0;  %Subject 7

CO14 = allco14g.*mask;
meanco14g_mod = sum(CO14,2)./sum(mask,2);

CO214=zeros(size(allco14g));
for i = 1: length (meanco14g_mod);
    CO214(i,:)=(CO14(i,:)-meanco14g_mod(i)).^2;
end

SDco14g_mod = (sum(CO214,2)./(sum(mask,2)-1)).^(1/2);
    plusSDco14g_mod = meanco14g_mod + SDco14g_mod;
    minusSDco14g_mod = meanco14g_mod - SDco14g_mod;
SEco14g_mod = SDco14g_mod./sqrt(sum(mask,2));
    plusSEco14g_mod = meanco14g_mod + SEco14g_mod;
    minusSEco14g_mod = meanco14g_mod - SEco14g_mod;

%% Diastolic Blood pressure 0g
mask = ones (size(alldia0g));

BP0 = alldia0g.*mask;
meandia0g_mod = sum(BP0,2)./sum(mask,2);

BP02=zeros(size(alldia0g));
for i = 1: length (meandia0g_mod);
    BP02(i,:)=(BP0(i,:)-meandia0g_mod(i)).^2;
end

SDdia0g_mod = (sum(BP02,2)./(sum(mask,2)-1)).^(1/2);
    plusSDdia0g_mod = meandia0g_mod + SDdia0g_mod;
    minusSDdia0g_mod = meandia0g_mod - SDdia0g_mod;
SEdia0g_mod = SDdia0g_mod./sqrt(sum(mask,2));
    plusSEdia0g_mod = meandia0g_mod + SEdia0g_mod;
    minusSEdia0g_mod = meandia0g_mod - SEdia0g_mod;

%% Diastolic Blood pressure 1.4g
mask = ones (size(alldia0g));
mask(9600:10400,1)=0;  %Subject 5
mask(8250:10500,3)=0;  %Subject 7
mask(11350:11950,10)=0;  %Subject 15

BP14 = alldia14g.*mask;
meandia14g_mod = sum(BP14,2)./sum(mask,2);

BP142=zeros(size(alldia14g));
for i = 1: length (meandia14g_mod);
    BP142(i,:)=(BP14(i,:)-meandia14g_mod(i)).^2;
end

SDdia14g_mod = (sum(BP142,2)./(sum(mask,2)-1)).^(1/2);
    plusSDdia14g_mod = meandia14g_mod + SDdia14g_mod;
    minusSDdia14g_mod = meandia14g_mod - SDdia14g_mod;
SEdia14g_mod = SDdia14g_mod./sqrt(sum(mask,2));
    plusSEdia14g_mod = meandia14g_mod + SEdia14g_mod;
    minusSEdia14g_mod = meandia14g_mod - SEdia14g_mod;

%% Mean Blood pressure 0g
mask = ones (size(allmbp0g));

MBP0 = allmbp0g.*mask;
meanmbp0g_mod = sum(MBP0,2)./sum(mask,2);

MBP02=zeros(size(allmbp0g));
for i = 1: length (meanmbp0g_mod);
    MBP02(i,:)=(MBP0(i,:)-meanmbp0g_mod(i)).^2;
end

SDmbp0g_mod = (sum(MBP02,2)./(sum(mask,2)-1)).^(1/2);
    plusSDmbp0g_mod = meanmbp0g_mod + SDmbp0g_mod;
```

```
    minusSDmbp0g_mod = meanmbp0g_mod - SDmbp0g_mod;
SEmbp0g_mod = SDmbp0g_mod./sqrt(sum(mask,2));
    plusSEmbp0g_mod = meanmbp0g_mod + SEmbp0g_mod;
    minusSEmbp0g_mod = meanmbp0g_mod - SEmbp0g_mod;

%% Mean Blood pressure 1.4g
mask = ones (size(allmbp0g));
mask(8250:10500,3)=0;  %Subject 7

MBP14 = allmbp14g.*mask;
meanmbp14g_mod = sum(MBP14,2)./sum(mask,2);

MBP142=zeros(size(allmbp14g));
for i = 1: length (meanmbp14g_mod);
    MBP142(i,:)=(MBP14(i,:)-meanmbp14g_mod(i)).^2;
end

SDmbp14g_mod = (sum(MBP142,2)./(sum(mask,2)-1)).^(1/2);
    plusSDmbp14g_mod = meanmbp14g_mod + SDmbp14g_mod;
    minusSDmbp14g_mod = meanmbp14g_mod - SDmbp14g_mod;
SEmbp14g_mod = SDmbp14g_mod./sqrt(sum(mask,2));
    plusSEmbp14g_mod = meanmbp14g_mod + SEmbp14g_mod;
    minusSEmbp14g_mod = meanmbp14g_mod - SEmbp14g_mod;

%% Systolic Blood pressure 1.4g
mask = ones (size(allsys0g));
mask(9600:10400,1)=0;  %Subject 5

SBP14 = allsys14g.*mask;
meansys14g_mod = sum(SBP14,2)./sum(mask,2);

SBP142=zeros(size(allsys14g));
for i = 1: length (meansys14g_mod);
    SBP142(i,:)=(SBP14(i,:)-meansys14g_mod(i)).^2;
end

SDsys14g_mod = (sum(SBP142,2)./(sum(mask,2)-1)).^(1/2);
    plusSDsys14g_mod = meansys14g_mod + SDsys14g_mod;
    minusSDsys14g_mod = meansys14g_mod - SDsys14g_mod;
SEsys14g_mod = SDsys14g_mod./sqrt(sum(mask,2));
    plusSEsys14g_mod = meansys14g_mod + SEsys14g_mod;
    minusSEsys14g_mod = meansys14g_mod - SEsys14g_mod;

%% Pulse pressure 1.4g
mask = ones (size(allpp0g));
mask(9600:10400,1)=0;  %Subject 5
mask(8250:10500,3)=0;  %Subject 7

PP14 = allpp14g.*mask;
meanpp14g_mod = sum(PP14,2)./sum(mask,2);

PP142=zeros(size(allpp14g));
for i = 1: length (meanpp14g_mod);
    PP142(i,:)=(PP14(i,:)-meanpp14g_mod(i)).^2;
end

SDpp14g_mod = (sum(PP142,2)./(sum(mask,2)-1)).^(1/2);
    plusSDpp14g_mod = meanpp14g_mod + SDpp14g_mod;
    minusSDpp14g_mod = meanpp14g_mod - SDpp14g_mod;
SEpp14g_mod = SDpp14g_mod./sqrt(sum(mask,2));
    plusSEpp14g_mod = meanpp14g_mod + SEpp14g_mod;
    minusSEpp14g_mod = meanpp14g_mod - SEpp14g_mod;

%% Stroke Volume 1.4g
mask = ones (size(allsv14g));
mask(9600:10400,1)=0;  %Subject 5
mask(8250:10500,3)=0;  %Subject 7
mask(11350:11950,10)=0;  %Subject 15

SV14 = allsv14g.*mask;
meansv14g_mod = sum(SV14,2)./sum(mask,2);
```

```
SV142=zeros(size(allsv14g));
for i = 1: length (meansv14g_mod);
    SV142(i,:)=(SV14(i,:)-meansv14g_mod(i)).^2;
end

SDsv14g_mod = (sum(SV142,2)./(sum(mask,2)-1)).^(1/2);
    plusSDsv14g_mod = meansv14g_mod + SDsv14g_mod;
    minusSDsv14g_mod = meansv14g_mod - SDsv14g_mod;
SEsv14g_mod = SDsv14g_mod./sqrt(sum(mask,2));
    plusSEsv14g_mod = meansv14g_mod + SEsv14g_mod;
    minusSEsv14g_mod = meansv14g_mod - SEsv14g_mod;

%% Peripheral resistance 1.4g
mask = ones (size(allr14g));
mask(8250:10500,3)=0;  %Subject 7
mask(19050:19700,4)=0;  %Subject 8
mask(20950:21840,4)=0;  %Subject 8
mask(11180:12010,10)=0;  %Subject 15
mask(1:4281,5)=0;  %Subject 9

R14 = allr14g.*mask;
meanr14g_mod = sum(R14,2)./sum(mask,2);

R214=zeros(size(allr14g));
for i = 1: length (meanr14g_mod);
    R214(i,:)=(R14(i,:)-meanr14g_mod(i)).^2;
end

SDr14g_mod = (sum(R214,2)./(sum(mask,2)-1)).^(1/2);
    plusSDr14g_mod = meanr14g_mod + SDr14g_mod;
    minusSDr14g_mod = meanr14g_mod - SDr14g_mod;
SEr14g_mod = SDr14g_mod./sqrt(sum(mask,2));
    plusSEr14g_mod = meanr14g_mod + SEr14g_mod;
    minusSEr14g_mod = meanr14g_mod - SEr14g_mod;

%% Peripheral resistance 0g
mask = ones (size(allr0g));
mask(1:1305,3)=0;  %Subject 7

R0 = allr0g.*mask;
meanr0g_mod = sum(R0,2)./sum(mask,2);

R20=zeros(size(allr0g));
for i = 1: length (meanr0g_mod);
    R20(i,:)=(R0(i,:)-meanr0g_mod(i)).^2;
end

SDr0g_mod = (sum(R20,2)./(sum(mask,2)-1)).^(1/2);
    plusSDr0g_mod = meanr0g_mod + SDr0g_mod;
    minusSDr0g_mod = meanr0g_mod - SDr0g_mod;
SEr0g_mod = SDr0g_mod./sqrt(sum(mask,2));
    plusSEr0g_mod = meanr0g_mod + SEr0g_mod;
    minusSEr0g_mod = meanr0g_mod - SEr0g_mod;
```

```
%% PLOT ALL SUBJECTS

close all
clear all
clc

getCVdata;
processCVdata;

%% Cardiac Output
%Plot modified including manual removal of misreading data
%1.4g
%mask(9600:10400,1)=0;  %Subject 5
%mask(8250:10500,3)=0;  %Subject 7
figure(2);
```

```
hold on;
boundedline (t_std , meanco0g, SEco0g, '-r','alpha',...
             t_std, meanco1g, SEco1g , '-b','alpha',...
             t_std , meanco14g_mod, SEco14g_mod, '-g', 'alpha');
plot(t_std,meanco0g,'LineWidth',3,'color','r');
plot(t_std,meanco1g,'LineWidth',3,'color','b');
plot(t_std,meanco14g_mod,'LineWidth',3,'color','g');
title('Cardiac Output (Mean and SE)','FontSize',20,'FontName','Times');
ylabel('Cardiac Output (liters per minute)','FontSize',18,'FontName','Times');
xlabel('Time (minutes)','FontSize',18,'FontName','Times');
legend('No Centrip','1G Centrip','1.4G Centrip','Location','NorthWest');
ax = gca;
set(ax,'FontSize',16);
box on;
axis([0,25,0,20]);


%% Diastolic Blood Pressure
%Plot modified including manual removal of misreading data
%0g
%mask(3000:25000,1)=0;  %Subject 5 (no)
%1.4g
% mask(9600:10400,1)=0;  %Subject 5
% mask(8250:10500,3)=0;  %Subject 7
% mask(11350:11950,10)=0;  %Subject 15
figure(5);
hold on;
boundedline (t_std , meandia0g_mod, SEdia0g_mod, '-r','alpha',...
             t_std, meandia1g, SEdia1g , '-b','alpha',...
             t_std , meandia14g_mod, SEdia14g_mod, '-g', 'alpha');
plot(t_std,meandia0g_mod,'LineWidth',3,'color','r');
plot(t_std,meandia1g,'LineWidth',3,'color','b');
plot(t_std,meandia14g_mod,'LineWidth',3,'color','g');
title('Diastolic BP (Mean and SE)','FontSize',20,'FontName','Times');
ylabel('Diastolic Blood Pressure (mmHg)','FontSize',18,'FontName','Times');
xlabel('Time (minutes)','FontSize',18,'FontName','Times');
legend('No Centrip','1G Centrip','1.4G Centrip','Location','NorthWest');
ax = gca;
set(ax,'FontSize',16);
%legend boxoff;
box on;


%% Heart Rate
figure(7);
hold on;
boundedline (t_std , meanhr0g, SEhr0g, '-r','alpha',...
             t_std, meanhr1g, SEhr1g , '-b','alpha',...
             t_std , meanhr14g, SEhr14g, '-g', 'alpha');
plot(t_std,meanhr0g,'LineWidth',3,'color','r');
plot(t_std,meanhr1g,'LineWidth',3,'color','b');
plot(t_std,meanhr14g,'LineWidth',3,'color','g');
title('Heart Rate (Mean and SE)','FontSize',20,'FontName','Times');
ylabel('Heart Rate (beats per minute)','FontSize',18,'FontName','Times');
xlabel('Time (minutes)','FontSize',18,'FontName','Times');
legend('No Centrip','1G Centrip','1.4G Centrip','Location','NorthWest');
ax = gca;
set(ax,'FontSize',16);
box on;


%% Mean Blood Pressure
%Plot modified including manual removal of misreading data
%0g
%mask(3000:25000,1)=0;  %Subject 5
%1.4g
% mask(8250:10500,3)=0;  %Subject 7
figure(10);
hold on;
boundedline (t_std , meanmbp0g_mod, SEmbp0g_mod, '-r','alpha',...
             t_std, meanmbp1g, SEmbp1g , '-b','alpha',...
```

```
            t_std , meanmbp14g_mod, SEmbp14g_mod, '-g', 'alpha');
plot(t_std,meanmbp0g_mod,'LineWidth',3,'color','r');
plot(t_std,meanmbp1g,'LineWidth',3,'color','b');
plot(t_std,meanmbp14g_mod,'LineWidth',3,'color','g');
title('Mean Blood Pressure (Mean and SE)','FontSize',18,'FontName','Times');
ylabel('Mean Blood Pressure (mmHg)','FontSize',18,'FontName','Times');
xlabel('Time (minutes)','FontSize',18,'FontName','Times');
legend('No Centrip','1G Centrip','1.4G Centrip','Location','NorthWest');
ax = gca;
set(ax,'FontSize',16);
box on;


%% Pulse Pressure
%Plot modified including manual removal of misreading data
%1.4g
% mask(9600:10400,1)=0;  %Subject 5 (No)
% mask(8250:10500,3)=0;  %Subject 7

figure(13);
hold on;
boundedline (t_std , meanpp0g, SEpp0g, '-r','alpha',...
             t_std, meanpp1g, SEpp1g , '-b','alpha',...
             t_std , meanpp14g_mod, SEpp14g_mod, '-g', 'alpha');
plot(t_std,meanpp0g,'LineWidth',3,'color','r');
plot(t_std,meanpp1g,'LineWidth',3,'color','b');
plot(t_std,meanpp14g_mod,'LineWidth',3,'color','g');
title('Pulse Pressure (Mean and SE)','FontSize',20,'FontName','Times');
ylabel('Pulse Pressure (mmHg)','FontSize',18,'FontName','Times');
xlabel('Time (minutes)','FontSize',18,'FontName','Times');
legend('No Centrip','1G Centrip','1.4G Centrip','Location','SouthWest');
ax = gca;
set(ax,'FontSize',16);
box on;
axis([0,25,10,80]);


%% Stroke Volume
%Plot modified including manual removal of misreading data
%1.4g
% mask(9600:10400,1)=0;  %Subject 5
% mask(8250:10500,3)=0;  %Subject 7
%mask(11350:11950,10)=0;  %Subject 15
figure(16);
hold on;
boundedline (t_std , meansv0g, SEsv0g, '-r','alpha',...
             t_std, meansv1g, SEsv1g , '-b','alpha',...
             t_std , meansv14g_mod, SEsv14g_mod, '-g', 'alpha');
plot(t_std,meansv0g,'LineWidth',3,'color','r');
plot(t_std,meansv1g,'LineWidth',3,'color','b');
plot(t_std,meansv14g_mod,'LineWidth',3,'color','g');
title('Stroke Volume (Mean and SE)','FontSize',20,'FontName','Times');
ylabel('Stroke Volume (mL)','FontSize',18,'FontName','Times');
xlabel('Time (minutes)','FontSize',18,'FontName','Times');
legend('No Centrip','1G Centrip','1.4G Centrip','Location','SouthWest');
ax = gca;
set(ax,'FontSize',16);
box on;
axis([0,25,50,130]);


%% Systolic Blood Pressure
%Plot modified including manual removal of misreading data
%1.4g
% mask(9600:10400,1)=0;  %Subject 5
figure(19);
hold on;
boundedline (t_std , meansys0g, SEsys0g, '-r','alpha',...
             t_std, meansys1g, SEsys1g , '-b','alpha',...
             t_std , meansys14g_mod, SEsys14g_mod, '-g', 'alpha');
plot(t_std,meansys0g,'LineWidth',3,'color','r');
```

```
plot(t_std,meansys1g,'LineWidth',3,'color','b');
plot(t_std,meansys14g_mod,'LineWidth',3,'color','g');
title('Systolic BP (Mean and SE)','FontSize',20,'FontName','Times');
ylabel('Systolic Blood Pressure (mmHg)','FontSize',18,'FontName','Times');
xlabel('Time (minutes)','FontSize',18,'FontName','Times');
legend('No Centrip','1G Centrip','1.4G Centrip','Location','SouthEast');
ax = gca;
set(ax,'FontSize',16);
box on;
axis([0,25,80,180]);


%% Resistance
%Plot modified including manual removal of misreading data
%1.4g
% mask(8250:10500,3)=0;  %Subject 7
% mask(19050:19700,4)=0;  %Subject 8
% mask(20950:21840,4)=0;  %Subject 8
% mask(11180:12010,10)=0;  %Subject 15
% mask(1:4281,5)=0;  %Subject 9
%0g
%mask(1:1305,3)=0;  %Subject 5

figure(22);
hold on;
boundedline (t_std , meanr0g_mod./1330, SEr0g_mod/1330, '-r','alpha',...
             t_std, meanr1g./1330, SEr1g/1330 , '-b','alpha',...
             t_std , meanr14g_mod./1330, SEr14g_mod/1330, '-g', 'alpha');
plot(t_std,meanr0g_mod/1330,'LineWidth',3,'color','r');
plot(t_std,meanr1g/1330,'LineWidth',3,'color','b');
plot(t_std,meanr14g_mod/1330,'LineWidth',3,'color','g');
title('Vascular Resistance (Mean and SE)','FontSize',20,'FontName','Times');
ylabel('Resistance (PRU: mmHg/ml/sec)','FontSize',18,'FontName','Times');
xlabel('Time (minutes)','FontSize',18,'FontName','Times');
legend('No Centrip','1G Centrip','1.4G Centrip','Location','NorthWest');
axis([0,25,0,2]);
ax = gca;
set(ax,'FontSize',16);
box on;
```

C. Nexfin Noninvasive Continuous Hemodynamic Monitoring

The Nexfin system (BMEYE B.V. Amsterdam, the Netherlands) allows accurate hemodynamic monitoring non-invasively. The only interface with the subject is a finger cuff that includes an infrared photo-plethysmograph sensor that measures the diameter of the finger arteries. The cuff inflates or deflates in order to keep the diameter of the "unload" arteries (no tensions in the walls) constant during the cardiac cycle, and this cuff pressure is directly measured as the real-time finger pressure waveform [95]. This is called the "volume clamp method"[69]. The arteries diameter set point level and periodic automatic adjustments are established using the "Physiocal" method, which is based on the curvature and sharpness of the plethysmogram during short periods of steady cuff pressure levels [74], [96]. The finger pressure waveform is then transformed to brachial pressure waveform to counteract both the pressure drop due to resistance, and the pressure wave amplification in peripheral measurements sites like the fingers.

Stroke volume and cardiac output are calculated using the CO-Trek pulse contour algorithm, summarized in Figure 92. This method incorporates a three-element Windkessel model, where C_w represents the sum of all compliances of all arteries, R_p equals the total peripheral resistance, and Z_c represents the characteristic impedance of the aorta, or in other words, the impedance that the ventricle encounters during ejection. C_w and Z_c are non-linear functions of pressure and they depend on patient age, weight, gender, and height. R_p is calculated iteratively as the ratio of mean arterial pressure (MAP) and CO. The aortic input impedance Zin is calculated from the three-element Windkessel model using non-linear relationships [82].

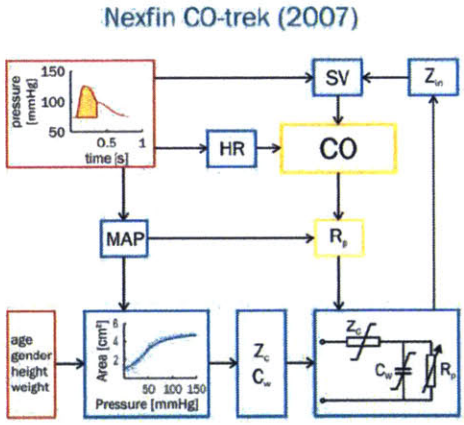

Figure 92 – Nexfin CO-Trek methodology (figure taken from [74]).

Stroke volume is obtained instantaneously by dividing the Pulsatile Systolic Area (PSA, time-integral of the systolic part of the arterial pressure wave) by the aortic input impedance Zin. Finally, cardiac output is calculated as the product of stroke volume and heart rate.

D. Forms for the Centrifuge Experiment

COUHES APPROVAL

MIT Committee On the Use of Humans as Experimental Subjects

MASSACHUSETTS INSTITUTE OF TECHNOLOGY
77 Massachusetts Avenue
Cambridge, Massachusetts 02139
Building E 25-143B
(617) 253-6787

To:	Laurence Young 37-219
From:	Leigh Firn, Chair COUHES
Date:	11/20/2014
Committee Action:	**Renewal**
Committee Action Date	11/20/2014
COUHES Protocol #	1301005479
Study Title	Artificial Gravity with Ergonomic Exercise: Development and Characterization of a Test Platform Meeting Requirements for Future Inflight Studies
Expiration Date	11/19/2015

The above-referenced protocol was given renewed approval following full board review by the Committee on the Use of Humans as Experimental Subjects (COUHES).

If the research involves collaboration with another institution then the research cannot commence until COUHES receives written notification of approval from the collaborating institution's IRB.

It is the Principal Investigator's responsibility to obtain review and continued approval before the expiration date. You may not continue any research activity beyond the expiration date without approval by COUHES. Failure to renew your study before the expiration date will result in termination of the study and suspension of related research grants.

Adverse Events: Any serious or unexpected adverse event must be reported to COUHES within 48 hours. All other adverse events should be reported in writing within 10 working days.

Amendments: Any changes to the protocol that impact human subjects, including changes in experimental design, equipment, personnel or funding, must be approved by COUHES before they can be initiated.

Prospective new study personnel must, where applicable, complete training in human subjects research and in the HIPAA Privacy Rule before participating in the study.

You must maintain a research file for at least 3 years after completion of the study. This file should include all correspondence with COUHES, original signed consent forms, and study data.

CONSENT FORM

CONSENT TO PARTICIPATE IN NON-BIOMEDICAL RESEARCH

Artifical Gravity with Ergonomic Exercise: Development and Characterization of a Test Platform to Meet Requirements for Future Inflight Studies

You are asked to participate in a research study conducted by Laurence Young, Sc.D., from the Department of Aeronautics and Astronautics at the Massachusetts Institute of Technology (M.I.T.). The results of this study may be published in a student thesis or scientific journal. You were selected as a possible participant in this study because you volunteered and meet the minimum health and physical requirements. You should read the information below, and ask questions about anything you do not understand, before deciding whether or not to participate.

PARTICIPATION AND WITHDRAWAL

Your participation in this study is completely voluntary and you are free to choose whether to be in it or not. If you choose to be in this study, you may subsequently withdraw from it at any time without penalty or consequences of any kind. The investigator may withdraw you from this research if circumstances arise which warrant doing so. Such circumstances include evidence that you do not meet the minimum health and physical requirements, or that during the study it becomes clear to the experimenter that you are becoming drowsy, unalert, or uncooperative.

You should not participate in this study if you have any medical heart conditions, respiratory conditions, musculoskeletal conditions, medical conditions which would be triggered if you develop motion sickness, are under the influence of alcohol, caffeine, anti-depressants, or sedatives, have suffered in the past from a serious head injury (concussion), or if there is any possibility that you may be pregnant. The experimenter will check to see if you meet these requirements.

PURPOSE OF THE STUDY

Short radius centrifugation is currently being investigated as a countermeasure to the deleterious effects of weightlessness experienced during long duration spaceflight. The purpose of this study is to characterize, both physiologically and mechanically, a proposed design for a short radius centrifuge that would fit within the confines of a spacecraft, as well as to develop an optimal centrifugation and exercise regimen for this centrifuge.

PROCEDURES

If you volunteer to participate in this study, we would ask you to do the following things: When you arrive at the lab, you will be briefed on the background of centrifugation, disqualifying medical conditions, the experiment protocol, and the various components of the centrifuge, including the emergency stop button, restraining belt, and data collection devices. Data collection devices include a tape measure, scale, heart a rate sensor, blood

pressure sensor, inertial sensors on your legs, EMG electrodes, and force sensors on the pedals of the cycle ergometer. Additional data will be collected from accelerometers on the centrifuge arm, though these sensors will not be attached to your body. After your briefing, the experimenter will record your answers to basic questions about your health, ask you to complete a pre-participation questionnaire, and take your height, weight, blood pressure, and heart rate.

During the experiment you will be on the centrifuge lying on your side with your head slightly to the side of the center of rotation. Two leg pads will be strapped to your lower leg, and two leg cuffs will be strapped around your upper leg. Your feet may be strapped into foot pedals of an exercise device, or left to rest on a platform. A three-point harness will be secured prior to beginning trials. After lying down, the experimenter may collect some data while the centrifuge is stationary. The experimenter will explain the centrifugation regimen, and ask you if you are ready before starting rotation. The regiment will meet the following requirements:

- Acceleration will be no greater than 5 rpm/second
- G-level along your body axis will not exceed 2.0 G at your feet (a "1G" is defined as the acceleration or force that you experience normally while standing on earth).
- Time of rotation will not exceed 30 minutes
- Exercise loads will not exceed 300 watts

During rotation the experimenter may direct you to start or stop exercising, and will alert you to changes in speed of rotation and exercise loads. You may opt to perform the trials in the dark to minimize motion sickness. When the experiment is complete, the centrifuge will be stopped, and the experimenter may collect some additional data.

After the experiment you will be asked to report your subjective experience via an exit survey. All data, including the surveys, will be recorded anonymously.

As a participant in experimental trials, you tentatively agree to return for additional trials (at most 10) requested by the experimenter. You may or may not be assigned to a study group that performs similar tasks. Other than the time required for rotation, the time commitment is 20 minutes for the first briefing, and 10-60 minutes for other procedures before and after rotation.

POTENTIAL RISKS AND DISCOMFORTS

During rotation you may develop a headache or feel pressure in your legs caused by a fluid shift due to centrifugation. You may experience discomfort from the restraint and leg harnesses, and fatigue from exercise. You may also experience nausea or motion sickness, especially as a result of head movements. The experimenter will frequently ask you about your motion sickness to ensure your comfort, and your alertness will be monitored through communication and through video cameras. You may stop centrifugation at any time by hitting the onboard kill switch, or by alerting the experimenter.

POTENTIAL BENEFITS TO SUBJECTS

You will receive no benefits from this research.

POTENTIAL BENEFITS TO SOCIETY

The potential benefits to science and society are a better understanding of how short radius centrifugation can enable long duration spaceflight.

PAYMENT FOR PARTICIPATION

Subjects will not be eligible for payment for their participation.

CONFIDENTIALITY

Any information that is obtained in connection with this study and that can be identified with you will remain confidential and will be disclosed only with your permission or as required by law.

Some of the data collected in this study may be published in scientific journals and student theses. The data may consist of height, weight, heart rate, blood pressure, EMG activity, leg motion, forces you apply to the ergometer, subjective ratings of your comfort and motion sickness, and descriptive data on the trials including the artificial gravity loads and exposure time, exercise loads, and accelerations on the centrifuge.

During the experiment, the experimenter will monitor you through video cameras capable of imaging in darkness. You will be monitored to ensure your state of well being and compliance with the experiment protocol. In some cases the video data will be recorded on digitally. You have a right to review and edit the file. Any recorded videos will be accessible only by members of the current Artificial Gravity research team.

Research data collected during the experiment is stored in coded files that contain no personal information. This coding of the data will prevent linking your personal data to research data when it is analyzed or archived. Research data is stored in Microsoft excel files and ASCII files, and there is no certain date for destruction. The data is stored in Man Vehicle Lab computers that remain accessible only by Artificial Gravity team members. The investigator will retain a record of your participation so that you may be contacted in the future should your data be used for purposes other than those described here.

IDENTIFICATION OF INVESTIGATORS

If you have any questions or concerns about the research, please feel free to contact:

Principle Investigator: Laurence Young (37-219) 77 Massachusetts Avenue Cambridge, MA 02139 (617) 253-7759	

EMERGENCY CARE AND COMPENSATION FOR INJURY

If you feel you have suffered an injury, which may include emotional trauma, as a result of participating in this study, please contact the person in charge of the study as soon as possible.

In the event you suffer such an injury, M.I.T. may provide itself, or arrange for the provision of, emergency transport or medical treatment, including emergency treatment and follow-up care, as needed, or reimbursement for such medical services. M.I.T. does not provide any other form of compensation for injury. In any case, neither the offer to provide medical assistance, nor the actual provision of medical services shall be considered an admission of fault or acceptance of liability. Questions regarding this policy may be directed to M.I.T.'s Insurance Office, (617) 253-2823. Your insurance carrier may be billed for the cost of emergency transport or medical treatment, if such services are determined not to be directly related to your participation in this study.

RIGHTS OF RESEARCH SUBJECTS

You are not waiving any legal claims, rights or remedies because of your participation in this research study. If you feel you have been treated unfairly, or you have questions regarding your rights as a research subject, you may contact the Chair-man of the Committee on the Use of Humans as Experimental Subjects, M.I.T., Room E25-143b, 77 Massachusetts Ave, Cambridge, MA 02139. Phone: 617-253-6787.

SIGNATURE OF RESEARCH SUBJECT OR LEGAL REPRESENTATIVE

I have read (or someone has read to me) the information provided above. I have been given an opportunity to ask questions and all of my questions have been answered to my satisfaction. I have been given a copy of this form.

BY SIGNING THIS FORM, I WILLINGLY AGREE TO PARTICIPATE IN THE RESEARCH IT DESCRIBES.

_____
Name of Subject

_____
Name of Legal Representative (if applicable)

_____ _____
Signature of Subject or Legal Representative Date

SIGNATURE OF INVESTIGATOR

I have explained the research to the subject or his/her legal representative, and answered all of his/her questions. I believe that he/she understands the information described in this document and freely consents to participate.

_____
Name of Investigator

_____ _____
Signature of Investigator Date (must be the same as subject's)

SIGNATURE OF WITNESS (If required by COUHES)

My signature as witness certified that the subject or his/her legal representative signed this consent form in my presence as his/her voluntary act and deed.

_____ _____
Name of Witness Date

CHECKLIST

SUBJECT: CONDITION: Date:

A. Setup

1. Control Room Comp..... .....ON
   Password: spinaround
2. Onboard Battery..... .....ON
3. Onboard Computer (OC) ..... ON
   Password: spinaround
4. Ergometer.....ON
5. From the control room computer, log in remotely to onboard computer via remote desktop:
   a. Computer: centrifugeOB
   b. Username: CentrifugeOB/Centrifuge
   c. Password (if asked): spinaround
6. OC: Open LEM
   a. Login (upper right corner)
      i. Username: lode
      ii. Password: service
   b. Add subject name
   c. Select "CV Testing1" protocol
7. OC: Open Logger Lite 1.6.1
   a. Check and ZERO the sensor inputs:
      i. **Force 1(left foot)**
      ii. **Force 2 (right feet)**
      iii. 3-axis accelerometer
   b. Check collection frequency and time interval of frequency (Experiment -> Data Collection)
      i. Duration: **30 min**
      ii. Sampling rate: **120 samples/min**
   c. File/Save as: **Subject_rpm**
8. Record room temperature and humidity
9. Disinfect HR belt
10. Ensure anchor on centrifuge main arm
11. Ergometer baseplate.....LOCKED
12. Ergometer on struts.....LOCKED
13. Chair.....LOCKED
14. Upper leg cuff mount.....LOCKED
15. Prepare consent, eligibility, and post-test survey documentation.
16. Check onboard camera feed: 192.168.0.13
    a. Username: admin
    b. Password: spinaround
    c. Use lower Login button (server push mode)
17. Open MMT in laptop

B. Subject Orientation

1. Review Consent Form with subject
2. Sign Consent Form
3. Administer Eligibility and Pre-Procedure Questionnaire
4. Check results to Questionnaire Clarification document to ensure eligibility.
5. Check subject clothing (no loose articles, nothing in pocket, proper shoes with toe covering)
6. Get subject's info
   a. Name:
   b. Weight (kg/lb):
   c. Height:
   d. Age:
   e. Date of birth:
7. Get a subject ID:
8. Enter data in the LEM profile
9. Enter data in the CCNexfin system
10. Enter weight (lb) in MMT

1

SUBJECT: CONDITION: Date:

C. Boarding

1. Don leg pads (2), if needed
2. Add saline solution to HR belt
3. Allow subject to don HR belt
4. Check Garmin for HR belt signal
5. Climb in and attach safety harness in all 3 positions
6. Adjust slider board to proper position (head at the center of rotation). Lock in place with strut sections and enter radial distance at the end of the slider board into the MMT
    a. Slider radius (m):
7. Adjust position of eye bolts as needed to align with upper and lower leg.
8. Strap feet into ergometer.
9. Don upper leg cuffs (2).
10. Adjust exerciser baseplate radially. Lock in place. with pins (1-2) and carriage locks. Enter positions into the MMT.
    a. Foot radius (m):
11. Adjust ergometer along struts. Lock in place with pins (2). Enter distance into the MMT.
    a. Ergometer offset (m):
12. Tighten upper leg cuffs.
13. Don blood pressure finger cuff.
14. Adjust headrest as needed.
15. Run MMT.
16. Add counterweights as specified.
    a. Counterweights:
17. Disconnect batteries from power strip. Store extension cord.
18. Flip on the kill switch circuit box (check for red light).
19. Check that subject can reach kill switch.
20. Unclamp centrifuge arm, stow clamp.
21. Push centrifuge arm 360° to check for clearances.

D. Preparation for data collection (Control Computer)

1. Configure LEM for data collection
    a. Test subject: Subject
    b. Test Ergometer: Angio 2003
    c. Test Protocol: CV Testing1
    d. Visualization: workload, rpm, protocol
2. LEM: click start and wait for the "Initialization successful" message
    a. If problem, check that the bike is ON and powered.
3. Start "Centrifuge Control" (green icon on the desktop)
    a. Click ok when the next message appears "New maximum velocity is 35 rpm"
4. Locate all the windows so they are all visible
    a. Camera
    b. LEM
    c. Logger Lite
    d. Centrifuge Control

SUBJECT: CONDITION: Date:

E. Trial

1. Start data collection at the same time:
    a. **TIME:**
    b. ccNexfin
    c. HR monitor
    d. LEM: "CV Testing" protocol
    e. Logger Lite
2. Start the metronome at 120 pedals/min
3. During 3 minutes check the status of the data collection, and prepare for the spin up
4. Manual control box .....OFF
5. Manual control box .....ON
6. Control type.....AUTO
7. Run type.....RUN
8. Direction.....FORWARD
9. RPM Dial.....0
10. Engage (click up once to 'Start').
11. After **TIME = 3min:**
12. Accelerate centrifuge to specified acceleration.
    a. Specified rpm:
    b. Speed up in jumps of 5 rpm
        i. Click "Start"
        ii. Introduce rpm (jumps of 5rpm)
        iii. Click "Set Velo"
13. Alert subject to adjust body position as needed. Ask about comfort and positioning of:
    a. Safety harness
    b. Lower leg pads
    c. Upper leg cuffs
    d. Position of ergometer
    e. Sensors
14. Check Logger Lite/LEM for active sensor readings.
15. Check video display for live feed.
16. Wait for the "AG exposure warm-up" time to complete
17. After **TIME = 6m:45s**
    a. Alert subject to begin cycling.
18. During trial, alert subject to upcoming changes in workload.
19. During trial, monitor:
    a. Subject via video and oral communication
    b. Sensor readouts
    c. Acceleration (speed). Adjust as necessary.
20. At the end of the exercise (workload=0), tell the subject to stop cycling, and continue the spinning for 2 min.
21. Alert subject that deceleration is coming (suggest closing eyes).
22. At **TIME = 23m:45s,**
    a. Decelerate centrifuge to 0 RPM.
        i. Click "Stop"
23. Leave the subject to rest for 1min15s minutes
24. Stop/save LEM protocol.
25. Stop/save Logger Lite data collection.
26. Stop/save CCNexfin data
27. Stop/save HR monitor data

3

SUBJECT: CONDITION: Date:

F. Post-Trial

1. Manual control box .....OFF
2. Lock centrifuge arm.
3. Unstrap subject:
    a. Safety harness
    b. Blood pressure cuff
    c. Ergometer foot straps
    d. Upper leg cuffs
    e. Lower leg pads (if any)
4. Allow subject to doff HR belt.
5. Plug batteries into power cord.
6. Administer exit survey.
7. Export LEM data. Exit software
8. Export Logger Lite data. Exit software.
9. Copy ccNexfin data in a USB key and save in desktop. Exit software
10. Save a copy of the MMT configuration
11. Get HR data.
12. Onboard Computer ..... OFF
13. Onboard Battery.....OFF
14. Ergometer.....OFF
15. Kill switch circuit box.....OFF
16. Control room computer.....OFF

QUESTIONNAIRES

Eligibility and Pre-Participation Questionnaire

Please mark one box for each of the following questions. For any question to which you answered "Yes" please briefly explain. Answering "Yes" does not automatically disqualify you from the study.

Yes ☐ No ☐ 1. Do you currently have any neck, back, chest, hip, knee, ankle, or foot pain/discomfort?

Yes ☐ No ☐ 2. Do you have arthritis in your ankle, knee, or hip?

Yes ☐ No ☐ 3. Are you currently using any cardiac, blood pressure, or muscle relaxation/stimulant medications?

Yes ☐ No ☐ 4. Do you have any history of neck, back, chest, hip, knee, ankle, or foot injuries? When did these occur?

Yes ☐ No ☐ 5. Have you ever had ACL, PCL, MCL, or ACL surgery? If so how long ago?

Yes ☐ No ☐ 6. Have you recently strained a leg muscle (hip, quad, calf, etc.)? If so how long ago?

Yes ☐ No ☐ 7. Have you ever herniated a disk in you back from heavy lifting? If so how long ago?

Yes ☐ No ☐ 8. Have you ever broken a bone in your leg, ankle, or foot? If so, which bone(s) and how long ago?

Yes ☐ No ☐ 9. Are you prone to dizziness or motion sickness?

Yes ☐ No ☐ 10. Do you exercise regularly?

If so, what form (circle)? Cardiovascular, Strength training

How many days per week? _____

How many hours per session?_____

Describe your typical routine (which exercises, weights/reps, etc.)

Yes ☐ No ☐ 11. Do you experience joint or muscle pain when exercising?

Yes ☐ No ☐ 12. Are you, or could you be, pregnant?

To Be Filled Out by Investigator

Subject Number: _____

Weight: _____

Height: _____

Target HR: _____

Subject: Condition: Date:

Exit Survey

1. On a scale of 1-5 how comfortable was cycling on the centrifuge and how natural did it feel (1=very comfortable/natural, 5=very uncomfortable/unnatural),? What, if any, components contributed to discomfort?

2. On a scale of 1-5 how strenuous do you feel the exercise regimen was (1=easy, 5= very strenuous)? If strenuous, was this because of the resistance on the exercise device, the duration of the exercise, or both?

3. Do any muscles or areas of your body feel sore?

4. Circle how much each symptom below is affecting you right now:

#	Symptom	Severity			
1.	General discomfort	None	Slight	Moderate	Severe
2.	Fatigue	None	Slight	Moderate	Severe
3.	Headache	None	Slight	Moderate	Severe
4.	Eye strain	None	Slight	Moderate	Severe
5.	Difficulty focusing	None	Slight	Moderate	Severe
6.	Salivation increased	None	Slight	Moderate	Severe
7.	Sweating	None	Slight	Moderate	Severe
8.	Nausea	None	Slight	Moderate	Severe
9.	Difficulty concentrating	None	Slight	Moderate	Severe
10.	"Fullness of the head"	None	Slight	Moderate	Severe
11.	Blurred vision	None	Slight	Moderate	Severe
12.	Dizziness with eyes open	None	Slight	Moderate	Severe
13.	Dizziness with eyes closed	None	Slight	Moderate	Severe
14.	*Vertigo	None	Slight	Moderate	Severe
15.	**Stomach awareness	None	Slight	Moderate	Severe
16.	Burping	None	Slight	Moderate	Severe

5. Did you experience motion sickness? If so, when did this occur?

On scale of 1 to 10, rate your overall motion sickness: _____

0 – no symptoms
1 - any symptom no matter how slight
2 – minimal warmth, fatigue
5 – stomach awareness
7 – moderate nausea
9 – incipient vomiting
10 - vomiting

6. Did you notice the Coriolis forces acting in the lateral direction that you were pedaling (as if pushing or pulling on your knees)?

7. Any other comments you'd like to share?

FOR CLARIFICATION ONLY, THIS PAGE NOT GIVEN TO SUBJECTS

Medical Screening

Subjects will be screened for medical conditions by the Eligibility/Pre-Participation Questionnaire. Of the 12 questions, there are five for which a "yes" answer would result in an automatic disqualification (#1, 2, 3, 11,12) as these indicate the subject has a current medical condition or is on medication that put them at risk.

There are five questions (#4, 5, 6, 7, 8) for which a "yes" answer would result in disqualification depending on the time period since the indicated injury. If subjects indicate the injury has occurred within the last 6 months they will be disqualified, otherwise they will be allowed to participate.

Question 9 pertains to motion sickness; if the subject indicates they are prone to motion sickness this will not disqualify them from the study, however it will alert the investigator to proceed slowly with ramping-up the centrifuge spin rate.

Question 10 pertains to the subject's exercise routine. This question is for data collection purposes and does not affect the subject's eligibility.

E. Analytical Solutions for the Transcapillary Flow and the Interstitial Fluid Volume

The following equations, taken from Heldt [63], provide an analytical solution for the intercapillary flow and interstitial volume change during gravitational stress. The solution has been divided in four regions, depending on the nature of the orthostatic stress. The regions are indicated in Figure 93.

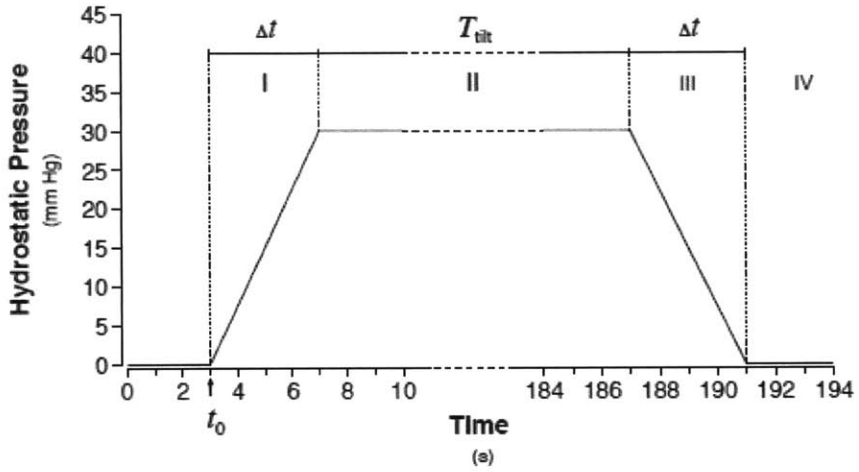

Figure 93 – Generic hydrostatic pressure profile. Figure taken from [63].

Region I: Gradual increase in orthostatic stress over a period of length Δt.

$$q(t) = \frac{V_{max}}{\Delta t} \cdot (1 - e^{-\frac{t}{\tau}}) \tag{E.1}$$

$$V(t) = V_{max} \cdot \left(\frac{t}{\Delta t} - \frac{\tau}{\Delta t}\left(1 - e^{-\frac{t}{\tau}}\right)\right) \tag{E.2}$$

Region II: Full orthostatic stress during period of duration T_{tilt}.

$$q(t) = \frac{V_{max}}{\Delta t} \cdot (1 - e^{-\frac{\Delta t}{\tau}}) \cdot e^{-\frac{t-\Delta t}{\tau}} \tag{E.3}$$

$$V(t) = V_{max} \cdot \left(1 - \frac{\tau}{\Delta t}\left(1 - e^{-\frac{\Delta t}{\tau}}\right) e^{-\frac{t-\Delta t}{\tau}}\right) \tag{E.4}$$

Region III: Gradual decline in orthostatic stress over a period of length Δt.

$$q(t) = \frac{V_{max}}{\Delta t} \cdot \left(1 + \left(1 - e^{-\frac{\Delta t}{\tau}}\right) e^{-\frac{T_{tilt}}{\tau}}\right) \cdot e^{-\frac{t-(\Delta t+T_{tilt})}{\tau}} - \frac{V_{max}}{\Delta t} \tag{E.5}$$

$$\begin{aligned} V(t) = {} & V_{max} \cdot \left(1 - \frac{t-(\Delta t+T_{tilt})}{\Delta t}\right) - V_{max} \cdot \frac{\tau}{\Delta t} \cdot \left(1 - e^{-\frac{\Delta t}{\tau}}\right) \cdot e^{-\frac{T_{tilt}}{\tau}} + \\ & + V_{max} \cdot \frac{\tau}{\Delta t} \cdot \left(1 + \left(1 - e^{-\frac{\Delta t}{\tau}}\right) e^{-\frac{T_{tilt}}{\tau}}\right) \cdot \left(1 - e^{-\frac{t-(\Delta t+T_{tilt})}{\Delta t}}\right) \end{aligned} \tag{E.6}$$

Region IV: Post-orthostatic stress recovery of unspecified length.

$$q(t) = -\frac{V_{max}}{\Delta t} \cdot \left(1 - e^{-\frac{\Delta t}{\tau}}\right) \cdot \left(1 - e^{-\frac{T_{tilt}+\Delta t}{\tau}}\right) \cdot e^{-\frac{t-(2\Delta t+T_{tilt})}{\tau}} \tag{E.7}$$

$$V(t) = V_{max} \cdot \frac{\tau}{\Delta t} \cdot \left(1 - e^{-\frac{\Delta t}{\tau}}\right) \cdot \left(1 - e^{-\frac{T_{tilt}+\Delta t}{\tau}}\right) \cdot e^{-\frac{t-(2\Delta t+T_{tilt})}{\tau}} \tag{E.8}$$

F. Finding Initial Conditions

The 23 non-linear algebraic equations to find the initial conditions used by Zamanian [65] are listed below. The first equation equates the right ventricular stroke volume and the left ventricular stroke volume. The following 21 equations describe the blood flow in the compartments assuming that the capacitors are not conducting. The last equation is based on the conservation of volume equating the difference between the total volume and the unstressed volume, and the distending volume in each compartment.

$$C_{ld}(P_{lvd} - P_{th}) - C_{ls}(P_{lvs} - P_{th}) = C_{rd}(P_{rvd} - P_{th}) - C_{rs}(P_{rvs} - P_{th}) \tag{F.1}$$

$$C_{ld}(P_{lvd} - P_{th}) - C_{ls}(P_{lvs} - P_{th}) = T_s^v \cdot \frac{P_{lvd}}{R_1} \tag{F.2}$$

$$T_s^v \cdot \frac{P_{lvd}}{R_1} = I_0 \cdot \left(\frac{P_1 - P_2}{R_2} + \frac{P_1 - P_6}{R_6}\right) \tag{F.3}$$

$$I_0 \cdot \frac{P_1 - P_2}{R_2} = I_0 \cdot \frac{P_2 - P_3}{R_3} \tag{F.4}$$

$$I_0 \cdot \frac{P_2 - P_3}{R_3} = I_0 \cdot \frac{P_3 - P_4}{R_{ub}} \tag{F.5}$$

$$I_0 \cdot \frac{P_3 - P_4}{R_{ub}} = I_0 \cdot \frac{P_4 - P_5}{R_4} \tag{F.6}$$

$$I_0 \cdot \frac{P_4 - P_5}{R_4} = I_0 \cdot \frac{P_5 - P_{ra}}{R_5} \tag{F.7}$$

$$I_0 \cdot \frac{P_1 - P_6}{R_6} = I_0 \cdot \frac{P_6 - P_7}{R_7} \tag{F.8}$$

$$I_0 \cdot \frac{P_6 - P_7}{R_7} = I_0 \cdot \left(\frac{P_7 - P_8}{R_8} + \frac{P_7 - P_{10}}{R_{10}} + \frac{P_7 - P_{12}}{R_{12}}\right) \tag{F.9}$$

$$I_0 \cdot \frac{P_7 - P_8}{R_8} = I_0 \cdot \frac{P_8 - P_9}{R_{rc}} \tag{F.10}$$

$$I_0 \cdot \frac{P_8 - P_9}{R_{rc}} = I_0 \cdot \frac{P_9 - P_{14}}{R_9} \tag{F.11}$$

$$I_0 \cdot \frac{P_7 - P_{10}}{R_{10}} = I_0 \cdot \frac{P_{10} - P_{11}}{R_{sc}} \tag{F.12}$$

$$I_0 \cdot \frac{P_{10} - P_{11}}{R_{sc}} = I_0 \cdot \frac{P_{11} - P_{14}}{R_{11}} \tag{F.13}$$

$$I_0 \cdot \frac{P_7 - P_{12}}{R_{12}} = I_0 \cdot \frac{P_{12} - P_{13}}{R_{lc}} \tag{F.14}$$

$$I_0 \cdot \frac{P_{12} - P_{13}}{R_{lc}} = I_0 \cdot \frac{P_{13} - P_{14}}{R_{13}} \tag{F.15}$$

$$I_0 \cdot \frac{P_{14} - P_{15}}{R_{14}} = I_0 \cdot \left(\frac{P_9 - P_{14}}{R_9} + \frac{P_{11} - P_{14}}{R_{11}} + \frac{P_{13} - P_{14}}{R_{13}} \right) \tag{F.16}$$

$$I_0 \cdot \frac{P_{14} - P_{15}}{R_{14}} = I_0 \cdot \frac{P_{15} - P_{ra}}{R_{15}} \tag{F.17}$$

$$I_0 \cdot \left(\frac{P_5 - P_{ra}}{R_5} + \frac{P_{15} - P_{ra}}{R_{15}} \right) = T_d^v \cdot \frac{P_{ra} - P_{rvd}}{R_{tri}} \tag{F.18}$$

$$T_d^v \cdot \frac{P_{ra} - P_{rvd}}{R_{tri}} = T_s^v \cdot \frac{P_{rvd} - P_{pa}}{R_{ro}} \tag{F.19}$$

$$T_s^v \cdot \frac{P_{rvd} - P_{pa}}{R_{ro}} = I_0 \cdot \frac{P_{pa} - P_{pv}}{R_{pv}} \tag{F.20}$$

$$I_0 \cdot \frac{P_{pa} - P_{pv}}{R_{pv}} = I_0 \cdot \frac{P_{pv} - P_{la}}{R_{li}} \tag{F.21}$$

$$I_0 \cdot \frac{P_{pv} - P_{la}}{R_{li}} = T_d^v \cdot \frac{P_{la} - P_{lvd}}{R_{mit}} \tag{F.22}$$

$$V_{total} - V_{total}^0 = \sum_{j \in \left\{ \begin{matrix} 1,2,\ldots,10, \\ 12,15,ra,rv, \\ pa,pv,la,lv \end{matrix} \right\}} C_j \cdot \Delta P_j + \sum_{k \in \{11,13,14\}} \left[\frac{2V_{maxk}}{\pi} \cdot arctan\left(\frac{\pi C_{0k}}{2V_{maxk}} \cdot \Delta P_k \right) \right] \tag{F.23}$$

G. Parameters of the Cardiovascular Model

The following table summarizes the parameters of the cardiovascular model.

Table 41 – Parameters of the cardiovascular model.

Index	Description	Units	Value
1	Arterial baroreflex set-point pressure P_A^{sp}	mm Hg	95
2	Arterial baroreflex scaling factor	mm Hg	18
3	R-R-interval sympathetic gain	$\frac{ms}{mm\,Hg}$	9
4	R-R-interval parasympathetic gain	$\frac{ms}{mm\,Hg}$	9
5	Arterial baroreflex R_{ub} gain	$\frac{PRU}{mm\,Hg}$	-0.05
6	Arterial baroreflex R_{rc} gain	$\frac{PRU}{mm\,Hg}$	-0.05
7	Arterial baroreflex R_{sc} gain	$\frac{PRU}{mm\,Hg}$	-0.05
8	Arterial baroreflex R_{lc} gain	$\frac{PRU}{mm\,Hg}$	-0.05
9	Arterial baroreflex V_{ub} gain	$\frac{ml}{mm\,Hg}$	5
10	Arterial baroreflex V_{rc} gain	$\frac{ml}{mm\,Hg}$	2
11	Arterial baroreflex V_{sc} gain	$\frac{ml}{mm\,Hg}$	13
12	Arterial baroreflex V_{lc} gain	$\frac{ml}{mm\,Hg}$	7
13	Arterial baroreflex C_{rs} gain	$\frac{ml}{mm\,Hg^2}$	0.022
14	Arterial baroreflex C_{ls} gain	$\frac{ml}{mm\,Hg^2}$	0.007
15	Cardio-pulmonary reflex set-point pressure	mm Hg	5
16	Cardio-pulmonary reflex scaling factor	mm Hg	5
17	Cardio-pulmonary reflex R_{ub} gain	$\frac{PRU}{mm\,Hg}$	-0.05
18	Cardio-pulmonary reflex R_{rc} gain	$\frac{PRU}{mm\,Hg}$	-0.05
19	Cardio-pulmonary reflex R_{sc} gain	$\frac{PRU}{mm\,Hg}$	-0.05
20	Cardio-pulmonary reflex R_{lc} gain	$\frac{PRU}{mm\,Hg}$	-0.05
21	Cardio-pulmonary reflex V_{ub} gain	$\frac{ml}{mm\,Hg}$	13
22	Cardio-pulmonary reflex V_{rc} gain	$\frac{ml}{mm\,Hg}$	3
23	Cardio-pulmonary reflex V_{sc} gain	$\frac{ml}{mm\,Hg}$	64
24	Cardio-pulmonary reflex V_{lc} gain	$\frac{ml}{mm\,Hg}$	30
25	Delay sympathetic impulse response	s	2
26	Peak sympathetic impulse response	s	5

27	End sympathetic impulse response	s	30
28	Nominal intra-thoracic pressure P_{th0}	mm Hg	-4
29	Upper body venous compliance C_4	$\frac{ml}{mm\,Hg}$	7
30	Kidney venous compliance C_9	$\frac{ml}{mm\,Hg}$	5
31	Splanchnic venous compliance C_{11}	$\frac{ml}{mm\,Hg}$	60
32	Lower body venous compliance C_{13}	$\frac{ml}{mm\,Hg}$	20
33	Abdominal venous compliance C_{14}	$\frac{ml}{mm\,Hg}$	1.3
34	Inferior vena cava compliance C_{15}	$\frac{ml}{mm\,Hg}$	0.5
35	Superior vena cava compliance C_5	$\frac{ml}{mm\,Hg}$	1.3
36	Right atrial diastolic elastance	$\frac{mm\,Hg}{ml}$	0.3
37	Right atrial end-systolic elastance	$\frac{mm\,Hg}{ml}$	0.74
38	Right ventricular diastolic elastance	$\frac{mm\,Hg}{ml}$	0.07
39	Right ventricular end-systolic elastance	$\frac{mm\,Hg}{ml}$	1.3
40	Pulmonary arterial compliance	$\frac{ml}{mm\,Hg}$	3.4
41	Pulmonary venous compliance	$\frac{ml}{mm\,Hg}$	9.0
42	Left atrial diastolic elastance	$\frac{mm\,Hg}{ml}$	0.50
43	Left atrial end-systolic elastance	$\frac{mm\,Hg}{ml}$	0.61
44	Left ventricular diastolic elastance	$\frac{mm\,Hg}{ml}$	0.13
45	Left ventricular end-systolic elastance	$\frac{mm\,Hg}{ml}$	2.5
46	Upper body microvascular resistance R_{ub}	PRU	3.3
47	Upper body venous outflow resistance R_4	PRU	0.11
48	Renal microvascular resistance R_{rc}	PRU	4.1
49	Renal venous outflow resistance R_9	PRU	0.11
50	Splanchnic microvascular resistance R_{sc}	PRU	2.4
51	Splanchnic venous outflow resistance R_{11}	PRU	0.07
52	Lower body microvascular resistance R_{lc}	PRU	3.9
53	Lower body venous outflow resistance R_{13}	PRU	0.10
54	Abdominal venous resistance R_{14}	PRU	0.019
55	Inferior vena cava resistance R_{15}	PRU	0.008
56	Superior vena cava resistance R_5	PRU	0.028
57	Tricuspid valve resistance R_{tri}	PRU	0.006

58	Right ventricular outflow resistance R_{ro}	PRU	0.006
59	Pulmonary microcirculation resistance R_{pv}	PRU	0.07
60	Pulmonary venous outflow resistance R_{li}	PRU	0.006
61	Mitral valve resistance	PRU	0.010
62	Left ventricular outflow resistance R_1	PRU	0.007
63	Total blood volume V_{tot}	ml	5150
64	Maximal splanchnic venous distending volume V_{maxsp}	ml	1500
65	Maximal lower body venous distending volume V_{maxll}	ml	1000
66	Maximal abdominal venous distending volume V_{maxab}	ml	650
67	Total zero pressure filling volume V_0	ml	4166
68	Upper body ZPFV	ml	645
69	Renal ZPFV	ml	30
70	Splanchnic ZPFV	ml	1146
71	Lower body ZPFV	ml	716
72	Abdominal venous ZPFV	ml	79
73	Inferior vena cava ZPFV	ml	33
74	Superior vena cava ZPFV	ml	16
75	Right atrial ZPFV	ml	14
76	Right ventricular ZPFV	ml	46
77	Pulmonary arterial ZPFV	ml	160
78	Pulmonary venous ZPFV	ml	430
79	Left atrial ZPFV	ml	24
80	Left ventricular ZPFV	ml	55
81	Nominal heart rate	beats/min	67
82	Ascending aorta compliance C_1	$\frac{ml}{mm\ Hg}$	0.28
83	Brachiocephalic arteries compliance C_2	$\frac{ml}{mm\ Hg}$	0.13
84	Descending thoracic aorta compliance C_6	$\frac{ml}{mm\ Hg}$	0.1
85	Upper body arteries compliance C_3	$\frac{ml}{mm\ Hg}$	0.2
86	Abdominal aorta compliance C_7	$\frac{ml}{mm\ Hg}$	0.1
87	Renal arteries compliance C_8	$\frac{ml}{mm\ Hg}$	0.21
88	Splanchnic arteries compliance C_{10}	$\frac{ml}{mm\ Hg}$	0.2

89	Leg arteries compliance C_{12}	$\frac{ml}{mm\,Hg}$	0.2
90	Brachiocephalic arteries resistance R_2	$\frac{ml}{mm\,Hg}$	0.003
91	Descending thoracic aorta resistance R_6	$\frac{ml}{mm\,Hg}$	0.011
92	Upper body arteries resistance R_3	$\frac{ml}{mm\,Hg}$	0.014
93	Abdominal aorta resistance R_7	$\frac{ml}{mm\,Hg}$	0.010
94	Renal arteries resistance R_8	$\frac{ml}{mm\,Hg}$	0.10
95	Splanchnic arteries resistance R_{10}	$\frac{ml}{mm\,Hg}$	0.07
96	Leg arteries resistance R_{12}	$\frac{ml}{mm\,Hg}$	0.09
97	P-R Interval	s	0.12
98	Atrial systole	s	0.2
99	Ventricular systole	s	0.3
100	Ascending aorta vertical length l_{v1}	cm	10.0
101	Brachiocephalic arteries vertical length l_{v2}	cm	4.5
102	Upper body arteries vertical length l_{v3}	cm	20.0
103	Upper body veins vertical length l_{v4}	cm	20.0
104	Superior vena cava vertical length l_{v5}	cm	14.5
105	Descending thoracic aorta vertical length l_{v6}	cm	16.0
106	Abdominal aorta vertical length l_{v7}	cm	14.5
107	Renal arteries vertical length l_{v8}	cm	0
108	Renal veins vertical length l_{v9}	cm	0
109	Splanchnic arteries vertical length l_{v10}	cm	10.0
110	Splanchnic veins vertical length l_{v11}	cm	10.0
111	Leg arteries vertical length l_{v12}	cm	85
112	Leg veins vertical length l_{v13}	cm	85
113	Abdominal veins vertical length l_{v14}	cm	14.5
114	Inferior vena cava vertical length l_{v15}	cm	6.0
115	Ascending aorta ZPFV	ml	21
116	Brachiocephalic arteries ZPFV	ml	5
117	Descending thoracic aorta ZPFV	ml	16
118	Upper body arteries ZVFV	ml	200
119	Abdominal aorta ZPFV	ml	10

120	Renal arteries ZPFV	ml	20
121	Splanchnic arteries ZPFV	ml	300
122	Body weight	kg	69

References

[1] A. E. Nicogossian and J. F. Parker, *Space Physiology and Medicine*. NASA, 1982.

[2] J. Buckey, *Space Physiology*. Oxford University Press, 2006.

[3] G. Clément and A. Bukley, *Artificial Gravity*. Springer, 2007.

[4] J. L. Edmonds, T. Jarchow, and L. R. Young, "Physiological benefits of exercise in artificial gravity: A broadband countermeasure to space flight related deconditioning," *Acta Astronaut.*, vol. 63, no. 1–4, pp. 2–7, Jul. 2008.

[5] P. Norsk, A. Asmar, M. Damgaard, and N. J. Christensen, "Fluid shifts, vasodilatation and ambulatory blood pressure reduction during long duration spaceflight," *J. Physiol.*, vol. 593, no. 3, pp. 573–584, 2015.

[6] P. Norsk, "Blood pressure regulation IV: Adaptive responses to weightlessness," *Eur. J. Appl. Physiol.*, vol. 114, no. 3, pp. 481–497, 2014.

[7] V. Marwaha, "A current understanding of the various factors of bone loss incorporated into the development of the Gravity Loading Countermeasure Skinsuit (GLCS)," International Space University, 2010.

[8] J. M. Waldie and D. J. Newman, "A gravity loading countermeasure skinsuit," *Acta Astronaut.*, vol. 68, no. 7–8, pp. 722–730, Apr. 2011.

[9] H. M. Frost, "Bone's mechanostat: a 2003 update.," *Anat. Rec. A. Discov. Mol. Cell. Evol. Biol.*, vol. 275, no. 2, pp. 1081–1101, 2003.

[10] V. Laurence, A. Christian, R. Bacabac, J. Van Loon, and J. Klein-Nulend, "Bone Overview ESA." 2004.

[11] H. M. Frost, "Why do marathon runners have less bone than weight lifters? A vital-biomechanical view and explanation," *Bone*, vol. 20, no. 3, pp. 183–9, Mar. 1997.

[12] D. R. Taaffe, T. L. Robinson, C. M. Snow, and R. Marcus, "High-impact exercise promotes bone gain in well-trained female athletes," *J. Bone Miner. Res.*, vol. 12, no. 2, pp. 255–260, 1997.

[13] S. M. Smith, M. a Heer, L. C. Shackelford, J. D. Sibonga, L. Ploutz-Snyder, and S. R. Zwart, "Benefits for bone from resistance exercise and nutrition in long-duration spaceflight: Evidence from biochemistry and densitometry," *J. Bone Miner. Res.*, vol. 27, no. 9, pp. 1896–906, Sep. 2012.

[14] R. H. Fitts, S. W. Trappe, D. L. Costill, P. M. Gallagher, a C. Creer, P. a Colloton, J. R. Peters, J. G. Romatowski, J. L. Bain, and D. a Riley, "Prolonged space flight-induced alterations in the structure and function of human skeletal muscle fibres.," *J. Physiol.*, vol. 588, no. Pt 18, pp. 3567–3592, 2010.

[15] R. Gopalakrishnan, K. O. Genc, A. J. Rice, S. M. C. Lee, H. J. Evans, C. C. Maender, H. Ilaslan, and P. R. Cavanagh, "Muscle volume, strength, endurance, and exercise loads during 6-month missions in space," *Aviat. Sp. Environ. Med.*, vol. 81, no. 2, pp. 91–102, 2010.

[16] B. F. Lujan and R. J. White, "Human Physiology in Space," *NSBRI*. [Online]. Available: http://www.nsbri.org/HumanPhysSpace/indexb.html.

[17] D. R. Hamilton, A. E. Sargsyan, K. Garcia, D. J. Ebert, P. a Whitson, A. H. Feiveson, I. V Alferova, S. a Dulchavsky, V. P. Matveev, V. V Bogomolov, and J. M. Duncan, "Cardiac and vascular responses to thigh cuffs and respiratory maneuvers on crewmembers of the International Space Station.," *J. Appl. Physiol.*, vol. 112, no. 3, pp. 454–62, Feb. 2012.

[18] B. D. Levine, "Maximal Exercise performance after adaptation to microgravity," *J. Appl. Physiol.*, vol. 81, no. 2, pp. 686 – 694, 1996.

[19] R. T. Jennings, "Managing space motion sickness," *J. Vestib. Res.*, vol. 8, no. 1, pp. 67–70, 1998.

[20] L. R. Young, "Spatial orientation and posture during and following weightlessness: human experiments on Spacelab Life Science," *J. Vestib. Res.*, vol. 3, no. 3, pp. 231–239, 1993.

[21] C. M. Oman, I. P. Howard, T. Smith, A. C. Beall, A. Natapoff, J. E. Zacher, H. L. Jenkin, and S. Assistants, "The Role of Visual Cues in Microgravity Spatial Orientation Authors," *Neurolab Spacelab Mission Neurosci. Res. Sp.*, 2003.

[22] C. Trigg, "Design and Validation of a Compact Radius Centrifuge Artificial Gravity Test Platform," Massachusetts Institute of Technology, 2013.

[23] S. Siceloff, "COLBERT Ready for Serious Exercise," 2009. [Online]. Available: http://www.nasa.gov/mission_pages/station/behindscenes/colberttreadmill.html.

[24] "NASA - Cycle Ergometer with Vibration Isolation and Stabilization System (CEVIS) - International Space Station," 2013. [Online]. Available: http://www.nasa.gov/mission_pages/station/research/experiments/841.html.

[25] NASA, "Advanced Resistive Exercise Device (ARED)," 2013. [Online]. Available: Advanced Resistive Exercise Device (ARED).

[26] "Institute of Adaptative & Spaceflight Physiology, Graz, Autria." [Online]. Available: http://www.meduni-graz.at/iap/proteinometer.htm.

[27] I. B. Kozlovskaya, a I. Grigoriev, and V. I. Stepantzov, "Countermeasure of the negative effects of weightlessness on physical systems in long-term space flights," *Acta Astronaut.*, vol. 36, no. 8–12, pp. 661–8, 1995.

[28] I. B. Kozlovskaya and A. I. Grigoriev, "Russian system of countermeasures on board of the International Space Station (ISS): The first results," *Acta Astronaut.*, vol. 55, pp. 233–237, 2004.

[29] "ESA - Human Spaceflight and Exploration," 2013. [Online]. Available: http://www.esa.int/Our_Activities/Human_Spaceflight/Astronauts/Andreas_Mogensen_set_for_Soyuz_mission_to_Space_Station_in_2015.

[30] G. Clément and A. Pavy-Le Traon, "Centrifugation as a countermeasure during actual and simulated microgravity: a review," *Eur. J. Appl. Physiol.*, vol. 92, no. 3, pp. 235–48, Jul. 2004.

[31] S. Trappe, D. Costill, P. Gallagher, A. Creer, J. R. Peters, H. Evans, D. a Riley, and R. H. Fitts, "Exercise in space: human skeletal muscle after 6 months aboard the International Space Station," *J. Appl. Physiol.*, vol. 106, pp. 1159–1168, 2009.

[32] D. Linnarsson, R. L. Hughson, K. S. Fraser, G. Clément, L. L. Karlsson, E. Mulder, W. H. Paloski, J. Rittweger, F. L. Wuyts, and J. Zange, "Effects of an artificial gravity countermeasure on orthostatic tolerance, blood volumes and aerobic power after short-term bed rest (BR-AG1)," *J. Appl. Physiol.*, vol. 118, no. 1, pp. 29–35, 2015.

[33] W. Paloski and J. Charles, "2014 Artificial Gravity Workshop - White Paper," Ames Research Center.

[34] B. Joosten, "Preliminary assessment of artificial gravity impacts to deep-space vehicle design," 2007.

[35] J. Kaderka, L. R. Young, and W. H. Paloski, "A critical benefit analysis of artificial gravity as a microgravity countermeasure," *Acta Astronaut.*, vol. 67, no. 9–10, pp. 1090–1102, Nov. 2010.

[36] J. E. Greenleaf, D. P. Gundo, D. E. Watenpaugh, G. M. Mulenburg, M. A. Mckenzie, A. R. Hargens, M. Field, and N. Aeronautics, "Cycle-Powered Short Radius (1.9 m) Centrifuge : Effect of Exercise Versus Passive Acceleration on Heart Rate in Humans," 1997.

[37] S. Iwase, Q. Fu, K. Narita, E. Morimoto, H. Takada, and T. Mano, "Effects of graded load of artificial gravity on cardiovascular functions in humans," *Environ. Med. Annu. Rep. Res. Inst. Environ. Med. Nagoya Univ.*, vol. 46, no. 1–2, pp. 29–32, 2002.

[38] S. Iwase, "Effectiveness of centrifuge-induced artificial gravity with ergometric exercise as a countermeasure during simulated microgravity exposure in humans," *Acta Astronaut.*, vol. 57, no. 2–8, pp. 75–80, Jul. 2005.

[39] C.-B. Yang, S. Zhang, Y. Zhang, B. Wang, Y.-J. Yao, Y.-C. Wang, Y.-H. Wu, W.-B. Liang, and X.-Q. Sun, "Combined short-arm centrifuge and aerobic exercise training improves cardiovascular function and physical working capacity in humans," *Med. Sci. Monit.*, vol. 16, no. 12, pp. 575–583, 2010.

[40] Y. Yang, M. Baker, S. Graf, J. Larson, and V. J. Caiozzo, "Hypergravity resistance exercise: the use of artificial gravity as potential countermeasure to microgravity," *J. Appl. Physiol.*, vol. 103, no. 5, pp. 1879–87, Nov. 2007.

[41] K. Katayama, K. Sato, and H. Akima, "Acceleration with Exercise during Head-Down Bed Rest Preserves Upright Exercise Responses," *Aviat. Sp. Environ. Med.*, vol. 75, no. 12, pp. 1029–1035, 2004.

[42] K.-I. Iwasaki, T. Shiozawa, A. Kamiya, D. Michikami, K. Hirayanagi, K. Yajima, S. Iwase, and T. Mano, "Hypergravity exercise against bed rest induced changes in cardiac autonomic control.," *Eur. J. Appl. Physiol.*, vol. 94, no. 3, pp. 285–291, 2005.

[43] K. R. Duda, T. Jarchow, and L. R. Young, "Squat Exercise Biomechanics during Short-Radius Centrifugation," *Aviat. Space. Environ. Med.*, vol. 83, no. 2, pp. 102–110, Feb. 2012.

[44] Y. Yang, A. Kaplan, M. Pierre, G. Adams, P. Cavanagh, C. Takahashi, A. Kreitenberg, J. Hicks, J. Keyak, and V. Caiozzo, "Space cycle: a human-powered centrifuge that can be used for hypergravity resistance training.," *Aviat. Sp. Environ. Med.*, vol. 78, no. 1, pp. 2–9, 2007.

[45] H. Akima, K. Katayama, and K. Sato, "Intensive Cycle Training with Artificial Gravity Maintains Muscle Size During Bed Rest," no. August, pp. 923–929, 2005.

[46] J. Rittweger, M. Pierre, G. Clément, D. Linnarsson, W. H. Paloski, F. Wuyts, J. Zange, and O. Angerer, "Short-arm centrifugation as a partially effective musculoskeletal countermeasure during 5-day head-down tilt bed rest — results from the BRAG1 study," *Eur. J. Appl. Physiol.*, 2015.

[47] A. C. Guyton, T. G. Coleman, and H. J. Granger, "Circulation: overall regulation," *Annu. Rev. Physiol.*, vol. 34, pp. 13–46, 1972.

[48] A. C. Guyton, C. E. Jones, and T. G. Coleman, *Circulatory Physiology: Cardiac Output and Its Regulation*, 2nd Ed. Philadelphia: WB Saunders, 1973.

[49] A. C. Guyton, A. E. Taylor, and H. J. Granger, *Circulatory Physiology II: Dynamics and Control of the Body Fluids*. Philadelphia: WB Saunders, 1975.

[50] B. N. Van Vliet and J. Montani, "Circulation and Fluid Volume Control," *Integr. Physiol.*, vol. C, pp. 43–66, 2005.

[51] J. Montani and B. N. Van Vliet, "Understanding the contribution of Guyton's large circulatory model to long-term control of arterial pressure," *Exp. Physiol.*, vol. 94, no. December 2008, pp. 381–397, 2009.

[52] L. Taelman, J. Degroote, P. Verdonck, J. Vierendeels, and P. Segers, "Modeling hemodynamics in vascular networks using a geometrical multiscale approach: numerical aspects," *Ann. Biomed. Eng.*, vol. 41, no. 7, pp. 1445–58, Jul. 2013.

[53] F. M. Melchior, R. S. Srinivasan, and J. B. Charles, "Mathematical modeling of human cardiovascular system for simulation of orthostatic response," *Am. J. Physiol.*, vol. 262, no. 102, pp. H1920–H1933, 1992.

[54] M. S. Olufsen, J. T. Ottesen, H. T. Tran, L. M. Ellwein, L. a Lipsitz, and V. Novak, "Blood pressure and blood flow variation during postural change from sitting to standing: model development and validation," *J. Appl. Physiol.*, vol. 99, pp. 1523–1537, 2005.

[55] T. Heldt, E. B. Shim, R. D. Kamm, and R. G. Mark, "Computational modeling of cardiovascular response to orthostatic stress," *J. Appl. Physiol.*, vol. 92, pp. 1239–1254, 2002.

[56] K. van Heusden, J. Gisolf, W. J. Stok, S. Dijkstra, and J. M. Karemaker, "Mathematical modeling of gravitational effects on the circulation: importance of the time course of venous pooling and blood volume changes in the lungs," *Am. J. Physiol. Heart Circ. Physiol.*, vol. 291, pp. H2152–H2165, 2006.

[57] E. Lim, G. S. H. Chan, S. Dokos, S. C. Ng, L. a Latif, S. Vandenberghe, M. Karunanithi, and N. H. Lovell, "A cardiovascular mathematical model of graded head-up tilt.," *PLoS One*, vol. 8, p. e77357, 2013.

[58] R. C. Croston, J. a. Rummel, and F. J. Kay, "Computer model of cardiovascular control system responses to exercise," pp. 301–307, 1973.

[59] F. M. Melchior, R. S. Srinivasan, P. H. Thullier, and J. M. Clère, "Simulation of cardiovascular response to lower body negative pressure from 0 to -40 mmHg," *J. Appl. Physiol.*, vol. 77, pp. 630–640, 1994.

[60] R. J. White, J. I. Leonard, and J. B. Charles, "Mathematical modeling of acute and chronic cardiovascular changes during extended duration orbiter (EDO) flights," *Acta Astronaut.*, vol. 23, pp. 41–51, 1991.

[61] R. J. White and C. G. Blomqvist, "Central venous pressure and cardiac function during spaceflight," *J. Appl. Physiol.*, vol. 85, no. 2, pp. 738–746, 1998.

[62] W. D. Lakin, S. a Stevens, and P. L. Penar, "Modeling intracranial pressures in microgravity: the influence of the blood-brain barrier," *Aviat. Sp. Environ. Med.*, vol. 78, no. 10, pp. 932–936, Oct. 2007.

[63] T. Heldt, "Computational Models of Cardiovascular Response to Orthostatic Stress," 2004.

[64] T. Heldt, R. Mukkamala, G. B. Moody, and R. G. Mark, "CVSim: An Open-Source Cardiovascular Simulator for Teaching and Research," *Open Pacing. Electrophysiol. Ther. J.*, vol. 3, pp. 45–54, Jan. 2010.

[65] S. A. Zamanian, "Modeling and Simulating Human Cardiovascular Response to Acceleration," Massachusetts Institute of Technology, 2007.

[66] ESA, "Artificial Gravity with Ergometric Exercise (AGREE) - Accommodation Feasibility Study." 2011.

[67] A. Diaz, C. Trigg, and L. R. Young, "Combining ergometer exercise and artificial gravity in a compact-radius centrifuge," *Acta Astronaut.*, vol. 113, pp. 80–88, 2015.

[68] "HUMAN INTEGRATION DESIGN HANDBOOK NASA SP-2010-3407," 2010.

[69] J. Penaz, "Photoelectric measurement of blood pressure, volume and flow in the finger," in *Digest 10th Int Conf Med Biol Engng*, 1973.

[70] "ccNexfin Operator's Manual." Bmeye B.V., 2012.

[71] P. R. Cavanagh, R. Gopalakrishnan, a J. Rice, K. O. Genc, C. C. Maender, P. G. Nystrom, M. J. Johnson, M. M. Kuklis, and B. T. Humphreys, "An Ambulatory Biomechanical Data Collection System for USe in Space: Design and Validation," *Aviat. Sp. Environ. Med.*, vol. 80, no. 10, pp. 870–881, 2009.

[72] K. O. Genc, R. Gopalakrishnan, M. M. Kuklis, C. C. Maender, a J. Rice, K. D. Bowersox, and P. R. Cavanagh, "Foot forces during exercise on the International Space Station," *J. Biomech.*, vol. 43, no. 15, pp. 3020–7, Nov. 2010.

[73] R. G. Mark, "Cardiovascular Mechanics." Massachusetts Institute of Technology, Cambridge, p. 70.

[74] J. Truijen, J. J. Van Lieshout, W. a. Wesselink, and B. E. Westerhof, "Noninvasive continuous hemodynamic monitoring," *J. Clin. Monit. Comput.*, vol. 26, pp. 267–278, 2012.

[75] J. R. Martina, B. E. Westerhof, J. van Goudoever, E. M. F. H. de Beaumont, J. Truijen, Y.-S. Kim, R. V. Immink, D. a. Jöbsis, M. W. Hollmann, J. R. Lahpor, B. a. J. M. de Mol, and J. J. van Lieshout, "Noninvasive Continuous Arterial Blood Pressure Monitoring with Nexfin®," *Anesthesiology*, vol. 116, no. 5, pp. 1092–1103, 2012.

[76] J. R. Martina, B. E. Westerhof, J. Van Goudoever, N. De Jonge, J. J. Van Lieshout, J. R. Lahpor, and B. a J. M. De Mol, "Noninvasive blood pressure measurement by the Nexfin monitor during reduced arterial pulsatility: a feasibility study," *ASAIO J.*, vol. 56, pp. 221–227, 2010.

[77] D. W. Eeftinck Schattenkerk, J. J. van Lieshout, A. H. van den Meiracker, K. R. Wesseling, S. Blanc, W. Wieling, G. a van Montfrans, J. J. Settels, K. H. Wesseling, and B. E. Westerhof, "Nexfin noninvasive continuous blood pressure validated against Riva-Rocci/Korotkoff.," *Am. J. Hypertens.*, vol. 22, no. 4, pp. 378–383, 2009.

[78] O. Broch, J. Renner, M. Gruenewald, P. Meybohm, J. Schöttler, a. Caliebe, M. Steinfath, M. Malbrain, and B. Bein, "A comparison of the Nexfin ® and transcardiopulmonary thermodilution to estimate cardiac output during coronary artery surgery," *Anaesthesia*, vol. 67, pp. 377–383, 2012.

[79] S. I. Bubenek-Turconi, M. Craciun, I. Miclea, and A. Perel, "Noninvasive continuous cardiac output by the nexfin before and after preload-modifying maneuvers: A comparison with intermittent thermodilution cardiac output," *Anesth. Analg.*, vol. 117, no. 2, pp. 366–372, 2013.

[80] L. W. J. Bogert, K. H. Wesseling, O. Schraa, E. J. Van Lieshout, B. a J. M. De Mol, J. Van Goudoever, B. E. Westerhof, and J. J. Van Lieshout, "Pulse contour cardiac output derived from non-invasive arterial pressure in cardiovascular disease," *Anaesthesia*, vol. 65, pp. 1119–1125, 2010.

[81] M. O. Fischer, R. Avram, I. Cârjaliu, M. Massetti, J. L. Gérard, J. L. Hanouz, and J. L. Fellahi, "Non-invasive continuous arterial pressure and cardiac index monitoring with Nexfin after cardiac surgery," *Br. J. Anaesth.*, vol. 109, no. July, pp. 514–521, 2012.

[82] N. Westerhof, J. W. Lankhaar, and B. E. Westerhof, "The arterial windkessel," *Med. Biol. Eng. Comput.*, vol. 47, pp. 131–141, 2009.

[83] H. Suga, "Time course of left ventricular pressure-volume relationship under various end-diastolic volumes," *Jpn. Heart J.*, vol. 10, no. 6, pp. 509–515, 1969.

[84] H. Suga, "Time course of left ventricular pressure-volume relationship under various extends of aortic occlusion," *Jpn. Heart J.*, vol. 11, no. 4, pp. 373–378, 1970.

[85] H. Suga, "Left Ventricular Time-varying Pressure-Volume Ratio in Systole as an Index of Miocardial Inotropism," *Jpn. Heart J.*, vol. 12, no. 2, pp. 153–160, 1971.

[86] H. Suga, K. Sagawa, and a a Shoukas, "Load independence of the instantaneous pressure-volume ratio of the canine left ventricle and effects of epinephrine and heart rate on the ratio," *Circ. Res.*, vol. 32, pp. 314–322, 1973.

[87] H. Senzaki, C.-H. Chen, and D. A. Kass, "Single-Beat Estimation of End-Systolic Pressure-Volume Relation in Humans: A New Method with the Potential for Noninvasive Application," *Circulation*, vol. 94, no. 10, pp. 2497–2506, Nov. 1996.

[88] R. W. de Boer, J. M. Karemaker, and J. Stracke, "Description of the Heart_Rate Variability Data in Accordance With a Physiological Model for the Genesis of Heartbeats," *Phychophysiology*, vol. 22, no. 2, pp. 147–155, 1985.

[89] Z. Samar, "Cardiovascular Parameter Estimation using a Computational Model," 2005.

[90] A. C. Guyton, *Textbook of Medical Physiology*. Harcourt College Pub.

[91] J. Mead and E. A. Geansler, "Esophageal and pleural pressures in man, upright and supine," *J. Appl. Physiol.*, vol. 14, no. 1, pp. 81–83, 1959.

[92] B. G. Ferris, J. Mead, and N. R. Frank, "Effect of body position on esophageal pressure and measurement of pulmonary compliance," *J. Appl. Physiol.*, vol. 14, no. 4, pp. 521–524, 1959.

[93] T. David, "Teaching Physiology Through Interactive Simulation of Hemodynamics," Massachusetts Institute of Technology, 1991.

[94] R. S. Johnston and L. F. Dietlein, *Biomedical Results from Skylab*, NASA SP-37. Washington D.C.: National Aeronautics and Space Administration (Scientific and Technical Information Office), 1977.

[95] A. Perel, W. Wesselink, and J. Settels, "The Nexfin Monitor – A Totally Non_Invasive Cardiac Output Monitor," in *Proceedings of the 23rd Annual Meeting - International Symposium on Critical Care Medicine*, 2011, pp. 103–108.

[96] K. H. Wesseling, B. de Wit, and G. M. A. vsn der Hoeven, "Physiocal, calibrating finger vascular physiology for Finapres," *Homeostasis*, vol. 36, no. 2–3, 1995.